Université catholique de Louvain
Secteur des sciences de la santé

Institut LOUVAIN DRUG RESEARCH INSTITUTE
DE DUVE INSTITUTE

Promoteurs Pr. Marie-Paule MINGEOT-LECLERCQ
Pr. Donatienne TYTECA

Résumé. Les saponines, des molécules amphiphiles retrouvées abondamment dans les plantes, attirent de plus en plus d'attention grâce à leurs activités biologiques telles que des propriétés anticancéreuses. L'activité de certaines saponines est attribuée à leur interaction avec le cholestérol membranaire. Dans ce travail, nous nous sommes intéressés à la saponine ginsenoside Rh2 que l'on retrouve dans la racine du *Panax ginseng*. Notre but était d'obtenir plus d'information sur l'activité membranaire et apoptotique du Rh2 et de comprendre l'importance respective du cholestérol et de la sphingomyéline pour ses activités. Les résultats obtenus sur des modèles membranaires artificiels et sur des membranes biologiques insistent sur l'importance de le la nature du lipide pour l'activité du Rh2. Nous avons montré le rôle critique de la sphingomyéline dans l'action du Rh2 alors que le cholestérol semble diminuer la sensibilité de la membrane au Rh2. A la fin de cette thèse, nous avons initié un travail à long terme visant à évaluer l'intérêt potentiel du Rh2 pour moduler l'invasion cellulaire tumorale. D'un point de vue plus global, l'interaction favorable d'une molécule avec un lipide membranaire pourrait servir à mettre en évidence ce lipide ou à cibler ce dernier dans un contexte physiopathologique tel que la croissance tumorale et les métastases.

Summary. Saponins, amphiphilic compounds widely found in plants, attract more and more attention based on their biological activities including anticancer properties. The activity for some saponins has been attributed to their interactions with membrane cholesterol. In this study, we focus on the saponin ginsenoside Rh2 found in *Panax ginseng* root. Our goal was to obtain detailed knowledge about the activity of Rh2 and to elucidate the respective importance of cholesterol and sphingomyelin for its activity. Results obtained in artificial and biological membranes clearly highlight the importance of membrane lipid nature for the Rh2 activity. We revealed the critical role of sphingomyelin in the activity of Rh2 while cholesterol seems to depress the sensitivity of the membrane to Rh2. At the end of th PhD thesis, we initiated a long-term study aiming at evaluating the potential interest of Rh2 to modulate tumor cell invasion. From a more global point-of-view, the favorable interaction of a molecule with a membrane lipid could provide a powerful tool to evidence this lipid or target the latter in a pathophysiological context such as tumor growth and metastasis.

Notice biographique
Sandrine Verstraeten obtient son diplôme de master en sciences biomédicales à l'UCLouvain en 2015. A l'issue de son master, elle effectue un stage au CRCHUM à Montréal. Dans le cadre d'un mandat Télévie sous la supervision des Professeurs M.P. Mingeot-Leclercq et D. Tyteca, elle s'intéresse à l'importance de certains lipides membranaires pour l'activité du ginsenoside Rh2, une molécule présente dans le *Panax ginseng*. Parallèlement à son parcours académique, Sandrine joue au hockey sur gazon, adore voyager et boire des mojitos entre amis. Elle rénove actuellement une maison à La Bruyère avec son compagnon.

2019

Sandrine Verstaeten

Importance of membrane lipids for the saponin activity

Contribution of membrane lipids to the activity of the saponin ginsenoside Rh2

Sandrine Verstraeten

November 2019

Thesis submitted to fulfil the requirements for the degree of
PhD in Biomedical and Pharmaceutical Sciences

Secteur des sciences de la santé

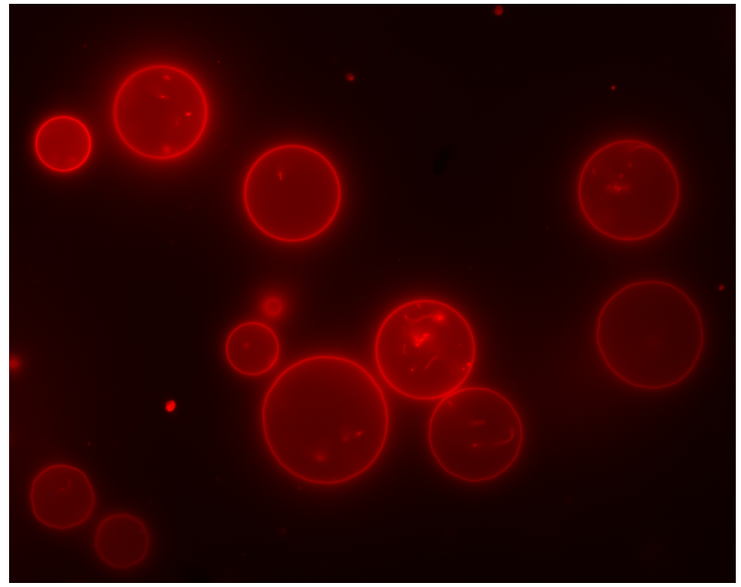

UCLouvain
Louvain Drug Research Institute & de Duve Institute
Cellular and Molecular Pharmacology & CELL biology unit

Contribution of membrane lipids to the activity of the saponin ginsenoside Rh2

Sandrine Verstraeten

November 2019

Supervisors: Prof. Marie-Paule Mingeot-Leclercq

Prof. Donatienne Tyteca

Thesis in view to obtain the degree of PhD in Biomedical and Pharmaceutical Sciences

Members of the jury

Prof. Pierre SONVEAUX (President)
UCLouvain

Prof. Marie-Paule MINGEOT-LECLERCQ (Promotor)
UCLouvain

Prof. Donatienne TYTECA (Co-promotor)
UCLouvain

Prof. Bénédicte JORDAN
UCLouvain

Prof. Jean-Baptiste DEMOULIN
UCLouvain

Prof. Stefan CONSTANTINESCU
UCLouvain

Prof. Véronique ROSILIO
Université Paris-Sud

Prof. François PARIS
Université de Nantes

Remerciements

Après ces quatre années de thèse, je voudrais prendre le temps de regarder en arrière et de remercier les nombreuses personnes qui m'ont permis d'accomplir ce travail, que ce soit par leur conseil, leur soutien intellectuel, ou affectif.

Je tiens en premier lieu à remercier mes deux promotrices, Marie-Paule Mingeot-Leclercq et Donatienne Tyteca. Merci de m'avoir épaulée et soutenue à 300% toute au long de cette thèse, et encore plus au cours de ces derniers mois. Je n'aurai vraiment pas pu rêver de mieux. J'ai réellement apprécié travailler à vos côtés, et une belle complémentarité scientifique et humaine s'est dégagée de cette enrichissante copromotion.

Marie-Paule, merci pour vos conseils et votre investissement durant cette thèse. Merci pour la confiance et la liberté de recherche que vous m'avez accordées. Merci de m'avoir donné l'opportunité de partir en congrès, et de m'avoir toujours poussée aux collaborations, qui ont indéniablement permis de faire avancer cette thèse. Au-delà d'une professeure et d'une chef, j'ai également appris à vous connaitre en dehors du cadre du travail, notamment lors de nos trajets en voiture vers Gembloux ou Louvain-La-Neuve. Merci pour votre positivité, votre bonne humeur, vos rires qui traversent les murs (mais aussi l'écho de vos sandales dans le couloir qui me prévienne qu'il est temps d'arrêter de papoter ave Hélène et de se remette au travail!). Un immense merci pour votre bienveillance et vos encouragements, qui m'ont toujours donnés l'envie de me surpasser, pour ne pas avoir de regrets mais également ne pas vous décevoir. Je vous souhaite une belle fin de carrière, et une transition heureuse vers plus de moments partagés avec votre famille. (PS : J'ai déjà chargé personnellement Hélène de prendre le relais si vous devez faire un skype!)

Donatienne, merci d'avoir fait une infidélité aux globules rouges pour m'aider à faire avancer ce projet de thèse. Merci pour toutes tes suggestions d'expériences et tes commentaires pertinents. Merci également pour ton investissement et les tonnes d'heures que tu as passé à corriger et peaufiner mes papiers et ma thèse (je suis tout particulièrement reconnaissante pour ces corrections où je pouvais juste cliquer sur accepter!). Merci aussi pour ton enthousiasme et ta passion pour la recherche, qui ont été de réelles sources de motivation! Je te souhaite une belle continuation professionnelle, et j'espère que ton projet sur les cellules cancéreuses apportera son lot de belles découvertes!

Je remercie également les membres de mon jury de thèse : les professeurs Bénédicte Jordan, Pierre Sonveaux, Jean-Baptiste Demoulin, Stefan Constantinescu qui m'ont

permis de faire avancer ce projet par leurs remarques constructives au fil des comités d'années, et de m'avoir convaincue d'aller explorer les méandres de la biophysique, malgré que ce n'était pas initialement ma tasse de thé! *Je tiens également à remercier les deux membres externes, Veronique Rosilio et François Paris, pour avoir accepté de se joindre au jury lors de ma thèse privée. Merci d'avoir pris votre rôle à cœur, et d'avoir rendu cette défense riche et stimulante.*

Merci également au Télévie qui m'a financée au long de ces quatre années et sans qui cette thèse n'aura jamais vu le jour!

Merci à Françoise, pour votre enjouement aux activités de labo et de vous êtes toujours donner à fond dans les épreuves/défis proposées lors de ces journées (Au point même d'utiliser des stratagèmes de filou comme bloquer l'ascenseur du LDRI ou cacher les indices pour gagner☺)

Merci Hussein alias HusHus ; tu as été le premier à m'accueillir dans l'équipe FACM et tu m'as aidé à y faire ma place. Merci pour ta bienveillance, tu as toujours été là pour m'aider et répondre à la moindre de mes questions. Merci aussi de m'avoir fait prendre goût à ces délicieuses épices, cacahuètes et noix de cajou du Liban!

Merci à mon binôme de cœur, Hélène! Je me rappellerai toujours quand Louise m'a parlé de toi pour la première fois en tant que bébé kot connu pour ses talents en gymnastique. J'ai d'abord été intriguée, puis au fil du temps tu es devenue une super copine bien plus qu'une collègue. Merci pour ta bonne humeur communicative en chantant Elton John « I'm still standing, yeah yeah yeah », merci pour ton enthousiasme dès qu'il s'agit de se lancer dans l'organisation d'un team building, merci pour ton oreille attentive et tes paroles réconfortantes. Tu as été un réel soutien durant toutes ces années.

Merci à Aline pour ta convivialité et tes rires dans le couloir qui poussent à sortir du bureau pour se joindre à la fête. Merci aussi d'avoir fédéré le laboratoire autour de tes délicieux desserts. Je peux l'avouer aujourd'hui, on essayait toujours de leur trouver un petit défaut, histoire que tu décides d'améliorer la recette et que tu en reprépares un pour le lendemain. Et ce pour le plus grand plaisir de nos papilles et un peu moins de nos régimes.

Merci également à tous les autres membres de la team FACM. J'ai réellement aimé l'ambiance conviviale qui y régnait, la solidarité qu'on a pu avoir entre nous, ainsi que les verres d'après travail qui font relativiser, surtout quand de dures semaines de manip se terminent en échec… Merci à Tamara, pour toutes ses heures

incalculables à discuter au bureau, au point que je me suis déjà demandé ce que j'avais fait de ma journée. Merci Virginie pour tout le temps que tu as consacré à me préparer les lignées cellulaires, merci pour tes conseils en potager et en maison, et ton enthousiasme de cette dernière année. Merci Albert d'avoir arbitré mon match de hockey, (il y a des chances que je te le redemande prochainement!). *Merci à Yvan, de m'avoir montré que des pokémons se cachaient dans la hotte. Merci à Vas, pour toutes ses parties de baby-foot dont j'espère que tu admettras que j'en sortais souvent gagnante. Merci à Fred, de m'avoir montré que certains Français pouvaient être modeste même lorsqu'ils gagnent contre la Belgique à la Coupe du monde (ouille je suis en train de réveiller un mauvais souvenir :p). Toutes mes félicitations pour ta petite fille Victoria. Merci à Gang de m'avoir montré qu'il était possible de travailler avec 1000 plaques de 96 puits sous une hotte sans les inverser. Merci à Alix, notre professeur d'escalade. Merci à Tiep, pour ta bonne humeur et ton sourire communicatif. Merci également à Perrin pour tes chants mélodieux à côté du bureau, il faut encore que tu travailles la justesse mais on tient quelque chose! Merci à Audrey, Alexandra, Perrine et Mandeep d'apporter votre fraicheur, enthousiasme et motivation de début de thèse. La thèse se termine mais j'espère de tout cœur encore partager des moments de convivialités avec chacun et chacune d'entre vous.*

Merci également aux anciens du labo qui m'ont accueillie, conseillée et permis de m'intégrer dans l'équipe. Merci à Marie-Claire. Tu m'auras fait un sacré parquet de cellules! Merci pour ta gentillesse, ton écoute et ton soutien lorsque j'étais la petite jeune doctorante sortie des études. Merci Ahaleyiah et Claire d'être aussi pétillantes et d'avoir la positive attitude comme dirait Lorie! Merci Lucy (alias gossip girl) pour ta bonne humeur et tes croustillants ragots dont on veut toujours plus, Merci à Alice, pour ton énergie débordante et ta motivation à organiser les Get together. Merci Catherine, pour ta folie et tes histoires plus farfelues les unes que les autres.

Merci à l'équipe du Lido, Patrick, Hélène et Louise pour votre aide pour le nombre incalculable de fois où je suis venu vous dire que le microscope ne marchait pas et qu'il faisait bien noir dans le binoculaire. Anne-Sophie pour ton humour pince-sans-rire et pour toutes les TLCs. Entre notre empoissonnement sous la hotte, le four et le vaporisateur qui ne fonctionne pas, on en aura bien bavé. Merci aussi à Mauriane pour tout le peps que tu dégages dans un si petit corps. Courage pour la suite du projet cellules cancéreuses, je te souhaite de belles découvertes !

Mais une thèse ne s'arrête pas dans l'enceinte d'un labo, et le soutien moral des amis m'a été essentiel pour persévérer ! Je remercie Mathilde et Louise, mes acolytes de voyage et de début de thèse! Merci pour tous ces moments inoubliables

partagés lors de notre stage à Montréal ou encore lors de nos city-trips. Mathilde, comme quoi échanger nos crachats lors d'un TP de bio en première année peut découler sur une amitié qui dure depuis déjà 10 ans. Louise, merci pour ta joie de vivre, tes youpiieees, et le fait que tu ries même à mes blagues les plus nulles. Merci d'avoir été une copine au top, en autre pour nos congrès de biophysiques. Mais pour nos futurs city-trip en compagnie de Myrtille, je m'occuperai quand même dorénavant du choix du logements, afin d'éviter de séjourner à nouveau dans un hôtel moribond aux chambres infestées de souris!

Merci à Cha d'être une vraie petite maman, toujours là pour prendre des nouvelles, pour écouter et réconforter (et même pour proposer une solution de logement au chaud pour ne pas devoir finaliser une thèse avoir les doigts gelés).

Merci également à toute la bande de copains de première année d'université : Nico, Sylvie, Ben, Flo, Adrien, Math, Alice, Dam et les +1 qui sont venus progressivement compléter la bande : Laure-Anne, Fred, Laurent Anouck, Astrid, Quentin, Nico DS. Ça fait du bien de pouvoir compter sur une bande d'amis en or comme vous.

Merci à Soso, Mad et Sarah pour tous ces moments partager à plaisanter autour d'un bon petit plat et à se poser des question très très existentielles (comme par exemple, savoir comment chacune se lave les oreilles!)

Merci à mon équipe de hockey, que ce soit celles qui sont parties (souvent tombées enceintes); les anciennes ou les nouvelles. Merci pour toutes les troisième mi-temps qu'on a passé (mon foie s'en rappelle encore) et les nombreux fou-rires qu'on a pu partager! Bien plus qu'un simple sport, le hockey c'est surtout l'occasion de revoir les copines!

Merci aux SBIMs, Benoit, Manon, Fanny, Séverine, Fabrice, Nora avec lesquelles on a partagé nos études dépeuplées et inconnues, nos galères de stage, et pour certains, nos galères de doctorats!

Merci à Sophie et à Eléonore, pour cette facilité à se retrouver autour d'un souper ou d'un verre au Chasseur Ardennais, même lorsqu'on ne s'est pas vues depuis longtemps.

Je remercie également ma famille. Papa, Maman. Je n'oublie pas que c'est en partie grâce à vous que j'en suis là aujourd'hui. Je souhaite de tout cœur qu'on puisse un jour retrouver la sérénité du passé. « Ne regarde pas en arrière les yeux plein de regrets ; regarde plutôt en avant, les yeux plein d'espoir ». Merci à mes deux grands

frérots Benoit et Sébastien et leurs petites tribus, pour leur soutien indéfectible. On s'exprime peu mais vous êtes profondément dans mon coeur! Un merci particulier à Ben, Marie Raphael et Elise de nous avoir hébergé, moi et Laurent au début des travaux. L'introduction de cette thèse a été pondu tout droit de votre studio. Je vous remercierai en babysitting, c'est promis!

Merci également à Etienne, Claire, Damien, Marine, Arthur, Olivier, Pauline de nous encourager, et aussi de nous aider dans notre projet de rénovation de maison.

J'ai également une pensée pour mon Papy et ma Mamy qui m'ont conduit à entreprendre des études scientifiques [illegible] investir dans la recherche.

Et je terminerai ces remerciements par toi, mon Lau. Je suis la plus heureuse qu'on se lance ensemble dans cette nouvelle aventure qu'est l'achat et la rénovation de notre maison. Merci pour le son doux et mélodieux du burineur et les secousses du marteau piqueur. Blague à part, merci pour tous les jours que tu as déjà passé à rénover notre maison pendant que j'écrivais cette thèse. Merci pour ton précieux soutien, tes conseils et tes encouragements qui m'aident à préserver dans tout ce que j'entreprends. Merci pour ton optimisme, ta détermination, tes yeux plissés quand tu souris et toute la joie et bonheur que tu m'apportes au quotidien.

« Il suffit d'une minute pour changer votre attitude et avec cette minute vous pouvez changer toute votre journée »

TABLE OF CONTENTS

ABBREVIATIONS

ACC, acetyl-CoA carboxylase
AFM, atomic force microscopy
AMP, antimicrobial peptide
BODIPY, 4,4-difluoro-5.7-dimethyl-4-bora-3a,4a-diaza-s-indacene-3-pentanoic
Cer, ceramide
CL, cardiolipin
Chol, cholesterol
DAG, diacylglycerol
DOPC, 1,2-dioleoyl-sn-glycero-3-phosphocholine
DPH, 1,6-diphenyl-1,3,5-hexatriene
DPPC, 1,2-dipalmitoyl-sn-glycero-3-phosphocholine
DRM, detergent resistance membrane
FA, fatty acid
FASN, fatty acid synthase
GPMV, giant plasma membrane vesicle
GPL, glycerophospholipid
GSL, glycosphingolipid
GUV, giant unilamellar vesicle
Ld, liquid-disordered
Lo, liquid-ordered
LUV, large unilamellar vesicle
MβCD, methyl-β-cyclodextrin
MDR, multidrug resistance
MOMP, mitochondrial outer membrane permeabilization
NBD, 7-nitrobenz-2-oxa-1,3-diazol-4yl
PA, phosphatidic acid
PC, phosphatidylcholine
PCC, Pearson's correlation coefficient
PE, phosphatidylethanolamine
PFT, pore-forming toxin
PG, phosphatidylglycerol
P-gp, P-glycoprotein
PI, phosphatidylinositol
PI3K, phosphoinositide 3-kinase
PIP2, phosphatidylinositol-4,5-bisphosphate
PIP3, phosphatidylinositol-3,4,5-bisphosphate
PL, phospholipid

PM, plasma membrane
PPD, protopanaxadiol
PPT, protopanaxatriol
PS, phosphatidylserine
RBC, red blood cell
SL, sphingolipid
SM, sphingomyelin
SMase, sphingomyelinase
S1P, sphingosine-1-phosphate
So, solid-ordered
Tm, melting temperature
TMA-DPH, 1-[4-(tri- methylamino)phenyl]-6-phenylhexa-l,3,5-triene

FOREWORD

Cholesterol (Chol) and sphingomyelin (SM) are known to cluster into domains which have been proposed to contribute to cellular signaling including cell survival and migration with potential implications in cancer development. Altogether, this makes those lipids an interesting target for pharmacological agents to modulate these pathways. Among these, saponins, amphiphilic compounds widely found in plants, attract more and more attention based on their biological activities including anticancer properties. The activity for some saponins has been attributed to their interactions with membrane Chol. In this study, we focus on the steroid saponin ginsenoside Rh2 found in *Panax ginseng* root. My goal was to obtain detailed knowledge about the activity of Rh2 and to elucidate the respective importance of membrane Chol and SM for this activity. In the first part, I evaluated the membrane-related effects induced by Rh2 in artificial membrane models containing Chol and/or SM (Verstraeten et al, Scientific Reports, 2019). In the second part, I turned my attention to biological membranes to study the importance of Chol and SM in the Rh2-induced apoptosis (Verstraeten et al, Toxicology and Applied Pharmacology, 2018). In the third part, we initiated a long-term study aiming at evaluating the potential interest of Rh2 to modulate tumor cell invasion (ongoing study).

In the introduction of this thesis, I will describe the plasma membrane (PM) organization, composition, biophysical properties and functions and expose some membrane lipid alterations found in cancer cells. As ginsenosides are saponins, molecules well-known to interact with the PM, I will then summarize the function and diversity of saponins and models of membrane-saponin interactions. I will thereafter review current literature data on the interaction of ginsenosides with different membrane models and cell membranes and their pharmacological activities. Then, I will regroup all results obtained regarding the membrane-related effects and the apoptosis induced by Rh2 with a particular attention to the role of membrane lipid Chol and SM. I will also expose our preliminary data on breast cancer cell lines characterization. In particular, we started to compare the cell lines for their migration/invasion, stiffness, lipid content and organization. I will finish by exposing the main limitations of this work, while discussing the role of PM, specific lipids and biophysical properties for the activity of Rh2 and debating the potential use of Rh2 as a chemotherapeutic agent.

CHAPTER I: INTRODUCTION

1. PLASMA MEMBRANE LIPID ORGANIZATION, COMPOSITION, BIOPHYSICAL PROPERTIES AND ROLES

In this chapter, we will be interested in the PM, the main target for the activity of the amphiphilic ginsenoside Rh2 that we investigated throughout this study. Firstly, we will expose a brief historical review regarding the membrane lipid organization (section 1.1). Secondly, we will depict the most abundant lipids present in the PM (section 1.2) and its biophysical membrane properties (section 1.3). Finally, we will focus on the role of these last two factors in two major pathways: cell survival/death and migration assessed during this work (section 1.4).

1.1 Membrane lipid organization: a brief historical review

In 1925, before the emergence of electron microscopy, Gorter and Grendel provided the first evidence that biological membranes consist of lipid bilayers **(Fig. 1A)**[1]. Such a discovery was based on the hypothesis that, if the PM is a lipid bilayer, then the surface area occupied by the lipid monolayer would be approximately twice the one occupied by the PM. To test this hypothesis, they isolated lipids from a known number of human red blood cells (RBCs) and, using a Langmuir film balance (section 1.3.6), they calculated the area covered by these lipids spread on water to form a monolayer. Comparison of both measurements revealed that the surface area of the lipid monolayer was approximately twice the one occupied by the RBC membrane which was in perfect agreement with their lipid bilayer prediction. However, in this model, the PM was seen as a static, passive and homogeneous simple cell barrier with the hydrophobic components in the internal part of the membrane and the hydrophilic components in the external part that maintains the aqueous cytoplasm separately from the extracellular medium. Hence, the role of membrane proteins was not taken into account. A decade later, Davson and Danielli refined the Gorter-Grendel model adding to the PM a layer of protein covering the surface of the membrane and preventing lipids to rotate freely **(Fig. 1B)**[2]. In 1972, Singer and Nicholson introduced the “fluid-mosaic model” **(Fig. 1C)**[3], in which lipids and proteins (partially or totally embedded in the PM) are randomly distributed into the PM.

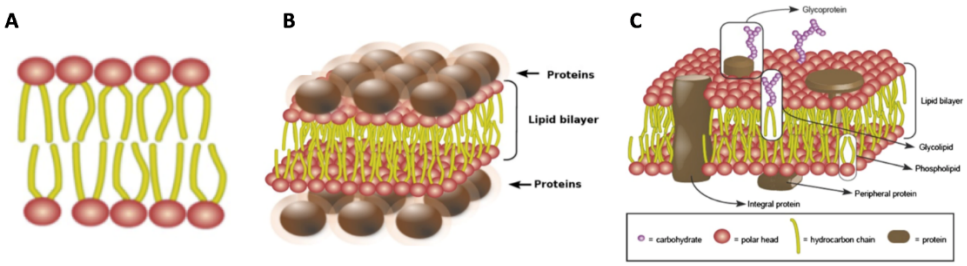

Fig 1. Evolution of the concepts of membrane structure and organization. **A.** In 1925, Gorter and Grended proposed that cells are surrounded by a static, passive and homogeneous lipid bilayer. **B.** In 1935, Danielli and Davson suggested that the lipid bilayer is sandwiched between two thin protein layers. **C**. In 1972, Singer and Nicolson postulated the « fluid-mosaic model » in which lipids and proteins are randomly distributed into the PM. Adapted from [4].

Today, this basic model remains relevant, although abundant evidences indicate that lipids and proteins do not homogeneously distribute into the membrane but present a multilevel of heterogeneity. After the observations that detergent-resistant fractions can be isolated from the cell membrane, Simons and Ikonen proposed the existence of lipid rafts which are unstable (sec) nanometric (20-200 nm), sterol- and sphingolipid-enriched membrane domains which could function as platforms for the attachment of proteins[5]. In 2011, Kusimi et al. proposed a hierarchical three-domain organization of the PM[6]. In addition to the lipid raft domains **(Fig. 2A)**, this model suggested that membrane exhibits compartment with a diameter of 40–300 nm, created via a partitioning of the entire PM, owing to its interactions with the actin-based membrane skeleton (fence) and transmembrane proteins anchored to the membrane-skeleton fence (pickets) (**Fig. 2B**). Dynamic protein complex domains constitute the third mesodomain in the hierarchical architecture and are composed of dimers/oligomers of integral membrane proteins with sizes generally between 3 nm and 10 nm in diameter **(Fig. 2C)**.

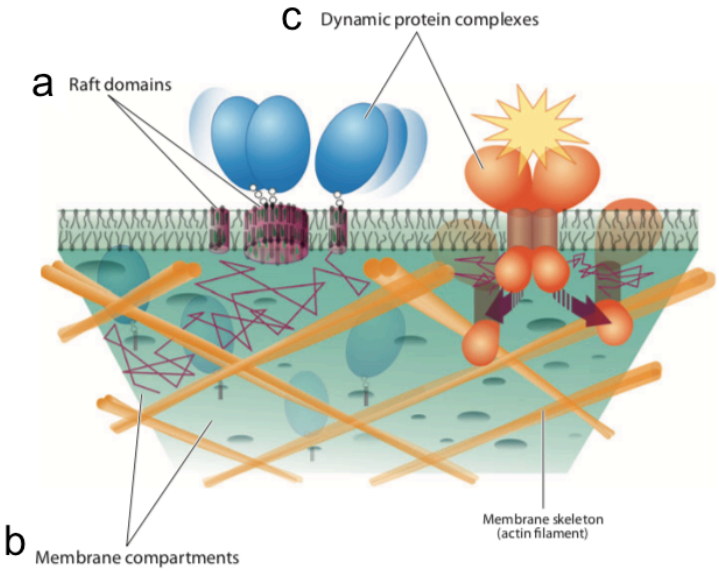

Fig 2. Three-tiered hierarchical mesoscale-domain architecture of the PM. A. Lipid rafts enriched in Chol and SLs. **B.** Membrane compartments generated/maintained through interactions with the actin-based membrane skeleton (fence) and transmembrane proteins anchored to the membrane-skeleton fence (pickets). **C.** Dynamic protein complexes composed of dimers/oligomers of integral membrane proteins[6].

In the past decade, due to the development of new probes and imaging methods, several groups have presented evidences of stable (min) submicrometric domains (> 200 nm) in a variety of living cells from prokaryotes to yeast and mammalian cells[7]. These domains will be further described in section 1.3.2.3.

Currently, the membrane is not just considered as a simple cell wall but also as an important platform for many pathways such as cell survival/death and migration (section 1.4) which are often altered in many diseases like cancers. Because of that, the cell membrane deserves attention for the development of new therapeutic strategies, *i.e.* the membrane lipid therapy. This emerging field is growing and evolving rapidly, providing treatments used for a multitude of diseases[8].

1.2 Most abundant lipid constituents of cell membrane

Cellular membranes are formed from a highly diverse set of lipids present in different proportions[9]. The major membrane lipids are classified into glycerophospholipids (GPLs), sphingolipids (SLs) and sterols. Fatty acids (FAs) are constituents of the first two.

Free FAs are only present in traces in the membrane but mostly found esterified to the lipid backbone structure. They differ from each other with respect to their hydrocarbon chain length and the degree and position of saturation. Generally, they possess 10 to 24 carbons and zero (saturated), one (monounsaturated) or more (polyunsaturated) carbon-carbon double bonds **(Table 1)**.

Name	Carbons	Double Bonds (Positions)
Myristate	14	0
Palmitate	16	0
Palmitoleate	16	1 (Δ9)
Stearate	18	0
Oleate	18	1 (Δ9)
Linoleate	18	2 (Δ9, Δ12)
Linolenate	18	3 (Δ9, Δ12, Δ15)
Arachidonate	20	4 (Δ5, Δ8, Δ11, Δ14)

Table 1. Common FAs of membrane lipids. FAs differ in chain length, degree of saturation and the position of double bonds[10].

Glycerophospholipids (GPLs) are the principal components of the membrane bilayer. Their basic structures are made of a glycerol moiety to which two FAs and a phosphoric acid are attached as esters forming a phosphatidic acid (PA). Generally, FA at the C1 tends to be saturated or monounsaturated and composed of 16 or 18 carbon atoms while FA at the C2 is longer and usually polyunsaturated. At the C3 position, glycerol backbone supports the GPL polar headgroup. The polar head could be an ethanolamine (phosphatidylethanolamine, PE), a choline (phosphatidylcholine, PC), a serine (phosphatidylserine, PS), a glycerol (phosphatidylglycerol, PG), an inositol (phosphatidylinositol, PI) and its phosphorylated derivatives, such as PI-4,5-bisphosphate (PIP2) or PI-3,4,5-trisphosphate (PIP3) **(Fig. 3)** or a phosphatidylglycerol (cardiolipin, CL) (structure not shown). The presence of both hydrophobic FAs and hydrophilic headgroup leads to the amphipathic nature of GPLs. In addition, every polar head presents different electric charges. For instance, PE and PC are zwitterionic PLs whereas PA, PS, PG, PI and CL are anionic PLs. It is well-established that PM is characterized by

an asymmetric distribution of lipids with anionic lipids mainly found in the inner leaflet (section 1.3.3) giving rise to a transmembrane potential.

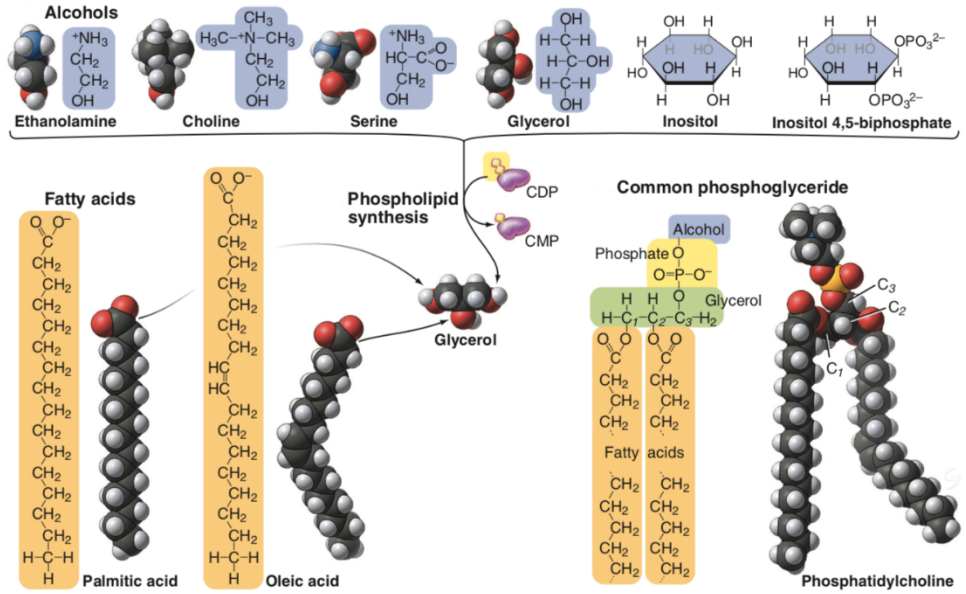

Fig 3. Structure and formation of GPLs. GPLs have a glycerol backbone with FAs (i.e palmitic or oleic acid) at C1 and C2 positions and with the headgroup consisting of a phosphate and an alcohol (ethanolamine, choline, serine, glycerol, inositol, inositol 4,5-bisphosphate) at the C3[10]. Cytidine diphosphate (CDP) provides the phosphate linking glycerol to the alcohol and forms cytidine monophosphate (CMP).

Sphingolipids (SLs) constitute another important class of structural lipids, constructed on a sphingoid base backbone, the sphingosine **(Fig. 4)**. The phosphorylation of sphingosine forms sphingosine-1-phosphate (S1P). A relatively long saturated FA chain (up to 24 carbon atoms) attached to sphingosine through amide linkage forms ceramide (Cer). The polar head attached to the hydroxyl function C1 of Cer can be a phosphocholine or an oligosaccharide forming sphingomyelin (SM) and glycosphingolipids (GSLs), respectively. There is an astonishing diversity of structurally different GSLs molecules. Among those, one can cite the gangliosides GM1, 2, 3 which are GSLs with terminal sialic acids linked to the sugar chain. Besides playing structural roles in cellular membranes, sphingosine, S1P and Cer represent bioactive signaling molecules involved in regulation of cell growth, differentiation, senescence, and apoptosis. We will enlarge this latter function of Cer in section (1.4.1.2).

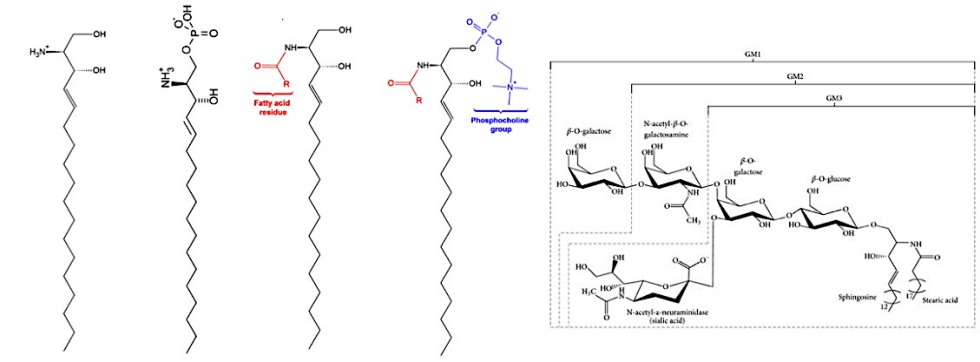

Fig 4. Major SL structures. Sphingosine, sphingosine-1-phosphate (S1P), Cer, SM, GM1,2,3. R represents the alkyl portion of a FA[11, 12].

Sterols are only present in eukaryotic cell membranes with the exception of some bacteria. Vertebrates contain mainly Chol while plants exhibit stigmasterol, campesterol and sitosterol and fungi are composed of ergosterol **(Fig. 5)**[13]. Chol is composed of four fused hydrocarbon rings in trans configuration forming the steroid structure. A polar hydroxyl group and a iso-octyl lateral chain are attached to the polycyclic structure in positions 3 and 17, respectively. The hydroxyl group is responsible for the slightly amphipathic character of Chol and is able to form hydrogen bonds with nearby carbonyl oxygen of GPL and SL headgroups. Unesterified Chol is primarily located in the PM (up to 90%)[14]. The latter could be esterified by lecithin-cholesterol acyltransferase forming cholesteryl ester which is much less polar than the former and appears to be the preferred form for secretion as lipoprotein and for storage as lipid droplets. Chol is also a biosynthetic precursor of steroid hormones, bile acids and lipid-soluble vitamins.

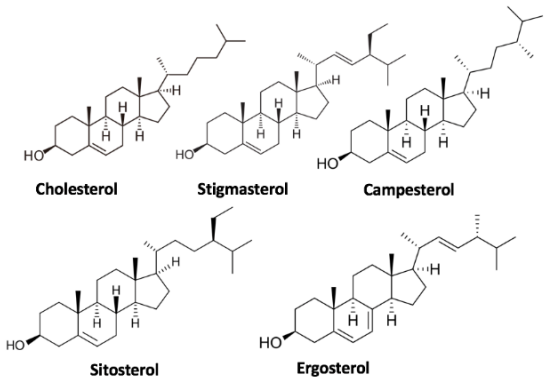

Fig 5. Molecular structures of different sterols. Vertebrates contain mainly cholesterol, plants stigmasterol, campesterol and sitosterol and fungi ergosterol[13].

PM composition largely differs between cells, especially for the Chol content **(Table 2)**. For instance, the PM of rat myoblasts or RBCs contains approximately equimolar quantities of Chol (± 45 mol%, whereas human alveolar macrophages exhibit only 8 mol% of Chol compared to the total lipid fraction. In subsequent sections of this thesis, we will focus specifically on the PM of mammals.

Molar %	Polar lipids						Sterol	Ref.
	PC	PE	PI	PS	PA	SLs	Chol	
Human RBCs	24	6	traces	3	traces	19	48	[15, 16]
Human platelets	18	20	1	12		16	32	[17, 18]
Fibroblast cell line (NIH 3T3)	43	16	8	6.5	1.5	12	13	[19]
Chinese hamster ovary cells (CHO)	25	21		7		12	35	[20]
Schwann cell line (NF1T)	27	9	6	2		18	38	[21]
Undifferentiated L6 myoblasts	24	9	2	6		16	42	[22]
Human alveolar macrophages	30	21		21		7	8	[16, 23]

Table 2. Lipid composition of the PM of different cells. PC, phosphatidylcholine; PE, phosphatidylethanolamine; PI, phosphatidylinositol; PS, phosphatidylserine; PA, phosphatidic acid; SLs, sphingolipids; SM, sphingomyelin; Chol, cholesterol. From [7, 16].

1.3 Biophysical membrane properties

The lipid bilayer is a 3D assembly with a rich variety of physical features that modulate cell signaling and protein function. Here we review five major membrane properties i) lipid motions and phases (section 1.3.1), ii) lateral heterogeneity (section 1.3.2), iii) transversal asymmetry (section 1.3.3), iv) fusion (section 1.3.4) and v) permeability (section 1.3.5). We will then describe artificial membrane models generally used to study membrane interactions and some of these biophysical properties (section 1.3.6).

1.3.1 Membrane lipid motions and phases

1.3.1.1 Lipid motions in the membrane

Lipids are highly dynamic structures and can undergo several types of movement within the membrane such as trans-gauche isomerization (**Fig. 6A)**, bond oscillations, protrusion, rotational and lateral diffusion in the same monolayer, transversal diffusion via flip-flop jumping from one leaflet to the other.

The membrane itself undergoes undulations**.** All these oscillations have different correlation times **(Fig. 6B)**.

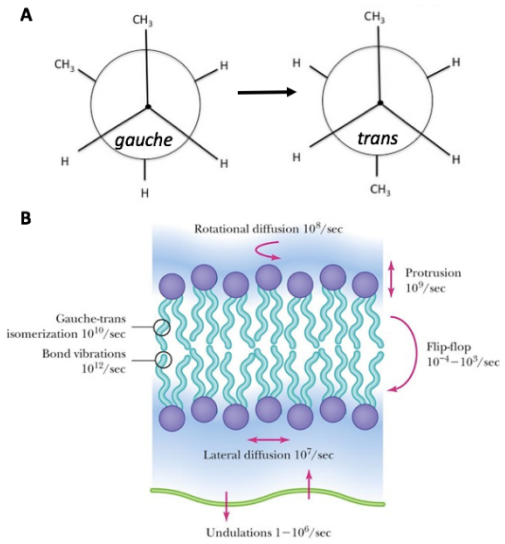

Fig 6. Lipid motions in the membrane. A. Isomerization of acyl chains from gauche to trans configuration. **B.** Approximate correlation times of lipid motions in membranes[24].

1.3.1.2 Lipid phases

According to the dynamic state of the membrane, different lamellar phases can be distinguished (solid-ordered, liquid-disordered, liquid-ordered) **(Fig. 7)**. These phases are characterized by the mobility of the lipid molecules within the bilayer as well as the lateral organization (section 1.3.2).

Membrane exhibits a **solid-ordered (So) or gel phase (Lβ)** when the hydrocarbon lipid chains display an all trans configuration and are elongated at the maximum giving rise to an extremely compact lipid network. In the **liquid-disordered (Ld) or liquid crystalline phase (Lα)**, the tails are not stretched and trans-gauche isomerization occurs, giving rise to a fluid and less packed membrane. The transition between the gel and fluid phases occurs at a specific temperature called melting or transition temperature (Tm). At temperatures below Tm, lipids are in So phase with packed and rigid membrane, while higher temperature will cause a transition to a Ld phase. The Tm depends mainly on the length of the acyl chains and the position and degree of unsaturation. The longer the PL tails, the more interactions between the tails are possible and the less fluid the membrane is. Thus, increasing chain length correlates with increasing Tm. Moreover, saturated lipids promote membrane packing and their straight hydrophobic chains interact

with each other tightly through Van der Waals interactions, which increase the Tm. In contrast, double bonds of unsaturated lipids distort the hydrophobic chain, preventing the tight packing through steric hindrance. This weakens inter-lipid Van der Waals interactions and lowers the Tm. In the presence of Chol, lipid bilayers can adopt a **liquid-ordered phase (Lo)** which is between the Ld and So phases[25]. Chol rigidifies the Ld phase and renders the So more fluid. Chol, due to its rigid structure, inhibits trans-gauche isomerization of acyl chains. It is worth nothing that in RBCs and most eukaryotic cells which present a high Chol concentration, lipid phase transition between the gel and fluid phase is abolished[26].

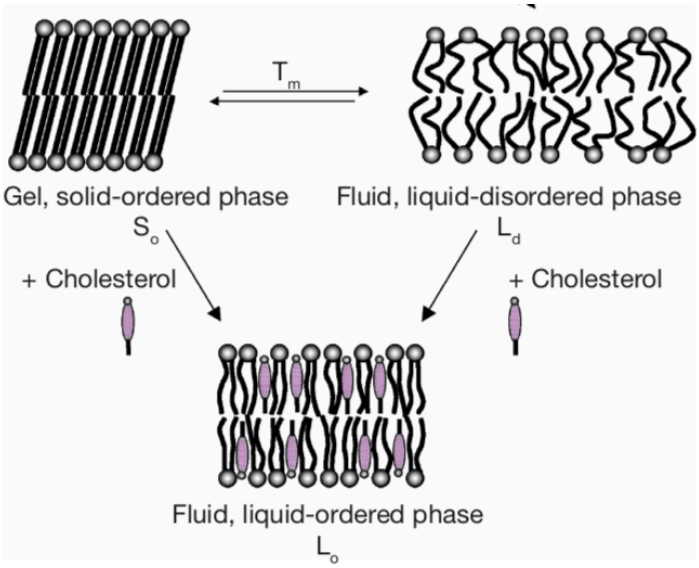

Fig 7. Different physical phases adopted by a lipid bilayer in aqueous medium. Membrane exhibits different phases including solid-ordered (So), liquid-ordered (Lo) and liquid-disordered (Ld) states with increasing packing[27].

The development of lipid phase diagrams allows to define the lipid phase behaviors for the combination of two or three lipids, any point within the triangle representing one defined membrane lipid composition **(Fig. 8)**. Depending on the mixture and the temperature, different lamellar phases can coexist in model membrane[28]. We describe hereunder those encountered in this thesis.

- Lo/Ld phase coexistence: Membranes consisting of relatively saturated lipids with a high Tm such as palmitoyl-SM (pSM), unsaturated PL species with a low Tm such as 1-palmitoyl-2-oleoyl-glycero-3-phosphocholine (POPC) and Chol can separate into two distinct liquid phases: Lo enriched

in saturated lipid species and Chol and Ld comprising mainly the unsaturated lipids. Lo phase is believed to represent a potential physical model of lipid rafts in cell membrane[29]. Contrary to lipid rafts, which are unstable structures, Lo/Ld phase coexistence in model membranes is stable upon time. It is worth nothing that many researchers have chosen this three-component mixture to model the outer leaflet of eukaryotic PM.

- So/Ld phase coexistence: This type of phase coexistence is observed when the membrane is composed of a binary system with two different lipids, one with a low and another with high Tm[30]. High sterol concentration favors the Lo phase and inhibits this phase coexistence. Therefore, this coexistence seems not to take place in eukaryotic membranes.

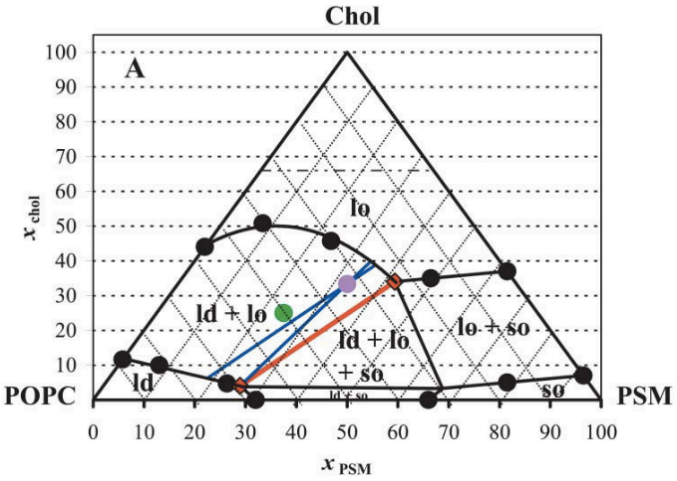

Fig 8. PSM/POPC/Chol phase diagram at 23°C. The red (quasi) tie-line on the tie-triangle describes the Lo/Ld composition at the right of which there is also So phase. The blue tie-lines are the interval for the possible tie-lines that contain the 1:1:1 composition. The purple point marks the 1:1:1 composition and the green point marks the 2:1:1 composition. The dashed horizontal line for Chol x = 0.66 represents the Chol solubility limit on the lipid bilayer[29].

1.3.1.3 Monitoring phase transition and membrane packing using laurdan, DPH and TMA-DPH

Transition between the gel and fluid phases in artificial membrane models can be monitored by a variety of techniques[31]. In this work, we used laurdan(6-dodecanoyl-2-dimethylaminonaphthalene) **(Fig. 9A)** to sense membrane phase transition but also determine the membrane packing. This molecule is located at

the hydrophilic-hydrophobic interface of the bilayer with the lauric acid tail anchored in the PL acyl chain region. It quantifies the lipid packing through its sensitivity to the polarity of its environment in the bilayer. Thus, variations in water content within the membrane cause shifts in the laurdan emission spectrum. Hence, the laurdan emission shifts from a maximum at 440 nm in gel to a maximum at 490 nm in fluid phase **(Fig. 9B)**. The spectral shift in emission is used to calculate the generalized polarization factor (GP), which is a relative quantitative measure for lipid packing [32, 33]. A high GP value reflects a high lipid ordering and therefore a low membrane fluidity. The transition between the gel and fluid phases occurs at Tm which correspond to the inflection point of a curve in a graph displaying the GPex of laurdan upon increasing temperatures.

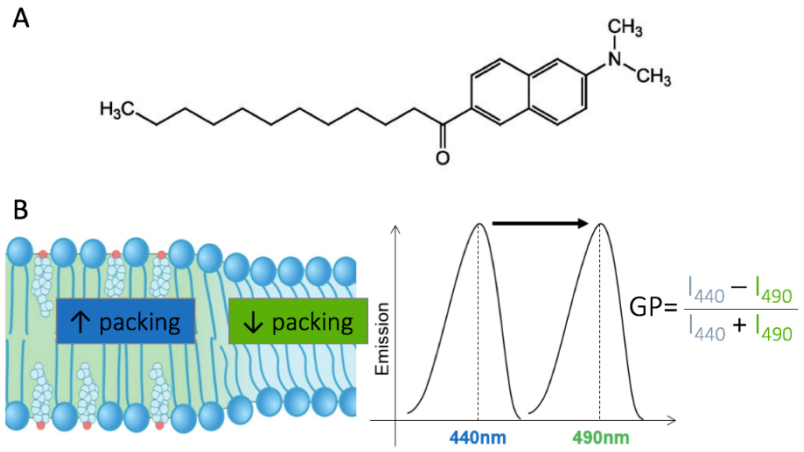

Fig 9. Determination of membrane phase transition and packing by the use of laurdan. A. Laurdan Structure. **B.** Laurdan exposes an emission spectrum shift upon increasing membrane packing, from 440 to 490 nm. Generalized Polarization (GP) ratiometric analysis from the emission intensity at those wavelengths can be used to measure changes in membrane order and phase transition (where I_{440} and I_{490} are the fluorescence intensities at those wavelengths).

Beside the evaluation of GP of laurdan, another common method widely used to probe membrane packing involves measurements of the anisotropy of the fluorescence polarization of probes incorporated into the membrane such as 1,6-diphenyl-1,3,5-hexatriene (DPH) or 1-[4-(tri- methylamino)phenyl]-6-phenylhexa-l,3,5-triene (TMA-DPH). One difference between those two probes is their insertion depth. DPH and TMA-DPH monitor the order in the membrane hydrophobic core and the interfacial packaging of the polar head of PLs, respectively **(Fig. 10)**[34].

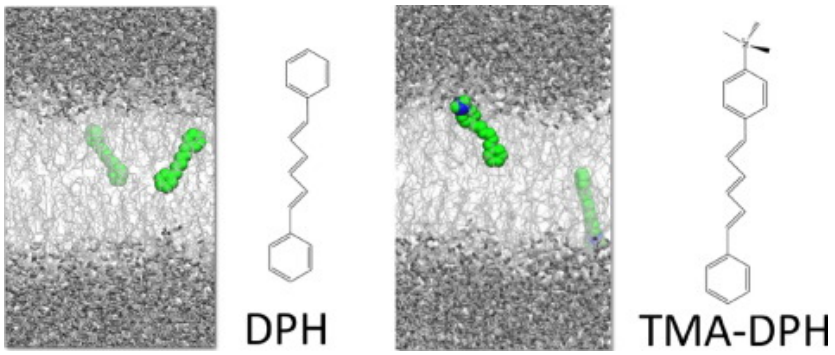

Fig 10. A comparative molecular dynamic simulation study of DPH and TMA-DPH inserted in pure POPC bilayers. DPH is employed as a reporter of the highly disordered hydrophobic core of the POPC bilayer (light area) while TMA-DPH is employed to probe the more ordered shallow regions of the bilayer (glycerol backbone and upper segments of the PL acyl chains) owing to its cationic group which purposely acts as an anchor to the water/bilayer interface[34].

These intrinsically fluorescent probes have excitation and emission dipoles parallel to their molecular axes. For this reason, rotations about the long molecular axis make essentially no contribution to the depolarization of polarized fluorescence, while rotations orthogonal to the long axis of those probes result in rapid fluorescence depolarization **(Fig. 11)**[35]. The resulting polarization of fluorescence is defined in terms of the steady-state fluorescence anisotropy (r). In other words, lipid bilayers which are more ordered and restrict the movement of DPH or TMA-DPH will have higher fluorescence polarization values as compared to more fluid membranes.

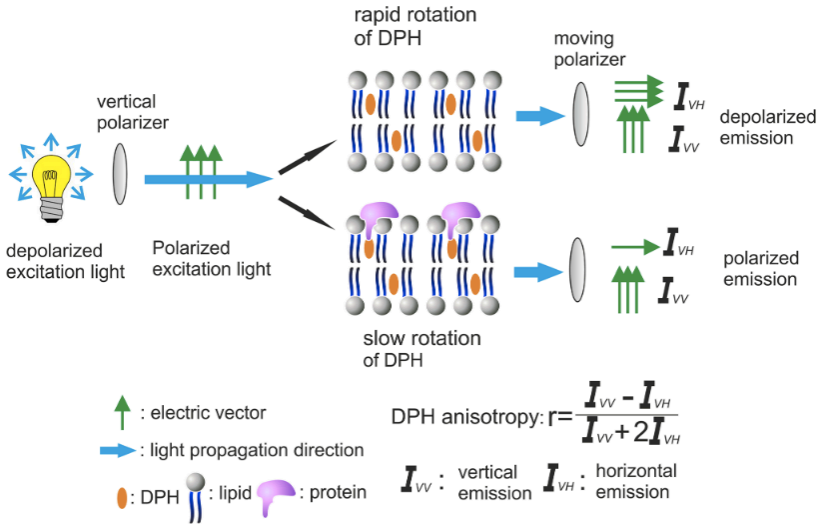

Fig 11. Theoretical explanation of fluorescence polarization measurement of DPH as an indicator of lipid bilayer fluidity. The steady state fluorescence anisotropy is associated to its rotational diffusion, which is sensitive to the order in the membrane. Ivv and Ivh are the intensities measured in directions parallel and perpendicular to the electric vector[36].

1.3.1.4 Physiological relevance of membrane packing

It is widely accepted that membrane packing influences many biological processes. For example, the transition from the Ld to So phase results to a low activity of Ca^{2+}-ATPase in liposome. So seems to promote an unfavorable protein conformational change for its activity[37]. The most apparent function of Lo domain is to segregate proteins and regulate their activities (see section 1.3.2). For example, studies have showed that molecules such as benzyl alcohol could affect the P-gp effux pump function preferentially located in lipid raft domain by reducing the membrane packing[38]. Finally, the fundamental importance of membrane fluidity is underlined by the fact that poikilothermic organisms including bacteria, fungi, reptiles, and fish which do not control their body temperature, must adapt their membrane lipid composition in order to maintain membrane fluidity when they are subjected to thermal change. This adaptive responsive is known as homeoviscous adaptation. For instance, acclimation to lower temperature results in an increase of the proportion of unsaturated FAs in membranes to maintain optimal membrane fluidity[39].

1.3.2 Lateral heterogeneity in the plasma membrane

Accumulating evidences suggest that cellular membranes are laterally heterogeneous, featuring a variety of distinct subcompartments that differ in their biophysical properties and composition. I will here briefly approach three types of lipid domains: transient nanometric lipid rafts (section 1.3.2.1) and caveolae (section 1.3.2.2) domains and stable submicrometric lipid domains (section 1.3.2.3).

1.3.2.1 Lipid rafts

The membrane raft is a subtype of such lateral membrane heterogeneity. Lipid rafts are defined as heterogeneous, highly dynamic (in terms of both lateral mobility and association-dissociation), Chol- and SL-enriched membrane nanodomains (10–200 nm) which form Lo domains that coexist with Ld domains in living cells **(Fig. 12A, B)**[5].

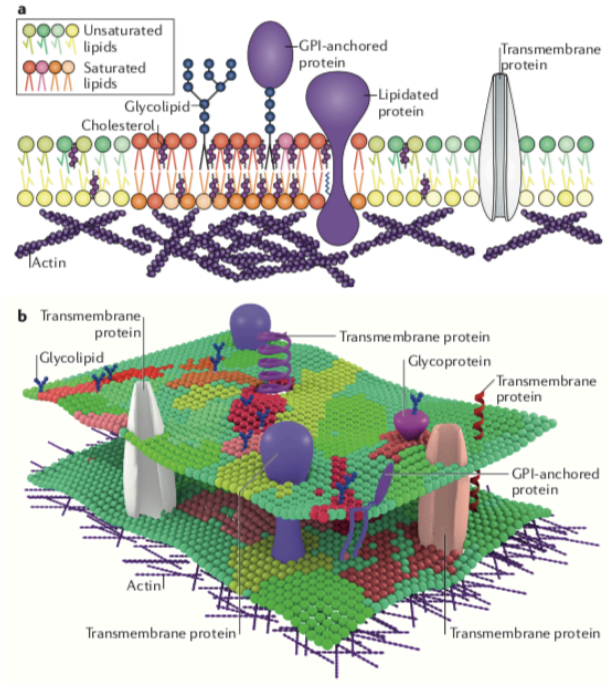

Fig 12. Lateral heterogeneity in the PM. A. Membrane model showing the formation of lipid rafts in the cell membrane. Rafts are composed of mainly saturated GPLs, Chol, GSLs, SM and transmembrane proteins. In addition to membrane components, cortical actin plays an active part in domain maintenance and remodeling. **B.** Membrane organization is probably not binary with highly distinct raft and non-raft regions, but instead membranes consist of various raft-like and non-raft domains with distinct compositions and properties[40].

1.3.2.1.1 METHODS TO STUDY LIPID RAFTS

The first evidence for membrane lateral heterogeneity was provided upon isolation of detergent-resistant membrane (DRM) complexes that float to low density during sucrose gradient centrifugation after treatment with nonionic detergents at 4°C [41]. DRMs have clearly distinct compositions from the rest of the membrane, being enriched in Chol, SLs and GPI-anchored proteins. Despite the ease and usefulness of the extraction, this method is not without pitfalls. Indeed, a raft protein can be strongly linked to the cytoskeleton and will not float after detergent extraction or inversely, its association with rafts can be so weak that it is solubilized by the detergent. Moreover, DRM experiments are plagued by the choice of detergent and temperature which isolate different subsets of rafts[42].

The use of agents or enzymes which manipulate the lipid raft constituents, is also well debated to study the lipid raft function[40]. As rafts are enriched in Chol, the most common raft-disrupting agent is methyl-β-cyclodextrin (MβCD), a water-soluble cyclic heptasaccharide, which selectively and efficiently extracts Chol from membranes. However, MβCD appears to preferentially remove Chol from Ld (non-raft) domains in model membranes[43]. To target SM, one can use agents that interfere with its synthesis (e.g. fumonisin B1) or structure (e.g. bacterial sphingomyelinase, SMase). However, these agents could lead to potential off-target effects such as the accumulation of Cers, which can potentially alter membrane properties in other ways[44]. Hence, Chol or SM depletion could have more global effects than only the rafts disruption[45].

Thus, direct studies were required to prove the real existence of rafts. However, since rafts are too small to be resolved by conventional optical microscopy (with a ±250 nm resolution), this field was for a long time in a stalemate. To overcome this limitation and evaluate whether nanoscale membrane domains could exist, super-resolution optical microscopy methods (±20-40nm) have been developed, including structured illumination microscopy (SIM), stimulated emission depletion (STED), stochastic optical reconstruction microscopy (STORM) and photoactivated localization microscopy (PALM) [40, 41, 46]. Please refer to [47] for an in-depth information about these techniques. Principal drawback of these tools resides in the fact that they do require fixation with formaldehyde or glutaraldehyde solutions, which is a serious limitation for lipid organization studies as it can lead to artefactual lipid redistribution. Moreover, all the above-mentioned methodologies rely on fluorescent labels. The major caveats for some fluorescent probes are their potential perturbation of native membrane organization, for example by inducing clustering of their binding partners, as is the case for cholera toxin inducing unphysiological clustering of GM1[48]. To address those concerns, atomic force microscopy (AFM) is one of the most accurate tools to provide high-

resolution membrane structures (1-10nm) and assess the lateral heterogeneity in the PM by avoiding cell fixation and without the necessity of external labelling. Despite the emergence of these tools, the presence and exact nature of rafts in live cells remains debated, particularly as different methodologies can often yield seemingly contradictory results[49].

1.3.2.1.2 PHYSIOLOGICAL RELEVANCE OF LIPID RAFT

The most important role of Lo nanodomains have been proposed to segregate specific elements in order to regulate their interactions with other membrane components and hence their activity. It is suggested that in the case of tyrosine kinase signaling, adaptors, scaffolds and enzymes are recruited to the cytoplasmic side of the PM as a result of ligand activation. their phosphorylation state can be modified by local kinases and phosphatases, resulting in downstream signaling involved in a range of cellular processes including cell survival[41]. This heterogeneity is potentially important for others various cellular functions such immune response, as well as apoptosis and cell migration that we will further described in section 1.4.

1.3.2.2 Caveolae

In addition to rafts, other nanoscale domains have been described at the PM of eukaryotic cells: caveolae. Caveolae are defined as 60-80 nm invaginations of the PM and are especially abundant in endothelia, smooth muscle and adipocytes (50% of the PM surface) while absent in leukocytes[50]. These bulb-shaped surface pits are mainly enriched with Chol and SLs, making them relatively rigid like lipid rafts. In fact, these bulb-shaped surface pits are often described as "invaginated lipid rafts" but they differ primarily by the presence of caveolin and cavin proteins.

1.3.2.2.1 METHODS TO STUDY CAVEOLAE

Many experimental approaches, including biochemical, pharmacological and microscopic methods used to study of membrane rafts have also been reported to study caveolae. An advantage of studying caveolae is that, unlike rafts, which are flat structures within membranes, caveolae have a distinct morphological structure (bulb-shaped) that is readily identifiable by electron microscopy and more equivocally by other microscopic techniques, for example, anti-caveolin antibodies and immunofluorescence[51]. In addition, caveolin protein overexpression and knockout has been used to examine the role of these domains and proteins in physiology and signal transduction. However, because caveolins act as regulators of several signal transduction pathways, alteration in their expression by such approaches cannot be directly correlated with the compartmentation of a particular signaling pathway in caveolae.

1.3.2.2.2 MAIN PHYSIOLOGICAL FUNCTIONS OF CAVEOLAE

Since caveolae protrude out from the cell surface, they have been linked to environmental sensing. It has been shown that caveolae can flatten in response to membrane stretch in endothelia, skeletal muscle, cardiomyocytes and fibroblasts and serve as a physiological membrane reservoir to accommodate sudden changes in PM tension. In addition, multitude of studies report that caveolae act as signaling platforms to a set of signaling molecules such as insulin receptors or epidermal growth factor receptors and may also play a role in endocytosis[52]. For more detail please refer to [52].

1.3.2.3 Stable submicrometric domains

During the past decade, owing to the development of new probes, the hypothesis that some lipids form large (submicrometric/ mesoscale vs nanometric rafts) and stable (> min vs sec) membrane domains has emerged[7]. Lipid membrane nanodomains could auto-associate within the membrane leaflets to form larger lipid platforms that become detectable by optical microscopy[53]. Several groups have presented evidences for submicrometric domains in artificial and biological membranes from yeast to mammalian cells. Artificial membrane models, such as giant unilamellar vesicles (GUVs) (see section 1.3.6), have highly contributed to better understand the lipid organization in cell membranes. For instance, GUVs composed of a sterol and two other lipid components (one with a high Tm and one with a low Tm) have been used to study the liquid-liquid phase separation. However, those GUVs do not authentically reflect biological membranes. Fortunately, submicrometric lipid domains have also been documented on various cell types. A substantial, non-exhaustive, list of examples is presented in [7]. Briefly, in yeast, major redistribution of PIP2 into membrane clusters upon osmotic stress has been clearly evidenced for both fission and budding yeast cells[54, 55]. In animals cells, Jurkat T cells exhibit SM-rich membrane domains spatially and functionally different from those enriched with the ganglioside GM1[56]. Non-senescent keratinocytes have also demonstrated submicrometric organization of lipid domains enriched in SM[57]. Using living red blood cells (RBCs), Tyteca's group provided evidence for stable submicrometric lipid domains enriched in Chol, SM, PC or ganglioside GM1 at the outer PM leaflet of RBCs[58-62].

1.3.2.3.1 METHODS TO STUDY SUBMICROMETRIC LIPID DOMAINS

Submicrometric lipid domains were first revealed on RBCs by vital fluorescence and/or confocal imaging thanks to the trace insertion at the external membrane leaflet of fluorescent lipid analogues such as BODIPY-SM, PC and GM1[60-62]. Since the substitution of the FA chain by a fluorochrome could have some caveats, exogenous fluorescent protein probes have been developed to

visualize endogenous membrane lipids. Based on toxins capable to bind to lipids, such as Chol-dependent cytolysins of Gram-positive bacteria or SM-dependent lysenin of earthworm *Eisenia foetida* (section 1.3.5.1), Tyteca group have generated non-toxic domain fragments coupled to fluorescent proteins to detect outer PM leaflet lipids. Those include fluorescent toxin fragments specific to endogenous SM (mCherry-lysenin, lysenin*) and Chol (Theta*) **(Fig. 13)**[58, 59]. Besides toxin fragments, other probes are based on protein domains which are able to bind endogenous PLs in the inner leaflet PM as well as cytoplasmic membranes of organelles and/or in the outer PM leaflet after transbilayer flip-flop. For instance, pleckstrin homology (PH) domain of PLCδ (PH-PLCδ) has a high affinity for PIP2 while the discoidin Lact-C2 domain is another probe, specific for PS[63, 64]. Since those domains have a diameter ± 0.5 µm, three representatives of high-resolution microscopy such as conventional confocal imaging, two-photon excitation microscopy and total internal reflection fluorescence (TIRF) have been used to visualize those domains in live cell imaging without requiring cell fixation. Therefore, the major limitations rest upon the use of fluorescent markers. However, AFM imaging have confirmed the presence of these submicrometric domains on unlabeled RBCs[65, 66].

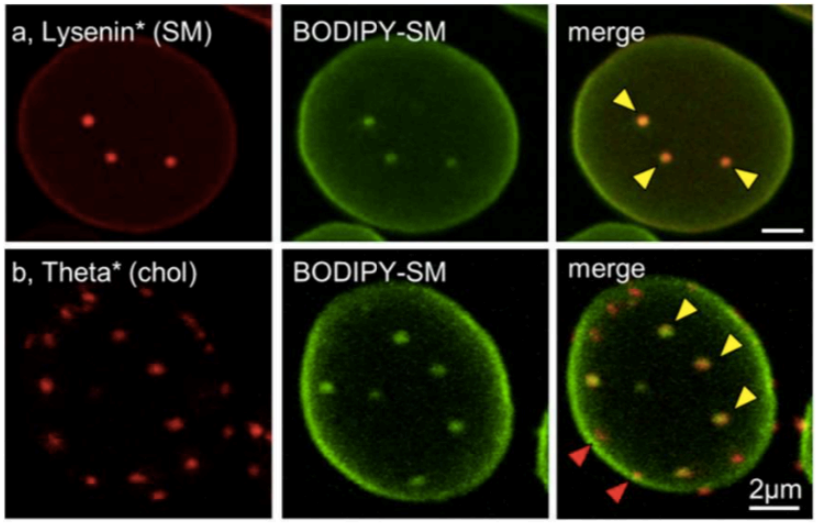

Fig 13. Evidence for submicrometric lipid domains at the RBC surface. Living RBCs spread onto poly-L-lysine pretreated coverslips and labelled with mCherry-lysenin (a; lysenin*, endogenous SM) or mCherry-Theta toxin fragments (b; endogenous Chol) and then by exogenous green BODIPY-SM. Lysenin* and BODIPY-SM perfectly colocalize whereas two types of Chol domains coexist: one containing both Chol and SM (yellow arrowheads) and the other mostly made of Chol (red arrowheads)[58, 59].

1.3.2.3.2 PHYSIOLOGICAL FUNCTIONS OF SUBMICROMETRIC DOMAINS IN RED BLOOD CELLS

Submicrometric lipid domains of RBCs have been showed to play a key role in the RBC deformation. Whereas Chol-enriched domains gather in increased curvature areas upon RBC deformation, low curvature- associated lipid domains increase in abundance either upon calcium influx during RBC deformation (GM1/PC/Chol-enriched domains) or upon secondary calcium efflux during RBC shape restoration (SM/PC/Chol-enriched domains)[67, 68].

1.3.3 Transversal asymmetry in the plasma membrane

1.3.3.1 Asymmetric transbilayer distribution

When studying biological membrane organization and function, one important aspect to consider is lipid asymmetry, meaning unequal distribution of lipids between the outer and inner PM leaflets[69, 70]. In mammalian cells, PS, PE and PI are prominent in the internal layer while PC, SM and GSL are essentially located in the outer leaflet. The distribution of Chol is not fully understood and even under intense debate. Unlike the PLs, Chol has a high rate of flip-flop across the PM ($t_{1/2}$ ±1s)[71]. However, since Chol preferentially interacts with SLs rather than unsaturated PLs and since those SLs are mainly found in the outer leaflet, other assume that the majority of Chol should be in the outer PM leaflet[72]. The transversal asymmetry leads to set an unequal electrical charge distribution with a neutral external leaflet vs a negatively-charged inner one. Therefore, even in the absence of ions, asymmetric distribution of lipids in the bilayer can generate a transmembrane potential. In addition, the fatty acyl chains in the outer leaflet are somewhat more saturated than those in the inner leaflet.

1.3.3.2 Generation and maintenance of lipid asymmetric distribution

Many evidences showed the transfer of lipids between the two leaflets. For example, SM are synthesized in the lumenal leaflet of the Golgi apparatus, suitably positioned to enter the lumenal leaflet of secretory vesicles for eventual deposition in the outer leaflet of the PM. These lipids can be considered to be topologically 'locked' in the outer leaflet of the PM[73]. However, some reports indicate the presence of a small amount of SM at the inner PM leaflet suggesting the existence of transporters. Indeed, the compositional asymmetry cannot be explained by spontaneous passage of polar head groups through the hydrophobic core given the large energy barrier (20-50 kcal/mol) that has to be overcome [74]. For instance, the transbilayer movement of GSLs would take one day as compared to seconds for diacylglycerol (DAG), Cer and Chol. This energetically unfavorable movement is facilitated by three specific types of transporters. At the expense of ATP hydrolysis,

flippases transport lipids from the exoplasmic to the cytosolic face (flip; out-to-in) while floppases do the opposite (flop in-to-out). Scramblases facilitate the bidirectional movement of lipids in an ATP-independent manner[73] **(Fig. 14A)**. The "credit card model" has been proposed to explain how such a transporter might work to flip-flop PLs **(Fig. 14B)**. In this model, the lipid polar headgroup (the magnetic strip on the card) traverses the membrane via the cavity (the groove in the card reader) while the hydrophobic tails remain embedded within the hydrophobic core.

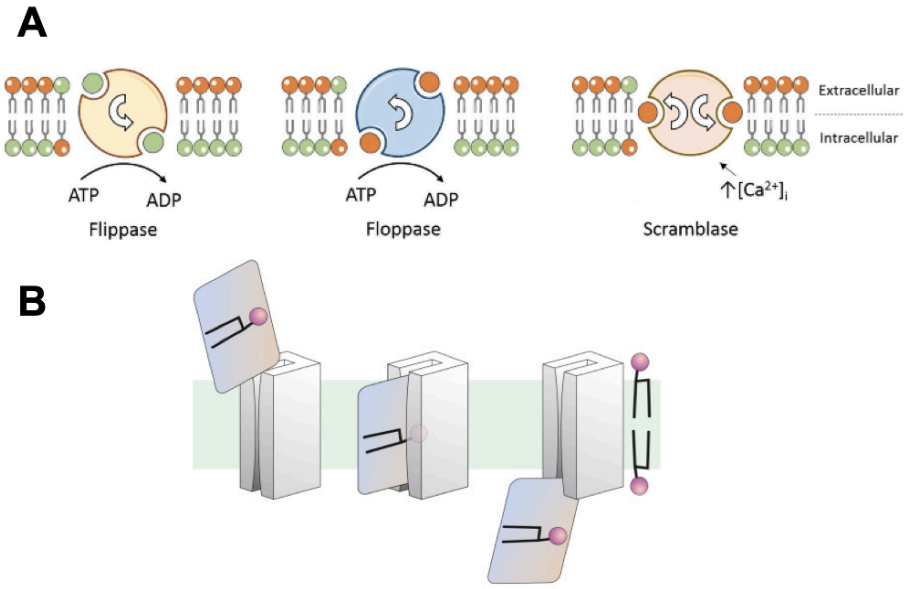

Fig 14. Proteins mediate the transbilayer movement of PLs and regulate membrane asymmetry. A. ATP-dependent flippases catalyze the translocation of lipids from the outer leaflet to the inner leaflet, whereas floppases mediate a reverse reaction. Scramblase, a group of homologous ATP-independent calcium-dependent enzymes, move all kinds of lipids bidirectionally[75]. **B.** The credit card model: translocation of a lipid from one side of the bilayer (light green) to the other is depicted as the swiping of a credit card through a card reader. The polar headgroup of the lipid (the magnetic strip on the card) is protected from the lipid environment by the protein (the groove in the card reader) during passage across the membrane, while the acyl chains of the lipid remain in the hydrophobic core of the membrane[73].

1.3.3.3 Methods to examine transbilayer distribution of lipids

Whereas asymmetric transbilayer lipid distribution in the PM is well recognized, methods to examine this parameter are limited in living cells. PM transbilayer lipid asymmetry was first assessed by biochemical technique using PM of RBCs (devoid of organelles). In intact RBCs, the amino PLs PE and PS cannot be modified by amine-reactive/membrane-impermeable reagents (2,4,6-trinitrobenzen sulfonic acid (TNBS) or N-Hydroxysuccinimide (NHS) esters of biotin (EZ-Link Sulfo-NHS-Biotin) except when the membrane is disrupted, suggesting that these lipids are located in the inner leaflet[76]. Chemical labeling has not been applied to PC and SM. In this case, selective hydrolysis of outer leaflet lipids by a variety of exogenous phospholipases has been widely employed and analyzed by thin-layer chromatography to quantify the fraction of a particular lipid that was located in the outer leaflet PM[73, 77]. A potential problem of this technique is that the reaction products (lysophospholipid, Cer, DAG) are membrane active and thus may reorganize membrane bilayer during treatment. This technique alllows to study lipid asymmetry in RBCs and Gram+ bacteria while application of these methods to multi-membrane systems such as nucleated cells requires additional measures to obtain highly purified membrane preparations[78]

Another method to study lipid asymmetry is sodium dodecyl sulphate (SDS)-digested freeze–fracture replica labelling (FRL) which combines the techniques of freeze–fracture sample preparation and immune-electron microscopy **(Fig.15)**[79]. In this method, cells are frozen extremely quickly, within milliseconds, and then physically cracked. The fracture plane passes through the hydrophobic center of the lipid bilayer separating the monolayers. Both exposed faces are treated with a vapor of platinum and carbon that forms a cast of membranes. After that treatment with SDS detergent removes unfractured membranes, cytoplasmic components, and membrane-associated proteins but keeps membrane lipids and integral proteins. Then the comparison of the membrane density of lipids between the outer and inner leaflet by transmission electron microscopy is possible using lipid-binding proteins, peptides and antibodies followed by colloidal gold-conjugated secondary antibodies[73, 78].

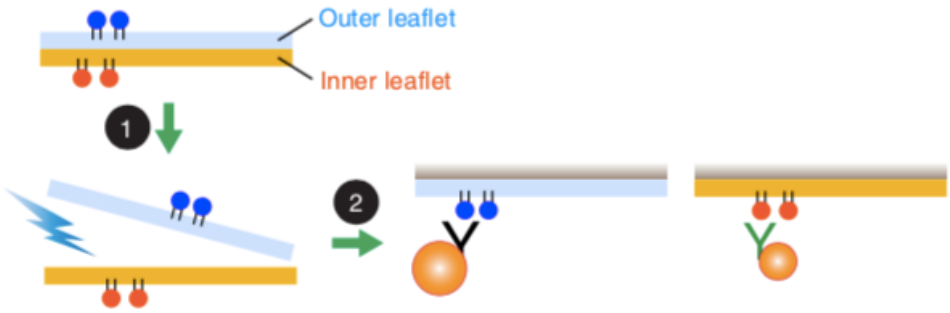

Fig 15. Sodium dodecyl sulphate (SDS)-digested freeze–fracture replica labelling (FRL) to evaluate membrane lipid asymmetry. (1) Cells are rapidly frozen and physically cracked, resulting in the separation of the two membrane leaflets. **(2)** Deposition of platinum/carbon on the exposed hydrophobic faces fixes lipids and proteins, so that lipid headgroups are exposed. After treatment with SDS detergent, lipids are detected by gold-conjugated reagents and their appearance in the outer or inner leaflet is quantified[73, 78].

1.3.3.4 Physiological relevance of membrane asymmetry

Generation and maintenance of membrane asymmetry is essential for the cells, as revealed by the following examples. First, PS is externalized on the surface of activated platelets during coagulation[80] while exposure of PS at the cell surface during apoptosis leads to cell recognition and phagocytosis by macrophages[81]. Second, negatively charged lipid headgroups in the inner leaflet such as PIP2 provide the binding surface for cytoskeletal proteins involved in the cell deformation (section 1.4.2.1). Third, PIP2 can also be hydrolyzed by phospholipase C into inositol 1,4,5-trisphosphate (IP3) and DAG, as soluble and membrane-bound second messengers, respectively. Fourth, lipid asymmetry can strongly influence the behavior of membrane-inserted proteins. Indeed, many transmembrane proteins have a positive charge on their cytosolic domain, which likely helps the protein orient toward the inner leaflet due to its large negative charge density[82, 83]. Finally, the lipid asymmetry is also responsible for membrane curvature which is essential for biological processes such as membrane fusion (section 1.3.4).

1.3.3.5 Interleaflet lipid coupling

Although transbilayer asymmetry has been well reported, the PM may display local regions of biophysical transbilayer symmetry via the colocalization of similar membrane domains in opposing leaflets. Indeed, current consensus is that outer leaflet lipids influence the physical properties of the inner leaflet and those properties of the two leaflets could be ‘coupled’. Asymmetric membranes have revealed that the tendency to phase-separate in one leaflet can induce phase separation in the other leaflet[84, 85]. Conversely, the lack of such a tendency can

prevent phase separation in the apposed leaf **(Fig. 16A)**. This coupling would offer a mechanism of communication between receptors on the extracellular leaflet and cytoplasmic components of signal transduction pathways even if transmembrane proteins also provide these signals. Proposed mechanisms for this inderdependence include acyl chain interdigitation, transmembrane protein, electrostatic interactions, membrane curvature and line tensions[86]. The dynamic interdigitation proposed that long saturated acyl chains of lipids in one leaflet may cross the midline of the bilayer to extend their hydrocarbon chains to the opposite leaflet, pinning the leaflets together **(Fig. 16B)**[87]. For example, it has been shown that transmembrane interactions between outer leaflet long acyl-chain lipids and inner leaflet PS are crucial in generating actin dependent clustering of cytofacial lipid-anchored proteins[88]. In addition, transbilayer interactions are necessary for the generation of Chol-dependent nanoclusters of GPI-anchored proteins[89].

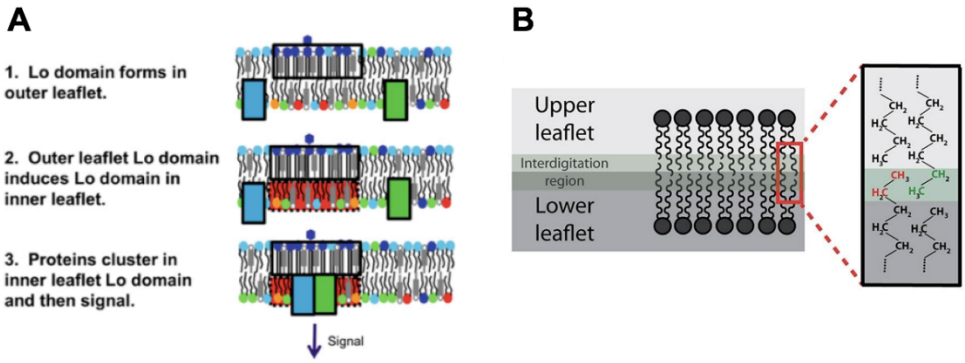

Fig 16. Schematic illustration of interleaflet lipid coupling and the role of acyl chain interdigitation. A. Lo forming outer leaflet lipids are shown inducing Lo domains in the inner leaflet. This in turn may cause protein clustering in inner leaflet Lo domains which regulates signal transduction[90]. **B.** Interdigitating lipid acyl chains in green-gray; zoom: interdigitating ethyl groups of upper (green) and lower (red) leaflets.

1.3.4 Membrane Fusion

Membrane fusion is one of the most important cellular process by which two distinct lipid bilayers merge their hydrophobic cores, resulting in one interconnected structure. Even long-term contacts between protein-free lipid bilayer vesicles do not result in fusion indicating that transient and localized instability of the bilayer structure must occur to induce membrane fusion. It has been found under certain conditions (i.e change of temperature, pH, osmolarity) that vesicles can be induced to fuse in the absence of any proteins which clearly indicates that lipid components are directly involved in the fusion process. The formation of fusion intermediates has been shown to correlate with their effective spontaneous curvature. A key controller of the bilayer's propensity to form curved structures is the average molecular shape of the lipid molecules and therefore the relative size of the headgroup vs the hydrophobic tails[91]. Lysophosphatidylcholine (LPC) or detergent exhibit higher head-to-tail proportion and have inverted cone-shapes, forming structures with a positive curvature, such as micelles **(Fig. 17A)**. PC and SM exhibit a cylindric shape based on head-to-tail proportion and preferentially form flat bilayer structures **(Fig. 17B)**. PE, PS, DAG, PA, Cer or CL are considered as cone-shaped lipids due to their small heads and form structures with a negative curvature such as the inverted hexagonal phase (H_{II}) **(Fig. 17C)**. This phase is characterized by long tubular associations composed of inverted micelles with headgroups inside and hydrophobic tails outside. Transitions between lamellar and hexagonal phases are thought to facilitate membrane fusion[92]. Therefore, the local shape of a membrane depends on its local composition. Interestingly, the compositional difference between the inner and outer leaflets suggests that the outer leaflet does not exhibit a curvature preference whereas the inner leaflet may have a preference for negative curvature which promotes the formation of vesicles toward the cytosol. Notice however that membrane lipids are not the only actors of membrane bending and proteins highly contribute to this process through curvature-sensing proteins (e.g. BAR-domain containing proteins) and cytoskeleton-induced mechanical forces, a.o.. For more detail, please refer to [93].

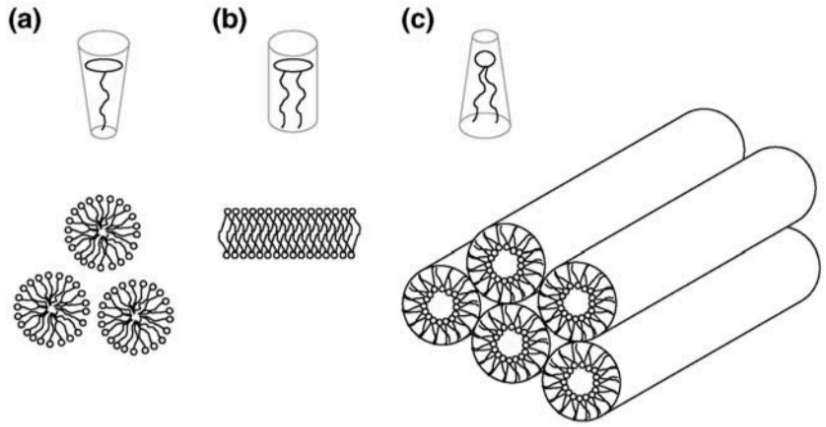

Fig 17. Structures formed by lipids with different shapes. A. Inverted conical lipids form normal micelles. **B.** Cylindrical-shaped lipids form lamellar phases or bilayers. **C.** Conical lipids favor inverted hexagonal phases (H_{II})[91].

1.3.4.1 Molecular mechanisms of fusion of protein-free lipid bilayers

Three distinct steps characterize the molecular mechanism of fusion: membrane aggregation, bilayer destabilization and merging of the membrane and internal contents. In the first step, during which membranes enter in close proximity, strong repulsive hydration forces must be overcome. This can be reached by decreasing the number of charges or water binding sites on membrane, facilitating the aggregation of both vesicles via Van der Waals attraction. A temporary destabilization of the bilayer in the contact region is required for vesicular merging. Destabilization can be introduced by alteration of some physical parameters such as surface tension or membrane curvature. Increase in surface tension or high curvature induction provoke defects in membranes in such a way that membranes get the required energy for fusion. Two possible mechanisms via formation of inverted micelle intermediates (IMI) or by stalk structure have been proposed during the merging of membrane lipids[94]. In the first model, the merging of outer monolayers leads to the transient formation of inverted micelles characterized by the headgroups at the center with the tails extending out **(Fig. 18A)**. The coordinate rupture of both inner monolayers in contact with the micelle leads to pore connecting both initial liposomes, allowing for fusion[92]. In the second model, first an hourglass-like connection is made between the outer monolayers **(Fig. 18B)**. This early hemifusion connection is referred to as the fusion stalk. At this stage, the outer monolayers begin to mix whereas the two inner monolayers are completely separated. This stalk then expands radially forming *trans* monolayer contact (TMC) which is followed by a direct fusion pore formation.

The fusion is finished when two separated lipid membranes merge into a single continuous bilayer and share the same internal contents.

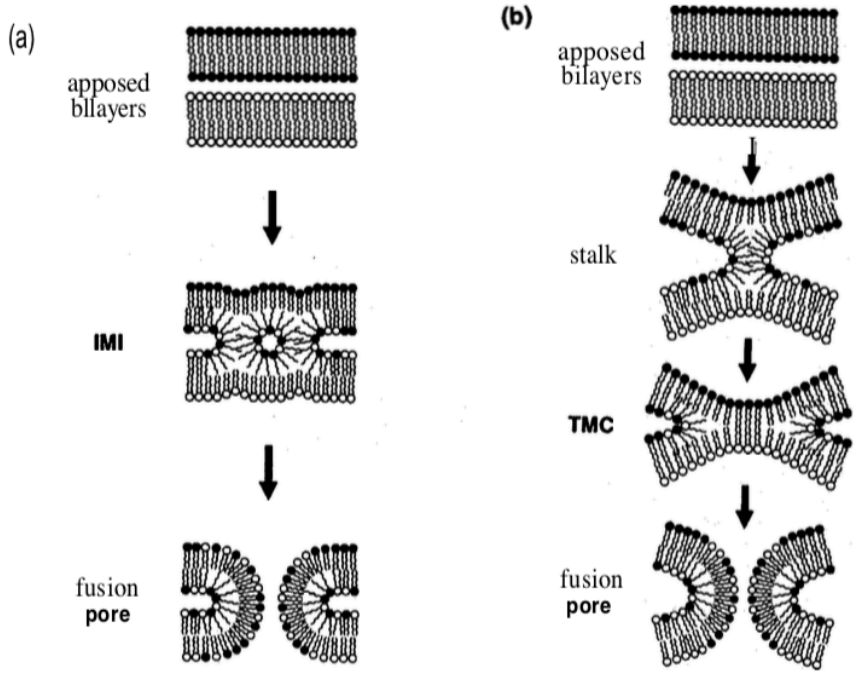

Fig 18. Lipid structures during the fusion process. Two possible fusion mechanisms have been proposed, i.e. through inverted micelle intermediates **(A)** or stalk structure **(B).** IMI: inverted micelle intermediates, TMC: trans monolayer contact[95].

1.3.4.2 Dynamic light scattering and fluorescence assays to monitor membrane fusion

Beside molecular dynamics simulations like coarse-grained modeling[96], majority of studies used lipid mixing assay to monitor membrane fusion with some variations regarding fluorescent markers. For more details regarding those markers please refer to [97, 98]. To study the role of proteins mediating fusion, fluorescence resonance energy transfert experiments (FRET) are often performed to elucidate protein-protein interactions[99]. In this work, membrane fusion was monitored by dynamic light scattering and fluorescence assays using octadecylrhodamine B in bilayer vesicles. The first step prior to the actual fusion is to bring vesicles together. This aggregation can be measured by the increase of light scattering due to polydisperse aggregates. Fluorescence assays are next used to monitor lipids mixing **(Fig. 19)**[100]. One set of vesicles is prepared with a self-quenching

concentration of membrane-bound dye (octadecylrhodamine B, R18) and is mixed with another set of vesicles without any probe. After fusion of the two sets of vesicles, an increase of fluorescence, which results from the relief of R18 self-quenching due to the decrease in its surface density, is measured.

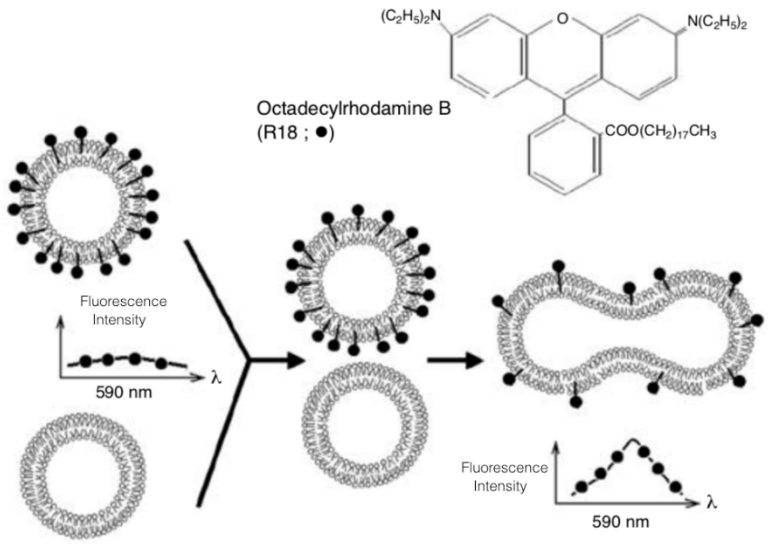

Fig 19. Lipid-mixing assay based on fluorescence self-quenching. Fluorescence of octadecylrhodamine B (R18) is quenched due to dye-dye interactions. Fusion between R18 labelled-membrane and unlabeled membrane results in the dispersion of the probe and an increase of fluorescence intensity at an emission wavelength of 590 nm[97].

1.3.4.3 Physiological relevance of membrane fusion

Membrane fusion is a biophysical reaction that is of fundamental importance in biological systems. Three major events illustrate the role of membrane fusion [101]. First, fusion is observed in intracellular transport vesicles such as between *trans*-Golgi and PM. SNARE complex formation appears to provide a driving force for the fusion of lipid bilayers[102]. Second, fusion of sperm with oocyte or formation of syncytia of muscle cells evidence extracellular fusion of eukaryotic cells. Third, viruses employ membrane fusion to introduce their genomes into host cells. To initiate fusion, hydrophobic portions of a viral protein are inserted into the target cell membrane and bring the viral membrane and the target cell membrane together (within a few Ångström) and to facilitate the fusion event. For example, Influenza viruses use hydrophobic fusion domains of the hemagglutinin.

1.3.5 Membrane permeability

The ability of lipids to provide a selective permeable barrier between the extracellular medium and the cytoplasm is also an important function of biological membranes. The permeability of a molecule can be quantitatively represented by its permeability coefficient (cm/s), which is a measure of how fast it can cross a membrane. Artificial lipid bilayers with different lipid compositions or cell lines monolayers are often used as model barriers. While the former allows passive permeation only, the latter also allows transporter mediated permeation[103]. Molecules that move through the membrane employ different transport mechanisms such as passive diffusion or protein transport[103]. All those mechanisms clearly indicate that PM permeabilization represents an important threat for any cells, since it compromises its viability by disrupting cell homeostasis. Given that ginsenoside Rh2 induces membrane permeability, we will describe how antimicrobial peptides (AMPs), pore-forming toxins (PFTs) and Cer permeabilize the membrane to better understand the underlying mechanisms.

1.3.5.1 Prototypes of permeabilizing proteins and lipids

PM is the front of pathogen attack and often serves as a primary target for secreted toxins. A variety of organisms produce AMPs to protect themselves against bacterial infection by permeabilizing bacterial membranes. AMPs are mostly positive cationic peptides that interact preferentially with negatively charged lipids such as PG or CL present in bacterial membranes. Pore formation induced by AMPs can be described by the toroidal **(Fig. 20A)** or barrel-stave **(Fig. 20B)** models[104]. **In the toroidal pore model**, AMPs insert perpendicularly in the lipid bilayer while the lipid tails are packed away from the surface of the pore, resulting in significant lipid disorder, and membrane curvature change. As a result, toroidal pores are accompanied by enhanced membrane hydration, as evidenced by significant water penetration into the membrane. In the **barrel stave model,** AMPs insert perpendicularly in the lipid bilayer and promote lateral peptide-peptide interactions, in a manner similar to that of membrane protein ion channels. Contrary to the toroidal pores, the hydrophobic and hydrophilic arrangement of the bilayer is not disrupted in barrel stave model. AMPs can also act without forming specific pores in the membrane. Some AMPs adsorb parallel to the lipid bilayer and reach a threshold concentration to cover the surface of the membrane, thereby forming a "**carpet**" **(Fig. 20C)**. As their surface concentrations reach a critical value, the membrane integrity is lost, producing a detergent-like effect, which eventually disintegrates the membrane by forming micelles. The final collapse of the membrane bilayer structure into micelles is also known as the detergent-like model.

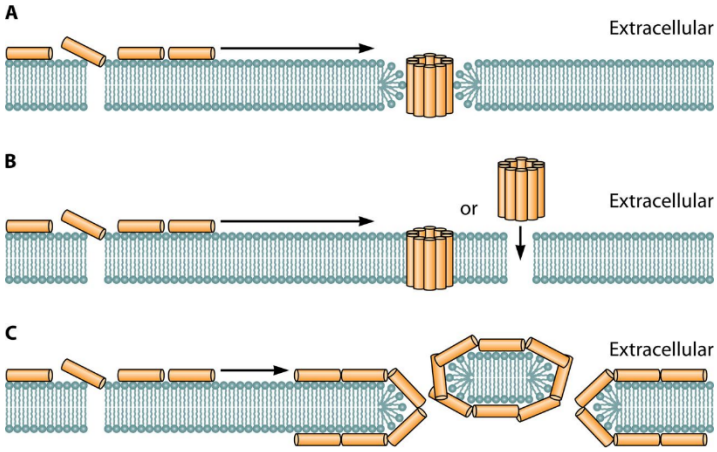

Fig 20. The proposed models of membrane-lytic mechanisms by AMPs. **A.** Toroidal pore model. **B.** Barrel-stave mode**l. C.** Carpet model[104].

Pathogenic bacteria but also earthworm produce key virulence determinants, pore-forming toxins (PFTs). Some PFTs require a specific lipid for their activity in the membrane[105]. For example, perfringolysin O from *Clostridium perfringens* triggers pore formation by binding to membrane Chol whereas lysenin from the earthworm *Eisenia foetida* binds to clustered SM (fewer than 10 lipid molecules) **(Fig. 21)**[106].

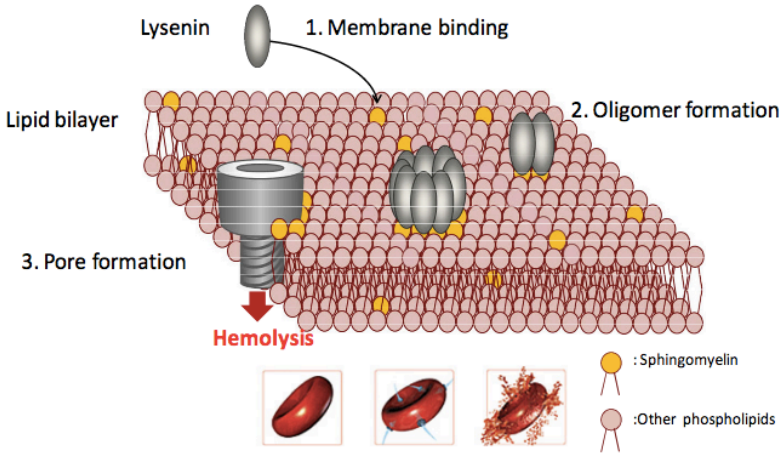

Fig 21. The interaction of lysenin with SM at the RBC membrane occurs in three stages. (1) Monomeric form of lysenin binds to membrane SM where (2) its oligomerization is induced and (3) leads to the formation of transmembrane pores, provoking hemolysis[106].

Studies have also revealed that Cer could form pores in model bilayers as well as in the outer membrane of isolated mitochondria through the formation of large cylinder membrane channels[107]. Colombini team reported a model of a Cer pore consisting of four to six Cers H-bonded via amide groups[108]. Formation of Cer channels does not rely on any particular protein.

1.3.5.2 Calcein release to monitor pore formation

Membrane pore formation induced by drugs could be predicted by digital simulation[109]or experimentally evaluated by AFM[110] or osmotic swelling assay[111]. Vesicles loaded with fluorescent molecules which have a different quantum yield depending on whether they are inside or outside the vesicles are also often used to detect pore opening[112]. In this work, we assessed membrane permeability using calcein release from artificial membrane vesicle[113]. Calcein, a membrane-impermeable fluorescent probe is entrapped at a self-quenching concentration into large unilamellar vesicles (LUVs) (see section 1.3.6). Molecule-induced calcein leakage results in dequenching and a concomitant increase in the calcein fluorescence. The percentage of fluorescence recovery is determined by comparing the molecule-induced calcein release with the value obtained after adding Triton X-100 to obtain a complete release of calcein. In addition, GUVs (section 1.3.6) allow the determination of the pore-forming activity by confocal microscopy. Indeed, GUVs are resuspended in a solution containing a fluorophore, and the filling of the vesicle is followed after pore formation.

1.3.6 Artificial membrane models to study drug interaction and biophysical properties

Biological membranes are hugely complex systems due to their diversity in lipid composition (section 1.2), organization in lipid domains (section 1.3.2), asymmetry (section 1.3.3) and association with proteins and cytoskeleton, making the biophysical interaction with molecules very difficult to investigate. Over the last century, model membranes have been proved to play a considerable role in the elucidation of the structure and the properties of biological membranes as well as in the understanding of biological processes that occur at the membrane surface or that are associated with cell membranes[16]. The ability to control their membrane composition is advantageous because it enables to investigate the lipid requirements, or preferences of a compound and its influence on biophysical membrane properties. The most well-known and common artificial membrane systems used are lipid monolayers and liposomes [16]. **Lipid monolayers** provide a simple model considered as half the bilayer of biological membranes. This model can be used to analyze the first steps of the interaction of a bioactive molecule with a membrane. Parameters such as the nature and the packing of the spread

molecules, the composition of the subphase (pH, ionic strength) and temperature can be varied in a controlled way and without limitation. Langmuir monolayers are formed by spreading lipids at the air-water interface of a Langmuir trough where the polar regions are in the aqueous phase and the acyl chains extend above the buffer. After stabilization of the lipid monolayer at a defined surface pressure (*Π*) compounds of interest are injected into the water subphase and the increase of the *Π* resulting from the interaction of molecules with the lipid monolayer is recorded **(Fig. 22)**. It is worth noting that this technique allows the formation of Chol monolayer whereas the formation of liposomes containing only Chol is not achieved.

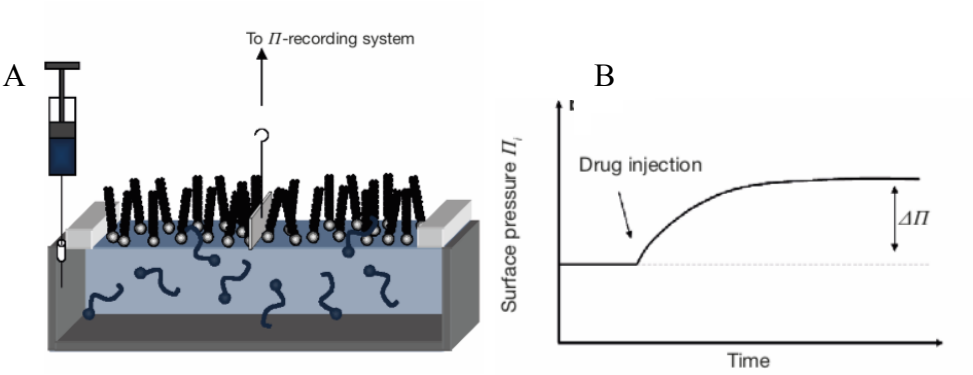

Fig 22. Schematic representation of the Langmuir trough. A. This technique is used for evaluating the penetration power of molecules into lipid monolayer. **B.** Penetration kinetic following the injection of the drug into the subphase[27].

Liposomes are small artificial vesicles of spherical shape composed of a single lipid bilayer, which are arranged in a way that is similar to that of biological membranes. According to the method of preparation and the size, different types of bilayer structures can be obtained[114]. In this study, we worked with large unilamellar vesicles (LUVs, ± 150 nm) or giant unilamellar vesicles (GUVs, ± 15 µm). LUVs are often used for studying binding processes (isothermal titration calorimetry, see below), fluidity (section 1.3.1.3), fusion (section 1.3.4.2), permeability (section 1.3.5.3) while GUVs that closely resemble biological membranes in curvature and size (10-20 µm), allow to visualize the lipid phase organization, shape deformation and permeability by fluorescence microscopy. In this work, we performed isothermal titration calorimetry to assess parameters like free energy of binding (ΔG), entropy (ΔS), enthalpy (ΔH), and binding affinities (K) values regarding the Rh2-membrane interaction. Briefly, this technique measures the heat released or adsorbed when two interacting components are brought together in the same environment and initiate a reaction. The changes in heat energy are assessed over time and measure the enthalpy changes due to the

interaction between titrated and titrating solutions[16].

1.4 Contribution of membrane lipid composition and biophysical properties to cell death/survival and migration

All biophysical membrane properties described above contribute to modulate a range of cell signaling pathways such as cell division, cell death and survival, exo- and endocytosis, cell squeezing, migration and invasion. We will here focus on cell death/survival (section 1.4.1) and migration/invasion (section 1.4.2) as they have been studied during this thesis through the activity of the ginsenoside Rh2.

1.4.1 Cell death and survival

Changes in biophysical membrane properties and lipid content such as Cer appear to be involved in the regulation of cell death. After an overview of apoptotic pathways (section 1.4.1.1), we will focus on the role of Cer (1.4.1.2), PIP2/PIP3 (1.4.1.3) and lipid rafts (1.4.1.4), well-known to be involved in the apoptosis.

1.4.1.1 Apoptotic pathways

Apoptosis, i.e. the programmed cell death in mammalian cells, is a key regulator of physiological growth control and of tissue homeostasis by eliminating "unnecessary cells". The typical morphological hallmarks of apoptosis include cell shrinkage, nuclear DNA fragmentation and membrane blebbing while the underlying cell signaling pathway varies depending on the cytotoxic stimulus. Apoptosis is mainly regulated by extrinsic and intrinsic signaling pathways through the formation of death receptor-mediated death-inducing signaling complex (DISC) and mitochondrial-derived apoptosome, respectively **(Fig. 23)**[115, 116]. The extrinsic route is mediated by the binding of ligands (FasL, TRAIL) to death receptors (Fas, TRAILR) located at the PM, which leads to receptor aggregation and the sequential recruitment of adaptor proteins such as Fas-associated death domain (FADD) and procaspases-8 and -10 forming the death-inducing signaling complex (DISC). It results in dimerization and activation of caspase-8 which can directly cleave and activate caspase-3 and -7 triggering extrinsic apoptotic signaling. The intrinsic mitochondrial-involved apoptotic pathway is engaged by a wide array of stimuli that are sensed intracellularly, including DNA damages or ER stresses. Stresses induce mitochondrial outer membrane permeabilization (MOMP) and release of second mitochondria-derived activator of caspases (SMAC) and cytochrome c from the mitochondria. SMAC prevents X-linked inhibitor-of-apoptosis protein (XIAP) to interact with caspase-3, -7, -9 and inhibit their activity. Cytochrome c released from the mitochondria binds to apoptotic protease-activating factor-1 (APAF-1) and procaspase-9 to form the so-called "apoptosome"

that activates caspase-3 and -7 and triggers the apoptotic cell death program. The extrinsic and intrinsic apoptotic pathways cross-talk through the BH3-interacting domain death agonist (Bid), a pro-apoptotic Bcl-2 family member protein. Bid is cleaved by caspase-8 to form truncated Bid, which translocates to mitochondria and interacts with Bcl-2–associated X protein (Bax) and Bcl-2 homologous antagonist killer (Bak). These two proteins insert into the outer mitochondrial membrane and induce MOMP and the release of the cytochrome c and SMAC. Anti-apoptotic Bcl-2 or Bcl-xl proteins can bind to Bid and inhibit its ability to induce oligomerization of Bax and Bak.

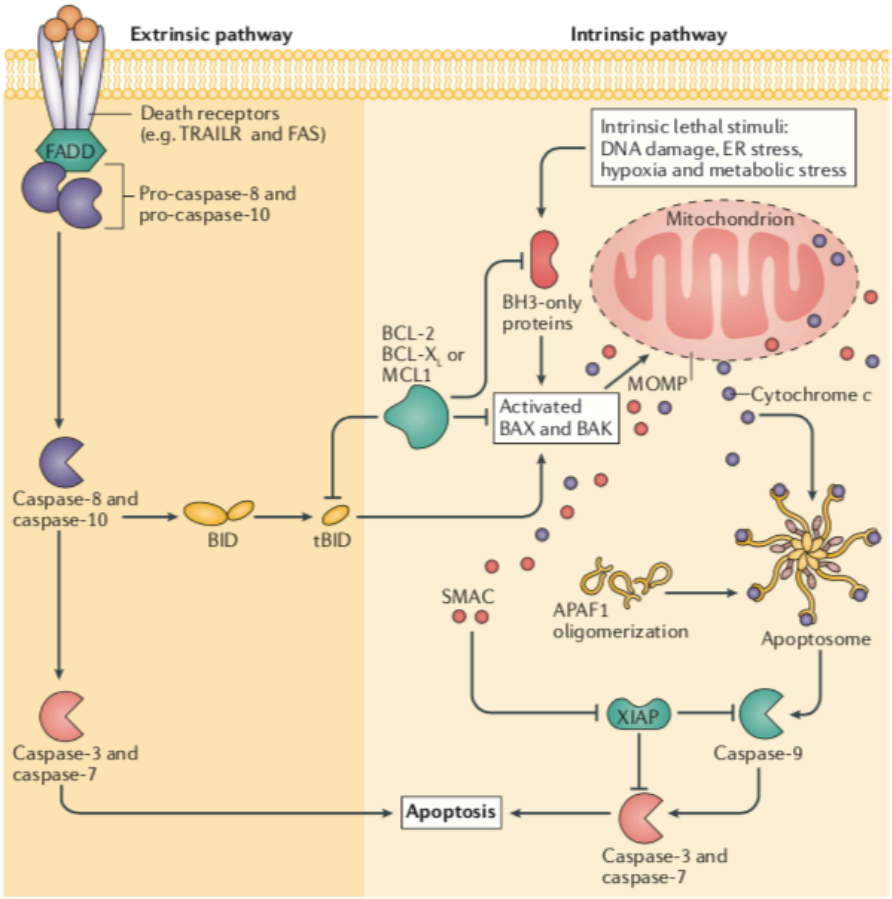

Fig 23. Extrinsic and intrinsic apoptotic signaling pathways. The extrinsic apoptotic pathway is initiated by the ligation of death receptor with its ligand, leading to the recruitment of FAS-associated death domain protein (FADD) and then caspase-8. It results in the dimerization and activation of caspase-8 which can directly cleave and activate caspase-3 and caspase-7, leading to apoptosis. Intrinsic apoptotic stimuli lead to mitochondrial outer membrane permeabilization (MOMP) and release of second mitochondria-derived activator of caspases (SMAC) and cytochrome c. Cytochrome c binds to apoptotic protease-activating factor 1 (APAF1) and caspase-9 forming the apoptosome. The latter triggers the autoproteolytic activation of caspase-9 which in turn activates executioner caspases, caspase-3 and caspase-7, leading to apoptosis. X-linked inhibitor-of-apoptosis protein (XIAP) is a direct inhibitor of caspase-3, -7, -9 activities. The anti-apoptotic Bcl-2 and Bcl-xl proteins can bind to Bid and inhibit Bid's ability to induce oligomerization of Bcl-2–associated X protein (Bax) and Bcl-2 homologous antagonist killer (Bak) leading to MOMP formation[115].

1.4.1.2 Ceramide: a key regulator of apoptotic pathways

Cer draws wide attention as a key regulator of programmed cell death[117, 118]. Multiple stress stimuli, including pro-apoptotic ligands such as FasL (section 1.4.1.1) as well as ionizing radiation[119] and chemotherapeutic drugs, have been shown to induce rapid generation of Cer levels through stimulation of *de novo* Cer synthesis and/or activation of SM hydrolysis via SMase[120]. The formation of Cer on the outer leaflet of the PM is thought to result in the formation of Cer-enriched membrane platforms, which induce death receptors clustering and amplification of the extrinsic apoptosis[121]. In addition, Cer cellular accumulation has been shown to inhibit PI3K/Akt pathway (see section 1.4.1.3) by activating protein phosphatases such as Cer-activated protein phosphatase (CAPP), resulting in the activation of the pro-apoptotic Bcl-2-family protein like Bcl-2 associated death promoter (Bad)[122]. Cer can also form pores in isolated mitochondria through the formation of large cylinder membrane channels leading to increase permeability of mitochondrial outer membranes and release of cytochrome c involved in the intrinsic apoptosis[107]. Anti-apoptotic proteins (specifically Bcl-xl and Bcl-2) are able to inhibit Cer channel formation whereas pro-apoptotic proteins (specifically Bax and Bak) promote its formation. Altogether, it has been suggested that Cer could act as a tumor suppressor lipid by promoting cancer apoptosis (section 2.2.1)[123].

1.4.1.3 PI3K/Akt pathway

There is a close relationship between cell death and survival. Lack of survival signals triggers apoptosis, a phenomenon called “death by neglect”. Survival signals such as growth factors, cytokines and some hormones activate the PI3K/Akt pathway[124]. One of the main function of PI3K is to phosphorylate PIP2 to PIP3. This leads to the recruitment of the kinases PDK1 and Akt through direct contact of their pleckstrin-homology (PH) domain with PIP3. PDK1 and mTORC2 active Akt through the phosphorylation at Thr308 (activation loop) and Ser473 (hydrophobic motif), respectively **(Fig. 24A)**. After that, Akt adopts an active conformation and interferes with the apoptotic machinery by phosphorylating and inhibiting capsase-9 and Bad **(Fig. 24B)**[125]. PI3K/Akt survival signaling is counteracted by phosphatase and tensin homolog deleted on chromosome 10 (PTEN) which dephosphorylates PIP3 to PIP2. Cancer cells have developed several mechanisms to inhibit apoptosis and prolong their survival. PI3K is overexpressed in several malignancies leading to a constitutively active survival signaling pathway which promotes the insensitivity of tumor cells to apoptosis induction. In addition, *PTEN* is one of the genes that is most frequently mutated or deleted in cancer[124].

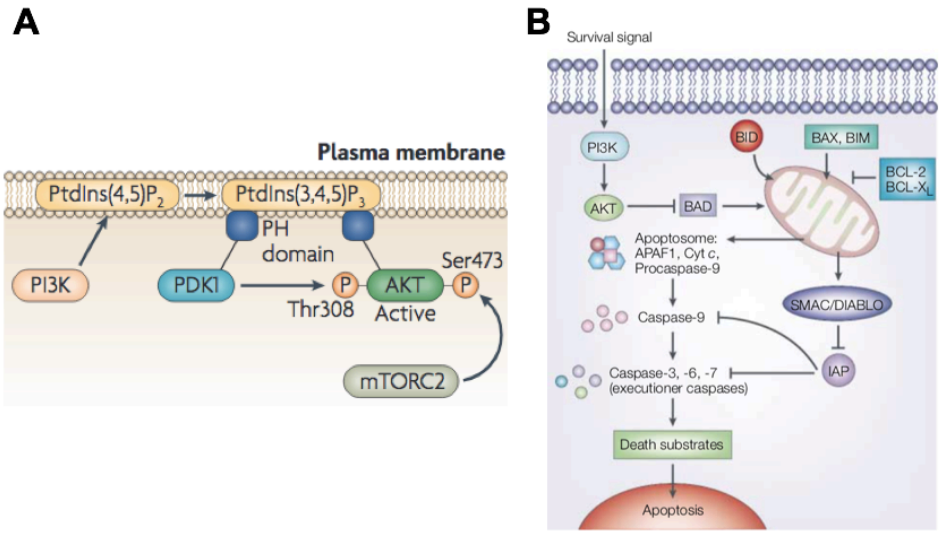

Fig 24. Activation of PI3K/Akt pathway promotes cell survival and inhibits apoptotic pathway. A. Phosphoinositide 3-kinase(PI3K) phosphorylates PIP2 to PIP3. Akt through direct contact of its PH domain with PIP3 is recruited within the PM and activated through the phosphorylation of its Thr308 and Ser473 by PDK1 and mTORC2, respectively. **B.** Akt phosphorylates and inhibits caspase-9 and the pro-apoptotic Bad resulting in the suppression of apoptotic pathway[124, 126].

1.4.1.4 Lipid raft: a floating island of death and survival

While many regulatory mechanisms of apoptosis are well elucidated, the role of lipid rafts in those pathways has only recently begun to be explored. It has been suggested that those domains could provide signaling platforms able of activating both pro-apoptotic and anti-apoptotic pathways. On one hand, given that the PM is the active site of PI3K/Akt pathway, the lipid raft compartmentalization seems to play a crucial role in triggering the PI3K/Akt signaling pathway, by facilitating Akt recruitment and activation upon PIP3 accumulation in the PM **(Fig. 25A)**[127, 128]. PDK1 seem also recruited in membrane rafts in response to growth factors, whereas the negative regulator of this pathway, PTEN is primarily located in nonraft regions[129]. Some studies have also demonstrated that disruption of lipid raft domains using MβCD results in impaired Akt phosphorylation and increases apoptosis in different tumor cell lines[130]. On the other hand, death receptors can aggregate and initiate the apoptosis independently of death receptor ligands. This phenomenon has been proposed to be due to the formation of clusters of apoptotic signaling molecule-enriched rafts (CASMERs) which refers to the co-aggregation of death receptors and their downstream apoptotic molecules **(Fig. 25B)**. CASMER represents a raft-

based supramolecular entity acting as a linchpin for launching apoptotic signals[131].

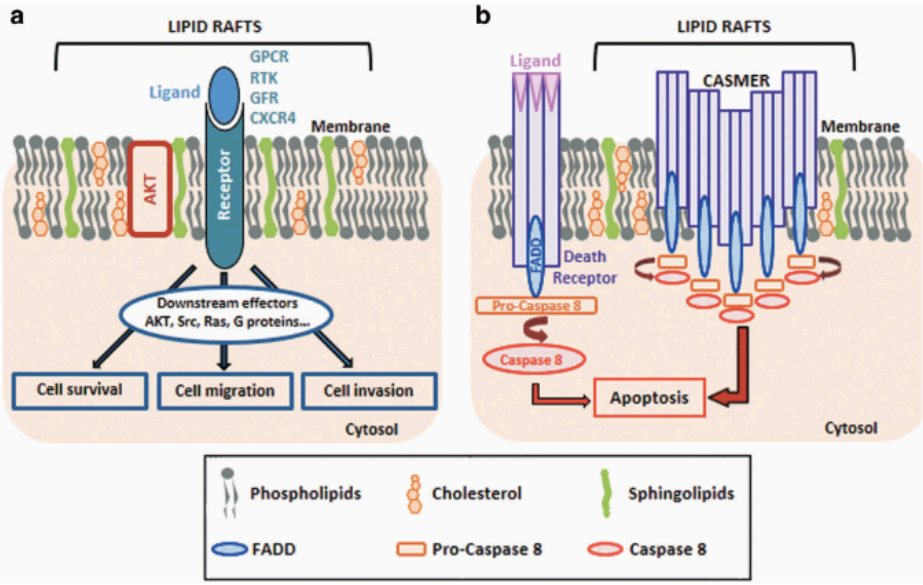

Fig 25. Lipid rafts as platforms for cell survival and apoptosis. A. Lipid rafts facilitate the recruitment of PI3K/Akt and cell survival **B.** Aggregation of death receptors in lipid rafts forms clusters of apoptotic signaling molecule-enriched rafts (CASMER) launching apoptotic signals[132].

1.4.2 Cell migration

Cell migration is critical for wound healing, immune responses, development, invasion, a.o. Cell migration needs the coordinated activation of several processes: cell polarization and elongation, formation of cell protrusions and attachment to extracellular matrix (ECM) at the front, and contraction of the cell body at the rear to deploy a force to pull the cell body forward[133]. These processes involve a continuous reorganization of the underlying cytoskeleton structure, which must be accompanied by appropriate restructuration of the PM. The effect of lipid composition on actin cytoskeleton dynamics is clearly demonstrated by *in vitro* experiments reporting that the formation of filopodia (finger–like protrusive structure based on actin filament) does not form on PC bilayer alone but requires negatively-charged lipids to promote actin polymerization[134]. We will here below focus on the contribution of lipid composition and organization to the cell migration process, while leaving aside the role of protein, extremely complex and beyond the scope of this thesis.

1.4.2.1 The importance of phosphoinositides

The best understood negatively-charged lipids that engage the regulation of the organization and dynamics of the actin cytoskeleton are the phosphoinositides (PIs). These lipids are dynamically regulated by phosphorylation and dephosphorylation. It has been reported that PIs directly interact and regulate the activities of actin-binding proteins[135]. Among different PIs, PIP2 is the best-characterized regulator of the actin cytoskeleton. Typically, PIP2 activates proteins that induce actin filament assembly and inhibits actin-binding proteins promoting actin filament disassembly. For example, PIP2 with the aid of Rho family GTPase (Cdc42) and a protein from the BAR-domain family containing an Src homology 3 domain (SH3) allow the recruitment ant the activation of Wiskott-Aldrich syndrome protein (WASP) at the membrane **(Fig. 26A).** In turn, activated Wasp containing VCA domain (verprolin, cofilin, acidic) activates actin-related protein complex 2/3 (Arp2.3) which induces actin filament nucleation and network growth. Regarding another actin binding protein, cofilin binds to and is inhibited by PIP2 in the PM **(Fig. 26B)**. However, upon EGF-stimulated PIP2 reduction, cofilin gets released and depolymerizes actin[136]. In mammary tumors, the activity status of cofilin is directly related to the invasion and metastasis[137].

High PIP3 concentration induced by the local PI3K activity at the leading edge and the regulated hydrolysis of PIP3 to PIP2 by PTEN at the retracting tail contribute to the cell migration towards the chemoattractant gradient **(Fig. 23C)**[135]. Cell migration also requires Rac GTPases to promote formation of actin polymers at cell's leading edge. An activator of Rac (a small GTPase of the Rho family), DOCK180, accomplishes the Rac relocalization by using its DHR-1 domain to bind PIP3[138]. Given the pronounced role of PIP2 and PIP3 in maintaining epithelial polarity, these lipids may be involved in epithelial to mesenchymal transition (EMT) of cancer cells. Indeed, during this transition, epithelial cells lose polarity and cell-cell adhesions, become motile, and invade surrounding tissues.

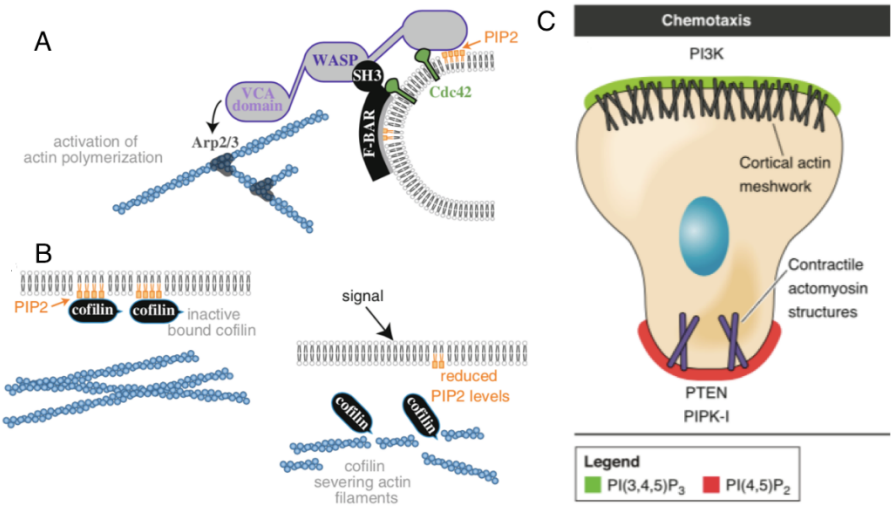

Fig 26. Importance of PIP2 and PIP3 for cell migration and polarization. A. Wiskott-Aldrich syndrome protein (WASP) is localized and activated at the membrane through the binding to PIP2 and the aid of Rho family GTPase (Cdc42) and a protein from the BAR-domain family containing an Src homology 3 domain (SH3). Activated WASP containing VCA domain (verprolin, cofilin, acidic) activates actin-related protein complex 2/3 (Arp2/3) which induces actin filament nucleation and network growth. **B.** PIP2 binds and inactivates cofilin. Reduced PIP2 level leads to release of membrane bound cofilin, which becomes active and severs actin filaments**. C.** During chemotaxis of neutrophils, PIP2 and PIP3 are located at the uropod and leading edge, respectively[135, 139].

1.4.2.2 The importance of glycosphingolipids and lipid rafts

Cell surface glycosphingolipids perform important functions through carbohydrate-specific interactions with membrane proteins such as integrins implicated in adhesion and mobility. It has reported that GM2 mediates tumor cell migration through interaction and activation of the integrin receptor[140]. On the other hand, GM3 was found to inhibit hepatoma cell motility. The low metastatic hepatoma cell line has high level of ganglioside GM3, whereas the high metastatic cell line contains a high level of ganglioside GM2. Interestingly, the increase in GM3 content in high metastatic cells inhibits their mobility and migration[141]. Moreover, migrating T lymphocytes exhibit an asymmetric redistribution of GM3- and GM1-enriched domains to the leading edge and to the uropod, respectively[142]. Altogether, this suggests complex and differential roles of gangliosides in cell growth and progression. Some studies have reported that lipid rafts are prerequisite for lamellipodia formation in melanoma cells through actin cytoskeleton-mediated recruitment of β1 and β3 integrin[143]. Rac1 association

with the PM requires lipid raft domains. When cells are detached, lipid raft markers are cleared from the cells surface through internalization[144]. In addition, lipid rafts are also critical for human neutrophil to amplify the chemoattractant gradient and maintaining cell polarization[145].

2. ALTERATIONS OF MEMBRANE LIPID COMPOSITION IN CANCER CELLS

Membrane lipids clearly contribute to cell survival/death and migration. As those physiological processes are often altered in tumors, we dedicate a section on alterations of membrane composition in cancer cells. In this chapter, we will provide a simplified overview of the synthesis of GPLs and SLs (section 2.1.1) and Chol (section 2.1.2) to better understand the next chapter dedicated to the alteration of lipid profile in cancer cells (section 2.2), especially breast cancer cells (section 2.2.5).

2.1 Simplified overview of lipid synthesis

"Normal" cells obtain lipids through the uptake of free FAs and lipoproteins from the bloodstream. New synthesis of FA and Chol involving the activity of hundreds of enzymes is restricted to a few specialized tissues like the liver, adipose tissue or the lactating breast. Although, in cancer cells, these restrictions are interrupted and new synthesis of lipids is observed[146]. This illustrates the fundamental role played by lipids in maintaining membrane homeostasis and normal function in healthy cells.

2.1.1 Glycerophospholipids and sphingolipids synthesis

FA synthesis starts with the generation of acetyl-CoA from citrate by the enzyme ATP-citrate lyase (ACLY). The carboxylation of acetyl-CoA to malonyl-CoA is performed by the enzyme acetyl-CoA carboxylase (ACC) **(Fig. 27)**. Acetyl-CoA and malonyl-CoA are then coupled via the enzyme fatty acid synthase (FASN). Repeated condensations of acetyl groups generate a basic 16-carbon saturated FA, the palmitic acid. Palmitic acid is further elongated and desaturated to synthesize the diverse spectrum of saturated and unsaturated FAs. One of the main desaturases in mammalian cells is the stearoyl-CoA desaturase (SCD), which introduces a double bond at the Δ9 position of palmitic and stearic acids to generate monounsaturated FAs. Then, FAs can be used to generate many different types of lipids. They could be transformed into diacylglycerides and triacylglycerides via the glycerol phosphate pathway, which uses the glycolytic intermediate glycerol-3-phosphate to form the glycerol backbone of these lipids. Intermediates of this pathway can be converted into different GPLs such as PC, PE, PG and PS. The sphingoid backbone is

also generated from FAs via the condensation of palmitoyl-CoA and serine by serine palmitoyltransferase (SPT), the rate-limiting enzyme of the SL biosynthesis pathway. The product of this reaction is 3-ketosphinganine. This is followed by other catalyzed reactions leading to the formation of Cer. Following conversion to Cer, sphingosine is released via the action of ceramidase. Inversely, sphingosine can serve as a substrate for Cer synthesis, through the actions of Cer synthases. The overall level of Cer in a cell is a balance between the need for sphingosine derivatives such as sphingosine-1-phosphate (S1P) and SM. S1P is formed by phosphorylation of sphingosine while SM are synthesized by the transfer of phosphorylcholine from PC to a Cer in a reaction catalyzed by SM synthases (SMS). Inversely, SM are degraded via the action of sphingomyelinases (SMase) resulting in release of Cer and phosphocholine[147]. For more detail regarding lipid synthesis please refer to [148].

2.1.2 Cholesterol synthesis

Chol is obtained from two sources, diet and *de novo* synthesis (liver represents the main site). The relative contribution of *de novo* Chol synthesis vs dietary intake has been estimated as ~70:30 for total body Chol. Chol is synthetized from acetyl-CoA through the initial steps of the mevalonate pathway (MVA) **(Fig. 26)**[149]. The most important rate-limiting step in the regulation of cholesterol synthesis is the conversion of 3-hydroxy-3-methylglutaryl-CoA (HMH-CoA) to mevalonate catalyzed by the 3-hydroxy-3-methylglutaryl-CoA reductase (HMG-CoA reductase), an enzyme that can be inhibited by statins.

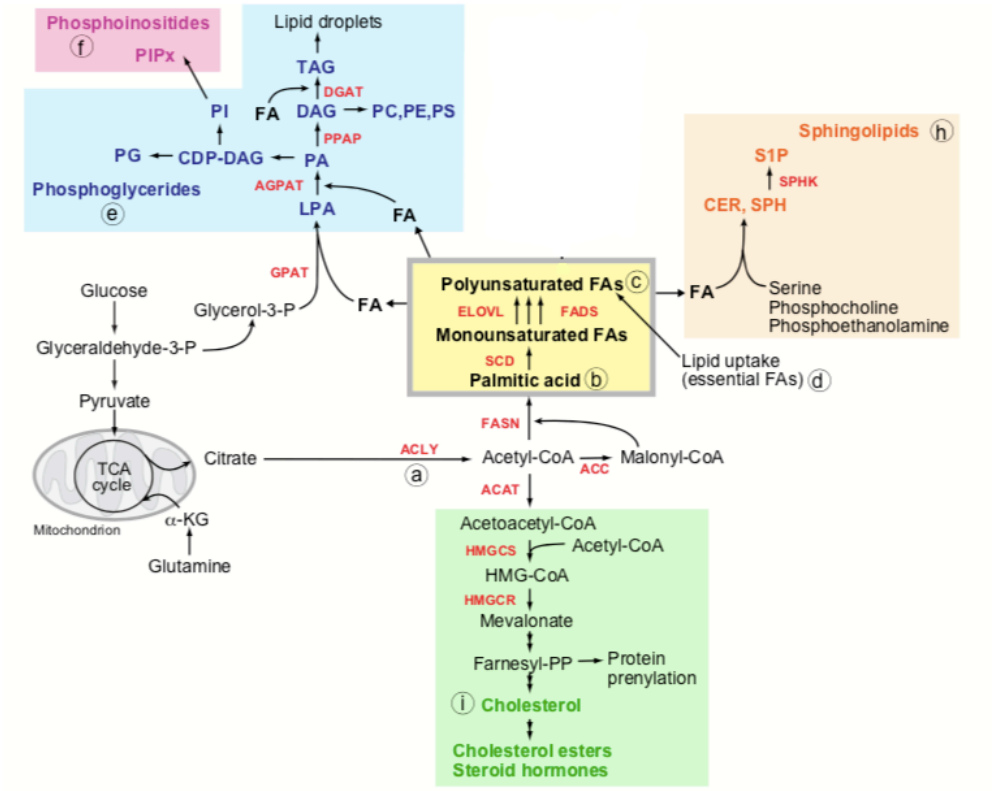

Fig 27. Lipid biosynthesis. Schematic overview of the pathways involved in the synthesis of FAs, Chol and PLs. Enzymes are indicated in red: ACAT, acetyl-CoA acetyltransferase; ACC, acetyl-CoA carboxylase; ACLY, ATP citrate lyase; AGPAT, 1-acylglycerol-3-phosphate O-acyltransferase; DGAT, diacylglycerol O-acyltransferase; ELOVL, fatty acid elongase; FADS, fatty acid desaturase; FASN, fatty acid synthase; GPAT, glycerol-3-phosphate acyltransferase; HMGCR, 3-hydroxy-3-methylglutaryl-CoA reductase; HMGCS, 3-hydroxy-3-methylglutaryl-CoA synthase; PPAP, phosphatidic acid phosphatase; SCD, stearoyl-CoA desaturase; SPHK, sphingosine-1-kinase. Metabolite abbreviations: α-KG, α-ketoglutarate; CDP-DAG, cytidine diphosphate-diacylglycerol; CER, ceramide; DAG, diacylglycerol; FA, fatty acid; LPA, lysophosphatidic acid; PA, phosphatidic acid; PC, phosphatidylcholine; PE, phosphatidylethanolamine; PG, phosphatidylglycerol; PI, phosphatidylinositol; PIPx, phosphatidylinositol phosphate; PS, phosphatidylserine; S1P, sphingosine-1-phosphate; SPH, sphingosine; TAG, triacylglyceride[147].

2.2. Main lipid alterations in cancer

Highly proliferative cancer cells show a strong lipid and Chol avidity to supply energy and building blocks[147]. Excessive lipids and Chol stored in lipid droplets are both established as a hallmark of cancer[150]. To increase lipid and Chol synthesis, cancer cells upregulate the expression of lipogenic enzymes, such as the FASN or ACC which correlate with their metastatic ability[149]. Targeting the lipid and Chol dependence of cancer cells through inhibitor agents directed against lipogenic enzymes (FASN or ACC) has been the subject of numerous studies; and their efficacy as anticancer therapies have been proven in various preclinical models of carcinogenesis[151]. However, high adverse side effects of FASN-targeting drugs have precluded their clinical development[151]. For more detail regarding the lipid metabolic reprogramming in cancer cells, please refer to [132, 152]. In agreement with lipid reprogramming in cancer, numerous lipidomic studies have shown that the lipid profile of tumor cells is altered with respect to non-tumor cells[153]. Although it appears that there is no one common pattern of membrane lipid alterations in different kinds of tumors, some trends are emerging in certain features of tumor lipid profiles regarding SL (section 2.2.1), FA saturation (section 2.2.2), PL asymmetry (section 2.2.3) and Chol (section 2.2.4) that we describe in this chapter.

2.2.1 Sphingolipids

Among SLs, Cer is considered as a tumor-suppressor lipid owing to its antiproliferative, and apoptotic responses in various cancer cells[117, 154]. Accordingly, an inverse correlation is observed between the levels of Cer and the degree of malignant progression and prognostic severity in patients with malignant astrocytoma[155]. Similarly, the total content of Cer is decreased in ovarian tumors as compared to normal ovarian tissues[156]. In line with this, enzymes within the SL metabolism pathway are frequently deregulated in cancer, resulting in lower Cer levels, which could cause resistance to chemotherapeutic treatment[154]. Conversely to Cer, S1P acts as a tumor-promoting lipid and promotes proliferation, angiogenesis and migration while blocking apoptosis[157, 158]. S1P has been shown to stimulate invasiveness of human glioblastoma cells [157], suggesting that tumors might accelerate the metabolism of Cer and generate increased levels of S1P. Interestingly, the decrease of Cer is not necessarily associated with an increase of SM. In human cancer cells (Human glioma (U118, 1321N1, SF767), human nonsmall lungadenocarcinoma (A549), Jurkat-T lymphoblastic leukemia cells have markedly lower levels of SM than nontumor (MRC-5 human fibroblast) cells. The low SM levels are associated with the tumorigenic transformation[159]. In addition, Wang et al. showed a decrease of SM level in highly invasive breast cancer lines as compared to poorly invasive breast cancer lines[160]. Another putative pro-

tumoral ganglioside is GM3.Indeed, the metastatic and invasive potential of mouse melanoma B16 seems to be correlated with the level of GM3 expression at the cell surface[161].

2.2.2 Fatty acid saturation

It has been reported that the shift from lipid uptake to *de novo* lipogenesis in cancer cells leads to increased membrane lipid saturation, resulting in higher levels of saturated and monounsaturated PLs, potentially protecting cancer cells from oxidative damage and chemotherapeutic drugs by reducing lipid peroxidation and increasing membrane packing, respectively[162]. Increased levels of saturated FAs are also found in aggressive breast cancers[147, 163]. Interestingly, consumption of mono- and polyunsaturated FAs, like linoleic and oleic acids, is believed to have a protective effect against tumorigenesis by influencing membrane composition and changing PM properties[164]. However, although human MT3 breast cancer cell line show a significant increase in the content of mono- and polyunsaturated FAs, this seems to promote metastasis[165].

2.2.3 Phospholipid asymmetry

The loss of lipid asymmetry seems to be common for many cancer cells. It has been reported that tumorigenic, murine erythroleukemic cells express 7- to 8-fold more PS in their outer leaflet than do their counterparts[166]. In agreement, the tumorigenic cells express 3–7-fold more PS than the nontumorigenic normal human epidermal keratinocyte line[167]. In tumor endothelial cells, PE is also found to be exposed in the outer leaflet[168].

2.2.4 Cholesterol

Chol also appears to be changed in cancer cells. Indeed, Van Blitterswijk at al. have reported lower content of membrane Chol in murine leukemic cell lines as compared to normal thymocytes[169]. In addition, MT3 breast cancer cells show a significant decrease of Chol which correlates with an increase in membrane fluidity and an increase of metastatic foci registered in lungs of mice[165]. However, opposite results have been obtained in other studies. For example, in lung cancer, Dessi et al. showed that the tumor contains 2-fold more total Chol and 3.5-fold more esterified cholesterol than normal lung tissues[170]. In addition, total Chol and esterified Chol are markedly increased in oral tumor tissues as compared to normal tissues[171]. Chol levels could be either lower or higher according to the type of cancer and stage[172]. It has been proposed that, in metastatic cells, lower Chol levels well correlate with a more deformable membrane increasing its ability to invade surrounding tissues[165, 173]. However, in multidrug resistant cells, higher values of Chol can be found, turning the membrane more rigid and, thus,

less permeable for drugs[174].

2.2.5 A focus to breast cancer

This last section focuses on human breast cancer since breast cancer cell lines have been used in the third part of my thesis. In this cancer, it is possible through lipid profile assessment to discriminate malignant cells from benign ones and to distinguish low- and high-grade tumors **(Table 3)**. It has been reported that the PL content is 4-fold higher while the triacylglycerol content tends to be 65% lower in the breast cancer tissues as compared to adjacent healthy tissues[175]. Hilvo et al. have shown specific lipids such PC 30:0 and 32:0 as associated with more aggressive breast tumors and poorer overall survival. Wang et al. have identified a total of 31 lipids, especially PG, PA, PE, PS, PC, PI species, as upregulated and eight lipids, such as SM and PE species, as downregulated in highly invasive breast cancer lines compared to poorly invasive breast cancer lines[163].. As already mentioned, MT3 breast cancer cells show a significant decrease of Chol which correlates with an increase in metastatic foci registered in lungs of mice[165]. Lipidomic changes are also associated with estrogen receptor (ER) status. PC, PE, PI and SMs are upregulated in ER– as compared to ER+ breast cancer samples[163].

Altogether changes in the amount of lipids can be associated with the different cancer states and might affect signaling cascades. Fundamental differences between the cell membrane composition of normal and cancer cells serve as new diagnostic but could also be used for the development of new chemotherapy given that membrane alteration can change the activity of membrane proteins such ion channels and receptors as well as the biophysical membrane properties.

Cell type	Sample	Lipids	Up	Down	Compared to	Ref.
High metastatic MDA-MB231	Cell line	PA, PI, alkylacyl PC	X		Non-malignant MCF10A	[176]
High metastatic MDA-MB231	Cell line	PC, PE, PS, PI	X		Non-malignant MCF10A	[177]
High metastatic MDA-MB231	Cell line	PS, PI	X		Low metastatic MCF-7	[177]
High metastatic MDA-MB231	Cell line	PE, PG		X	Low metastatic MCF-7	[177]
High metastatic MDA-MB231	Cell line	PI 36:1, PC 36:1, 36:2	X		BT-20, MCF-7, SK-BR-3, MDA-MB-157, MDA-MB-361	[178]
High metastatic BT-549 and MA-MB-231	Cell line	PG, PA, PE, PS, PC, PI	X		Low metastatic MCF7 and T47D	[160]
High metastatic BT-549 and MA-MB-231	Cell line	SM, PE		X	Low metastatic MCF7 and T47D	[160]
High metastatic MDA-MB-157	Cell line	PI 36:1, PC 28:0, SM 34:1		X	BT-20, MCF-7, SK-BR-3, MDA-MB-231, MDA-MB-361	[178]
Low metastatic MCF-7	Cell line	PE 38:4, 38:5,36:4, PC 36:1		X	BT-20, SK-BR-3, MDA-MB-231, MDA-MB-157, MDA-MB-361	[178]
Low metastatic MCF-7	Cell line	PC, PE, PG	X		Non-malignant MCF10A	[177]
Low metastatic T47-D and high metastatic MDA-MB231	Cell line	PE		X	Non-malignant MCF10A	[176]

BT-20, MCF-7, SK-BR-3, MDA-MB-231, MDA-MB-157 and MDA-MB-361	Cell line	SM 34:0, PC 38:4, PI 38:4, Polyunsatured lipids		X	Non-malignant MCF10A	[178]
BT-20, MCF-7, SK-BR-3, MDA-MB-231, MDA-MB-157, and MDA-MB-361	Cell line	PC 32:1, 30:0	X		Non-malignant MCF10A	[178]
MT3 with prolongation of proliferation time	Cell line	Chol		X	MT3	[165]
Breast cancer	Tissue	PC 34:1	X		Adjacent normal tissue	[179]
Triple negative breast cancer	Tissue	PC 32:1 30:0	X		Luminal and HER2 breast cancer	[179]
Breast cancer	Tissue	PI 36:1, 38 :3	X		Normal mammary gland	[180]
Breast cancer	Tissue	PC, PE, PI	X		Adjacent normal tissue	[163]
ER- breast cancer	Tissue	PC, PE, PI, SM	X		ER+ breast cancer tissue	[163]
Grade 3 breast cancer	Tissue	PC 30:0, 32:0, 32:1, 32:3	X		Grade 1 breast cancer tissue	[163]
Breast cancer	Tissue	PC 40:6, 38:6, 34:1 Majority of PI species	X		Adjacent normal tissue	[181]

		SM 34:1, PE 34:1, 36:2				
Breast cancer	Tissue	PC 20:4, Exception: PI 38:4, 36:4, 38:5, SM 36:3, 40:2, PE 36:4, 38:5, 38:4		X	Adjacent normal tissue	[181]
Malignant breast cancer	Tissue	PE, PI, PC	X		Benign breast	[182]
Breast cancer	Tissue	PC,PE	X		Adjacent normal tissue	[175]

Table 3. Lipid biomarkers in human breast cancer. The table lists specific lipids evaluated in human breast cancer, specifying if these have been found to be up or down-regulated in the respective sample type. Estrogen receptor (ER) and progesterone receptor (PR)

3. FUNCTION, DIVERSITY AND MEMBRANE INTERACTION OF SAPONINS

After having developed PM and described alterations of its composition in cancer cells, we now focus on saponins, amphiphilic compounds interacting with PM and attracting more and more attention based on their anticancer properties. We will briefly describe the function and diversity of saponins (section 3.1) and expose models of interaction of saponin with membrane (section 3.2). After that we will focus on ginsenosides and the structure–activity relationships in their anticancer activities (section 3.3). We will close this chapter by highlighting the importance of PM for their actions (section 3.4).

3.1 Function and diversity

Saponins are key ingredients in traditional Chinese medicines and found in a wide variety of plants, edible legumes (lentils, chickpeas, a.o.) and some marine organisms like sea cucumbers (Holothuriidae) and sea stars (Asteroidea). Their biosynthesis follows the same mevalonic acid pathway as Chol. Their roles are still not fully understood but they have been shown to serve primarily as defensive molecules against bacteria, fungi, yeast and insect invasion. Beside their role in plant defense, saponins are of growing interest for drug research as they provide valuable pharmacological properties such as anti-inflammatory, anti-bacterial and anti-cancer activities[183]. They are also of interest as adjuvants due to the formation of immunostimulating complexes. Saponins have been shown to swell and rupture erythrocytes causing a release of hemoglobin. The effect of saponin on erythrocyte death or hemolysis may limit the therapeutic use of the substances. The saponin name comes from the Latin “sapo” which means soap which is due to their soap-like behavior in aqueous solution and their ability to produce foam by reducing the surface tension of the water. Structurally, saponins are amphiphilic molecules characterized by a lipophilic aglycone structure referred to as the sapogenin and one or more hydrophilic head group. Different hydrophilic sugar moieties and variations of the aglycone structure confer them a high degree of structural diversity exhibiting specific biological activities. Traditionally, saponins are subdivided based on the nature of their aglycone: pentacyclic triterpene (or triterpenoid) **(Fig. 28A)** and steroid (or steroidal) **(Fig. 28B)**. The aglycone of triterpene saponins consists of a C30 skeleton while the steroid aglycone consists of a C27 skeleton but they are both derived from 2,3-oxidosqualene, a central metabolite in sterol biosynthesis. Saponins possess different types and numbers of

carbohydrates (i.e, hexose, pentose)[184]. Best-known saponins are monodesmosidic saponins which means that only one position of the aglycone is glycosylated. In most monodesmosidic saponins the sugar chain is attached at the C3 hydroxyl group. Bidesmosidic saponins contain another sugar chain at C-26 or C-28.

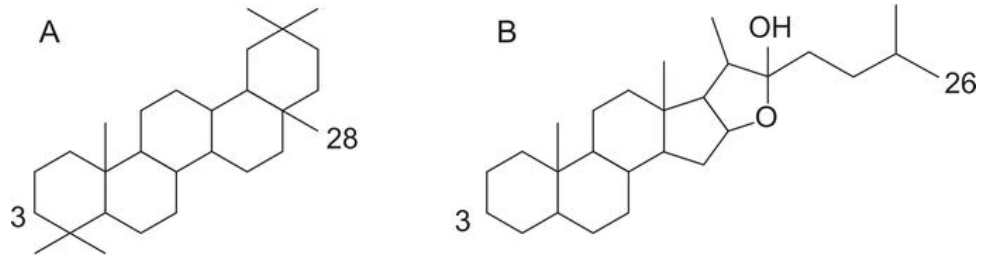

Fig 28. Saponins are classified in two groups based on the nature of their aglycone part. **A.** Pentacyclic triterpene (or triterpenoid) **B.** Steroid (or steroidal).

3.2 Models of interaction with membrane

The amphipathic properties of saponins give them the potential ability to interact with cell membrane. In this section, we will describe several models of action of different saponins established over time. Majority of models suggest the formation of a complex saponin/Chol (section 3.2.1), although some studies argued in favor of a Chol-independent activity for few saponins (section 3.2.2). Interestingly, some Chol-dependent saponins (avenacin A-1, α and δ-hederin) can insert into Chol-free membranes without inducing any changes. The formation of Chol:saponin complex induces membrane budding (digitonin, dioscin, δ-hederin) but also membrane vesiculation for certain saponins (glycoalkaloids, hederagenin). All these models are in agreement with the fact that saponin induces pore formation as a final step, exception has been made with hederagenin[185]. Regarding the Chol-independent activity, PC could play a major role in the action of few saponins (akebia Saponin B and C, ginsenoside Rc).

3.2.1 Cholesterol-dependent saponin activity

3.2.1.1 Model of Doursmashkin-Glauert (1962): Crude saponin extract

Glauert, Dourmashkin et al. demonstrated the presence of holes (diameter around 80 Angstrom) in the surface membrane of Rous sarcoma viruses and erythrocytes after treatment with “saponin”, described here as commercial mixture of saponins. They suggested that saponin has the ability to form a complex

with Chol at a 1:1 molar ratio and proposed that the pores are formed by the arrangement of twenty saponin molecules in a circular structure with a distinguishable space between each lipophilic headgroup **(Fig. 29)**[186].

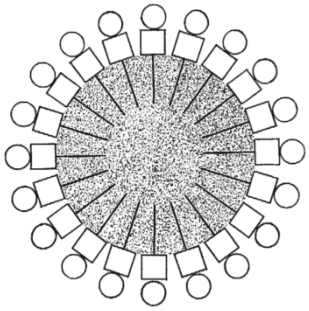

Fig 29. Crude saponin extract-Chol interaction: Model of Doursmashkin-Glauert. Hypothetical micellar-type arrangement of saponin within the membrane (□–) with cholesterol (O). The central speckled area represents the water phase[186].

3.2.1.2 Model of Nishikawa and Frenkel (1984 and 2014): Digitonin

Digitonin is a steroid saponin from the plant of the foxglove, *Digitalis purpurea.* The digitonin aglycone is attached to an unbranched chain of five sugar moieties **(Fig. 30A)**. Nishikawa et al. observed that digitonin induces membrane permeability in Chol-containing liposomes but not in Chol-free liposomes[187]. They proposed a model where the saponin forms a rigid complex with Chol with an equimolar stoichiometry. The formation of this complex leads to membrane rupturing. Interestingly, removal of subsequent sugar residues results in the progressive loss of digitonin activity. Recently, Frenkel et al. proposed the following mechanism of interaction between digitonin and Chol molecules in 1-stearoyl-2-oleoyl-sn-glycero-3-phosphocholine (SOPC)-Chol bilayers **(Fig. 30B)**[188]. First, digitonin penetrates within the membrane and binds to Chol molecules. The formation of Chol–saponin aglycone aggregates do not lead to any significant membrane destruction, but Chol is removed from the hydrophobic core region. Finally, the sterical hindrance between saccharide residues in those aggregates may induce changes in the curvature of the membrane outer leaflet, leading to an increase in the membrane permeability.

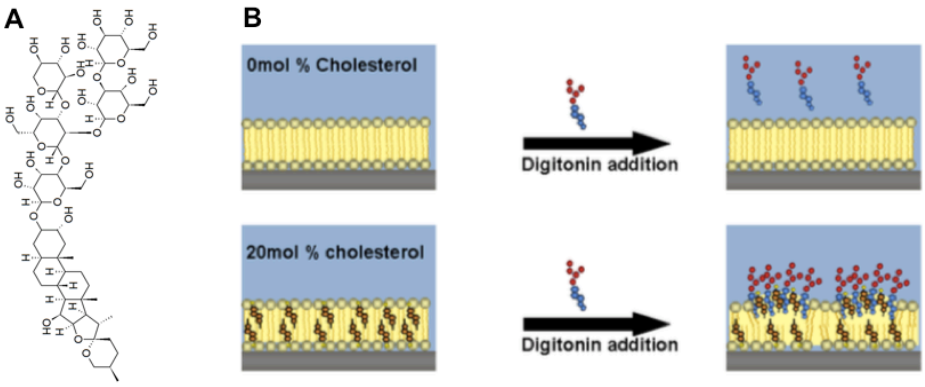

Fig 30. Digitonin-Chol interaction. A. Structure of Digitonin from *Digitalis purpurea.* **B.** Model of Nishikawa and Frenkel with steroid digitonin. Digitonin could not interact and affect membranes in the absence of Chol. However, digitonin penetrates into membranes containing Chol and forms Chol–saponin aglycone aggregates, leading to membrane curvature and permeability[188].

3.2.1.3 Model of Keukens (1995): Glycoalkaloids

Keukens et al. demonstrated that steroid glycoalkaloids such as ***α***-chaconine and ***α***-tomatine interact with membrane Chol and induce the formation of tubular (***α***-chaconine) and spherical (***α***- tomatine) structures and membrane disruption[189]. ***α***-solanine, which has the same aglycon structure but a different trisaccharide moiety as compared to ***α***-chaconine, has hardly an effect, highlighting the importance of the type of sugar moiety to interact with Chol **(Fig. 31A)**. Basically, after membrane insertion of ***α***-chaconine independently of Chol, its aglycon part bound to Chol in a 1:1 ratio **(Fig. 31B, step 1,2)**. After that, the interaction between the sugar moieties of glycoalkaloids initiate the formation of a stable irreversible matrix of glycoalkaloid/Chol complexes **(Fig. 31B, step 3, 4)**. Since Chol in the outer leaflet gets immobilized, Chol of the inner leaflet could flip to compensate for the loss of Chol. The membrane layer will bud due to the fact that glycoalkaloid/sterol complex has a relatively large polar headgroup forming a positive curvature **(Fig. 31B, step 5).** This curvature could result in the formation of hemitubular protuberance that may eventually lead to sterol extraction via vesiculation **(Fig. 31B, step 6)**.

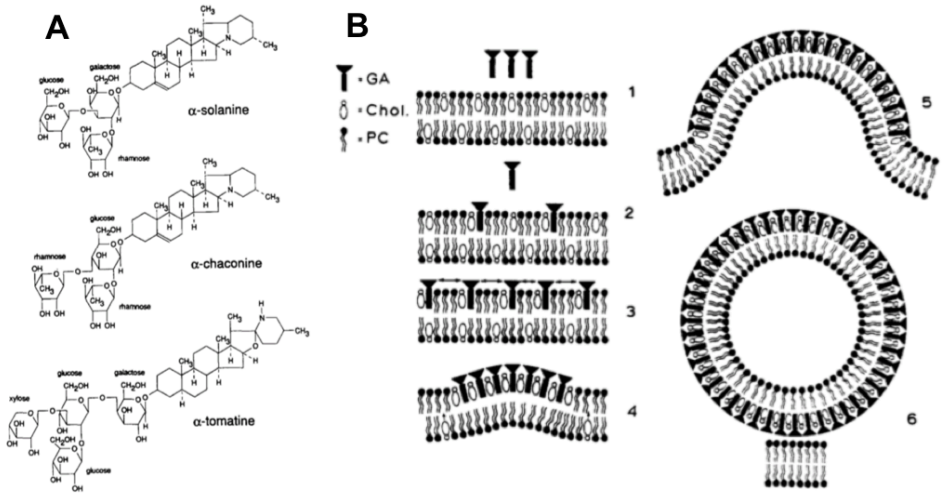

Fig 31. Glykoalkaloid-Chol interaction. A. Structures of ***α***-solanine***, α***-chaconine and ***α***-solanine. **B.** Model of Keukens with steroid glycoalkaloids. (1) Glycoalkaloids arriving at to the membrane. (2) Insertion of glycoalkaloids into the membrane, (3,4) formation of glycoalkaloids-Chol complexes, (5,6) budding of the membrane and formation of final tubular structure with glycoalkaloids-Chol layer on the outside and pure PC layer on the inside[189].

3.2.1.4 Model of Armah (1999): Avenacin A-1

Chol is also required for the triterpenoid saponin avenacin A-1 to induce bilayer permeabilization and to decrease the lateral diffusion of the fluorescent probes NBD-PE and NBD-Chol **(Fig. 32A)**. In lipid bilayers without Chol, avenacin A-1 does not affect those parameters even though the saponin is able to insert within the membrane as reported by its capacity of reducing the surface tension of POPC:DOPE (7:3) monolayers. In the model proposed by Armah et al., first the aglycone part of avenacin A-1 inserts into the outer leaflet in a Chol-independent manner[190]. Secondly, avenacin A-1 bound to the membrane Chol and the sugar residues of the avenacin A-1 interacts and causes the aggregation of Chol-avenacin A-1 complex. This may lead to the rearrangement of the bilayer lipids and the formation of transmembrane pore **(Fig. 32B)**.

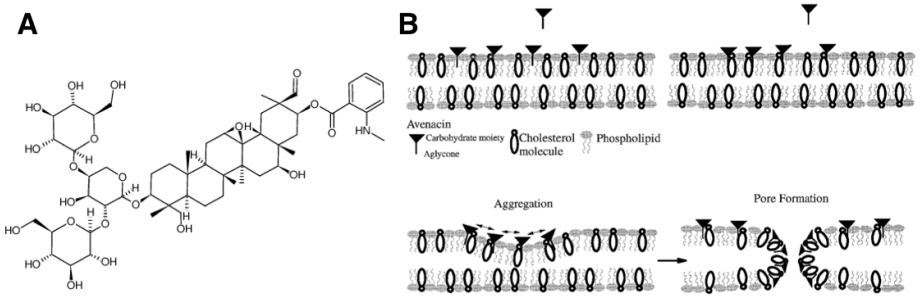

Fig 32. Avenacin A-1-Chol interaction. A. Structure of avenacin A-1, **B**. Model of Armah with triterpenoid avenacin A-1. Insertion of avenacin A-1 into Chol-free membranes followed by binding to Chol and formation of the transmembrane pore[190].

3.2.1.5 Model of Lin and Wang (2010): Dioscin

According to a coarse-grained molecular dynamic simulation (CGMD), the dioscin-Chol complex is energetically more favorable than the Chol-Chol complex **(Fig.33A)**[191]. Dioscin, a steroid saponin shown to interact with Chol, sequesters Chol from interactions with SM causing the disruption of lipid raft structures **(Fig. 33B)**. The accumulation of dioscin in the lipid raft changes the membrane morphology and provokes severe curvature of the lipid bilayer, which could lead to membrane deconstruction and RBC hemolysis.

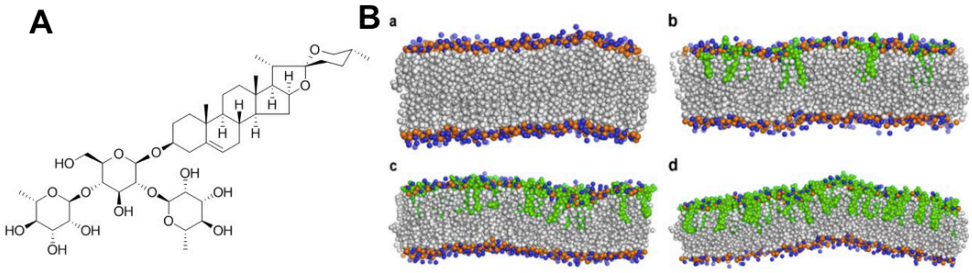

Fig 33. Dioscin-Chol interaction. A. Structure of dioscin. **B.** Model of Lin and Wang with steroid dioscin. Snapshots of CGMD simulations of the interaction of dioscin with the bilayer membrane (a) POPC:PSM:Chol without dioscin; (b) penetration of dioscin (*green*) into the membrane and binding to Chol; (c) sequestration of Chol from its interaction with SM and damage the structure of the lipid raft; (d) accumulation of saponin-Chol at lipid raft domains caused changes of membrane curvature[191].

3.2.1.6 Model of Lorent (2013): α-hederin and δ-hederin

α-hederin is a monodesmosidic triterpenoid compound with two sugar moieties attached at C3 of the aglycone (hederagenin) while δ-hederin possesses only one sugar moiety **(Fig. 34A)**. Lorent et al. showed that membrane permeabilization is dependent on the presence of membrane Chol and saponin sugar chains. There is a clear correlation between the number of sugars and membrane permeability: α-hederin>δ-hederin>hederagenin. The activities of α– and δ-hederin involve a three-step mechanism **(Fig. 34B)**[185]. The first step involves Chol-independent binding to the external leaflet of the membrane which increases GPex of laurdan. Second, these saponins interact with Chol and decrease GPex of laurdan. The glycoside residues could act like "umbrellas" shielding the nonpolar part of Chol from water, and preventing polar interactions between Chol and PLs. In a third step, α-hederin show a greater ability to induce pore formation and δ-hederin being more efficient in inducing budding. Hederagenin induces the formation of intravesicular buds but no formation of pore.

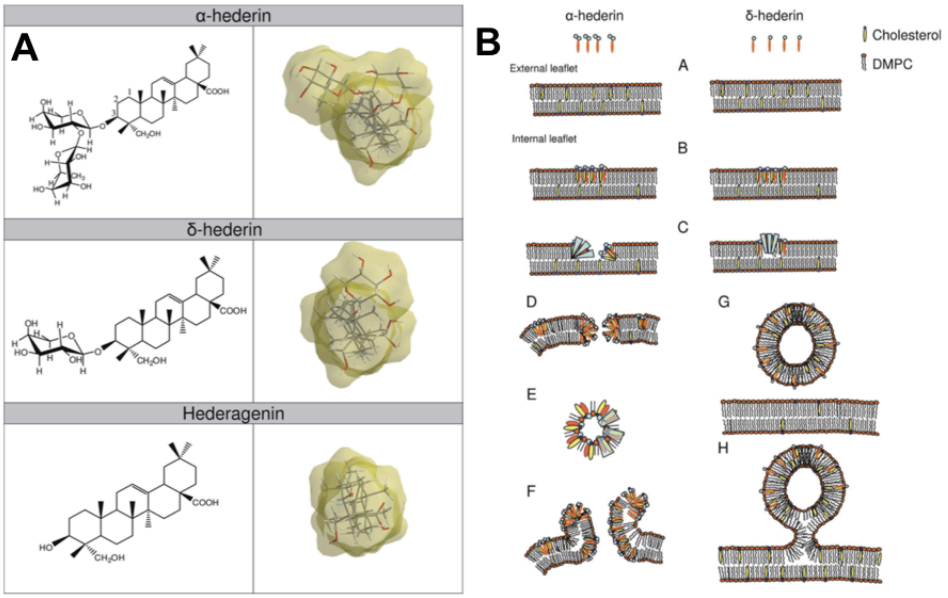

Fig 34. *α*- and δ-hederin and hederagenin-Chol interaction. A. Structure of ***α***- and δ-hederin and hederagenin. **B.** Model of Lorent with triterpenoid ***α***-hederin and δ-hederin. (A) ***α***- and δ-hederin interacted with the membrane in a Chol-independent manner and were integrated into the outer leaflet. (B) Interaction between these saponins and Chol lead to the formation of a region with a higher Chol concentration. (C) Sugar moieties of saponins in these regions increased spontaneous curvature inducing (D) membrane permeabilization or (G, H) budding. (D, E) Pores were stabilized by the sugar moieties pointing to the exterior of the membrane and reducing line tension. (F) Inhomogeneous distribution of ***α***-hederin between the inner and the outer leaflet caused rolled rims. (G) Intermediate curvature of δ-hederin was responsible for the immediate budding with complete fission from the GUVs at the beginning of incubation and (H) for the later budding with the bud still connected to the GUV at longer incubation times[185].

3.2.2 Cholesterol-independent saponin activity

Although the principal target of saponins is assumed to be Chol, some studies have shown that Chol does not always serve as a specific binding site for saponin activities. For example, the activity of triterpenoid glycyrrhizin and steroid ginsenoside chikusetsusaponin III saponins were somewhat higher for Chol-free liposomes than for Chol-containing liposomes **(Fig. 35)**. Hu et al. observed that some saponins glycosylated at both C3 and C28 of their oleanolic acids induce ePC (egg PC) membrane permeability without cholesterol[192]. Using dilauroyl-,

dimyristoyl-, dipalmitoyl- and distearoyl-PC vesicles, from short to high FA chain length. Nakamura et al. noticed the importance of PCs and the influence of the lengths of their acyl chains for the action of triterpenoid akebia Saponin B and C[193]. The sensitivity of vesicles toward those saponins decreases with the increased chain length and the underlying increased of membrane rigidity. This was also reported for the ginsenoside Rc-induced agglutinability which is more effective for PCs with short and/or unsaturated fatty acyl chains[194]. In addition, ginsenoside Rc showed strong agglutinability with ePC than ePE, ePA, PS and SM from bovine brain. No lytic activity was detected for saponins steroid chikusetsupsaponin V also named ginsenoside Ro (structure presented in section 3.4.2.1) and triterpenoid akebia saponin E and Pk (carrying two sugar chains) in ePC vesicles, with or without Chol, [193].

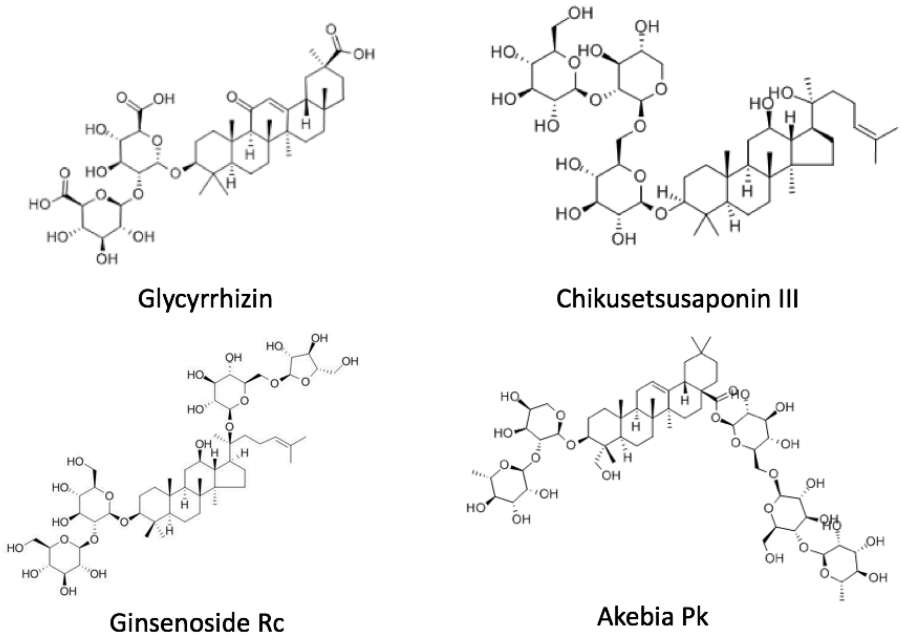

Fig 35. Structure of saponins having Chol-independent activities. Structure of triterpenoid glycyrrhizin and akebia Pk, steroid chikusetsusaponin III and ginsenoside Rc.

3.3 Ginsenosides and structure-activity relationship in their anticancer activities

The interesting properties of saponins have led us to the investigation of the saponin ginsenoside. Ginsenosides are the major pharmacologically active components of ginseng root (containing 2-3% ginsenosides). The basic structures of ginsenosides are similar, and most ginsenosides consist of a dammarane steroid nucleus with 17 carbon atoms arranged in four rings. Structurally, most of the ginsenosides belong to PPD and PPT groups (see section 3.4.2.1). Ginsenoside structures are named as Rx according to their mobility on TLC plates, with polarity decreasing from index “a” to “h”[195]. Ginsenosides are amphipathic in nature and their activities are mostly determined by the numbers and sites of polar hydroxyl groups on each ginsenoside. These compounds have been reported to display antioxidant potential (section 3.4.4.6), anti-bacteria and fungi activities (section 3.4.6.1 and 3.4.6.2) and anti-tumor efficacy (section 3.4.5.1). Interestingly, structure-activity relationship studies have shown that the anticancer activity of ginsenosides is inversely correlated to the number of sugar groups that they possess[196].While Rd with three sugar residues weakly inhibits the growth of cancer cell[197], Ginsenosides Rg3 (two sugar residues), Rh2 (one sugar residue) and PPD (no sugar residues) inhibit different types of cancer cells. Rh2 and PPD show 5- to 15-fold relatively stronger anti-proliferative effects than Rg3[198]. A correlation has been observed between thee cytotoxicity (IC50) and hydrophobicity (logP) of ginsenosides[197]. The presence of sugar moieties reduces the hydrophobic character of ginsenosides and probably decrease their interactions with the cell membranes. Sugar linkage positions also influence anticancer activities. A sugar group at C-6 decreases the anticancer activity of ginsenosides while sugar linkages at C-3 promotes it[230]. Notice that the backbone of ginsenoside Rh2 has one sugar group attached at C-3. It seems that the presence of a sugar moiety at C-6 increases the steric hindrance and prevent interaction with membrane proteins[199]. This kind of study may contribute to more effective ginsenoside design as the incidence of chemotherapeutic resistance increases.

The vast majority of studies reports the beneficial activity of ginsenoside through the modulation of many pathways such as cell cycle regulation, growth signals, cell death or inflammation for more detail please refer to [196, 200]. However, only few studies consider the PM for the activity of ginsenosides. Therefore, in the next section, we will review the key role played by PM for their activity and pharmacological benefits. The following section 3.4 will be submitted soon as a review as first author.

3.4 Lipid membranes as key targets for the pharmacological actions of ginsenosides

3.4.1 Introduction

The PM is the natural interface between inter- and intracellular space. One of its major functions is to delegate signals from the cell exterior to the interior, making it an interesting target for pharmacological agents able modulate signaling and thereby provoke a cellular response. The majority of drugs act on membrane proteins but it becomes clear that lipids are also important for signal transduction. Lipids can collectively form signaling platforms or lateral domains which include or exclude certain type of proteins[201]. Analysis of the PM lipidome has pointed out the colossal variety of membrane lipids[202]. It remains to be seen if each individual lipid has its own function or if this huge collective of lipids confers certain biophysical properties to the membrane, modulating cellular functions. Saponins, and especially, ginsenosides (a class of steroidal saponins) found in ginseng have been shown in the past to be membrane active substances and to influence the membrane as a collective by modulating its dynamics and its lateral organization in domains[203-205]. Interestingly, the mechanism of most ginsenosides does not seem to involve the formation of pores or holes in the membrane as it was observed with other saponins such as digitonin[183], reducing thereby the risk of hemolysis. The traditional use of ginseng has also proven that ginsenosides are relatively harmless *in vivo* and constitute interesting pharmacological agents. In this review, we will focus on the activity of ginsenosides on membranes and possibly related effects from physicochemical, biophysical and pharmacological viewpoints **(Table. 4)**.

3.4.2 Structural diversity of ginsenosides

The structural diversity of ginsenosides is mainly due to the high variety of sugar chains connected to different aglycone backbones. Hundreds of different ginsenosides have been reported and eliciting them is not in the scope of this review. For a detailed review on structural variety of the *Panax L*. species, including all ginsenosides which have been reported till 2012, please refer to [206, 207]. Globally, ginsenosides share a dammare-type triterpenoid saponin structure. Most ginsenosides belong to a family of steroids with a four trans-ring rigid steroid skeleton. Protopanaxadiol (PPD) and protopanaxatriol (PPT) are the two main groups of ginsenosides. In the PPD group, sugar residues are attached to the hydroxyl group at C-3 and/or C-20 while in the PPT group, sugar moieties are attached to the hydroxyl group at C-6 and/or C-20 **(Fig. 36)**. Minor ginsenosides include ocotillo-type (F11) oleanane-type (Ro) ginsenosides and other isolated

compounds can be classified as modified C-20 side-chain ginsenosides (Rh4, Rg5)[207]. An older classification of ginsenosides was based on their chromatographical profile. This ancient nomenclature has nowadays simply become the trivial name of ginsenosides (Ginsenoside Rb1, Rb2, Rc,…)[206].

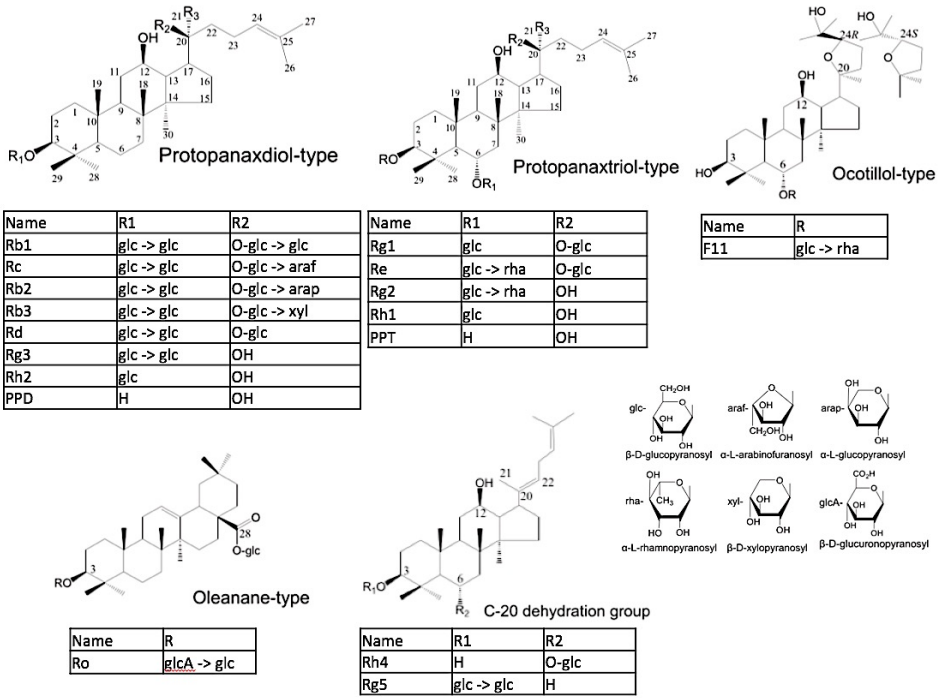

Name	R1	R2
Rb1	glc -> glc	O-glc -> glc
Rc	glc -> glc	O-glc -> araf
Rb2	glc -> glc	O-glc -> arap
Rb3	glc -> glc	O-glc -> xyl
Rd	glc -> glc	O-glc
Rg3	glc -> glc	OH
Rh2	glc	OH
PPD	H	OH

Name	R1	R2
Rg1	glc	O-glc
Re	glc -> rha	O-glc
Rg2	glc -> rha	OH
Rh1	glc	OH
PPT	H	OH

Name	R
F11	glc -> rha

Name	R
Ro	glcA -> glc

Name	R1	R2
Rh4	H	O-glc
Rg5	glc -> glc	H

Fig 36. Chemical structure of the main ginsenosides discussed in this review. Protopanaxdiol- and protopanaxatriol- type (R3 = CH_3), ocotillol-, oleanane type and C-20 side-chain ginsenosides[207].

3.4.3 Interaction with amphiphilic molecules and assembly into nanostructures

Saponins area amphiphilic molecules and have the property to accumulate at hydrophobic/hydrophilic interfaces and to self-aggregate upon a certain concentration (critical micelle concentration)[208]. Those properties provided the etymological background for the name “saponin” (‘*sapo*’ latin for soap) which are able to solubilize hydrophobic molecules in aqueous solution and have the same cleaning properties as other detergents. Specific aggregation of saponins with phospholipids and cholesterol, can lead to the formation of nanoparticles in aqueous solution which can be used as carriers for drugs. Those football-shaped nanoparticles named ISCOMs (immunostimulating complexes) are able to enhance

the immune response toward certain antigens [209]. Ginsenosides also have the potential to induce the formation of similar nanoparticles and could hence be used as nanocarriers for vaccines or potential anticancer drugs. More specifically, ginsenosides Ro, Rb1 and Rg1 are able to form nanoscopic aggregates in solution when combined with glucuronic acid and other saponins[210]. Ginsenoside Ro forms stable nanoscopic structures which have a vesicular shape. Rb1 forms worm like and spherical micelles whereby a higher number of sugars in the ginsenoside increase the number of binding sites in between those constructs[211, 212]. It has been shown that ginsenosides, extracted from red ginseng, are able to build nanoscopic aggregates in the presence of cholesterol and phospholipids, called ginsomes. Ginsomes have shown to enhance immune response in mice and are interesting candidates for nanoparticle carriers used in vaccines [213].

3.4.4 Ginsenoside-membrane interactions

3.4.4.1 Membrane insertion

The amphiphilic character of ginsenosides allows for adsorption or insertion into membranes, which are themselves nothing else than lamellar aggregates of amphiphilic phospholipids. The hydrophilic sugar moiety of saponins interacts with the interfacial part of the membrane, containing numerous glycolipids and glycoproteins. The saponin osidic part can induce the formation of intramolecular hydrogen bonds whereas the steroid or triterpenoid part interacts with membrane sterols. In accordance with those results, the interaction with liposomes of protopanaxadiol ginsenosides Rb1, Rb2, Rc and Rd is stronger than protopanaxatriol ginsenosides Re, Rf, Rg2, highlighting the importance of the sugar moiety position to membrane-related effects of ginsenosides[214]. Moreover, Fukuda et al. reported that ginsenoside-Rc having a a-L-arabinofuranose residue exhibits remarkable agglutinability toward egg yolk phosphatidylcholine vesicles, while other saponins (Rb1, Rb2, Rd, Re and Rg2) lacking this characteristic sugar residue show less or no agglutinability. The three-dimensional structure of the saponin is ultimately decisive for its aggregation with other lipids and the formation of lateral membrane domains[185, 189, 203]. In detail, in contrast to ginsenoside Rh1, Rh2 found in the lipid fraction extracted from crude plasma membrane, is able to induce flattening, increases adhesiveness to plastic surfaces and agglutinability of B16 melanoma cells. Those changes of surface properties could probably be linked to an increase of O-glycosidic oligosaccharides[215].

Regarding the preferential interaction between membrane lipids and saponin, the activity of some saponins, such as digitonin[216, 217] or alpha-hederin [203], is usually attributed to their interactions with membrane cholesterol. However, it has been reported that cholesterol is not necessary to protopanaxadiol

Rb1-induced liposomal membrane permeability but at the opposite suppresses its activity whereas protopanaxatriol Rg1 does not induce membrane permeability with or without cholesterol[218]. In addition, egg phosphatidylcholine vesicles are strongly agglutinated by ginsenoside-Rc, although egg phosphatidylethanolamine, egg phosphatidic acid, phosphatidylserine and sphingomyelin from bovine brain are no or less agglutinated. These results indicate that ginsenoside-Rc should recognize not only phosphorylcholine but also the glycerol backbone of phospholipids. They also show that the agglutinability of ginsenoside-Rc is more effective for phosphatidylcholines with short or unsaturated fatty acyl chains[194]. Moreover, we recently showed that cholesterol, contrary to sphingomyelin, delays the cytotoxicity of Rh2 in human monocytic leukemia U937 cells[219], an observation that has been confirmed by a large panel of biophysical approaches on lipid monolayers or LUVS[220]. To the best our knowledge, it is the first time that the saponin activity is ascribed to a preferential interaction with sphingomyelin and not cholesterol.

3.4.4.2 Effect on dynamic membrane properties

The dynamic behavior of lipids ultimately determines the diffusive properties of membrane proteins. Membranes with a high molar ratio of cholesterol, saturated phospholipids and sphingomyelin are considered to be tightly packed and thereby restrict the diffusion of lipids and proteins. Conversely, membranes with a high percentage of unsaturated phospholipids and low cholesterol content are rather disordered which allows for faster diffusion of intrinsic molecules. Several signaling pathways depend on the packing of lipid membranes and hence a transient change of lipid membrane dynamics by xenobiotics can have huge repercussions on cellular physiology. Several saponins seem to largely influence membrane dynamics and thus its function[183]. A broad variety of protopanaxadiol and –triol type ginsenosides (Rb2, Rc, Rd Re, Rf, Rg1, Rg2, Rh2) are able to reduce membrane order at the interfacial part of Hela cell membrane, as measured by laurdan. The aglycone protopanaxadiol itself can also decrease membrane order, hence this activity is not related to the sugar moieties[221]. Conversely, Fukumuda et al. highlighted the importance of arabinopyranosyl sugar residue of ginsenoside Rc and Rb2 for their interaction with both polar head groups and fatty acyl groups of egg phosphatidylcholine vesicles[194]. This insertion into the lipid bilayer reduces the segmental mobility of phosphatidylcholine. In melanoma cells, Rh2 increases lipid membrane order as determined by DPH fluorescence anisotropy but no fluorescence change is observed with TMA-DPH, suggesting that it is the lipid order of the inner hydrophobic core that is increased[215, 222]. Ginsenoside Rg3 increases fluorescence anisotropy of DPH and TMA-DPH in multidrug resistant KB V20 cells but not in the parental KB cell[205]. In bovine adrenal chromaffin cells, Rg3

increases the fluorescence anisotropy of DPH leading to the inhibition of the Na^+ and Ca^{2+} channel activity[223]. Ginsenoside Re reduces mitochondrial membrane order of brain cells after cerebral ischemia injuries in rats (DPH anisotropy)[224]. In addition, a ginseng extract of Korean red ginseng is able to reduce drastically DPH fluorescence anisotropy in *Candida albicans* suggesting that its antifungal activity is related to membrane activity (see section 3.4.6)[225, 226]. Finally, we recently published that Rh2 compacts the hydrophobic core of lipid bilayer (DPH anisotropy) and relaxes the interfacial packaging of the polar head of phospholipids (TMA-DPH anisotropy) in U937 cells[219]. Accordingly, by measuring the GPex of laurdan and the anisotropy of DPH, we observed that liposomal membrane rigidity is increased at a low ginsenoside Rh2/lipid ratio in the presence of egg sphingomyelin and the absence of cholesterol.

3.4.4.3 Effect on membrane lateral organization

Lipids rafts are Chol and SLs-enriched membrane nanodomains considered to facilitate protein signaling via the recruitment of specific proteins[201]. Their disruption could therefore potentially impact several signaling pathways or protein transport[221, 227]. Rp1 redistributes lipid rafts and inactivates the drug efflux pump P-gp, increasing the accumulation of doxorubicin in doxorubicin-resistant cells [228]. Rg3 has been found to reduce Aβ levels in cultured primary neurons and in the brain of mouse model with Alzheimer's disease by decreasing the association of presenilin-1 (PS1) with lipid rafts and inhibiting γ-secretase activity [229]. Rh2 also helps to prevent Alzheimer's disease symptoms by promoting nonamyloidgenic cleavage of amyloid precursor protein (APP) via the reduction of cholesterol and lipid rafts levels [230]. In addition, Rh2 has been reported disrupt lipid raft leading to apoptosis, via either the death receptor FAS oligomerization in human cervical cancer Hela cells[221] or inactivation of the serine/threonine kinase Akt in human epidermoid carcinoma A431 and breast cancer MBA-MB-231 cells[204, 221]. In contrast, another study has shown that membrane cholesterol depletion suppresses the dendrite formation of melanoma cells induced by Rh2 without affecting lipid rafts[222]. Interestingly, results suggest that ginsenoside activity is cell type specific. Indeed, Akt activity was decreased in lipid rafts of glioma cell line U87 MG cells but increases in neuroblastoma cell N2a by protopanaxadiol through regulating raft-associated dephosphorylation and without changing the levels of cholesterol. As protopanaxadiol has a chemical structure closed to cholesterol, it has been speculated that this ginsenoside could intercalate itself into the lipid rafts to cause changes in the microenvironment of the membrane[231]. It was proposed that this raft-disrupting ability of protopanaxadiol leads to activation of neutral sphingomyelinase and successive transformation of sphingomyelin into pro-apoptotic Cer[232].

3.4.4.4 Pore formation

In general, pore formation by saponins has been shown to depend on the interaction with cholesterol and phospholipids and the resulting three-dimensional aggregates which are formed in the membrane[185, 189]. Ginsenosides Rh2 and Rg3 very effectively form pores in red blood cells, inducing thereby hemolysis and intensity heme-induced hemolysis. Conversely, numerous ginsenosides at the same concentration (Rc>Rd>Re - Rb1>Rg1>Rh1>Rb3 - Rg2 - R1 - F11 - PPT) are able to protect erythrocytes towards heme-induced hemolysis[233]. These results indicate that a sugar moiety at C20 and hydroxyl group at C3 play a key role for the protective effect of protopanaxadiol and protopanaxatriol, respectively[233]. An extract of red ginseng root (Panax Ginseng C.A. Meyer) has the same toxicity on *Candida albicans* as amphotericin, a well-known antifungal compound most probably by disrupting the cellular membrane[226]. The hemolytic activity seems therefore not to be a common feature among ginsenosides, which makes them interesting pharmacophores because of their reduced toxicity compared to other saponins. Using calcein-filled liposomes, we observed that ginsenoside Rh2 induces membrane permeability in the presence of egg sphingomyelin but the absence of cholesterol[220].This result could be at a first glance opposing given that red blood cells membranes are particularly enriched in cholesterol[15, 16] but we do not exclude the influence of membrane organization or the importance of other lipids such as phosphatidylcholine (see section 3.4.4.1) involved in the membrane activity of Rh2. In addition, it has to be kept in mind that liposomes have some limitations as they do not capture the whole complexity of biological membrane such as membrane asymmetry and a large number of diverse membrane proteins.

3.4.4.5 Direct interaction with membrane proteins

Although ginsenosides are able to intercalate into the plasma membrane and change its dynamic and diverse cell signaling, numerous reports have also observed the ability of ginsenosides to directly interact with proteins embedded into the membrane such as voltage-dependent or ligand-gated ion channels or pumps like P-gp efflux pump (section 3.4.5.1.3)[234]. Rg3 has been shown to interfere with ion channel activity such as human Kv1.4 channel or the 5-hydroxytryptamine receptor type 3 (5-HT_{3A})[235]. Rg3 inhibits 5-HT_{3A} receptor channel activity by interacting with residues V291, F292 and I295 in the channel gating region of transmembrane domain 2[236, 237]. Moreover, in cultured hippocampal neurons, the activation of glutamate (NMDA) receptors is attenuated by ginsenoside Rh2 and Rg3 via a competitive interaction with its polyamine- or glycine-binding site, respectively[238, 239]. A comparative study has evidenced that protopanaxadiol-based (Rd, Rg3, Rh2, F2 and compound K) but not protopanaxtatriol-based ginsenosides (Rh1, F1 and Rg1) inhibit the sodium-glucose cotransporter (SGLT1), suggesting that the sugar moieties attached at the C6

position of the dammarane structure may interrupt the affinity for this cotransporter[240]. In agreement with this result, Chen et al. showed that ginsenosides with sugar moieties attached to the C3 position (such as PPD, Rh2 and Rg3) inhibit membrane-bound Na+/K+ ATPase activity. However, this inhibition is reduced or completely abolished when a monosaccharide is linked to the C-6 or C-20 position of ginsenoside[199].

3.4.4.6 Membrane antioxidant effects

Plasma membranes exhibit an asymmetric lipid distribution upon leaflets with a higher content of unsaturated acyl chains in the inner than the outer leaflet [77, 241], which reduces its membrane packing and increases the efficiency of protein insertion[201]. However, in situations of high oxidative stress, reactive oxygen species (ROS) (such as hydroxyl radical (OH•) or hydrogen peroxide (H_2O_2)) can oxidize polyunsaturated lipids and thereby induce a radical chain reaction leading to protein oxidation, cellular damage and the induction of signaling pathways which can promote diseases such as cancer, atherosclerosis or neurodegenerative diseases[242, 243]. Some types of ginsenosides have been shown to present a high potential for antioxidant activity and since they efficiently insert into membranes, it is reasonable to assume that their antioxidant activity targets cellular membranes. This is supported by the fact that many ginsenosides exhibit antioxidative properties mainly related to the suppression of lipid peroxidation products especially in the context of brain and myocardial injuries[224]. Rd attenuates lipid peroxidation and neuronal oxidative damage by decreasing the formation of major end-products of oxidation of polyunsaturated fatty acids in a rat model of focal cerebral ischemia[244]. Rb1 and Rg1 exhibit neuroprotective effects and prevent cardiac ischemia via the reduction of hydrogen peroxide and hydroxyl radicals [245]. Regarding the structure antioxidant-activity relationship of ginsenosides, sugar moieties at position C-20 or C-6 provide antioxidant activity. The order of antioxidative ability is classified as follows: Rc > Rb1 and Re > Rd > R1 > Rg1 > Rb3 > Rh1 [246]. At the opposite, the absence of sugar moieties at the C-20 position procures a rather pro-oxidant activity. This might come in pair with the fact that ginsenosides Rh2, Rh4 and Rg3 induce apoptosis via the formation of radical species and the depolarization of the mitochondrial membrane potential [247, 248]. Those results highlight the complex behavior of ginsenosides towards oxidative stress.

3.4.5 Potential use of ginsenosides as anticancer agents

Several ginsenosides have been shown to exert anticarcinogenic effects through different mechanisms such as direct cytotoxic, growth and metastasis

inhibitory effects against tumor cells[196]. Some mechanisms could be related to their membrane activities such as the alteration of lipid raft organization (section 3.4.5.1.1) and the modulation of ROS production (section 3.4.51.2). In addition, some ginsenosides inhibit the efflux pumps (section 3.4.5.1.3) which probably enhance conventional chemotherapeutic agents (section 3.4.5.1.4).

3.4.5.1 GINSENOSIDES AFFECT LIPID RAFT ORGANIZATION

The cell membrane, especially lipid rafts, attract more and more attention as key factors in cancer treatment and development of new therapeutic strategies. Lipid rafts serve as platforms for a number of cellular pathways related to cell survival, proliferation and apoptosis which are often altered in cancer cells[249]. For this reason, it could be of great advantage to use ginsenosides as potential anti-tumor drugs to modulate these domains and associated-pathways. In this regard, several studies have demonstrated that ginsenosides Rg3 or Rh2 interfere with lipid rafts (see section 1.4.1.4) and induce antiproliferative and apoptotic effects in various cancer cells[250-252]. For example, Rh2 blocks the growth of glioblastoma through the inhibition of receptor tyrosine kinase EGFR and PI3K/Akt signaling, which are suggested to be associated to lipid rafts (section 1.4.1.3)[253, 254].

3.4.5.2 GINSENOSIDES MODULATE ROS PRODUCTION

The regulation of oxidative stress is essential in both tumor growth and responses to anticancer therapies. ROS play a pivotal role during tumor growth and metastasis. At low levels, ROS may contribute to tumor emergence either by acting as signaling molecule or by promoting DNA mutation. At high levels caused by aberrant metabolism and signaling in cancer cells, ROS promote cell death and severe cellular damage. To combat this, cancer cells have enhanced antioxidant defense mechanism to reduce ROS levels even if this level stays higher than in normal cells[255]. Thus, increasing oxidative stress by ROS generation could be an efficient approach for the specific killing of cancer cells. The mechanism of ROS-mediated anticancer activities of ginsenoside depends on the specific type of cancer cells involved and the ginsenoside structure. On one hand, ginsenosides with sugar moieties at position C-20 or C-6 could mediate their antioxidant action through free radical scavenging to prevent tumor initiation. On the other hand, ginsenoside with no sugar moieties at the C-20 position could generate ROS to promote apoptosis during tumor progression, invasion and metastasis. For a detail review regarding the role of ROS in anticancer therapy with ginsenosides please refer to [256].

3.4.5.3 GINSENOSIDES INHIBIT EFFLUX PUMPS

Moreover, the anticancer potential of ginsenosides could result from their abilities to inhibit efflux pumps such as the P-glycoprotein (P-gp). The P-gp

overexpression is responsible to the development of multidrug resistance (MDR) causing major failure in cancer chemotherapy. Several ginsenosides inhibit P-gp and thus promote the activity of chemotherapy drugs against cancer cells[257]. Rg3 inhibits P-gp activity by decreasing membrane fluidity in human fibroblast carcinoma VCR-resistant KB V20C [205, 258]. Rp1 redistributes lipid rafts resulting in the relocalization of P-gp and its inhibition[228]. Finally, Rg5 interacts and reverses P-gp efflux pump activity which has been demonstrated by molecular docking analysis[259].

3.4.5.4 GINSENOSIDES ENHANCE THE ACTIVITY OF CONVENTIONAL CHEMOTHERAPEUTIC AGENTS

The combined application of ginsenosides with conventional chemotherapy agents could offer a promising strategy in cancer treatment. The combination of ginsenoside Rh2 with cisplatin enhances the inhibition of the growth of human ovarian tumor cells in nude mice as a result of synergistic action[260]. In combination with alkylating agent cyclophosphamide, ginsenosides Rg3 and Rh2 decrease tumor growth in mice[261]. Beside their own anticancer activities, it is tempting to speculate that ginsenosides could promote these synergistic effects by facilitating the entry of chemotherapeutic agents through the increase of membrane permeability and decrease of their efflux.

3.4.5.5 RESTRICTION AS ANTICANCER AGENTS

Saponins are still not used nowadays in chemotherapy due to their intrinsic hemolytic activity and poor bioavailability caused mainly by low aqueous solubility, instability in the gastrointestinal tract and extensive metabolism in the body. Nevertheless, some saponins have shown low or no hemolytic effect depending on their chemical structure[262]. Re, Rh1 and Rh2 show adjuvant potential with a low hemolytic activity [263-265]. Numerous drug delivery systems, such as liposomes or nanostructures (section 3.4.3), have been developed to avoid the fast plasma elimination of ginsenosides and to increase their solubility leading to the improvement of anticancer performance while preventing hemolytic activity[266]. Indeed, Rh2-loaded methoxy poly(ethylene glycol)-poly(lactide) (mPEG-PLA) liposome (Rh2-PLP) suppresses tumor growth in HepG2-xenografted mice without any significant toxicity[267]. Ginsenoside compound K encapsulated in phosphatidylcholine and phosphatidylethanolamine polyethylene glycol (PEG) enhances solubility and oral bioavailability as compared to free compound K. This micellar system improves ginsenoside anticancer effects such as the cell-cycle arrest and the decrease of the xenograft tumor growth in mice with low toxicity[268]. In addition, the treatment with Rg3 bile salt-phosphatidylcholine-based mixed micelle systems does not induce hemolysis in erythrocytes and exhibits higher antiproliferative activity against tumor cells than free Rg3[269].

Finally, a new drug delivery system based on ginsenoside Rh2-treated highly porous graphene has been recently generated and shown to improve their anticancer activities[270].

3.4.6 Potential use against invasive microorganisms

3.4.6.1 Fungi

Many saponins have shown antifungal properties acting as host chemical defenses to protect plants from fungal invasion[271]. The major mechanism behind is through the formation of complexes with membrane sterols, leading to loss of membrane integrity[189]. The importance of sterol for saponin activity is emphasized by the isolation of insensitive mutants (*F. solani)* to saponin due to their low sterol content[272]. Fungi also counter saponin activity by producing saponin-detoxifying enzymes. Ginseng root pathogens*, C. destructans and P. irregular,* hydrolyze monosaccharide moieties attached at the C3 and C20 position of PPD-type ginsenoside through the activity of extracellular glycosidase, rending them resistant to ginsenoside toxicity[273, 274]. In agreement, the removal of the sugar chain attached to C3 position has been shown to restrict the membrane binding of saponin to 3β-hydroxyl sterols[275]. The position and the number of sugar moieties of ginsenoside also influence their antifungal activity. Indeed, regarding the position of sugar moieties, protopanaxatriol-type ginsenoside fraction (PPT-GF; Re, Rg1) from the roots *Panax ginseng* C.A. Meyer shows higher growth inhibition against 5 ginseng non-pathogens as compared to protopanaxadiol-type ginsenoside fraction (PPD-GF; Rb2, Rc, Rd)[273]. Second, the antifungal activity of ginsenosides is negatively correlated with the number of their sugar moieties. Fungi membranes are disrupted to a higher extent after exposure to less polar ginsenoside (ginsenoside-Rk3, -Rh4, -Rh5) compared to polar ginsenosides (notoginsenodise-R1, ginsenoside Rg1, -Re, Rb2, Rd). One major reason could be that less polar ginsenosides interact more easily with fungal membranes as compared to more polar ginsenosides. Mechanistically, the interaction between ginsenosides isolated from Korean red ginseng with *C. albicans* membrane has been reported to decrease DPH fluorescence anisotropy and disrupt the structure of the cell membrane[226]. Interestingly, plant cells contain phytosterols such as campesterol, sitosterol and stigmasterol in their membranes, whereas fungal plant pathogens contain ergosterol, suggesting that targeting fungal sterols via ginsenoside synthesis seems to be an effective and non-toxic host defense strategy for plants to counter fungal infections[275].

3.4.6.2 Bacteria

With the abuse of antibiotics, the increased development of bacterial resistance to antibiotics raises interest in alternative therapies and particularly in

the therapeutic use of products isolated from plants. Plants have developed many mechanisms of defense to survive against fungal infection but also microbial invasion via the synthesis of saponins. Antimicrobial effects of ginseng have been described toward pathogenic Gram-positive and Gram-negative bacteria [276]. As observed in antifungal activities, less polar ginsenosides (-Rg2, -Rg3, -Rg6, -F4, -Rg5 and –Rk1) show higher antimicrobial activity against three bacteria species (*F. nucleatum*, *C. perfringens* and *P. gingivalis*) as compared to polar ginsenosides (-Rg1, -Rc, Rb2 and –Rd) by disrupting more easily bacterial membranes[277]. Interestingly, combination of Korean red ginsenosides and kanamycin antibiotics improves antibacterial activity against methicillin-resistant *S. aureus* (MRSA). The partial disruption of the bacterial membrane by ginsenosides is believed to facilitate the entry of kanamycin and could explain this synergistic antibacterial effects[225]. In addition, it has been reported that non-toxic dose of ginsenoside Rh2 enhances the susceptibilities of *S. aureus* and *E. coli* strains to ciprofloxacin antibiotic *in vitro* and *in vivo[278]*. This effect of Rh2 could be attributed to the increased accumulation of ciprofloxacin via the inhibition of NorA efflux pump embedded into bacteria membrane[279]. Regarding this activity, ciprofloxacin-loaded polymeric micelles (poloxamer/phosphatidylcholine/cholesterol) including ginsenoside Rg3 have been designed and shown to simultaneously inhibit P-gp efflux pump and improve ciprofloxacin solubility [280]. Since bacterial membranes do not possess sterols, it is tempting to speculate that the antibacterial activity of ginsenosides could result from interaction with haponoids (pentacyclic triterpenoids structurally similar to steroids) or from other unrelated mechanisms.

3.4.7 Conclusion

The membrane is a key target for ginsenosides, both through the modulation of essential membrane proteins and the reorganization of lipid bilayers. This review provides an overview of different studies investigating the physicochemical properties of different ginsenosides and their effects on membrane components embedded in both artificial and biological membranes. It highlights that ginsenosides exhibit many diverse effects, which could result from the following features. Firstly, more than hundred ginsenosides have been isolated and differ in their amphiphilic structure, conferring them specific and multiple membrane activities. Secondly, membrane activities of ginsenosides seem to change depending on the cell type which could be explained by differences of lipid membrane composition between cell lines. Thirdly, a single ginsenoside, by changing membrane dynamics, may alter a range of membrane proteins altering diverse cell signaling. Interestingly, the ability of several ginsenosides to suppress cell proliferation, induce apoptosis and inhibit efflux pumps suggest they could represent promising candidates for drug development in cancer cells as well as in

bacteria and fungi infections. However, few clinical trials have been undertaken in humans and the use of ginsenosides has been limited to cells and animal models, mainly due to their intrinsic hemolytic activity and low aqueous solubility[281]. Recently, a number of effort have been made on solving these problem by developing effective delivery systems and a variety of administration routes to improve the bioavailability of ginsenosides, resulting in remarkable improvements in their bioavailability.

Direct effects of ginsenoside	Ginsenoside	Methods	Models	Pharmacological consequences	Ref.
Membrane dynamics					
Compact the hydrophobic membrane core	Rh2	Fluorescence anisotropy of DPH	B16 melanoma cells	Induce flattening, increase adhesiveness to plastic surfaces, Agglutinability of B16 cells	[215]
Compact the hydrophobic membrane core Relax the interfacial packaging of the polar head of PL	Rh2	Fluorescence anisotropy of DPH and TMA-DPH	U937 leukemia cells	Inactive Akt and induce cancer cells apoptosis	[219]
Compact the hydrophobic membrane core	Rh2	Fluorescence anisotropy of DPH and TMA-DPH	B16 melanoma cells	Induce dendrite formation in melanoma cells	[222]
Increase membrane fluidity	Rb2, Rc, Rd Re, Rf, Rg1, Rg2, Rh2, PPD	Two-photon fluorescence microscopy with carboxy-laurdan	Hela cervical carcinoma cells	Active death receptors and induce cancer cells apoptosis	[221]
Compact the hydrophobic membrane core	Rh1	Fluorescence anisotropy of DPH	B16 melanoma cells	Do not induce cell morphology change and exert not effect on cell adhesiveness	[215]
Compact the hydrophobic membrane core	Rg3	Fluorescence anisotropy of DPH	Bovine chromaffin cells	Inhibit catecholamine secretion from cells stimulated by acetycholine	[223]

Compact the hydrophobic membrane core and the interfacial packaging of the polar head of PL	Rg3	Fluorescence anisotropy of DPH and TMA-DPH	KB V20C (resistant) and parental KB (sensitive) cells	Inhibit efflux pumps in KB V20C	[205]
Relax the hydrophobic membrane core	Re	Fluorescence anisotropy of DPH	Brain mitochondria membrane from Male Wistar rats	Protect rat brain against cerebral ischemia/reperfusion injuries	[224]
Relax the hydrophobic membrane core	Rg1	Fluorescence anisotropy of DPH	Old cortical cells from Wistar rats	Exhibit an antiaging action	[282]
Relax the hydrophobic membrane core	Korean red ginseng (Rb1, Rg1, Re, Rb2)	Fluorescence anisotropy of DPH	Candida Albicans	Disrupt the fungal membrane	[226]
Reduce the segmental mobility of the spin-labeled eggPC	Rc	Electron Spin Resonance	MLVs containing eggPC	Exhibit agglutinability toward eggPC vesicles	[283]
Reduce the segmental mobility of the spin-labeled eggPC	Rb2	Electron Spin Resonance	MLVs containing eggPC	Do not exhibit agglutinability toward eggPC vesicles	[283]
Interaction with rafts					
Redistribute lipid rafts	Rp1	DRM, immunofluorescence GM-1 staining	OVCAR-8 (sensitive), NCI/ADR-RES cells	Redistribue raft-associated MDR-1 protein	[228]

			(resistant)	Enhance doxorubicin accumulation in drug-resistant cells	
Disrupt the integrity of lipid rafts	Rg3	DRM, immunocytochemistry Flotillin-1 staining	CHO cells, mouse primary neurons Brains of mouse model with Alzheimer's disease	Reduce association of presenilin 1 (PS1) fragments with lipid rafts Inhibit **γ**-secretase activity decrease amyloid-β (Aβ) levels	[229]
Reduce cholesterol and lipid raft levels	Rh2	Amplex Red Cholesterol Assay Kit, immunofluorescence GM-1 staining	Mouse primary neurons	Reduce Aβ secretion, amyloid precursor protein (APP) endocytosis Improve learning and memory function in Alzheimer's disease	[230]
Reduce lipid rafts and caveolae levels Increase their internalization	Rh2	Immunofluorescence GM-1 and caveolin-1 staining, DRM	A431, MBA-MB-231, PC3 and HEK293 cells	Inactive raft-associated Akt signaling and induce cancer cells apoptosis	[204]
Disrupt the integrity of lipid rafts	Rb2, Rc, Rd Re, Rf, Rg1, Rg2, Rh2, PPD	Detergent-resistant membrane, immunofluorescence caveolae staining	Hela cervical carcinoma cells	Active death receptors and induce cancer cells apoptosis	[221]
Disrupt the integrity of lipid rafts	PPD	Immunofluorescence SM and CHOL staining, Western blot of lipid raft-associated proteins (IGF-1R, P-Akt)	K562, HT29 cells, K562-xenografted BALB/c nude mice	Active neutral SMase 2 and induce cancer cells apoptosis Reduce tumor volumes in xenograft mouse model	[232]

Membrane destruction and pore formation					
Disturb osmotic behavior of liposomes with or without Chol	Rb1	Absorbance measurement	MLVs composed of eggPC, PA with or without Chol	Induce liposomal membrane permeability	[218]
Disrupt the fungal membrane	Korean red ginseng (Rb1, Rg1, Re, Rb2)	Colony forming units (CFUs), fluorescence anisotropy of DPH	Candida Albicans	Decrease membrane potential and exhibit antifungal effects	[226]
Disrupt the bacterial membrane	Korean red ginseng (Rb1, Rg1, Re, Rb2)	Calcein release in liposome, colony forming units	Liposome composed of PC/PG (1:1), S. aureus, S. epidermidis, S. typhimurium	Enhance kanamycin activity and exhibit antibacterial effects	[226]
Form membrane pore	Rh2, Rg3	Measurement of the absorbance of the supernatant	Red blood cells	Induce hemolysis	[233]
Permeabilize lysosomal membrane	Octyl Ester derivative of Rh2	Acridine orange relocation	HepG2 liver cells	Release of cathepsin from lysosome to cytosol compartiment Induce cancer cells apoptosis	[284]
Disrupt the fungal membrane	Rg2, Rg3, Rg6, F4, Rg5, Rk1	Minimal fungicidal concentration (MFC),	E. floccosum, T. rubrum, T. mentagrophytes	Decrease membrane potential and exhibit antifungal effects	[277]
Disrupt the bacterial membrane	Rg2, Rg3, Rg6, F4, Rg5, Rk1	Minimal bactericidal concentration (MBC), cell constituents release into cell	F. nucleatum, C. perfringens, P. gingivalis	Decrease membrane potential and exhibit antibacterial effects	[277]

		suspension			
Interaction with membrane proteins					
Decrease the activity of raft-associated Akt	PPD	DRM	U87 MG glioma cells	Enhance the chemotoxicity of Paclitaxel or Vinblastine	[231]
Increase the activity of raft-associated Akt	PPD	DRM	N2a neuroblastoma cells	Attenuate the excitotoxicity of N-methyl-D- aspartate	[231]
Interact with 5-HT3A receptor and human Kv1.4 channel	Rg3	Ligand-gated ion currents measured via two-electrode voltage clamp technique, site-directed mutagenesis	Xenopus laevis oocytes	Inhibit 5-HT3A receptor-mediated ion currents and K+ currents flowing of the human Kv1.4 channel	[235, 285]
Interact with NMDA receptor	Rg3, Rh2	Ligand-gated ion currents measured via two-electrode voltage clamp technique	Cultured rat hippocampal neurons	Antagonize NMDA receptors	[238, 239]
Interact with the NorA efflux pump	Rh2	In silico molecular docking, Rhodamine 123 retention assay	S. aureus in vivo, S. aureus infected peritonitis mice	Promote ciprofloxacin accumulation	[279]
Interact with Na+/K+ ATPase	PPD, Rh2, Rg3	measurement of the inorganic phosphate liberated from ATP and molecular modeling and docking	Na+/K+-ATPase from the porcine cerebral cortex	Inhibit Na+/K+ ATPase activity Exhibit cardiac therapeutic effects	[199]
Bind to the P-gp efflux pump	Rg3	Rhodamine 123 retention assay and competition assay with [3H]azidopinen for binding to P-gp	Multidrug resistant P388/DOX cells	Block drug efflux and enhance anticancer drug accumulation	[258]

ROS production					
Attenuate lipid peroxidation	Re	Antioxidant enzymes and reactive oxygen species measurement	Ischemic brain tissues of male Wistar rats	Protect rat brain against cerebral ischemia/reperfusion injuries	[224]
Inhibit MPTP by free radical scavenging action	Rg3	ROS measurement	Isolated rat brain mitochondria	Exhibit neuroprotective effect after cerebral ischemia	[286]
Inhibit hydroxyl radical formation	Rd	ROS measurement	Rat model of focal cerebral ischemia	Exert neuroprotection in transient focal ischemia,	[287]
Inhibit lipid peroxidation	Rb1, Rg1	ROS measurement	Rat liver and brain microsomes	Prevent cardiac ischemia	[245]
Exhibit anti-oxidative effects	Rc > Rb1 and Re > Rd > R1 > Rg1 > Rb3 > Rh1	Measurement of the absorbance of the supernatant of the erythrocytes	2-amidinopropane hydrochloride) -induced hemolysis of erythrocytes	Reduce Hemolysis	[246]
Exhibit pro-oxidative effects	Rh2, Rg3	ROS measurement	Jurkat leukemia cells	Induce cancer cells apoptosis	[248]
Exhibit pro-oxidative effects	Rh4	ROS measurement	Human colorectal cancer xenograft mouse model	Inhibit tumor growth	[288]

Table 4. Physicochemical activities of ginsenosides and interaction with membranes.

CHAPTER II: AIMS AND STRATEGIES

As explained in the Introduction section, Chol and SM are able to cluster into domains (section 1.3.2.1) which could participate in cellular signaling related to cell survival/death (section 1.4.1) and migration/invasion (section 1.4.2) with potential implications in cancer development. Chol and SM therefore represent interesting targets for pharmacological agents to modulate these pathways. Among these, saponins attract more and more attention based on their biological activities including anticancer properties (section 3). In this study, we focus on the steroid saponin ginsenoside Rh2, one of the active principles of *Panax ginseng*. Rh2 exhibits the most potent anticancer activity. It has been reported that orally administered and subcutaneously injected Rh2 inhibits growth of human ovarian cancer cells transplanted into nude mice and significantly prolongs the survival times of the mice[289]. Mechanistically, Rh2 is the only ginsenoside (with the exception of PPD[232]) which has been reported to disrupt lipid rafts leading to apoptosis, via either the death receptor FAS oligomerization in human cervical cancer Hela cells or inactivation of the serine/threonine kinase Akt in human epidermoid carcinoma A431 and breast cancer MBA-MB-231 cells[204, 221]. However, the respective role of Chol and SM in the activity of Rh2 is still poorly understood. Our goal was thus to obtain detailed knowledge about the membrane-related effects and the apoptosis induced by Rh2 and to elucidate the respective importance of Chol and SM in this process.

For this purpose, in the first part of thesis, we decided to work on simplified model membranes. The great advantage of artificial model membranes is the ability to control their membrane composition allowing to understand the importance of specific lipids. Using Langmuir through, we evaluated the interaction of Rh2 with lipid monolayers composed of egg sphingomyelin (eSM), egg phosphatidylcholine (ePC), DOPC or Chol. Since lipid monolayers consist of only one lipid leaflet, we decided to use lipid vesicles (LUVs or GUVs) made of two lipid leaflets and composed of eSM (*i.e.* eSM:ePC, 1:1) or Chol (*i.e.* ePC:Chol, 1:1) or both of them (*i.e.* eSM:ePC:Chol, 1:1:1). Using LUVs, we measured the affinity of Rh2 with membranes (isothermal titration calorimetry) and examined its effect on different parameters: size (dynamic light scattering), fluidity (fluorescence anisotropy of diphenylhexatriene and generalized polarization of laurdan), fusion (R18 dequenching) and permeability (calcein release). In addition, GUVs allowed us to visualize the effects of Rh2 on lipid phase organization, shape deformation and permeability by fluorescence microscopy. Our results revealed that eSM promotes and accelerates membrane-related effects induced by Rh2 whereas

Chol slows down and depresses these effects. This first set of investigation is included in a first research paper as first author (Verstraeten SL et al, Scientific Report, 2019).

In the second part of this work, we turned our attention to biological membranes as a more relevant model than artificial membranes and studied the respective importance of membrane Chol and SM for the Rh2-induced apoptosis. To evaluate apoptosis, I benefited from another study ongoing when I joined the host laboratory and to which I contributed as a fourth author (Denamur S et al, Toxicology and Applied Pharmacology, 2016; Appendix). The aim was to assess the apoptosis induced by gentamicin, an aminoglycoside antibiotic used to treat serious and life-threatening infections caused by Gram-negative aerobes but which is nephrotoxic, a serious limiting factor in their daily use. To determine the effects of Chol in Rh2-induced apoptosis, I used three cell lines exhibiting differential membrane Chol levels: carcinomic human alveolar basal epithelial A549 > human monocytic leukemia THP-1 > U937 cells. In the three cell lines, non-depleted or depleted in Chol with methyl-β-cyclodextrin, we examined the time and concentration dependence of the Rh2-induced apoptosis and determined whether the Rh2-induced apoptosis could be Chol-dependent. Then, focusing on the Chol-auxotroph U937 cell line, we evaluated the role of SM in the Rh2-induced apoptosis through its hydrolysis by bacterial sphingomyelinase. After that, we studied the effect of Rh2 on PM fluidity measuring the DPH and TMA-DPH anisotropy and investigated the Rh2-induced intrinsic apoptotic pathway (mitochondrial membrane potential, caspase-9 and -3). Finally, the time course of Rh2 uptake was investigated in cells depleted or not in Chol by HPLC MS/MS. This work evidenced that membrane Chol, contrary to SM, could delay the apoptotic activity of ginsenoside Rh2. This second set of investigation is included in a second research paper as first author (Verstraeten SL et al, Toxicology and Applied Pharmacology, 2018). Results obtained in biological membranes correlated with those obtained in artificial membranes and clearly highlight the importance of membrane lipid nature for the Rh2 activity. These results reveal the critical role of SM in membrane-related effects induced by Rh2 while Chol seems to depress the sensitivity of the membrane to Rh2. Lipid specificity is a key factor for the detailed understanding of the penetration and activity of Rh2.

In the third part of this thesis, we initiated a long-term study aiming at evaluating whether Rh2 could be used as a potential agent for breast cancer treatment. Before that, it was crucial to compare the different breast cancer cell lines for their migration/invasion potential but also for their membrane lipid composition,

organization and biophysical properties. We chose as cell lines the human mammary epithelial MCF10A cell line series, which offers the same genetic background but an increasing malignancy potential: the normal human mammary epithelial cells MCF-10A, the pre-malignant MCF-10AT and the malignant MCF-10CaCl1[290]. We investigated the Akt phosphorylation, spontaneous migration, oriented motility and invasion, membrane stiffness and SM and Chol content in the three cell lines. We also started to characterize lipid organization in these cells using fluorescent toxin fragments and insertion of fluorescent BODIPY-lipid analogs in the PM. The identification of lipid domains potentially contributing to tumor cell motility and invasion is essential for understanding how motility is initiated in tumor cells and could provide new targets for the treatment of metastatic cancer. Our ultimate goal will be to determine whether ginsenoside Rh2 could affect tumor migration by targeting specific lipid domains. The data of this third set of investigations is included in a third research paper as co- author and which will be continued by Mauriane Maja (Tyteca's group, DDUV Institute).

CHAPTER III: RESULTS

1. Elucidate the respective importance of cholesterol and sphingomyelin in the membrane-related effects of Rh2 in artificial membrane models

In the first part of this work, we found that Rh2 interacts more favorably with monolayers composed of eSM and DOPC than with Chol and ePC. In LUVs, the interaction of Rh2 increases vesicle size, decreases membrane fluidity, induces membrane fusion and permeability. The activity of Rh2 is highly dependent on the lipid composition. For instance, the eSM:ePC composition is the more susceptible to the membrane-perturbing effects induced by Rh2, followed by eSM:ePC:Chol and then by ePC:Chol liposomes. On Giant Unilamellar Vesicles (GUVs), we evidenced that Rh2 generates positive curvatures in eSM-containing GUVs and small buds followed by intra-luminal vesicles in eSM-free GUVs. Our data indicate that eSM promotes and accelerates membrane-related effects induced by Rh2 whereas Chol slows down and depresses these effects.

SCIENTIFIC REPORTS

OPEN

The activity of the saponin ginsenoside Rh2 is enhanced by the interaction with membrane sphingomyelin but depressed by cholesterol

Received: 3 October 2018
Accepted: 12 April 2019
Published online: 13 May 2019

Sandrine L. Verstraeten[1,2], Magali Deleu[3], Maria Janikowska-Sagan[4], Emily J. S. Claereboudt[3], Laurence Lins[3], Donatienne Tyteca[2] & Marie-Paule Mingeot-Leclercq[1]

The membrane activity of some saponins, such as digitonin or alpha-hederin, is usually attributed to their interaction with membrane cholesterol (Chol). This contrasts with our recent publication showing that Chol, contrary to sphingomyelin (SM), can delay the cytotoxicity of the saponin ginsenoside Rh2, challenging the usual view that most saponins mediate their membrane effects through interaction with Chol. The aim of the present study was to elucidate the respective importance of Chol and SM as compared to phosphatidylcholine (PC) species in the membrane-related effects of Rh2. On simple lipid monolayers, Rh2 interacted more favorably with eggSM and DOPC than with Chol and eggPC. Using Large Unilamellar Vesicles (LUVs) of binary or ternary lipid compositions, we showed that Rh2 increased vesicle size, decreased membrane fluidity and induced membrane permeability with the following preference: eggSM:eggPC > eggSM:eggPC:Chol > eggPC:Chol. On Giant Unilamellar Vesicles (GUVs), we evidenced that Rh2 generated positive curvatures in eggSM-containing GUVs and small buds followed by intra-luminal vesicles in eggSM-free GUVs. Altogether, our data indicate that eggSM promotes and accelerates membrane-related effects induced by Rh2 whereas Chol slows down and depresses these effects. This study reconsiders the theory that Chol is the only responsible for the activity of saponins.

Cholesterol (Chol) and sphingomyelin (SM) are essential components of mammalian plasma membranes, constituting around 35 and 25% of total lipids present in the outer plasma membrane leaflet, respectively[1]. It was for a long time believed that these lipids are randomly distributed into the plasma membrane[2]. However, studies over the last decades have suggested for the presence of transient nanometric domains enriched in Chol and SM, forming a liquid-ordered (L_o) phase[3–5]. These highly ordered membrane domains have been proposed to serve as platforms for signaling pathways involved in cell adhesion and migration as well as cell survival and proliferation with potential implications in cancer development[6]. Altogether, this makes the lipids present in L_o domains an interesting target for pharmacological agents to modulate these pathways.

Among these, saponins, amphiphilic compounds widely found in plants, are attracting more and more attention based on their numerous biological activities including anticancer properties. Many of these effects seem to be related to their ability to interact and modify the plasma membrane properties, such as fluidity or permeability[7]. These membrane-related mechanisms are not completely understood yet, but the activity of some saponins such as alpha-hederin[8,9], digitonin[10,11] and alpha-tomatine[12,13] have been attributed to their interaction with membrane Chol by forming complexes[14].

[1]Université catholique de Louvain, Louvain Drug Research Institute, Cellular & Molecular Pharmacology Unit, 1200, Brussels, Belgium. [2]Université catholique de Louvain, de Duve Institute, Cell Biology Unit, 1200, Brussels, Belgium. [3]Université de Liège (ULiège), Gembloux-Agro-Bio Tech, Molecular Biophysics at Interfaces Unit, 5030, Gembloux, Belgium. [4]Jagiellonian University, Faculty of Physics, Astronomy and Applied Computer Science, 30-348, Krakow, Poland. Correspondence and requests for materials should be addressed to M.-P.M.-L. (email: marie-paule.mingeot@uclouvain.be)

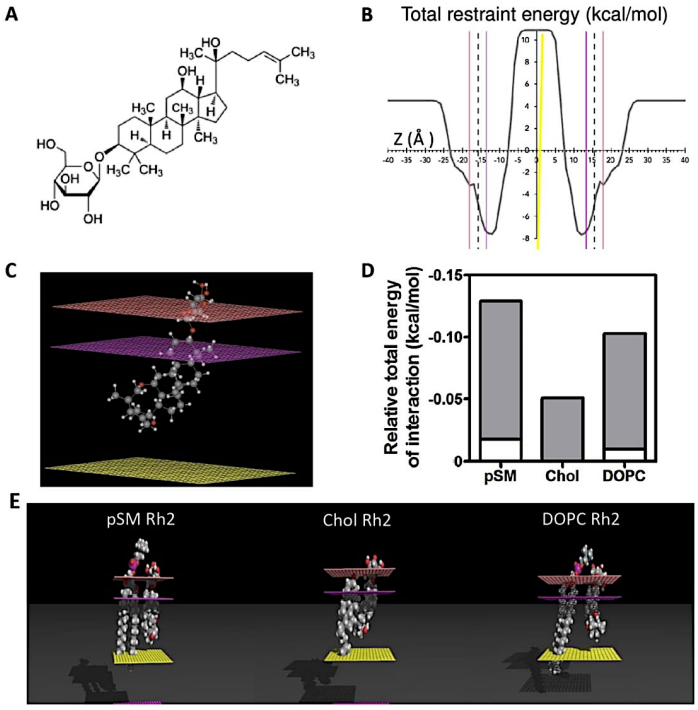

Figure 1. Rh2 interacts more favorably with membrane pSM and DOPC than with Chol. (**A**) Chemical structure of Rh2. (**B**,**C**) IMPALA simulation of the most favorable position of Rh2 into an implicit membrane 36 Å thick. (**B**) Energy profile of Rh2 traversing an implicit lipid bilayer. X-axis corresponds to the position of the center of mass of the saponin across the bilayer expressed in Ångström. Y-axis corresponds to total restraint energy expressed in kcal/mol. The solid vertical lines in different colors represent the different planar surfaces from the left to the right: water/membrane interface (pink), the lipid polar head/alkyl chain interface (purple), and the center of the bilayer (yellow). The vertical dotted line at ±15.75 Å corresponds to the interface between the hydrophobic and hydrophilic parts of the bilayer. (**C**) The most stable position of Rh2 into the implicit bilayer. The different planar surfaces represent the same solid vertical lines described in (**B**). Carbon atoms are dark grey, Hydrogens white, Nitrogens light blue and Oxygens red. (**D**,**E**) Interaction between Rh2 and pSM, Chol or DOPC was calculated by Hypermatrix docking method. (**D**) Relative total energy of interaction values for the interaction between a central molecule Rh2 and surrounding pSM, Chol or DOPC. Grey and white portions are the apolar and polar components of the energies, respectively. (**E**) Molecular assemblies of a Rh2 molecule interacting with a single pSM, Chol or DOPC molecule.

In this study, we focus on the ginsenoside Rh2 (structure presented in Fig. 1A), found in *Panax ginseng* and responsible to some extent for its medicinal properties and health benefits[15]. This well-known steroid saponin has been reported to disrupt L_o domains leading to apoptosis, via either the death receptor FAS oligomerization in human cervical cancer Hela cells[16] or inactivation of the serine/threonine kinase Akt in human epidermoid carcinoma A431 and breast cancer MBA-MB-231 cells[16,17]. In addition, our recent publication showed that the cytotoxicity of Rh2 is accelerated by membrane Chol depletion but delayed by SM depletion in human monocytic leukemia U937 cells[18]. These observations led to the hypothesis that, contrary to membrane SM, Chol could delay the activity of ginsenoside Rh2. The aim of the present study was thus to obtain detailed knowledge about the membrane-related effects of Rh2 and to elucidate the respective importance of Chol and SM.

To these aims, we first evaluated the interaction of Rh2 with membrane *in silico* and Langmuir experiments on simple lipid monolayers composed of egg sphingomyelin (eSM), egg phosphatidylcholine (ePC),

LUVs	K (mM^{-1})	ΔH ($KJ.mol^{-1}$)	TΔS ($KJ.mol^{-1}$)	ΔG ($KJ.mol^{-1}$)
eSM	18.03 ± 7.11	15.88 ± 3.31	49.91 ± 2.43	−34.03 ± 0.93
ePC	4.95 ± 4.65	1.06 ± 0.17	29.42 ± 4.46	−28.36 ± 4.29
DOPC	33.67 ± 1.80	−1.29 ± 0.20	34.47 ± 0.09	−35.75 ± 0.13

Table 1. Preferential binding of Rh2 to DOPC > eSM > ePC vesicles is accompanied by exo- (DOPC) or endothermic reactions (eSM, ePC). Thermodynamic parameters measured by isothermal titration calorimetry for the binding of Rh2 to LUVs composed of eSM, ePC or DOPC at a Rh2/lipid ratio of 0.02 at 25 °C.

1,2-dioleoyl-sn-glycero-3-phosphocholine (DOPC) or Chol. In a second step, we evaluated the consequences of Rh2 membrane adsorption on liposome size and a set of biophysical parameters (fluidity, fusion, lipid phase organization, shape deformation and permeability) determined on Large Unilamellar Vesicles (LUVs) or Giant Unilamellar Vesicles (GUVs) containing eSM (*i.e.* eSM:ePC, 1:1) or Chol (*i.e.* ePC:Chol, 1:1) or both of them (*i.e.* eSM:ePC:Chol, 1:1:1).

Data provided in our paper indicate that, in contrast to eSM, Chol slows down and depresses the membrane-related effects induced by Rh2. To the best of our knowledge, this study is the first to reveal the protective role of Chol in membrane-related effects induced by Rh2.

Results

Rh2 interacts more favorably with pSM and DOPC than Chol as revealed by molecular modeling. Firstly, molecular modeling was used to investigate the structure and molecular interactions of Rh2 with rigid 3D structures of palmitoylsphingomyelin (pSM), Chol and DOPC. The IMPALA method was used to predict the potential insertion of Rh2 into an implicit lipid bilayer[19]. The apolar aglycone moiety of Rh2 was deeply embedded into the bilayer as indicated by its most energetically stable position at ±12 Å (Fig. 1B). Interaction energies between the saponin and the aqueous medium outside of the membrane were highly positive, thus less favorable, suggesting that the most favorable state of Rh2 was within the bilayer (Fig. 1C). In addition, high energies were predicted at the bilayer center, suggesting that Rh2 would not be able to cross the bilayer. A docking method called Hypermatrix[20] was used to calculate the energies of interaction between the central molecule, Rh2, and the surrounding lipids. These molecular assemblies showed more favorable interactions between Rh2 and pSM or DOPC in comparison to Chol molecules (Fig. 1D,E). Calculations predicted that the interactions were mainly apolar in nature (grey bars in Fig. 1D).

Rh2 binds to lipid bilayer vesicles with the following preference: DOPC > eSM > ePC. Isothermal Titration Calorimetry (ITC) experiments were then applied to thermodynamically quantify the interaction of Rh2 with liposomes containing eSM, ePC or DOPC. Notice however that formation of liposomes with Chol was not achieved. LUVs were injected in steps into the sample cell containing Rh2 (Rh2/lipid ratio of 0.02) at 25 °C and thermodynamic parameters were determined (Table 1). The free energy of binding values (ΔG) were negative and relatively similar for the three compositions examined, indicating a favorable and spontaneous interaction. The entropy values (ΔS) were all positive, clearly indicating that the binding of Rh2 with the three types of vesicles was entropically favored but with differences depending on the lipid (eSM > DOPC > ePC). Regarding binding constants, the affinities of Rh2 with lipid bilayers occurred with the following preference: DOPC > eSM > ePC. This could be linked with the difference between DOPC and eSM or ePC liposomes in their interactions with Rh2 as revealed by the enthalpy values (ΔH). For instance, the interaction of Rh2 with eSM and ePC was endothermic (ΔH > 0) with higher positive enthalpic changes of eSM compared to ePC whereas Rh2 binding with DOPC was found to be exothermic (ΔH < 0).

Rh2 adsorbs to a higher extent with eSM and DOPC than with Chol and ePC monolayers. To explore Rh2:Chol interaction in comparison with that of Rh2 with eSM, ePC and DOPC, we pursued our study on lipid monolayers made of these lipids by measuring adsorption kinetics via the Langmuir trough method. Lipids were spread at the water-air interface to obtain an initial surface pressure of approximately 30 ± 2 mN/m. Rh2 was then injected into the buffer subphase at the final concentration of 10 μM and its adsorption to the different films was determined by measuring the surface pressure (Π) variations as a function of time with a constant film area. The injection of Rh2 beneath the eSM, Chol, ePC or DOPC monolayers gave rise to a rapid increase of Π over time (Fig. 2A). The ΔΠ upon the adsorption of Rh2 to lipid monolayers was observed with the following preference: eSM > DOPC > ePC and Chol monolayers (Fig. 2B) in agreement with results from Hypermatrix.

Rh2 increases eSM packing and transition temperature. Since Rh2 was able to highly adsorb to eSM monolayers, we then determined the effect of Rh2 on the eSM hydration and main transition temperature by evaluating the generalized polarization (GPex) of Laurdan upon increasing temperatures (Fig. 3)[21,22]. A transition temperature (T_m) around 41 °C was observed for eSM, *i.e.* close to the values reported in the literature using differential scanning calorimetry[23,24]. A Rh2/lipid ratio of 1 increased the value of Tm to 45 °C. In addition, whatever the temperature, the GPex was higher in presence of Rh2 suggesting that the ginsenoside decreased hydration of eSM. Thus, we suggest that upon addition of Rh2, the packing order would be reinforced giving rise to lower lipid lateral diffusion coefficients. These results are in agreement with the impairment of eSM:water hydrogen-bonds and packing induced by Rh2 as suggested by ITC.

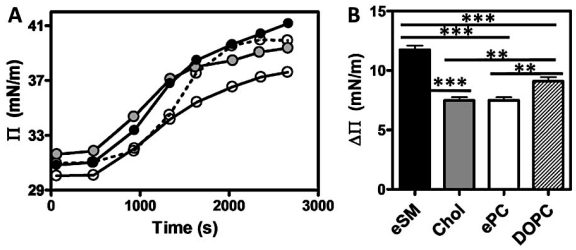

Figure 2. Rh2 adsorbs to a higher extent with eSM and DOPC than with Chol and ePC monolayers. Adsorption kinetics recorded at 25 °C of Rh2 on pure lipids (eSM (black), Chol (grey), ePC (white), DOPC (dotted line)). (**A**) Surface pressure – time (Π – t) curves for pure lipid monolayers at 30 ± 2 mN/m initial surface pressure recorded directly after the injection into the buffer subphase of Rh2 at the final concentration of 10 μM. (**B**) ΔΠ is the difference between the final and initial surface pressures. The curves are representative of three independent experiments and histogram data are means of these triplicated assays. One-way ANOVA with Bonferroni's multiple comparison post test. $^{**}p < 0.01$; $^{***}p < 0.001$.

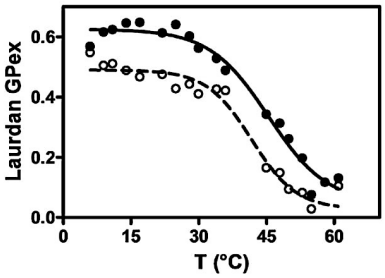

Figure 3. Rh2 increases eSM packing and transition temperature. Laurdan generalized polarization (GPex) was assessed at multiple temperatures from 4 to 60 °C in LUVs composed of eSM combined with Laurdan (0.5% mol) and treated for 5 min with 1% DMSO (dashed line) or at a Rh2/lipid ratio of 1 (black line). The λ_{ex} was set at 340 nm and the λ_{em} at 440 and 490 nm. The lines correspond to a non-linear regression (Hill's function) of data values and the inflexion points correspond to the transition temperature. The curves are representative of two independent experiments.

Rh2 adsorption on mixed lipid monolayers is enhanced in the presence of eSM and the absence of Chol. We next investigated the interaction of Rh2 with binary or ternary lipid systems. We first determined if and how Rh2 could adsorb to lipid monolayers made of either eSM:ePC (1:1), ePC:Chol (1:1) or eSM:ePC:Chol (1:1:1). Rh2 increased the Π within 500 s in eSM:ePC monolayer but only after 1400 s in monolayers containing Chol (Fig. 4A). A plateau was observed in all conditions at 2600 s but a higher ΔΠ was measured for eSM:ePC as compared to eSM:ePC:Chol and ePC:Chol monolayers (Fig. 4B). These data indicated that Rh2 adsorbed on mixed lipid monolayers with the following preference: eSM:ePC > eSM:ePC:Chol and ePC:Chol membrane.

Rh2 increases the size of LUVs containing eSM but no Chol at a low Rh2/lipid ratio. Having shown the favorable adsorption of Rh2 with mixed lipid monolayers in the presence of eSM and the absence of Chol, we then turned our attention to mixed lipid bilayers as a more relevant model system. We first assessed the size of LUVs by dynamic light scattering (Fig. 5). At a Rh2/lipid ratio of 0.4, the size of eSM:ePC liposomes increased from ~140 to ~190 nm, while vesicles containing Chol remained unchanged. However, at a Rh2/lipid ratio of 2, the size of vesicles increased regardless of the liposome composition with an average vesicle diameter of ~225, ~210 and ~190 nm for eSM:ePC, eSM:ePC:Chol and ePC:Chol, respectively. These results indicated that Rh2 increased more favorably the LUV size in the presence of eSM and the absence of Chol in agreement with the preferential binding of Rh2 with monolayers containing eSM but no Chol (Fig. 4).

Rh2 increases membrane rigidity in the presence of eSM and the absence of Chol at a low Rh2/lipid ratio. To next determine if Rh2 could affect membrane biophysical properties to a differential extent

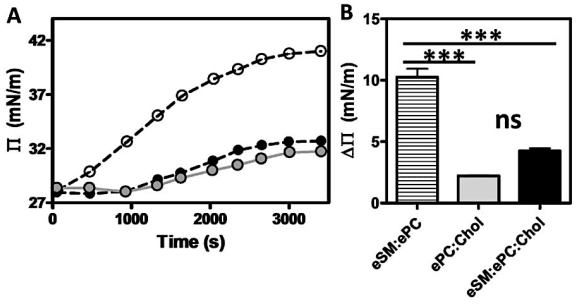

Figure 4. Rh2 adsorbs to a higher extent with complex lipid monolayers containing eSM but no Chol. Adsorption kinetics recorded at 25 °C of Rh2 on mixed lipids (eSM:ePC (striped bars), ePC:Chol (grey bars), eSM:ePC:Chol (black bars)). (**A**) Surface pressure – time (Π – t) curves for mixed lipid monolayers at 30 ± 2 mN/m initial surface pressure recorded directly after the injection into the buffer subphase of Rh2 at the final concentration of 10 μM. (**B**) ΔΠ is the difference between the final and initial surface pressures. The curves are representative of three independent experiments and histogram data are means of these triplicated assays. One-way ANOVA with Bonferroni's multiple comparison post test. ns: non-significant; ***$p < 0.001$.

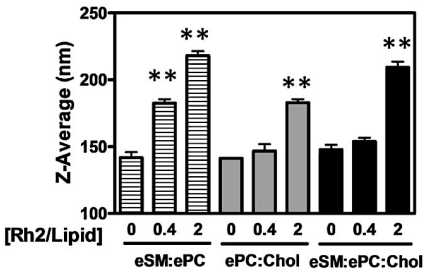

Figure 5. LUV size is increased at a low Rh2/lipid ratio in the presence of eSM and the absence of Chol. LUVs composed of eSM:ePC (1:1, striped bars), ePC:Chol (1:1, grey bars) or eSM:ePC:Chol (1:1:1, black bars) were incubated for 5 min with 1% DMSO or increasing Rh2/lipid ratios at 25 °C and vesicle size was determined by dynamic light scattering. Data are means of triplicated assays. One-way ANOVA with Dunnett's post tests to compare control *versus* Rh2-treated LUVs. **$p < 0.01$.

based on membrane composition, we started by evaluating membrane fluidity by the Laurdan generalized polarization (GPex; Fig. 6A) and the DPH fluorescence anisotropy (r; Fig. 6B) on the three liposome compositions. Laurdan locates at the level of the lipid glycerol backbone and allows to detect variations in membrane phase properties through its sensitivity to the environment polarity[22] while the DPH probe is in the hydrophobic core of the membrane and is sensitive to changes in lipid acyl chain physical properties[25]. The increase of these parameters indicates a higher rigidity in the lipid core region. In the absence of Rh2, membranes composed of eSM:ePC, ePC:Chol and eSM:ePC:Chol were characterized as the more fluid to the more rigid. After 5 min of incubation with Rh2 at a 0.4 molar ratio, GPex and anisotropy values were increased in Chol-free liposomes (eSM:ePC) but not in Chol-containing liposomes (ePC:Chol and eSM:ePC:Chol). At a Rh2/lipid molar ratio of 1, Rh2 significantly increased the eSM:ePC:Chol membrane rigidity whereas ePC:Chol exhibited no significant rigidity increase as compared to the control condition. A Rh2/lipid molar ratio of 2 was needed to increase the rigidity of the ePC:Chol system. Thus, it clearly appears that after addition of a low Rh2/lipid ratio, membrane rigidity only increased in the presence of eSM and the absence of Chol.

Rh2 induces membrane fusion to a faster and higher extent in the absence of Chol. We next evaluated the ability of Rh2 to induce membrane fusion by using the self-quenching probe R_{18} (octadecyl rhodamine B chloride). Fusion of R_{18}-labeled liposomes was monitored via the increase of fluorescence over time,

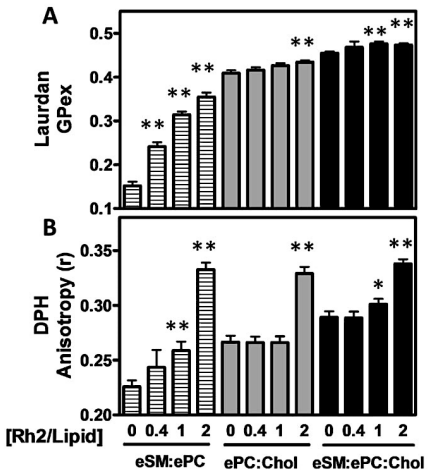

Figure 6. Membrane rigidity is increased at a low Rh2/lipid ratio in the presence of eSM and the absence of Chol. LUVs composed of eSM:ePC (1:1, striped bars), ePC:Chol (1:1, grey bars) or eSM:ePC:Chol (1:1:1, black bars) combined with Laurdan (0.5% mol, **A**) or DPH (0.5% mol, **B**) were incubated for 5 min with 1% DMSO or increasing Rh2/lipid ratios at 25 °C. Laurdan generalized polarization (GPex) and DPH fluorescence anisotropy (r) were measured following Rh2 treatment. The λ_{ex} was respectively set at 340 nm (Laurdan) and 365 nm (DPH) and the λ_{em} at 440 and 490 nm (Laurdan) and 425 nm (DPH). Results are means of three independent experiments in triplicates. One-way ANOVA with Dunnett's post tests to compare control *versus* Rh2-treated LUVs. *$p < 0.05$; **$p < 0.01$.

which results from the relief of R_{18} self-quenching due to the decrease in its surface density. At a Rh2/lipid ratio of 0.4 which increased the membrane rigidity in eSM:ePC system (Fig. 6), no R_{18} dequenching was observed (Fig. 7, ratio of 0.4). In contrast, at higher Rh2/lipid ratios, a plateau was reached after 25 s for all liposome compositions (Fig. 7, ratios of 1, 2 and 4). Importantly, Rh2 provoked faster and higher increase of R_{18} dequenching over time in Chol-free liposomes (eSM:ePC) as compared to Chol-containing liposomes (eSM:ePC:Chol and ePC:Chol). These results suggested that Rh2-induced membrane fusion to a faster and higher extent in the absence of Chol.

Rh2 accelerates liposome permeability in the presence of eSM and the absence of Chol. To investigate if the insertion of Rh2 into the membrane could induce membrane permeability, the release of calcein from LUVs was measured. Membrane permeabilization is evaluated by measuring the increase of fluorescence emission of LUVs entrapping self-quenched calcein in case of release across the permeabilized membrane. At a Rh2/lipid molar ratio of 4 for which Rh2 was able to induce membrane fusion (Fig. 7), there was no calcein release (Fig. 8, ratio of 4). At a ratio of 10, the fluorescence profile of the three types of liposomes can be discriminated. For instance, after 50 s of incubation with Rh2 (at which a plateau was obtained), 50% of calcein was released from eSM:ePC, ~25% from eSM:ePC:Chol while no release was measured from ePC:Chol liposomes (Fig. 8, ratio of 10). Treatment with a Rh2/lipid ratio of 20 induced a time-dependent increase of fluorescence (Fig. 8, ratio of 20). These results showed that Rh2 accelerated membrane permeability in the presence of eSM and the absence of Chol.

Rh2 induces positive membrane curvature in the presence of eSM and small buds followed by intra-luminal vesicles in its absence. We then took benefit from the resemblance of GUVs with cell membranes in terms of size and membrane curvature to visualize if Rh2 could change the GUV morphology. To this aim, GUVs were labeled with 1,2-dioleoyl-sn-glycero-3-phosphoethanolamine-N-(lissamine rhodamine B sulfonyl) (Rhod-PE, red channel) and N-(7-Nitrobenz-2-Oxa-1,3-Diazol-4-yl)-1,2-Dihexadecanoyl-sn-Glycero-3-Phosphoethanolamine (NBD-PE, green channel) to probe the liquid-disordered (L_d) and liquid-ordered (L_o) phases, respectively[26]. The time course of morphology changes was studied by incubating GUV suspensions with a fixed Rh2/lipid ratio of 3, for which membrane fusion but not permeability occurred (see above results). Control GUVs exhibited a spherical shape with no detectable morphology changes for the whole duration of the experiment (data not shown). In control eSM:ePC GUVs, solid-ordered phases (S_o) were observed (dark areas, white arrows at Fig. 9A, 0 min), as expected[27,28]. Following the same GUV upon addition of Rh2, the progressive formation of positive membrane curvature was accompanied by the progressive vesicle budding after 1 and 2 min

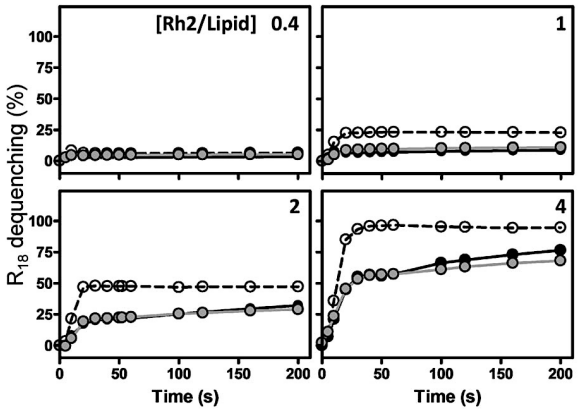

Figure 7. Rh2-induced membrane fusion occurs to a faster and higher extent in the absence of Chol. LUVs composed of eSM: PC (1:1, dashed lines), ePC:Chol (1:1, grey lines) or eSM:ePC:Chol (1:1:1, black lines) labeled with R_{18} were incubated with increasing Rh2/lipid ratios (indicated in the top right corner of each graph) at 25 °C. Membrane fusion of LUVs was assessed by R_{18} fluorescence dequenching. The change of fluorescence intensity was measured during 200 s, using λ_{ex} and λ_{em} at 560 nm and 590 nm, respectively. Fluorescence intensities were normalized as described in ≪Material and methods≫. The results are means of two independent experiments in triplicates.

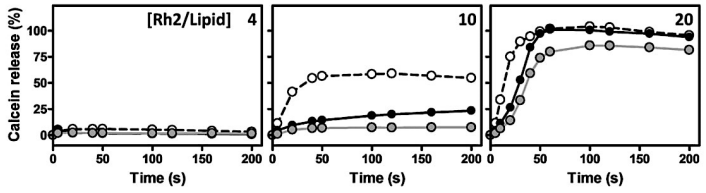

Figure 8. Rh2-induced membrane permeability is faster in the presence of eSM and the absence of Chol. LUVs composed of eSM:ePC (1:1, dashed lines), ePC:Chol (1:1, grey lines) or eSM:ePC:Chol (1:1:1, black lines) entrapping calcein at self-quenching concentrations were incubated with increasing Rh2/lipid ratios (indicated in the top right corner of each graph) at 25 °C. Membrane permeability was determined by the release of calcein from LUVs. The changes of fluorescence intensities were measured during 200 s, using λ_{ex} and λ_{em} at 472 nm and 512 nm, respectively. Fluorescence intensities were normalized as described in ≪Material and methods≫. Results are means of three independent experiments in triplicates.

(Fig. 9A, 1 and 2 min). Then, we were able to evidence membrane fusion and fission from 5 to 8 min (Fig. 9A, 5 to 8 min). In ePC:Chol GUVs, no phase separation was observed in the absence of Rh2 (Fig. 9B, 0 min). After 1 min, Rh2 promoted the formation of small buds (grey arrows) around the membrane that remained connected to the parent GUV, consistent with the induction of membrane curvature changes (Fig. 9B, 1 min). After 9 min, the small buds progressively disappeared but inward budding of GUV membranes appeared (white arrowheads at Fig. 9B, 9 min), leading to intra-luminal vesicles (ILVs) after 10 min (grey arrowheads at Fig. 9B, 10 min). In eSM:ePC:Chol, lipid phase separation was observed, as expected[23,28] (Fig. 9C, 0 min). Over the course of Rh2 treatment, positive membrane curvature occurred and L_d domain preferentially localized into these highly curved domains (Fig. 9C, 1 and 10 min). These results suggested that the insertion of Rh2 into the membrane promoted positive membrane curvature in the presence of eSM and the formation of small buds followed by ILV formation in the absence of eSM.

Rh2-induced morphology changes are not directly associated with membrane permeabilization. To determine the potential link between GUV morphology changes and Rh2-induced membrane permeability,

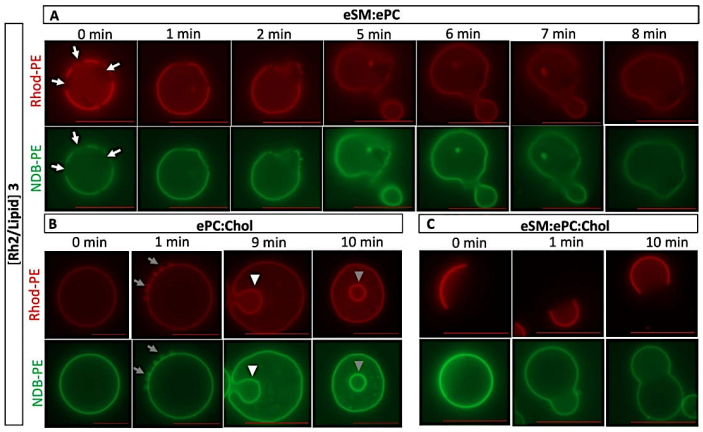

Figure 9. Rh2 induces positive membrane curvature in the presence of eSM and small buds followed by intra-luminal vesicles in its absence. GUVs composed of eSM:ePC (**A**), ePC:Chol (**B**) and eSM:ePC:Chol (**C**) were labeled with Rhod-PE (red) and NBD-PE (green) to reveal the liquid-disordered (L_d) and liquid-ordered (L_o) phases, respectively. GUVs were incubated with 1% DMSO (control, 0 min) or Rh2/lipid ratio of 3 and visualized at the indicated times at room temperature with a Zeiss wide-field fluorescence microscope (Observer.Z1) using a plan-Apochromat 40x/1.4 oil Ph3 objective. White arrows point to solid-ordered phases (S_o), grey arrows to small buds, white arrowheads to inward membrane budding and grey arrowheads to intra-luminal vesicles. Scale bars, 20 µm. Images are representative of two independent experiments.

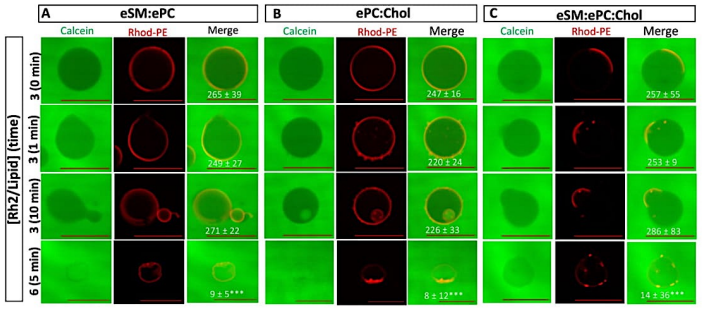

Figure 10. Morphology changes lead to visible membrane permeability only at a Rh2/lipid ratio of 6. GUVs composed of eSM:ePC (**A**), ePC:Chol (**B**) or eSM:ePC:Chol (**C**) were labeled with Rhod-PE (red) and diluted in 0.2 M glucose supplemented with 20 µM calcein (green). GUVs were incubated with either 1% DMSO (line 1) or with Rh2 at a Rh2/lipid ratio of 3 after 1 or 10 min (lines 2 and 3, respectively), or of 6 for 5 min (line 4) at 22 °C. The difference of green fluorescence intensities between outside and inside vesicles was measured and indicated in the merge panel. GUVs were visualized by confocal microscope with Axio Observer 1 inverted microscope equipped with a spinning disk microscope. Scale bars, 20 µm. One-way ANOVA with Bonferroni's multiple comparison. ***$p < 0.001$. Images are representative of two independent experiments and at least 15 GUVs were analyzed per experiment.

GUVs were placed in IBIDI chambers filled with glucose and calcein and were observed by confocal microscopy. Control GUV membranes containing sucrose were impermeable to free calcein present in the solution, showing a difference of fluorescence intensity between outside and inside of the GUVs (values noted in the merge panels;

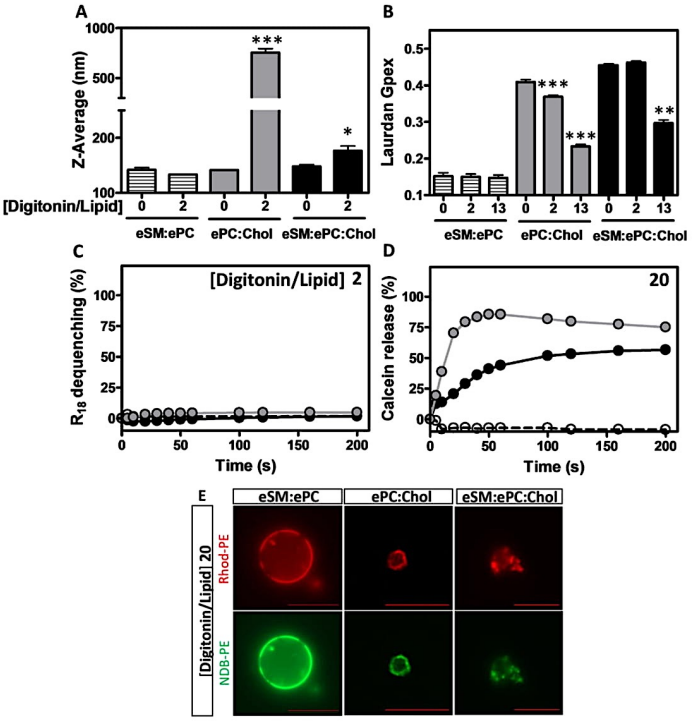

Figure 11. Digitonin changes membrane biophysical properties in a Chol-dependent manner. (**A**–**D**) LUVs composed of eSM:ePC (1:1, striped bars or dashed lines), ePC:Chol (1:1, grey bars or lines) or eSM:ePC:Chol (1:1:1, black bars or lines) were incubated with 1% DMSO or increasing digitonin/lipid ratios as indicated at 25 °C. (**A**) LUV size was determined by dynamic light scattering. Unpaired t-test was used to compare control *versus* digitonin-treated LUVs. (**B**) Fluidity was determined by GPex values on LUVs labeled with Laurdan. One-way ANOVA with Dunnett's post tests to compare control *versus* digitonin-treated LUVs. *$p < 0.05$; **$p < 0.01$; ***$p < 0.001$. (**C**,**D**) Membrane fusion and permeability were assessed by R_{18} fluorescence dequenching (**C**) and calcein self-quenching release (**D**), respectively. All the results are means of two independent experiments in triplicates. (**E**) GUVs composed of eSM:ePC, ePC:Chol or eSM:ePC:Chol were labeled with Rhod-PE (red) and NBD-PE (green) and were incubated with a digitonin/lipid ratio of 20 at room temperature. After 2 min following digitonin treatment, pictures were taken with a Zeiss wide-field fluorescence microscope (Observer.Z1) using a plan-Apochromat 40x/1.4 oil Ph3 objective. Scale bars, 20 μm. Images are representative of two independent experiments.

Fig. 10 A–C; line 1). This difference was maintained for the whole duration of the incubation with DMSO (data not shown). At a Rh2/lipid ratio of 3 and in the presence of eSM, the membrane budding induced by Rh2 reported in Fig. 9A,C was clearly visible but did not allow the entry of calcein into the GUVs (Fig. 10A,C; lines 2 and 3). In ePC:Chol GUVs, the formation of calcein-free small buds mediated by outward budding of GUV membranes was observed already after 1 min (Fig. 10B; line 2) while the formation of ILVs was noticed after 10 min (Fig. 10B; line 3). The difference of fluorescence intensity between outside the GUVs and inside those ILVs was 80 ± 36 which was lower than the difference between outside and inside control GUVs. This indicated that the calcein contained in the solution was encapsulated inside small vesicles during their formation, consistent with the formation of calcein-containing ILVs through inward indentation of the limiting GUV membrane[29]. Thus, Rh2-induced morphology changes were not directly associated with membrane permeability. A Rh2/lipid ratio of 6 was needed to induce wrinkled borders and entry of calcein through the membrane of the three GUV compositions, leading to

the suppression of difference of fluorescence intensities between outside and inside of GUVs (Fig. 10A–C; line 4). The latter results are compatible with the creation of membrane pores by Rh2 whatever the GUV composition.

In contrast to Rh2, digitonin modulates membrane biophysical properties in a Chol-dependent manner. Altogether, the data reported above indicated that Rh2 modified to a higher extent biophysical properties of LUVs in the presence of SM and the absence of Chol. Since those results challenged the usual view that some saponins mediate their membrane effects through interaction with Chol, the same series of experiments were carried out with digitonin, a steroid saponin known to require Chol for its membrane-related effects[11]. Using the same three liposome compositions, we evaluated the effects of digitonin on vesicle size (dynamic light scattering, Fig. 11A), membrane fluidity (Laurdan, Fig. 11B), fusion (R_{18} dequenching, Fig. 11C) and permeability (calcein release, Fig. 11D). The results clearly showed that treatment with digitonin increased vesicle size, membrane fluidity and permeability only in Chol-containing systems without any effect on membrane fusion even at a Rh2/lipid ratio of 13 (data not shown). Interestingly, ePC:Chol vesicles were more susceptible to digitonin as compared to eSM:ePC:Chol, suggesting an influence of Chol concentration. Consistently, digitonin rapidly disrupted the GUV membrane in the presence of Chol but not in its absence (Fig. 11E) even after long time (2 hours, data not shown). Altogether, these results supported the essential role of Chol in the membrane-related effects induced by digitonin and corroborated our observations that Rh2 interacted with the membrane in a differential way.

Discussion

The membrane-related effects of saponins are often considered as Chol-dependent. Our recent observations with the saponin ginsenoside Rh2 let us to reconsider this purpose and to propose that, in contrast to eSM, membrane Chol could decrease the activity of Rh2[18]. We here tested this hypothesis by determining Rh2:membrane interaction by *in silico* experiments as well as *in vitro* studies on lipid monolayers and bilayers while modulating the lipid composition, *i.e.* the presence or absence of Chol or eSM. *In silico* studies clearly revealed higher relative interaction energy between Rh2 and pSM or DOPC in comparison to Chol, which could result from higher hydrophobic and van der Waals forces but also higher hydrogen bond energies. Accordingly, studies on lipid monolayers showed that Rh2 adsorbed to a higher extent to eSM or DOPC in comparison to Chol and ePC monolayers.

As revealed by ITC, interactions between Rh2 and both eSM and DOPC are favorable with negative values for variation of free energy. They differ however since interaction with eSM was endothermic and mainly driven by entropy whereas interaction with DOPC was slightly exothermic with lower values for variations of entropy. Regarding the interaction of Rh2 with ePC and DOPC, the binding affinity between Rh2 and ePC was lower than with DOPC vesicles which could indicate that variations in the fatty acyl chain lengths, the number of unsaturation found in ePC composition (containing around 30% DOPC) and the resulting biophysical membrane properties could reduce membrane binding of Rh2.

To be closer to physiological condition, we then turned to mixed lipid bilayers. Even if biological membranes are more complex than artificial lipid bilayers (due to the presence of membrane and cytoskeletal proteins but also of membrane asymmetry), our data are consistent with those previously obtained in human cancer cell lines (A549, THP-1, and U937) which highlighted that membrane Chol depletion accelerates Rh2-induced apoptosis[18]. It can be deduced that Rh2 did not specifically interact with Chol which could instead delay and/or decrease the Rh2-induced membrane-related effects. Several hypotheses can be proposed to explain such a delayed/decreased effect. First, due to space constriction, Rh2 could have to at first remove Chol from the membrane, a mechanism reported for digitonin which extracts Chol and forms a complex with the latter[30]. However, three lines of evidence reported here do not support this possibility. Firstly, digitonin increased the size and induced membrane lysis only in Chol-containing liposomes, as previously observed by Sudji *et al.*[11], whereas the action of Rh2 was instead delayed and depressed by the presence of membrane Chol. Secondly, Rh2 was able to modulate membrane biophysical properties even without Chol or eSM. Thirdly, based on GPex value of Laurdan, we observed that digitonin increased membrane fluidity whereas Rh2 decreased it, suggesting that Rh2 could preferentially stay into the membrane. To reinforce this idea, hydroxypropyl-β-cyclodextrin (HPβCD), also known to capture Chol from the membrane, has been shown to decrease the surface pressure (II) of Chol monolayers[31], in contrast to Rh2. Moreover, like digitonin, alpha-hederin increases membrane fluidity and membrane permeability due to the formation of saponin:Chol complexes. The differential effect between Rh2 and alpha-hederin could be related to the less profound insertion into the membrane hydrophobic core of Rh2 than alpha-hederin owing to two sugar chains, thereby increasing the surface of interaction with Chol and preventing polar interactions between Chol and phospholipids[32]. This highlights the importance of saponin nature since other saponins than Rh2, including chikusetsusaponin III or oleanolic acid glycosylated at both C-3 and C-28, induce Chol-independent membrane disruption[33,34].

A second hypothesis for explaining the protective role of Chol is through its effect on membrane rigidity, decreasing the possibility for Rh2 to adsorb and interact with the membrane. In agreement with this hypothesis, eSM:ePC liposomes were more fluid than liposomes containing Chol and were also the most sensitive to Rh2. However, even if ePC:Chol and eSM:ePC:Chol liposomes were classified from the more fluid to the more rigid, ePC:Chol vesicles were less susceptible to the action of Rh2 as compared to eSM:ePC:Chol vesicles.

Third, the delayed/depressed effect of Chol could also be explained through its favorable interaction with SM in lipid domains and its similarity with Rh2 structure. Chol could compete with Rh2, thereby depressing Rh2:SM interaction and related effects. Such interaction between Rh2 and lipid clusters is in agreement with previous studies showing the disruption of lipid domains by Rh2[16,17]. Rh2 insertion could in turn increase membrane rigidity and line tension, resulting into the formation of positive membrane curvature to finally reduce the line tension[35]. Accordingly, using coarse-grained molecular dynamics simulations, Lin and Wang have shown that the interaction of dioscin saponin with membrane Chol leads to the destabilization of the L_o-phase and the formation of positive membrane curvature which may eventually result in the hemolysis of red blood cells[36].

The favorable interaction of Rh2 with eSM monolayer is reminiscent to the specific binding to membrane SM of pore-forming proteins actinoporins (*e.g.* equinatoxin and sticholysin)[37,38]. Hence, binding of the toxins and their permeabilization ability only occur in model systems exhibiting phase coexistence (L_o and L_d)[39]. Based on our data related to GUV phase separation and LUV membrane permeability, we rule out a similar mode of action for Rh2. For instance, whatever the presence and the type of GUV phase boundaries, Rh2 induced alterations of GUV morphology and membrane permeability.

In conclusion, our work challenged the usual view that most saponins mediate their membrane-related effects through an interaction with Chol. Here the activity of Rh2 is enhanced by the interaction with membrane SM but depressed by Chol. Further studies are required to determine the structure-activity relationship between different saponins and eventually predict the mechanisms of their interactions with membrane.

Materials and Methods

Materials. Ginsenoside Rh2, calcein, Sephadex® G-50, LH-20 and 1,6-diphenyl-1,3,5-hexatriene (DPH) were purchased from Sigma-Aldrich (St. Louis, MO, USA). Ginsenoside Rh2 (chemical purity ≥97.0%) was dissolved in 100% ethanol. Rh2 residue was evaporated and resolubilized in buffer solution (10 mM Tris-HCl, 159 mM NaCl pH 7.4, containing 1% DMSO). Calcein was dissolved in 6 N NaOH and subjected to size-exclusion chromatography through a Sephadex® LH-20 column. The L-α-phosphatidylcholine (ePC – Egg, Chicken), sphingomyelin (eSM – Egg, Chicken), cholesterol (Chol - Ovine Wool), 1,2-dioleoyl-*sn*-glycero-3-phosphocholine (DOPC) and 1,2-dioleoyl-*sn*-glycero-3-phosphoethanolamine-*N*-(lissamine rhodamine B sulfonyl) (ammonium salt) (Rhod-PE) were purchased from Avanti Polar Lipids Inc. (Alabaster, AL, USA). *N*-(7-Nitrobenz-2-Oxa-1,3-Diazol-4-yl)-1,2-Dihexadecanoyl-*sn*-Glycero-3-Phosphoethanolamine, Triethylammonium Salt) (NBD-PE) were ordered by Life technologies (Leusden, Netherlands). 6-Dodecanoyl-2-Dimethylaminonaphthalene (Laurdan) and Octadecyl Rhodamine B Chloride (R_{18}) were acquired from Thermo scientific (Rockford, IL USA). Lipids and lipid probes were dissolved in $CHCl_3$, except DPH, which was dissolved in tetrahydrofuran (THF), and were kept at −20 °C. All organic solvents used were from VWR (Radnor, PA, USA).

***In silico* methods.** IMPALA and Hypermatrix methods have been previously described in details[40].

Adsorption kinetics. The adsorption kinetics of Rh2 into lipid monolayer was measured by following changes in the surface pressure. Experiments were assayed in an automated Langmuir trough (KSV Mini-trough KSV instruments Ltd., Helsinki, Finland- width = 7.5 cm, length = 20 cm) with two hydrophophilic Delrin mobile barriers, a platinum Wilhelmy plate and a temperature probe. The system was enclosed in a Plexiglas box, and the temperature was maintained at 25 ± 1 °C. Lipid mixed solutions were dissolved at a concentration of 1 mM in $CHCl_3$ and were added at the air-water interface with a micro-syringe (Hamilton, USA) until surface pressure (Π) reached 30 ± 2 mN/m. After reaching the equilibrium, ginsenoside Rh2 was carefully injected into the 80 ml subphase (buffer 10 mM Tris-HCl, 159 mM NaCl pH 7.4) beneath the lipid monolayer. The subphase is stirred with magnetic stirrer using specialized injection supports. The variation of the surface pressure was recorded in function of time immediately after the injection of Rh2 until a plateau was observed.

Preparation and analysis of Large Unilamellar Vesicles. LUVs composed of eSM:ePC (1:1), eSM:ePC:Chol (1:1:1) or ePC:Chol (1:1) (molar ratio) were prepared by the extrusion from Multilamellar Lamellar Vesicles (MLVs)[41]. In brief, lipids were diluted $CHCl_3$ at the desired molar ratio. The organic solvent was then removed by evaporation in rotary evaporator (Buchi Rotavapor R-200, Switzerland). The residual lipid films after drying under vacuum overnight were hydrated with buffer solution (10 mM Tris-HCl, 135 mM NaCl pH 7.4). This suspension was submitted to five cycles of freezing/thawing. The latter were extruded through a polycarbonate Nuclepore Track Etch membrane filter (100 nm pore size filter, 19 times) using a mini-extruder system (Avanti Polar Lipids) to form LUVs. The quality control of LUVs was determined by the polydispersity index (PDI) (PDI < 0.2) and particle size distribution (z-average ± 150 nm) via dynamic light scattering (see below). Total phospholipids were determined by phosphorus assay and diluted to the desired final concentration in the buffer solution[42].

Isothermal Titration Calorimetry. Isothermal Titration Calorimetry techniques were assessed using a VP-ITC (MicroCal Northampton, MA, USA) to provide a complete thermodynamic description of the interaction between Rh2 and LUVs made with eSM, ePC and DOPC. All solutions were prepared with the same buffer constituted of 10 mM Tris-HCl, 159 mM NaCl pH 7.4. Prior each analysis, all solutions were degassed using sonicator bath. The cell (volume 1.4045 ml) for the ITC measurement was filled with Rh2 solution at a concentration of 40 μM and stirred at a speed of 305 rpm. The reference cell is filled with milliQ water Titration was carried out at 25 °C using 300 μl syringe filled with the LUV suspension at 2 mM and series of injections of 10 μl were made with a delay of 360 s between each succession injection to allow steady state to be attained. Data were processed by software ORIGIN 7 (Originlab, Northampton, MA, USA) using the cumulative model as described in Razafindralambo *et al.*[43].

Size of Large Unilamellar Vesicles. The average diameter of liposomes was determined in a 12 mm square polystyrene cuvette containing LUV suspension by dynamic light scattering (DLS) technique at 25 °C using a Zetasizer Nano SZ equipment (Malvern Instruments Ltd, UK) equipped with a helium-neon laser and added back scattering detection at 173°.

Liposomal membrane fluidity and transition temperature. The effect of Rh2 on liposomal membrane fluidity was determined by measuring the values of generalized polarization (GPex) of Laurdan and the

fluorescence anisotropy of DPH[25,44] at 25 °C. The solution of Laurdan or DPH were added at 0.5% mol to the mixed lipid suspension before the evaporation. GPex of Laurdan was measured from the equation (1).

$$GP_{ex} = (I_{440} - I_{490})/(I_{440} + I_{490}) \quad (1)$$

where I_{440} and I_{490} are the λ_{em} at 440 and 490 nm, respectively recorded with the λ_{ex} at 340 nm. To determine transition temperature of eSM liposomes, Laurdan generalized polarization was assessed at multiple temperatures from 4 to 60 °C.

The fluorescence anisotropy value (r) of DPH was determined via the equation (2):

$$(r) = (I_{vv} - GI_{vh})/(I_{vv} + 2.G/I_{vh}) \quad (2)$$

where I_{vv} and I_{vh} are the fluorescence intensities with the excitation and emission polarization filters in vertical (v) and horizontal (h) orientations, respectively. The G factor is an inherent factor to the spectrophotometer used. The fluorescence polarization was measured at λ_{ex} and λ_{em} of 365 nm and 425 nm, respectively.

Membrane permeability of Large Unilamellar Vesicles. The leakage from LUVs of entrapped calcein at self-quenching concentration was followed to determine the effect of Rh2 on membrane permeability[45]. Briefly, the dried lipid film was hydrated with a solution of 10 mM Tris-HCl, 135 mM NaCl pH 7.4 containing purified calcein (73 mM). LUVs were then eluted through a Sephadex-G50 column to remove the non-encapsulated calcein. Fluorescence intensities were continuously recorded during 200 s at 25 °C after the addition of increasing concentrations of Rh2 in the liposome suspension. The λ_{ex} and λ_{em} were 472 and 512 nm, respectively. The percentage of calcein release from liposomes was calculated using the equation (3):

$$\%release = [(F_t - F_{ctrl})/(F_{tot} - F_{ctrl})] * 100 \quad (3)$$

where F_t represents the fluorescence intensity at the time t following the treatment with Rh2. F_{ctrl} corresponds to the baseline fluorescence of liposomes at the same time and F_{tot}, maximum fluorescence is the fluorescence measured after the addition of 0.1% Triton X-100 to induce maximum release.

Membrane fusion of Large Unilamellar Vesicles. Lipid mixing assay is based on self-quenching of R_{18} (octadecyl rhodamine B chloride) in LUVs[46]. The R_{18} hydrophic probe was incorporated at 5.7% mol into a lipid mixture before its evaporation. R_{18} labeled liposomes were mixed at a ratio of 1:4 with unlabeled liposomes adjusted to the same concentration. The changes of fluorescence intensity were measured during 200 s at 25 °C, using λ_{ex} and λ_{em} at 560 nm and 590 nm, respectively. The percentage of liposomal fusion was calculated using the equation (3).

Preparation and analysis of Giant Unilamellar Vesicles. GUVs were prepared using the electroformation method[47]. To investigate phase separation, mixtures of eSM:ePC (1:1), eSM:ePC:Chol (1:1:1) or ePC:Chol (1:1) combined with 0.2% mol Rhod-PE and 0.5% mol NBD-PE were prepared. A small volume of lipid solution was spread and dried inside the chamber of 1 mm thick silicon gasket placed on the surface of an ITO coated glass lamella. The electroformation chamber was filled with 0.2 M sucrose and overlaid with a second ITO-coated slide. The GUVs were formed by exposure to a sinusoidal alternating current of 10 Hz and 1 V for 2 h at 60 °C. The volume containing GUVs were collected from the slide and lipid concentration was determined based on a calibration curve of NBD-PE fluorescence intensity. GUVs were diluted in 0.2 M glucose and placed in a μ-Slide 8-well chamber from IBIDI (Martinsried, Germany) and observed in the red channel for Rhod-PE (λ_{ex}, 561 nm and λ_{em}, 617 nm) and in the green channel for NDB-PE (λ_{ex}, 488 nm and λ_{em}, 530 nm) at room temperature. To investigative the permeabilizing effect of Rh2, same GUV compositions combined with 0.2% mol Rhod-PE were diluted in 0.2 M glucose supplemented with 20 μM calcein and the difference of fluorescence intensity between outside and inside vesicle was measured. GUVs were visualized either with a Zeiss wide-field fluorescence microscope (Observer.Z1) using a plan-Apochromat 40x/1.4 oil Ph3 objective or a Axio Observer 1 inverted microscope equipped with a model CSU-X1 Yokogawa spinning disk and Plan-Apochromat 40x/1.40 oil DIC. Images were analyzed with the Carl Zeiss AxioVision 4.8.2 software.

Fluorescence spectroscopy measurement. All fluorescence measurements were carried out with a LS55 luminescence spectrometer from Perkin Elmer (Waltham, MA, USA). The spectrophotometer was equipped with a temperature-controlled sample holder being set at 25 °C.

Data Availability

Data are expressed as means ± SEM. All statistical analyses were performed with the GraphPad Prism 4.03 software (GraphPad software, San Diego, CA, USA).

References

1. van Meer, G., Voelker, D. R. & Feigenson, G. W. Membrane lipids: where they are and how they behave. *Nat Rev Mol Cell Biol* **9**, 112–124, https://doi.org/10.1038/nrm2330 (2008).
2. Singer, S. J. & Nicolson, G. L. The fluid mosaic model of the structure of cell membranes. *Science* **175**, 720–731 (1972).
3. Simons, K. & Ikonen, E. Functional rafts in cell membranes. *Nature* **387**, 569–572, https://doi.org/10.1038/42408 (1997).
4. Lingwood, D., Kaiser, H. J., Levental, I. & Simons, K. Lipid rafts as functional heterogeneity in cell membranes. *Biochem Soc Trans* **37**, 955–960, https://doi.org/10.1042/BST0370955 (2009).
5. Carquin, M., D'Auria, L., Pollet, H., Bongarzone, E. R. & Tyteca, D. Recent progress on lipid lateral heterogeneity in plasma membranes: From rafts to submicrometric domains. *Prog Lipid Res* **62**, 1–24, https://doi.org/10.1016/j.plipres.2015.12.004 (2016).

6. Mollinedo, F. & Gajate, C. Lipid rafts as major platforms for signaling regulation in cancer. *Adv Biol Regul* **57**, 130–146, https://doi.org/10.1016/j.jbior.2014.10.003 (2015).
7. Lorent, J. H., Quetin-Leclercq, J. & Mingeot-Leclercq, M. P. The amphiphilic nature of saponins and their effects on artificial and biological membranes and potential consequences for red blood and cancer cells. *Org Biomol Chem* **12**, 8803–8822, https://doi.org/10.1039/c4ob01652a (2014).
8. Lorent, J. *et al.* Domain formation and permeabilization induced by the saponin alpha-hederin and its aglycone hederagenin in a cholesterol-containing bilayer. *Langmuir* **30**, 4556–4569, https://doi.org/10.1021/la4049902 (2014).
9. Lorent, J. H. *et al.* alpha-Hederin Induces Apoptosis, Membrane Permeabilization and Morphologic Changes in Two Cancer Cell Lines Through a Cholesterol-Dependent Mechanism. *Planta Med* **82**, 1532–1539, https://doi.org/10.1055/s-0042-114780 (2016).
10. Korchowiec, B. *et al.* Impact of two different saponins on the organization of model lipid membranes. *Biochim Biophys Acta* **1848**, 1963–1973, https://doi.org/10.1016/j.bbamem.2015.06.007 (2015).
11. Sudji, I. R., Subburaj, Y., Frenkel, N., Garcia-Saez, A. J. & Wink, M. Membrane Disintegration Caused by the Steroid Saponin Digitonin Is Related to the Presence of Cholesterol. *Molecules* **20**, 20146–20160, https://doi.org/10.3390/molecules201119682 (2015).
12. Sucha, L. *et al.* The cytotoxic effect of alpha-tomatine in MCF-7 human adenocarcinoma breast cancer cells depends on its interaction with cholesterol in incubation media and does not involve apoptosis induction. *Oncol Rep* **30**, 2593–2602, https://doi.org/10.3892/or.2013.2778 (2013).
13. Keukens, E. A. *et al.* Glycoalkaloids selectively permeabilize cholesterol containing biomembranes. *Biochim Biophys Acta* **1279**, 243–250 (1996).
14. Bangham, A. D., Horne, R. W., Glauert, A. M., Dingle, J. T. & Lucy, J. A. Action of saponin on biological cell membranes. *Nature* **196**, 952–955 (1962).
15. Nag, S. A. *et al.* Ginsenosides as Anticancer Agents: *In vitro* and *in vivo* Activities, Structure-Activity Relationships, and Molecular Mechanisms of Action. *Front Pharmacol* **3**, 25, https://doi.org/10.3389/fphar.2012.00025 (2012).
16. Yi, J. S. *et al.* Ginsenoside Rh2 induces ligand-independent Fas activation via lipid raft disruption. *Biochem Biophys Res Commun* **385**, 154–159, https://doi.org/10.1016/j.bbrc.2009.05.028 (2009).
17. Park, E. K. *et al.* Induction of apoptosis by the ginsenoside Rh2 by internalization of lipid rafts and caveolae and inactivation of Akt. *Br J Pharmacol* **160**, 1212–1223, https://doi.org/10.1111/j.1476-5381.2010.00768.x (2010).
18. Verstraeten, S. L. *et al.* Membrane cholesterol delays cellular apoptosis induced by ginsenoside Rh2, a steroid saponin. *Toxicol Appl Pharmacol* **352**, 59–67, https://doi.org/10.1016/j.taap.2018.05.014 (2018).
19. Ducarme, P., Rahman, M. & Brasseur, R. IMPALA: a simple restraint field to simulate the biological membrane in molecular structure studies. *Proteins* **30**, 357–371 (1998).
20. Brasseur, R., Killian, J. A., De Kruijff, B. & Ruysschaert, J. M. Conformational analysis of gramicidin-gramicidin interactions at the air/water interface suggests that gramicidin aggregates into tube-like structures similar as found in the gramicidin-induced hexagonal HII phase. *Biochim Biophys Acta* **903**, 11–17 (1987).
21. Bagatolli, L. A., Parasassi, T., Fidelio, G. D. & Gratton, E. A model for the interaction of 6-lauroyl-2-(N,N-dimethylamino) naphthalene with lipid environments: implications for spectral properties. *Photochem Photobiol* **70**, 557–564 (1999).
22. Parasassi, T., De Stasio, G., d'Ubaldo, A. & Gratton, E. Phase fluctuation in phospholipid membranes revealed by Laurdan fluorescence. *Biophys J* **57**, 1179–1186, https://doi.org/10.1016/S0006-3495(90)82637-0 (1990).
23. Filippov, A., Oradd, G. & Lindblom, G. Sphingomyelin structure influences the lateral diffusion and raft formation in lipid bilayers. *Biophys J* **90**, 2086–2092, https://doi.org/10.1529/biophysj.105.075150 (2006).
24. Jimenez-Rojo, N., Garcia-Arribas, A. B., Sot, J., Alonso, A. & Goni, F. M. Lipid bilayers containing sphingomyelins and ceramides of varying N-acyl lengths: a glimpse into sphingolipid complexity. *Biochim Biophys Acta* **1838**, 456–464, https://doi.org/10.1016/j.bbamem.2013.10.010 (2014).
25. do Canto, A. *et al.* Diphenylhexatriene membrane probes DPH and TMA-DPH: A comparative molecular dynamics simulation study. *Biochim Biophys Acta* **1858**, 2647–2661, https://doi.org/10.1016/j.bbamem.2016.07.013 (2016).
26. Juhasz, J., Davis, J. H. & Sharom, F. J. Fluorescent probe partitioning in giant unilamellar vesicles of 'lipid raft' mixtures. *Biochem J* **430**, 415–423, https://doi.org/10.1042/BJ20100516 (2010).
27. de Almeida, R. F., Fedorov, A. & Prieto, M. Sphingomyelin/phosphatidylcholine/cholesterol phase diagram: boundaries and composition of lipid rafts. *Biophys J* **85**, 2406–2416, https://doi.org/10.1016/S0006-3495(03)74664-5 (2003).
28. Goni, F. M. *et al.* Phase diagrams of lipid mixtures relevant to the study of membrane rafts. *Biochim Biophys Acta* **1781**, 665–684, https://doi.org/10.1016/j.bbalip.2008.09.002 (2008).
29. Drucker, P., Pejic, M., Galla, H. J. & Gerke, V. Lipid segregation and membrane budding induced by the peripheral membrane binding protein annexin A2. *J Biol Chem* **288**, 24764–24776, https://doi.org/10.1074/jbc.M113.474023 (2013).
30. Augustin, J. M., Kuzina, V., Andersen, S. B. & Bak, S. Molecular activities, biosynthesis and evolution of triterpenoid saponins. *Phytochemistry* **72**, 435–457, https://doi.org/10.1016/j.phytochem.2011.01.015 (2011).
31. Dos Santos, A. G. *et al.* Changes in membrane biophysical properties induced by the Budesonide/Hydroxypropyl-beta-cyclodextrin complex. *Biochim Biophys Acta* **1859**, 1930–1940, https://doi.org/10.1016/j.bbamem.2017.06.010 (2017).
32. Lorent, J., Le Duff, C. S., Quetin-Leclercq, J. & Mingeot-Leclercq, M. P. Induction of highly curved structures in relation to membrane permeabilization and budding by the triterpenoid saponins, alpha- and delta-Hederin. *J Biol Chem* **288**, 14000–14017, https://doi.org/10.1074/jbc.M112.407635 (2013).
33. Nakamura, T. *et al.* Interaction of saponins with red blood cells as well as with the phosphatidylcholine liposomal membranes. *J. Pharmacobiodyn* **2**, 374–382, https://doi.org/10.1248/bpb1978.2.374 (1979).
34. Hu, M., Konoki, K. & Tachibana, K. Cholesterol-independent membrane disruption caused by triterpenoid saponins. *Biochim Biophys Acta* **1299**, 252–258, https://doi.org/10.1016/0005-2760(95)00214-6 (1996).
35. Garcia-Saez, A. J., Chiantia, S. & Schwille, P. Effect of line tension on the lateral organization of lipid membranes. *J Biol Chem* **282**, 33537–33544, https://doi.org/10.1074/jbc.M706162200 (2007).
36. Lin, F. & Wang, R. Hemolytic mechanism of dioscin proposed by molecular dynamics simulations. *J Mol Model* **16**, 107–118, https://doi.org/10.1007/s00894-009-0523-0 (2010).
37. Bakrac, B. *et al.* Molecular determinants of sphingomyelin specificity of a eukaryotic pore-forming toxin. *J Biol Chem* **283**, 18665–18677, https://doi.org/10.1074/jbc.M708747200 (2008).
38. Bakrac, B. & Anderluh, G. Molecular mechanism of sphingomyelin-specific membrane binding and pore formation by actinoporins. *Adv Exp Med Biol* **677**, 106–115 (2010).
39. Schon, P. *et al.* Equinatoxin II permeabilizing activity depends on the presence of sphingomyelin and lipid phase coexistence. *Biophys J* **95**, 691–698, https://doi.org/10.1529/biophysj.108.129981 (2008).
40. Claereboudt, E. J. S., Eeckhaut, I., Lins, L. & Deleu, M. How different sterols contribute to saponin tolerant plasma membranes in sea cucumbers. *Sci Rep* **8**, 10845, https://doi.org/10.1038/s41598-018-29223-x (2018).
41. Hope, M. J., Bally, M. B., Webb, G. & Cullis, P. R. Production of large unilamellar vesicles by a rapid extrusion procedure: characterization of size distribution, trapped volume and ability to maintain a membrane potential. *Biochim Biophys Acta* **812**, 55–65 (1985).
42. Bartlett, G. R. Phosphorus assay in column chromatography. *J Biol Chem* **234**, 466–468 (1959).

43. Razafindralambo, H., Dufour, S., Paquot, M. & Deleu, M. Thermodynamic studies of the binding interactions of surfactin analogues to lipid vesicles. *J Therm Anal Calorim* **95**, 817–821, https://doi.org/10.1007/s10973-008-9403-6 (2009).
44. Harris, F. M., Best, K. B. & Bell, J. D. Use of laurdan fluorescence intensity and polarization to distinguish between changes in membrane fluidity and phospholipid order. *Biochim Biophys Acta* **1565**, 123–128 (2002).
45. Weinstein, J. N., Yoshikami, S., Henkart, P., Blumenthal, R. & Hagins, W. A. Liposome-cell interaction: transfer and intracellular release of a trapped fluorescent marker. *Science* **195**, 489–492 (1977).
46. Hoekstra, D., de Boer, T., Klappe, K. & Wilschut, J. Fluorescence method for measuring the kinetics of fusion between biological membranes. *Biochemistry* **23**, 5675–5681 (1984).
47. Rodriguez, N., Pincet, F. & Cribier, S. Giant vesicles formed by gentle hydration and electroformation: a comparison by fluorescence microscopy. *Colloids Surf B Biointerfaces* **42**, 125–130, https://doi.org/10.1016/j.colsurfb.2005.01.010 (2005).

Acknowledgements

We thank AG. dos Santos (UCL, LDRI) for guiding us in GUV preparation and P. Van Der Smissen (UCL, DDUV) for training in fluorescence microscopy. S. Verstraeten is doctoral fellow of the Télévie. M. Janikowska-Sagan acknowledges financial support from Polish Ministry of Science and Education subsidy for her position as young researcher. This work was supported by the Belgian Fonds de la Recherche Scientifique (F.S.R-FNRS) and The Actions de Recherche Concertées (ARC, UCL).

Author Contributions

S.L.V. designed experiments, conducted *in vitro* work and wrote the manuscript. M.D. provided equipment to perform the surface pressure-time and isothermal titration calorimetry and the expertise in data treatment and interpretation. M.J. helped for the LUVs and GUVs preparations. EJSC performed in silico experiments and L.L. provided the expertise. D.T. and M.P.M. designed experiments and supervised the writing of the manuscript. All authors revised the manuscript.

Additional Information

Competing Interests: The authors declare no competing interests.

Publisher's note: Springer Nature remains neutral with regard to jurisdictional claims in published maps and institutional affiliations.

2. Elucidate the importance of cholesterol in the Rh2-induced apoptosis in biological membranes

In the second part of this study, we used three cell lines exhibiting differential membrane Chol level: carcinomic human alveolar basal epithelial A549 cells > human monocytic leukemia THP-1 > human monocytic leukemia U937 cells. We demonstrated that Rh2 induces apoptosis in a concentration- and time-dependent manner in the three cell lines. More importantly, A549, THP-1 and U937 can be classified from the more resistant to the more susceptible to the Rh2-induced apoptosis. Mechanistically, Rh2 alters PM fluidity leading to inhibition of Akt phosphorylation and the activation of the intrinsic pathway of apoptosis (loss of mitochondrial membrane potential, caspase-9 and -3 activation). Apoptosis, fluidity changes and Akt phosphorylation are induced earlier and in a higher extent in Chol-depleted cells, which could be explained by a higher cell accumulation of Rh2 in these conditions. Altogether, Chol seems to depress the sensitivity of the membrane to Rh2. In contrast to Chol removal, SM depletion confers resistance towards Rh2-induced apoptosis. This work is the first reporting that membrane Chol could delay the cytotoxic activity of the ginsenoside Rh2, renewing the idea that the activity of most saponins is only ascribed to an interaction with membrane Chol.

Contents lists available at ScienceDirect

Toxicology and Applied Pharmacology

journal homepage: www.elsevier.com/locate/taap

Membrane cholesterol delays cellular apoptosis induced by ginsenoside Rh2, a steroid saponin

Sandrine L. Verstraeten[a,b], Marie Albert[a], Adrien Paquot[c], Giulio G. Muccioli[c], Donatienne Tyteca[b], Marie-Paule Mingeot-Leclercq[a,*]

[a] Louvain Drug Research Institute (LDRI), Cellular & Molecular Pharmacology Unit (FACM), Université catholique de Louvain (UCL), Brussels 1200, Belgium
[b] de Duve Institute (DDUV), Cell Biology Unit (CELL), Université catholique de Louvain (UCL), Brussels 1200, Belgium
[c] Louvain Drug Research Institute (LDRI), Bioanalysis and Pharmacology of Bioactive Lipids Research Group (BPBL), Université catholique de Louvain (UCL), Brussels 1200, Belgium

ARTICLE INFO

Keywords:
Ginsenoside
Saponin
Cholesterol
Membrane
Apoptosis
Akt

ABSTRACT

Saponins exhibit several biological and pharmacological activities, such as antibacterial, anti-inflammatory and anticancer effects. Many studies attribute their activities to their interactions with cholesterol. In this study, we focus on the steroid saponin ginsenoside Rh2, one of the active principles of *Panax ginseng* root. Some evidence suggests that lipid rafts, defined as nanodomains enriched in cholesterol and sphingolipids, could be involved in the Rh2-induced apoptosis. However, the role of membrane lipids, especially cholesterol, in this process is still poorly understood. Here, we demonstrate that (i) A549, THP-1 and U937 cells are all susceptible to the Rh2-induced apoptosis but to a differential extent and (ii) the cytotoxic effect inversely correlates with the cell membrane cholesterol content. Upon cholesterol depletion via methyl-β-cyclodextrin, those three cells lines become more sensitive to Rh2-induced apoptosis. Then, focusing on the cholesterol-auxotroph U937 cell line, we showed that Rh2 alters plasma membrane fluidity by compacting the hydrophobic core of lipid bilayer (DPH anisotropy) and relaxing the interfacial packaging of the polar head of phospholipids (TMA-DPH anisotropy). The treatment with Rh2 conducts to the dephosphorylation of Akt and the activation of the intrinsic pathway of apoptosis (loss of mitochondrial membrane potential, caspase-9 and -3 activation). All these features are induced faster in cholesterol-depleted cells, which could be explained by faster cell accumulation of Rh2 in these conditions. This work is the first reporting that membrane cholesterol could delay the activity of ginsenoside Rh2, renewing the idea that saponin cytotoxicity is ascribed to an interaction with membrane cholesterol.

1. Introduction

Saponins, mainly produced by plants, are widely used in medicine for their multiple biological and pharmacological activities including immunomodulatory, anti-inflammatory or anti-cancer (Lorent et al., 2014a). Cytotoxic and hemolytic activities for most saponins (e.g. digitonin (Korchowiec et al., 2015; Sudji et al., 2015; Frenkel et al., 2014), α-tomatine (Keukens et al., 1996), α-hederin (Lorent et al., 2016; Lorent et al., 2014b), seem to be ascribed to their ability to interact with membrane lipids, especially cholesterol (de Groot and Muller-Goymann, 2016). For example, digitonin induces membrane permeability in the presence of cholesterol by removing cholesterol from the membrane and forming complexes with the latter (Sudji et al., 2015).

Cholesterol plays a crucial role in the stability, dynamics and organization of the plasma membrane, serving as a spacer between hydrocarbon chains of phospho- and sphingo-lipids (Ikonen, 2008). It is distributed heterogeneously in the plasma membrane (Carquin et al., 2016), notably enabling the formation of "lipid rafts" (Simons and Sampaio, 2011; Lingwood and Simons, 2010; Simons and Ikonen, 1997), transient ordered nanometric domains enriched in cholesterol and sphingolipids. Rafts are proposed to serve as platforms capable of promoting various cellular signaling including pro- and anti-apoptotic pathways such as the Fas death receptor and the phosphatidylinositol-3 kinase (PI3K)/Akt cell survival pathways, respectively (George and Wu, 2012; Mollinedo and Gajate, 2015).

Among steroid saponins, ginsenosides are the active components of ginseng, a well-known chinese medicinal plant. More than hundreds of different ginsenosides have been isolated from ginseng and have shown in the past to be membrane active substances and to influence the

* Corresponding author at: FACM/LDRI-UCL – Cellular and Molecular Pharmacology Unit of the Louvain Drug Research Institute, Université catholique de Louvain, Avenue E. Mounier 73, B1.73.05, B-1200 Brussels, Belgium.
E-mail address: marie-paule.mingeot@uclouvain.be (M.-P. Mingeot-Leclercq).

https://doi.org/10.1016/j.taap.2018.05.014
Received 19 December 2017; Received in revised form 4 May 2018; Accepted 14 May 2018
Available online 18 May 2018
0041-008X/

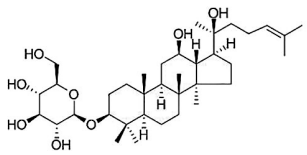

Fig. 1. The chemical structure of the ginsenoside Rh2, a steroid saponin.

membrane by modulating lipid membrane dynamics (Qi et al., 2011; Tsuchiya, 2015; Kwon et al., 2008). In this study, we focus on the ginsenoside Rh2 (Fig. 1), phytosterol from *Panax ginseng*. To the best of our knowledge, only two studies have reported the disruption of lipid rafts by Rh2 leading to apoptosis, via either the FAS oligomerization in Hela cells (Yi et al., 2009) or inactivation of Akt in human epidermoid carcinoma A431 cells and in human breast cancer MBA-MB-231 cells (Park et al., 2010). Taken together, these data suggest that rafts could be involved in Rh2-induced apoptosis. However, mechanistic understanding of the mode of interactions between Rh2 and membrane lipids and the exact subsequent apoptotic pathways are still poorly understood.

Since lipid rafts are enriched in cholesterol and since some saponins have been shown to interact with cholesterol, the aim of the present study was to explore the role of membrane cholesterol in the cytotoxic activity of Rh2. To this end, we used three cell lines exhibiting differential membrane cholesterol level: carcinomic human alveolar basal epithelial A549 > human monocytic leukemia THP-1 > U937 cells. We demonstrated that Rh2 induced apoptosis in a concentration- and time-dependent manner in the three cell lines. More importantly, A549, THP-1 and U937 cells can be classified from the more resistant to the more susceptible to the Rh2-induced apoptosis. In addition, upon cholesterol depletion via methyl-β-cyclodextrin (MβCD), those three cell lines became more sensitive to Rh2-induced apoptosis. To explore the mechanistic behind this observation, we then focused on the cholesterol-auxotroph U937 cell line (Billheimer et al., 1987). We showed that Rh2 altered plasma membrane fluidity, induced Akt dephosphorylation and the activation of the intrinsic pathway of apoptosis. Fluidity changes, Akt dephosphorylation and apoptosis appeared faster in cholesterol-depleted cells, which could be explained by a faster cell accumulation of Rh2 in these conditions.

This work is the first reporting that membrane cholesterol could delay the activity of ginsenoside Rh2, renewing the idea that saponin cytotoxicity is only ascribed to an interaction with membrane cholesterol.

2. Materials and methods

2.1. Cells and materials

Ginsenoside Rh2, methyl-β-cyclodextrin (MβCD), ethidium bromide, acridine orange, 4′,6-diamidino-2-phenylindole (DAPI), digoxin, 1,6-diphenyl-1,3,5-hexatriene (DPH), protease and phosphatase inhibitor cocktails and *Bacillus cereus* sphingomyelinase (SMase) were purchased from Sigma-Aldrich (St. Louis, MO, USA). U937, THP-1 and A549 cell lines were purchased from ATCC. RPMI-1640 medium and trypsin were ordered from Life technologies (Paisley, SL, UK). Delipidated serum was purchased from Labconsult (BE). Blue trypan, bicinchoninic protein assay, caspase-9 colorimetric assay kit, JC-1, NuPAGE reagents, PVDF membrane, Supersignal West Pico and Amplex® red cholesterol assay kit were purchased from Thermo scientific (Rockford, IL, USA). 1-(4-trimethylammoniumphenyl)-6-phenyl-1,3,5-hexatriene (TMA-DPH) was ordered from Molecular Probes (Eugene, OR, USA). Caspase-9 inhibitor (*Z*-LEHD-FMK) was purchased from R & D System (Minneapolis, MN, USA). Anti-phospho-Akt (Ser^{473}) (#4060) and anti-Akt (#9272) were purchased from Cell Signaling Technology (Beverly, MA, USA). Anti-β actin (sc-47778) and anti-caspase-3 (sc-7148) were purchased from Santa Cruz Biotechnology (Santa Cruz, CA, USA). TLC silica gel 60F was purchased from Merck Millipore (Billerica, MA, USA). All other reagents were purchased from VWR International (Atlanta, GA, USA) and were of analytical grade.

2.2. Cell culture and incubation with ginsenoside Rh2

Cells were cultured in suspension in RMPI-1640 medium supplemented with 10% fetal calf serum at 37 °C in 5% CO_2. Ginsenoside Rh2 was dissolved in absolute ethanol. After evaporation of the solvent, the residue was resolubilized in RPMI-1640 medium supplemented with 10% delipidated serum containing 0.1% DMSO in an ultrasonic bath for 5 min. Cells were incubated with 60 μM ginsenoside Rh2 (unless otherwise stated) in RMPI-1640 medium with 10% delipidated serum to avoid interaction between Rh2 and lipids in the serum and to prevent cholesterol and sphingomyelin replenishment at the membrane after cholesterol and sphingomyelin depletion with MβCD and SMase, respectively. After treatment with Rh2, cells were washed twice in Phosphate Buffered Saline (PBS) (10 mM Na_2HPO_4, 137 mM NaCl and 2.7 mM KCl).

2.3. Plasma membrane cholesterol or sphingomyelin depletion and assay

In serum-free RPMI-1640 supplemented with 1 mg/ml BSA, THP-1 cells were treated with 3 mM MβCD for 2 h whereas A549 and U937 cells were treated with 5 mM MβCD for 45 min and 2 h, respectively. In some experiments, U937 were also treated with raising concentration of MβCD (0 to 7 mM) for 2 h or SMase (0 to 60 mU/ml) for 1 h. Cells were then washed with serum-free RPMI and incubated with Rh2 for the indicated times. After the treatment with MβCD, cells were directly quantified for their cholesterol by the Amplex® red cholesterol assay and phospholipid contents by phosphorus assay after lipid extraction (Gamble et al., 1978; Bartlett, 1959). The ratio of cholesterol/phospholipid was determined and expressed by reference to the control. To evaluate sphingomyelin content, lipids were directly extracted after SMase treatment (Bartlett, 1959), separated on silica gel TLC plates in chloroform:methanol:$CaCl_2$ (15 mM) (65:35:8; v/v/v) and detected by charring in the presence of 10% cupric sulfate in 8% O-phosphoric acid (Kritchevsky et al., 1973; Carquin et al., 2014). Band intensity of sphingomyelin was quantified and expressed by reference to bands corresponding to phospholipids from the same sample and then expressed as percentage of control.

2.4. Apoptotic/non-apoptotic cell death

DAPI assay was carried out to quantify apoptosis as previously described (Servais et al., 2006). Briefly, cells presenting a fragmented and condensed nucleus were counted as apoptotic. Data were expressed as the percentage of apoptotic nuclei relative to total number of nuclei counted. A total number of 200 cells was counted per sample. Acridine orange/ethidium bromide (AO/EB) assay was performed to distinguish between living, death cells and early and late apoptotic cells (Kasibhatla et al., 2006). After treatment with Rh2, cells were incubated with the AO/EB solution and directly observed by fluorescence microscopy. A total number of 200 cells was counted per sample.

2.5. Trypan blue exclusion assay

Cell death was quantified by the trypan blue exclusion assay. Cells colored in trypan blue were considered as non-viable and the percentage of non-viable cells was calculated as the number of death cells divided by the total number of cells.

2.6. Quantification of intracellular ginsenoside Rh2 by HPLC MS/MS

After treatment with ginsenoside Rh2, cell pellets were resuspended in H_2O and digoxin (internal standard; 1 mg/ml) was added. Cells were lysed by sonication for 10 min and proteins were precipitated by adding a mixture of acetonitrile and methanol (MeOH) (21:4, v/v). After 20 min at −20 °C, lysates were centrifuged at 11,000 *g* for 5 min at room temperature. Supernatants were collected and dried. The dried samples were reconstituted in MeOH:H_2O (1:1, v/v) and injected on a Supelcosil LC-18 (150 × 4 mm; 3 μm) column preceded by a C-18 Supelguard precolumn maintained at 25 °C. Tandem quadrupole mass spectrometry was used to detect the ginsenoside Rh2 and digoxin. The negative ionization mode was selected for analysis. The mobile phase A consisted in MeOH:H_2O (1:1, v/v) and the mobile phase B was 100% MeOH (both containing 0.1% NH_4OH). The gradient consisted in a linear increase from 0% B to 100% B in 7.5 min followed by a 7.5 min plateau maintained before requilibrating the column. The data analysis was achieved by using the *MassLynx® software* to integrate peaks corresponding to the quantification transitions selected for the ginsenoside Rh2 (621.4 → 160.9) and for the digoxin (779.4 → 85.0). Qualification transitions were also used for both ginsenoside Rh2 (621.4 → 459.4) and digoxin (779.4 → 519.3) to further confirm the nature of the peak analyzed. The ratio of the area under the curve (AUC) of ginsenoside over the AUC of digoxin was determined and the amount of Rh2 in the cells was calculated using a calibration curve. Nine calibration solutions ranging between 0 and 60 pmol (on column) were prepared and the slope (0.056), intercept (0.029) and coefficient of determination (R^2: 0.9981) of the calibration curve were determined. Based on the calibration curve, the LOD and LOQ were also determined and found to be 0.0095 pmol and 0.0445 pmol on column, respectively. The accuracy expressed as bias (in %) was determined at four levels ranging from 0.117 to 60 pmol. The values were included between 0.006% and 0.097. The intracellular accumulation of Rh2 was then reported to the total protein amount determined by the BCA method using bovine serum albumin as a standard.

2.7. Plasma membrane fluidity

DPH or TMA-DPH were dissolved in tetrahydrofuran at a concentration of 2 mM. After incubation with Rh2, cells were washed and mixed with 2 μM DPH or TMA-DPH dispersed in PBS for 30 min or 5 min at 37 °C in the dark, respectively. The fluorescence anisotropy values (r) were determined using the equation:

$$(r) = (I_{vv} - G.\ I_{vh})/(I_{vv} + 2.\ G/I_{vh})$$

where Ivv and Ivh are the fluorescence intensities with the excitation and emission polarization filters in vertical (v) and horizontal (h) orientations, respectively. The G factor is an inherent factor to the spectrometer. The fluorescence polarization was measured at 37 °C at excitation and emission wavelengths of 365 nm and 425 nm, respectively, using a LS55 luminescence spectrometer connected to a circulating water bath.

2.8. Western blot

After treatment with Rh2, cells were resuspended in RIPA buffer (25 mM Tris-HCl, pH 7.4; 150 mM NaCl; 1% NP-40; 0.1% SDS; 1% sodium deoxycholate) supplemented with protease and phosphatase inhibitor cocktail. After 15 min on ice, cell lysates were centrifuged for 15 min at 14,000 *g* at 4 °C to pellet any insoluble material. The protein concentration of the supernatant was assessed using the BCA method. Western blots were performed using the NuPAGE electrophoresis system. 50 μg from each sample was mixed to 4× NuPAGE LDS sample buffer and 10× NuPAGE reducing agent, then heated at 70 °C for 10 min. Samples were separated on acrylamide gels (NuPAGE Bis-Tris Gel) and transferred to PVDF membranes (0.45 μm). Membranes were blocked in 5% non-fat dry milk in Tris-buffered saline containing 0.05% Tween-20 (TBST) and then incubated with appropriate diluted primary antibodies (Akt and p-Akt: 1/1000; β-actin and caspase-3: 1/200) at 4 °C overnight. Membranes were washed three times with TBST buffer and exposed to appropriate horseradish peroxidase-coupled secondary antibodies for 1 h. Blots were revealed by chemiluminescence (SuperSignal West Pico).

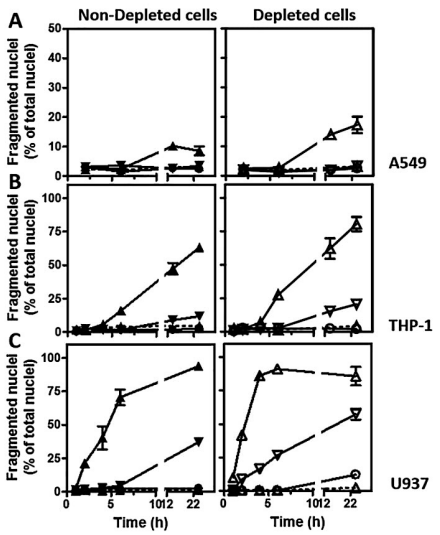

Fig. 2. Ginsenoside Rh2 induces faster cell cytotoxicity upon membrane cholesterol depletion in a concentration-dependent manner. Cells were kept untreated (left panel) or treated with MβCD (right panel). THP-1 (B) were treated with 3 mM for 2 h whereas A549 (A) and U937 (C) cells were treated with 5 mM MβCD for 45 min and 2 h, respectively. Cholesterol-depleted cells with MβCD (open symbol, right panel) or not (closed symbol, left panel) were incubated for the indicated times with increasing concentrations of Rh2: 20 μM (circle), 40 μM (inverted triangle), 60 μM (triangle) or with 0.1% DMSO (vehicle, dotted line, triangle). The number of fragmented nuclei was determined by DAPI. Results are the mean ± SEM of at least two independent experiments performed in triplicate. Where not visible, error bars are included in the symbols.

Table 1
Cellular cholesterol content in cells depleted or not in cholesterol by MβCD. Cells were kept untreated (second column) or treated with MβCD (third column). THP-1 were treated with 3 mM MβCD for 2 h whereas A549 and U937 cells were treated with 5 mM MβCD for 45 min and 2 h, respectively.

Cell lines	Chol (μg/mg protein) Non-depleted	Chol (μg/mg protein) Depleted
A549	34.58 ± 6.36	17.1 ± 7.17
THP-1	20.13 ± 4.04	10.52 ± 3.22
U937	10.68 ± 1.68	5.30 ± 2.95

2.9. Caspase-9 activity

Caspase-9 activity was measured using colorimetric protease assay kit. Briefly, cells treated with Rh2 were washed and resuspended in RIPA lysis buffer for 15 min on ice. After centrifugation (14,000 *g*,

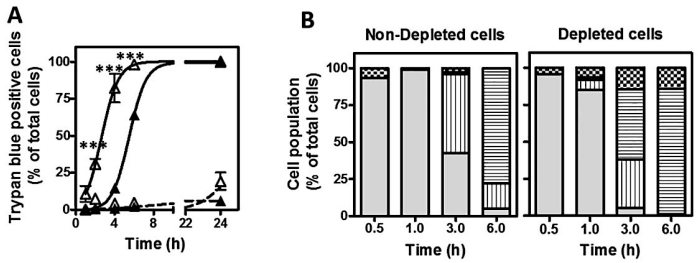

Fig. 3. Ginsenoside Rh2 induces faster U937 cell cytotoxicity upon membrane cholesterol depletion. A, B U937 cells cholesterol-depleted with 5 mM MβCD for 2 h (open triangle) or not (closed triangle) were incubated for the indicated times with 60 μM Rh2 (solid line) or with 0.1% DMSO (vehicle, dotted line). A. The number of dead cells was determined by trypan blue. Results are the means ± SEM of at least three independent experiments performed in triplicate. Two-way ANOVA with Bonferroni post-tests to compare points between non-depleted versus depleted cells treated with Rh2. The lines correspond to a non-linear regression (Hill's function) of data values. B. Cells were stained with acridine orange/ethidium bromide dyes. Staining method distinguished between living cells (grey bars), early apoptosis (vertical bars), late apoptosis (horizontal bars) and necrosis (check board bars). The result is the mean of two independent experiments done in triplicate. Depleted vs non-depleted conditions: ***, $p < 0.001$.

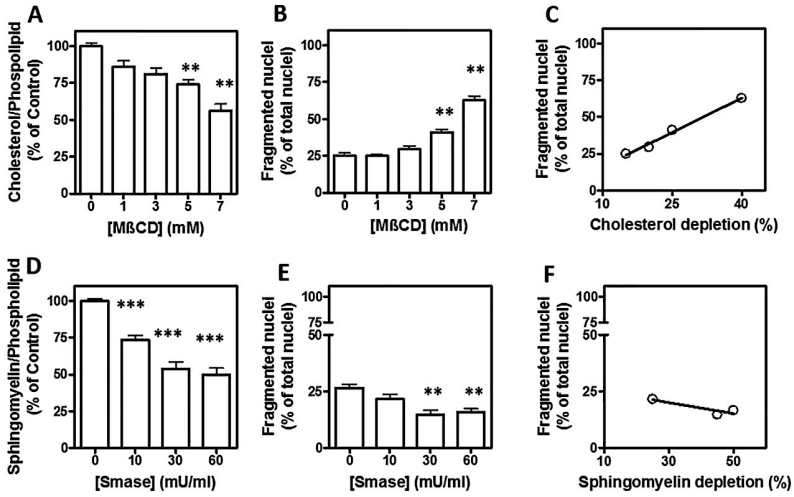

Fig. 4. Ginsenoside Rh2 induces stronger U937 cell cytotoxicity upon membrane cholesterol depletion and the opposite upon membrane sphingomyelin depletion. A, D. U937 cells were treated with raising MβCD (A) or Smase (B) concentrations for 2 h and 1 h, respectively. The cholesterol/phospholipid and sphingomyelin/phospholipid ratios were measured and expressed by reference to the control. One-way ANOVA with Dunnett's post test to compare points for control versus cells incubated with MβCD or Smase. **, $p < 0.01$; ***, $p < 0.001$. B, E. After treatment with increasing MβCD or SMase, cells were exposed for an additional 2 h with 60 μM Rh2 (in the absence of MβCD or SMase) and DAPI assay was performed. The experiment was repeated at least two times independently, each time in triplicate. One way ANOVA with Dunnett's post test. **, $p < 0.01$. C, F. Correlation between the cytotoxicity effect induced by Rh2 and the percentage of cholesterol or sphingomyelin reduction expressed by reference to the control. The line corresponds to a linear regression of data values with $R^2 = 0.99$ or $R^2 = 0.8124$ for cholesterol or sphingomyelin depletion, respectively.

15 min), protein concentration of the supernatants was measured using the BCA method. Amount of 50 μg of proteins diluted in 50 μl of buffer RIPA were mixed with 2× reaction buffer in a 96 well microplate and 5 μl of peptide substrates of caspase-9 (Ac-LEHD-pNA) was added. After 24 h incubation in the dark at 37 °C, the absorbance of the samples was read in a microplate reader at 400 nm. In some experiments, caspase-9 inhibitor (*Z*-LEHD-FMK, 125 μM) was added to fresh medium 1 h before the treatment with Rh2.

2.10. Loss of mitochondrial membrane potential

Loss of mitochondrial membrane potential was determined using the mitochondrial membrane potential sensitive cationic dye JC-1. Briefly, Rh2-treated cells were stained with 10 μM JC-1 for 30 min at

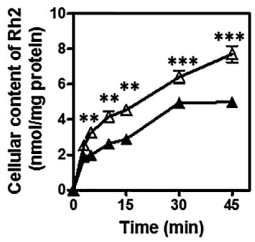

Fig. 5. Uptake of Rh2 by U937 cells is accelerated upon membrane cholesterol depletion. U937 cells were cholesterol-depleted (5 mM MβCD, open triangles) or not (closed triangles) and then incubated with 60 μM Rh2 over time. The amount of Rh2 in cell lysates was measured using HPLC MS/MS and expressed by reference to the amount of proteins. Each symbol is the mean ± SEM of at least three independent experiments done in triplicate. Two-way ANOVA with Bonferroni post-tests to compare points for non-depleted vs depleted cells. **, $p < 0.01$; ***, $p < 0.001$.

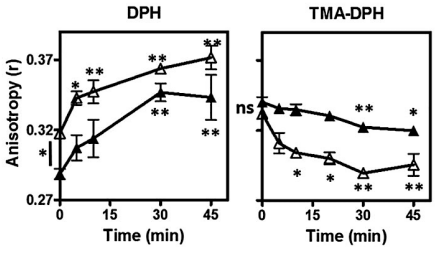

Fig. 6. Rh2 induces faster rigidification of the hydrophobic core (DPH) and fluidification of the interfacial region (TMA-DPH) of the U937 lipid bilayer upon membrane cholesterol depletion. U937 cells non-depleted (closed triangles) or cholesterol-depleted (5 mM MβCD, open triangles) were treated with 60 μM Rh2 at the indicated times and then incubated with DPH (left panel) or TMA-DPH (right panel) for 30 or 5 min, respectively. The anisotropy (r) values were measured. Results are means ± SEM of two independent experiments in triplicate. Student's t-test was performed to compare control depleted and non-depleted cells. One-way ANOVA with Dunnett's post-test to compare control cells vs cells incubated with Rh2. ns, not significant, *, $p < 0.05$; **, $p < 0.01$.

37 °C in the dark. Cells were washed and resuspended with PBS and the fluorescence was detected with a microplate reader at an excitation wavelength of 490 nm and emission wavelengths of 525 and 590 nm.

2.11. Data analysis

Data are expressed as means ± SEM. All statistical analyses were performed with the GraphPad Prism 4.03 software (GraphPad software, San Diego, CA, USA).

3. Results

In a first series of experiments, we examined the time and concentration dependence of the Rh2-induced apoptosis in A549, THP-1 and U937 cells. To this aim, cells were treated with increasing concentrations of Rh2 (20, 40 and 60 μM) for increasing periods of time (1 h to 24 h) and tested for apoptosis by DAPI staining. As shown in the left panel of Fig. 2, the Rh2-induced apoptosis extent was Rh2 concentration- and incubation time- as well as cell line-dependent. For instance, the U937 cell line (C) was more susceptible to the Rh2-induced apoptosis than THP-1 cells (B), themselves more susceptible than A549 cells (A). After 6 h of incubation, 60 μM Rh2 induced ~50% of fragmented nuclei in U937, ~15% in THP-1 without any effect in A549 cells. Since U937, THP-1 and A549 cells exhibited increasing membrane cholesterol (Table 1), those results suggested an inversed correlation between susceptibility to Rh2 and membrane cholesterol content: higher the cholesterol content, lower the Rh2-induced apoptosis. To further test this hypothesis, the same experiment was performed in cells depleted in cholesterol (right panel of Fig. 2). For this purpose, THP-1 were pretreated with 3 mM MβCD, whereas A549 and U937 cells were pretreated with 5 mM MβCD, a cholesterol-sequestering agent (Zidovetzki and Levitan, 2007). Those non-cytotoxic MβCD concentrations reduced by ~50% the ratio of cholesterol/protein in the three cell lines (Table 1). As shown in the right panel of Fig. 2, in all the conditions investigated, cholesterol-depleted cells were more sensitive to Rh2-induced apoptosis, corroborating the idea that a decrease in cholesterol content correlated with an increased number of apoptotic cells induced by Rh2.

To further investigate the role of cholesterol in the Rh2-induced cytotoxicity, we then focused on the U937 cell line, which is cholesterol auxotroph and considered as a valuable model to study the importance of cholesterol in membrane structure and function (Billheimer et al., 1987), and used the effective concentration of 60 μM Rh2. We started by analyzing the effect of Rh2 on membrane permeability and cell death via trypan blue assay. Depletion of cholesterol by MβCD effectively increased and accelerated the Rh2-induced cell death, confirming the results obtained with DAPI staining (Fig. 3A). Noteworthy, the apoptosis was observed before the appearance of cell death in non-depleted cells. Acridine orange/ethidium bromide staining was also performed to visualize membrane permeabilization in parallel with nucleus morphology changes (Lorent et al., 2016). The treatment with Rh2 conducted first to apoptosis observed by nuclear fragmentation followed in a second step by the loss of plasma membrane integrity and necrosis (Fig. 3B). > 45% of the cells lost their membrane integrity after 3 h of incubation with 60 μM of Rh2 in cholesterol-depleted cells while this phenomenon was not yet observed in non-depleted cells. In all the conditions investigated, depletion of cholesterol accelerated the cytotoxic effect of Rh2.

To confirm the protective role of membrane cholesterol in the Rh2-induced apoptosis, U937 cells were pretreated with 0 to 7 mM MβCD. Upon treatment with 5 mM and 7 mM MβCD, the cholesterol/phospholipid ratio was reduced to ~75% and 60% of that of control cells, respectively (Fig. 4A). Cells with varying contents of cholesterol were then treated with 60 μM Rh2 for 2 h and DAPI assay was performed to determine the percentage of fragmented nuclei (Fig. 4B). As expected, the increase of membrane cholesterol depletion via the pretreatment with raising concentrations of MβCD correlated with an increased number of apoptotic cells following Rh2 treatment (Fig. 4C). These data confirm that lower the cholesterol level is, higher the Rh2-induced apoptosis is. To determine whether those effects are specific to membrane cholesterol depletion, cells were incubated with 0 to 60 mU/ml *Bacillus cereus* sphingomyelinase (SMase) for sphingomyelin depletion. In these conditions, the reduction of sphingomyelin content reached ~50% of that of control cells (Fig. 4D) without inducing any cell death (data not shown). As shown in Fig. 4E, F, the increase of sphingomyelin depletion via the pretreatment with raising concentration of SMase correlated with a decreased number of apoptotic cells following Rh2 treatment. Therefore, in contrast to cholesterol removal, sphingomyelin depletion confers resistance towards Rh2-induced apoptosis, indicating that the cytotoxic activity of Rh2 depends on the membrane lipid nature.

To investigate whether the faster cytotoxic effect of Rh2 upon cholesterol depletion could result from a difference in Rh2 cell accumulation, the time course of Rh2 uptake was investigated in cells depleted or not in cholesterol. Cells were incubated with Rh2 over time

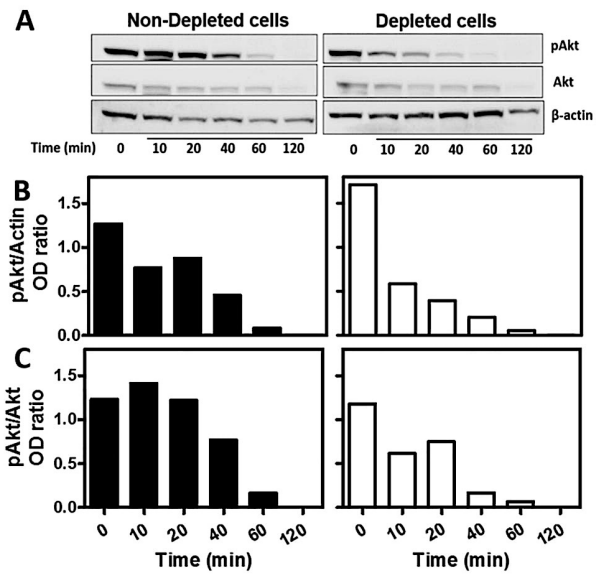

Fig. 7. Rh2 decreases the phosphorylation of Akt faster upon cholesterol depletion in U937 cells. Non-depleted (left panel) or cholesterol-depleted cells (5 mM MβCD, right panel) were incubated with 60 μM Rh2. A. Equal amounts of cell extracts were subjected to western-blot analysis for pAkt, Akt and β-actin protein. B, C. Densitometry analysis shows the band density ratios of pAkt over actin (B) and pAkt over Akt (C) in non-depleted cells (left panel, black bars) and cholesterol-depleted cells (right panel, white bars). This is a representative result from one of two independent experiments.

and the amount of Rh2 in cells was measured by HPLC MS/MS (Fig. 5). After 10 min of treatment, cholesterol-depleted cells accumulated two-fold more Rh2 as compared to non-depleted cells and this difference was maintained until 45 min. These results indicated faster cellular uptake of Rh2 upon cholesterol depletion.

To next ask whether Rh2 could affect plasma membrane biophysical properties, we measured plasma membrane fluidity, a highly regulated property, including by cholesterol. To this aim, we used DPH and TMA-DPH that respectively monitor the fluidity in the hydrophobic core and in the interfacial region of the lipid bilayer (do Canto et al., 2016). In the absence of Rh2, whereas no significant difference was observed for TMA-DPH anisotropy, DPH anisotropy value (*r*) of cholesterol-depleted cells was significantly higher than in non-depleted cells (Fig. 6), suggesting a higher rigidity in the lipid core region. Rh2 significantly increased the fluorescence polarization of DPH within 5 min in cholesterol-depleted cells but only after 30 min in non-depleted cells as compared with respective controls, suggesting that Rh2 compacted faster the lipid core region of cholesterol-depleted membranes. In contrast, Rh2 decreased the anisotropy value of TMA-DPH within 10 min in cholesterol-depleted cells and after 30 min in non-depleted cells, suggesting that Rh2 relaxed earlier the interfacial region of the lipid bilayer upon cholesterol depletion. Based on all these results, we propose that Rh2 affected faster the physical state of lipid bilayers in cholesterol-depleted cells than in non-depleted cells.

To elucidate whether membrane fluidity changes could impact on signaling pathways, we examined the effects of Rh2 on the activation of Akt, a lipid raft-associated protein kinase, which promotes cell survival and blocks the apoptotic pathways. Upon pretreatment with 5 mM MβCD and in the absence of Rh2, the levels of phospho-Akt and Akt were similar between cells depleted or not in cholesterol (Fig. 7). This observation could be at a first glance surprising since several papers show the dephosphorylation of Akt after cholesterol depletion via MβCD treatment (Calay et al., 2010; Gotoh et al., 2014). However, upon treatment with 5 mM MβCD (same concentration than our experimental condition) for 4 h, Upadhyay AK. et al. do not observe any effect neither on the Akt phosphorylation nor on the apoptosis in human breast cancer lines MCF-7 and MDA-MB-231 (Upadhyay et al., 2006). Therefore, we propose that differential incubation conditions with MβCD, i.e. dose and incubation time, could reconcile the different observations in distinct cell models. Additionally, the treatment with Rh2 decreased the level of the phosphorylated form of Akt (Ser^{473}) earlier in cholesterol-depleted cells. Regarding the disappearance of total Akt amount after 2 h of treatment with Rh2, different non-mutually exclusive explanations can be provided. Firstly, at this time, we have shown that Rh2 activated caspase-3 and could lead to the cleavage of Akt protein due to its critical role in the cell growth and its anti-apoptotic signaling properties, as suggested by Widmann C et al. (Widmann et al., 1998). Secondly, a recent study demonstrated that 60 μM Rh2 reduces Akt expression and its phosphorylation in glioma cell lines A172 without affecting the β-actin level (Li et al., 2018). Finally, it was also reported that Akt molecules can be degraded by macroautophagy (Calay et al., 2010).The dephosphorylation of Akt in a time-dependent manner resulting in the loss of its enzymatic activity could suggest the inhibition of Akt-dependent survival signaling pathways and the activation of the intrinsic apoptotic pathway by Rh2 (Franke et al., 2003).

To test for this hypothesis, apoptosis markers including loss of mitochondrial membrane potential (ΔΨ) and caspase-9 and -3 activations were investigated. ΔΨ was analyzed using the JC-1 dye. As shown in Fig. 8A, the treatment with Rh2 led to the early increase of the fluorescence intensity ratio at 525 nm (green) over 590 nm (red) upon cholesterol depletion. This result evidenced that Rh2 induced mitochondrial membrane depolarization faster in cholesterol-depleted than in non-depleted cells. Further downstream in the intrinsic apoptotic pathway, caspase-9 activity was monitored by detecting the cleavage of a specific caspase-9 substrate (Ac-LEHD-pNA). Rh2

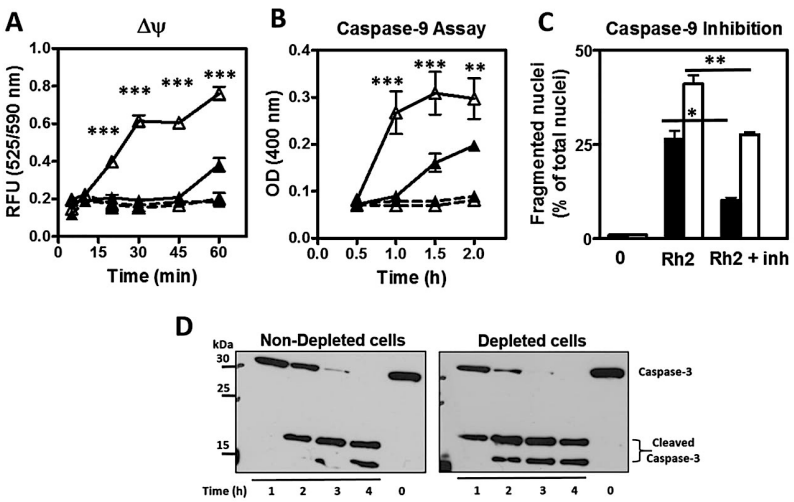

Fig. 8. Rh2 accelerates mitochondrial membrane depolarization and caspase-9 and -3 activations upon membrane cholesterol depletion in U937 cells. U937 cells were treated as at Fig. 2C. A, B. Non-depleted (closed triangles) or cholesterol-depleted cells (5 mM MβCD, open triangles) were incubated with 60 μM Rh2 (solid line) or with vehicle (dotted line) over time. A. Loss of mitochondrial membrane potential (ΔΨ) was determined by using the dye JC-1. B. Time course of caspase-9 activation was assessed by using a specific chromogenic substrate (Ac-LEHD-pNA). The experiments were repeated two times independently, each time in triplicate. Two-way ANOVA with Bonferroni post-tests to compare points for non-depleted vs depleted cells treated with Rh2. C. Non-depleted cells (black bars) or cholesterol-depleted cells (white bars) were pretreated with or without caspase-9 inhibitor (Z-LEHD-FMK) and then treated with 60 μM Rh2 or with vehicle for 2 h. DAPI assay was carried out as described previously. Results are means ± SEM of at least three independent experiments done in triplicate. Student's t-test was performed to compare cells depleted or not in cholesterol without and with caspase-9 inhibitor. D. The presence of active forms of caspase-3 was determined by western-blot in both cell types treated with 60 μM Rh2. This is a representative result from one of three experiments. *, $p < 0.05$; **, $p < 0.01$; ***, $p < 0.001$.

activated faster caspase-9 upon cholesterol depletion (Fig. 8B). To further address the caspase-9 involvement, cells were pretreated with specific caspase-9 inhibitor (Z-LEHD-FMK) followed by Rh2 treatment. The fragmented nuclei percentage was decreased more significantly by caspase-9 inhibitor in cholesterol-depleted cells as compared to non-depleted cells (Fig. 8C). Moreover, throughout the treatment with Rh2, the caspase-3 was progressively cleaved into two fragments resulting to its activation. As shown in Fig. 8D, the cleavage fragment (19 kDa) was detected after 2 h in non-depleted cells and only 1 h in cholesterol-depleted cells. As the caspase-9 activity, the caspase-3 activation was faster in cholesterol-depleted cells. Those data reported faster activation of the intrinsic apoptotic pathway by Rh2 observed via the depolarization of ΔΨ and the activation of caspase-9 and -3.

4. Discussion

Although many studies have investigated the Rh2-induced apoptosis in cancer cells (Shi et al., 2016; Lv et al., 2016; Choi et al., 2011), the role of membrane cholesterol in this process remains largely unclear. We here showed that cholesterol depletion enhanced the cellular accumulation of Rh2 in U937 cells that could result into faster Rh2-induced cytotoxicity. Based on the observation by Lorent et al. that α-hederin-induced apoptosis is reduced in cholesterol-depleted human leukemic U937 (Lorent et al., 2016), we suggest that the faster Rh2-induced cytotoxicity in cholesterol-depleted cells does not result from an unspecific mechanism due to pretreatment with MβCD. We also excluded the possibility that the observed effect could be cell-dependent, as revealed by a similar protective role of cholesterol in the Rh2-induced apoptosis in A549 and THP-1 cells.

Although we were not able to determine whether Rh2 is mostly inserted into the plasma membrane or localized inside the cell, it is tempting to speculate, based on similarity of Rh2 and cholesterol structures that Rh2 could intercalate easier and faster into the membrane of cholesterol-depleted cells by taking the place of cholesterol and modulating the membrane fluidity.

In order to determine whether the faster Rh2-induced apoptosis is specific of cholesterol depletion, we determined the cytotoxic effect of Rh2 in cells depleted or not in sphingomyelin, another abundant plasma membrane lipid exhibiting enrichment in lipid rafts. We showed that, in contrast to cholesterol depletion, sphingomyelin decrease reduced Rh2-induced apoptosis, suggesting the essential role of sphingomyelin in the cytotoxic activity of Rh2. To corroborate this idea, it has been shown that protopanaxadiol (aglycon of ginsenoside Rh2) mediates cytotoxic effects through the activation of neutral sphingomyelinase 2 leading to the hydrolysis of membrane sphingomyelins into pro-apoptotic intracellular ceramides (Park et al., 2013). Altogether, our results highlight the importance of membrane lipid composition for the ginsenoside Rh2-induced apoptosis.

To further define the interaction of Rh2 with interfacial and hydrophobic domains of the membrane, fluorescence anisotropy measurements using TMA-DPH and DPH were carried out. Both probes are located within the bilayer, with a shallower depth for TMA-DPH (do Canto et al., 2016). The steady state fluorescence anisotropy is associated to their rotational diffusion, which is sensitive to the order in the membrane. TMA-DPH fluorescence anisotropy values were not affected by cholesterol depletion in accordance with the literature, whereas

cholesterol-depleted cells showed higher rigidity in the lipid core region as compared to non-depleted cells (Prasad et al., 2009; Goodwin et al., 2005). Like cholesterol, we report here that Rh2 compacted the bilayer hydrophobic core. In addition, Rh2 relaxed the interfacial packaging of the phospholipid polar heads. These features were altered faster upon cholesterol depletion.

To investigate whether changes of the plasma membrane fluidity could potentially elicit cellular responses, we measured the effect of Rh2 on the lipid raft-associated Akt signaling and on the apoptotic pathway. We observed decreased levels of phosphorylated Akt and the activation of the intrinsic apoptotic pathway faster upon cholesterol depletion. Apoptosis markers manifested rapidly in Rh2 treated cells and only 20 to 90 min were necessary to induce the mitochondrial membrane depolarization and the activation of caspase-9 leading to apoptosis. These findings suggest that the primary action of Rh2 involved rapid pathways including phenomena such as dephosphorylation or cleavage of proteins which take less time than slower events like protein expression. Our results do not exclude the involvement of other pathways in the cytotoxic activity of Rh2 as suggest by the partial inhibition of Rh2-induced apoptosis by caspase-9 inhibitor. It has been reported that Rh2 also mediates apoptosis via the death receptor signaling leading to the activation of caspase-8 in Hela cells (Guo et al., 2014) and in A549 cells (Cheng et al., 2005).

In addition with the effect of cholesterol to delay the apoptosis induced by Rh2, two other cell effects of ginsenoside Rh2 are attributed to cholesterol-dependent mechanisms: (i) the induction of dendrite formation by Rh2 (18 μM, 2 h) is suppressed by depletion of cholesterol upon MβCD in B16 melanoma cells (Jiang et al., 2010); and (ii) a protective effect on the Aβ-induced amyloid pathology in primary neurons by Rh2 (3 μM, 12 h) is induced by reduction of cholesterol and lipid rafts (Qiu et al., 2014). These two studies could be at first glance in disagreement with the data we reported here. However, in the context of our study and the anticancerous effect of Rh2 we worked at higher concentrations (60 μM). Therefore, a differential ratio between cholesterol and Rh2 in the membrane could reconcile the different observations in distinct cell models treated with differential Rh2 concentrations.

Even if ginsenoside Rh2 was considered as a saponin like alpha-hederin or digitonin, it seems to interact differently with the lipid bilayer. Although the alpha–hederin induced cytotoxicity is well ascribed to its interaction with cholesterol, this study is the first to report that cholesterol slows down the cytotoxic activity of ginsenoside Rh2. This work highlights the need to distinguish different activities of molecules classified as saponins. Next step will be to investigate the mode of interaction of Rh2 with membranes at a molecular level using lipid monolayers and liposomes as useful models for studying membrane biophysical properties.

Acknowledgements

We thank M.C. Cambier and V. Mohymont for technical assistance and A.S. Cloos (UCL, DDUV) for guiding us in Thin Layer Chromatography experiments. S. Verstraeten is doctoral fellow of the *Télévie*. This work was supported by the Belgian *Fonds de la Recherche Scientifique* (F.S.R-FNRS).

References

Bartlett, G.R., 1959. Phosphorus assay in column chromatography. J. Biol. Chem. 234 (3), 466–468.
Billheimer, J.T., Chamoun, D., Esfahani, M., 1987. Defective 3-ketosteroid reductase activity in a human monocyte-like cell line. J. Lipid Res. 28 (6), 704–709.
Calay, D., et al., 2010. Inhibition of Akt signaling by exclusion from lipid rafts in normal and transformed epidermal keratinocytes. J. Investig. Dermatol. 130 (4), 1136–1145.
Carquin, M., et al., 2014. Endogenous sphingomyelin segregates into submicrometric domains in the living erythrocyte membrane. J. Lipid Res. 55 (7), 1331–1342.
Carquin, M., et al., 2016. Recent progress on lipid lateral heterogeneity in plasma membranes: from rafts to submicrometric domains. Prog. Lipid Res. 62, 1–24.
Cheng, C.C., et al., 2005. Molecular mechanisms of ginsenoside Rh2-mediated G1 growth arrest and apoptosis in human lung adenocarcinoma A549 cells. Cancer Chemother. Pharmacol. 55 (6), 531–540.
Choi, S., Oh, J.Y., Kim, S.J., 2011. Ginsenoside Rh2 induces Bcl-2 family proteins-mediated apoptosis in vitro and in xenografts in vivo models. J. Cell. Biochem. 112 (1), 330–340.
do Canto, A., et al., 2016. Diphenylhexatriene membrane probes DPH and TMA-DPH: a comparative molecular dynamics simulation study. Biochim. Biophys. Acta 1858 (11), 2647–2661.
Franke, T.F., et al., 2003. PI3K/Akt and apoptosis: size matters. Oncogene 22 (56), 8983–8998.
Frenkel, N., et al., 2014. Mechanistic investigation of interactions between steroidal saponin digitonin and cell membrane models. J. Phys. Chem. B 118 (50), 14632–14639.
Gamble, W., et al., 1978. Procedure for determination of free and total cholesterol in micro- or nanogram amounts suitable for studies with cultured cells. J. Lipid Res. 19 (8), 1068–1070.
George, K.S., Wu, S., 2012. Lipid raft: a floating island of death or survival. Toxicol. Appl. Pharmacol. 259 (3), 311–319.
Goodwin, J.S., et al., 2005. Ras diffusion is sensitive to plasma membrane viscosity. Biophys. J. 89 (2), 1398–1410.
Gotoh, K., et al., 2014. The antitumor effects of methyl-beta-cyclodextrin against primary effusion lymphoma via the depletion of cholesterol from lipid rafts. Biochem. Biophys. Res. Commun. 455 (3–4), 285–289.
de Groot, C., Muller-Goymann, C.C., 2016. Saponin interactions with model membrane systems - Langmuir monolayer studies, hemolysis and formation of ISCOMs. Planta Med. 82 (18), 1496–1512.
Guo, X.X., et al., 2014. p53-dependent Fas expression is critical for Ginsenoside Rh2 triggered caspase-8 activation in HeLa cells. Protein Cell 5 (3), 224–234.
Ikonen, E., 2008. Cellular cholesterol trafficking and compartmentalization. Nat. Rev. Mol. Cell Biol. 9 (2), 125–138.
Jiang, Y.S., et al., 2010. Cholesterol-dependent induction of dendrite formation by ginsenoside Rh2 in cultured melanoma cells. Int. J. Mol. Med. 26 (6), 787–793.
Kasibhatla, S., et al., 2006. Acridine orange/ethidium bromide (AO/EB) staining to detect apoptosis. CSH Protoc. 2006 (3).
Keukens, E.A., et al., 1996. Glycoalkaloids selectively permeabilize cholesterol containing biomembranes. Biochim. Biophys. Acta 1279 (2), 243–250.
Korchowiec, B., et al., 2015. Impact of two different saponins on the organization of model lipid membranes. Biochim. Biophys. Acta 1848 (10 Pt A), 1963–1973.
Kritchevsky, D., Davidson, L.M., Kim, H.K., 1973. Quantitation of serum lipids by a simple TLC-charring method. Clin. Chim. Acta 46 (1), 63–68.
Kwon, H.Y., et al., 2008. Selective toxicity of ginsenoside Rg3 on multidrug resistant cells by membrane fluidity modulation. Arch. Pharm. Res. 31 (2), 171–177.
Li, K.F., et al., 2018. Ginsenoside Rh2 inhibits human A172 glioma cell proliferation and induces cell cycle arrest status via modulating Akt signaling pathway. Mol. Med. Rep. 17 (2), 3062–3068.
Lingwood, D., Simons, K., 2010. Lipid rafts as a membrane-organizing principle. Science 327 (5961), 46–50.
Lorent, J.H., Quetin-Leclercq, J., Mingeot-Leclercq, M.P., 2014a. The amphiphilic nature of saponins and their effects on artificial and biological membranes and potential consequences for red blood and cancer cells. Org. Biomol. Chem. 12 (44), 8803–8822.
Lorent, J., et al., 2014b. Domain formation and permeabilization induced by the saponin alpha-hederin and its aglycone hederagenin in a cholesterol-containing bilayer. Langmuir 30 (16), 4556–4569.
Lorent, J.H., et al., 2016. Alpha-Hederin induces apoptosis, membrane permeabilization and morphologic changes in two cancer cell lines through a cholesterol-dependent mechanism. Planta Med. 82 (18), 1532–1539.
Lv, Q., et al., 2016. Antitumoral activity of (20R)- and (20S)-ginsenoside Rh2 on transplanted hepatocellular carcinoma in mice. Planta Med. 82 (8), 705–711.
Mollinedo, F., Gajate, C., 2015. Lipid rafts as major platforms for signaling regulation in cancer. Adv. Biol. Regul. 57, 130–146.
Park, E.K., et al., 2010. Induction of apoptosis by the ginsenoside Rh2 by internalization of lipid rafts and caveolae and inactivation of Akt. Br. J. Pharmacol. 160 (5), 1212–1223.
Park, B., et al., 2013. Neutral sphingomyelinase 2 modulates cytotoxic effects of protopanaxadiol on different human cancer cells. BMC Complement. Altern. Med. 13, 194.
Prasad, R., et al., 2009. Membrane cholesterol depletion from live cells enhances the function of human serotonin(1A) receptors. Biochem. Biophys. Res. Commun. 389 (2), 333–337.
Qi, L.W., Wang, C.Z., Yuan, C.S., 2011. Ginsenosides from American ginseng: chemical and pharmacological diversity. Phytochemistry 72 (8), 689–699.
Qiu, J., et al., 2014. Ginsenoside Rh2 promotes nonamyloidgenic cleavage of amyloid precursor protein via a cholesterol-dependent pathway. Genet. Mol. Res. 13 (2), 3586–3598.
Servais, H., et al., 2006. Gentamicin causes apoptosis at low concentrations in renal LLC-PK1 cells subjected to electroporation. Antimicrob. Agents Chemother. 50 (4), 1213–1221.
Shi, Q., et al., 2016. Anticancer effect of 20(S)-ginsenoside Rh2 on HepG2 liver carcinoma cells: activating GSK-3beta and degrading beta-catenin. Oncol. Rep. 36 (4), 2059–2070.
Simons, K., Ikonen, E., 1997. Functional rafts in cell membranes. Nature 387 (6633), 569–572.
Simons, K., Sampaio, J.L., 2011. Membrane organization and lipid rafts. Cold Spring Harb. Perspect. Biol. 3 (10), a004697.
Sudji, I.R., et al., 2015. Membrane disintegration caused by the steroid saponin digitonin is related to the presence of cholesterol. Molecules 20 (11), 20146–20160.
Tsuchiya, H., 2015. Membrane interactions of phytochemicals as their molecular

mechanism applicable to the discovery of drug leads from plants. Molecules 20 (10), 18923–18966.
Upadhyay, A.K., et al., 2006. Methyl-beta-cyclodextrin enhances the susceptibility of human breast cancer cells to carboplatin and 5-fluorouracil: involvement of Akt, NF-kappaB and Bcl-2. Toxicol. Appl. Pharmacol. 216 (2), 177–185.
Widmann, C., Gibson, S., Johnson, G.L., 1998. Caspase-dependent cleavage of signaling proteins during apoptosis. A turn-off mechanism for anti-apoptotic signals. J. Biol. Chem. 273 (12), 7141–7147.
Yi, J.S., et al., 2009. Ginsenoside Rh2 induces ligand-independent Fas activation via lipid raft disruption. Biochem. Biophys. Res. Commun. 385 (2), 154–159.
Zidovetzki, R., Levitan, I., 2007. Use of cyclodextrins to manipulate plasma membrane cholesterol content: evidence, misconceptions and control strategies. Biochim. Biophys. Acta 1768 (6), 1311–1324.

3. Characterize membrane lipid composition, organization and biophysical properties in breast cancer cell lines with increasing malignancy potential as a preliminary step before the evaluation of Rh2-membrane effects

In the third part of this thesis, I initiated a long-term study aiming at evaluating whether Rh2 could be used as a potential agent for breast cancer treatment. As a first step, we characterized membrane lipid composition, organization and biophysical properties in human mammary epithelial MCF10A cell line series, which offers the same genetic background but an increasing malignancy potential: the non-invasive mammary epithelial cells MCF-10A, the pre-malignant MCF-10AT and the malignant MCF-10CaCl1. The goal is to elucidate whether and how a different lipid composition and/or organization could contribute to tumor cell motility and invasion. Our ultimate goal is to determine whether ginsenoside Rh2 could affect tumor migration by targeting specific lipid regions.

3.1 Introduction and aims

The course of tumor metastasis entails complex multistep processes which include local tumor cell invasion, entry into the vasculature followed by the exit of cancer cells from the circulation and colonization at distal sites leading to the formation of secondary tumors, largely responsible for the mortality and morbidity of cancer[291, 292]. During the initial phases of tumor dissemination, many changes that occur (e.g. loss of cell adhesion, modification in cell shape and acquisition of cell motility) are characteristic of invasive pre-malignant cells at the primary site. After that, cancer cells initiate the invasion-metastasis cascade and need to squeeze through confined and narrow spaces of blood and lymphatic vessels to spread around tissues. Each step of cancer cell migration and invasion requires extensive deformation of the PM (e.g. distortion, deformation, compression and expansion). However, how PM composition, organization in lipid domains and biophysical properties participate to those deformations are poorly understood.

Regarding membrane composition, some studies discriminated, through lipid profile assessment, breast malignant cells from benign ones as well as low- and high-grade tumors[163, 172]. Wang et al. identified a total of 31 lipids, especially phosphatidylcholine (PC), phosphatidylserine (PS), phosphatidylinositol (PI) species, as

upregulated and eight lipids, such as sphingomyelin (SM) and phosphatidylethanolamine (PE) species, as downregulated in highly invasive breast cancer lines as compared to poorly invasive breast cancer lines[160]. Moreover, MT3 breast cancer cells show a significant decrease of Chol which correlates with an increase of membrane fluidity and metastatic foci registered in mice lungs[165].

Moving to membrane organization, several groups have provided evidence for submicrometric lipid domains at the surface of various cell types[56, 66]. Thus, using living red blood cells (RBCs) subjected to severe and regular deformation during its 120-days lifetime, Tyteca's group observed the coexistence of several types of lipid domains at their outer PM leaflet[58, 59]. Those domains were revealed thanks to (i) the use of fluorescent toxin fragments specific to endogenous SM (lysenin*) and Chol (Theta*); and (ii) the insertion of fluorescent BODIPY-lipids at trace levels in the PM. Three types of domains coexist, showing differential lipid enrichment, membrane biophysical properties and contribution to RBC deformation. Indeed, Chol-enriched domains gather in highly curved areas upon RBC stretching whereas GM1/PC/Chol- and SM/PC/Chol-enriched domains increase in abundance upon calcium influx during RBC deformation and calcium efflux during RBC shape restoration, respectively[68, 293]. However, only few studies addressed submicrometric lipid domains in cancer cell lines. Nevertheless, imaging by atomic force microscopy (AFM) of membranes purified by ultracentrifugation from MDA-MB-231 breast cancer cells revealed the presence of submicrometric domains[66]. Jurkat-T lymphoblastic leukemia cells exhibit SM-rich membrane domains spatially and functionally different from those enriched with the ganglioside GM1[56].

Finally, concerning membrane biophysical properties[294], a loss of membrane lipid asymmetry has been observed in several types of cancer, as revealed by the exposure of the negatively-charged PS at the outer PM leaflet[295, 296]. Membrane fluidity also appears to be altered in cancer cells and could be correlated with their malignant potential and capability to metastasize. For example, lymphoma and lung carcinoma cells exhibit higher membrane fluidity than their normal counterparts[173, 297]. In contrast, other cancer cells, such as the hepatoma tumor cell line, present decreased membrane fluidity[298].

While lipid profile reprogramming is now considered as a potential marker for aggressive tumors[163, 172], the distribution pattern of membrane lipids and their specific contribution to breast cancer invasiveness remain poorly understood. In this study, we aimed to address some of those questions in the human mammary epithelial MCF10A cell line series, which offers the same genetic background[290]. Those cells were first characterized using as read-outs (i) the level of Akt phosphorylation, a well-

known deregulated protein in various cancer cell types[299]; (ii) the extent of migration and invasion; and (iii) the membrane stiffness. We then started to ask whether differences in migration/invasion and stiffness could be related to differential global SM and Chol contents and PM lipid spatial distribution.

Those characterizations represent an essential step to understand how motility is initiated in tumor cells and to elucidate whether membrane lipids could provide new diagnostic approaches and/or targets for the treatment of cancer. Among drugs, one can consider to test the ginsenoside Rh2, which induces apoptosis upon Chol depletion and preferentially interacts with SM[219, 220]. This compound has been shown to reduce cell migration and invasion in MDA-MB-231 and MCF-7 human breast cancer cell lines[300] but the potential implication of membrane lipids in this activity is still not investigated.

3.2 Methods and preliminary data

The MCF-10A cell line series with increasing malignancy potential, i.e. the normal human mammary epithelial cells MCF-10A, the pre-malignant MCF-10AT and the malignant MCF-10CaCl1[290], were first characterized regarding the Akt phosphorylation state. Indeed, increased activation of the PI3K/Akt signaling pathway is often associated with tumors and correlates with excessive cell survival and proliferation. According to[301, 302], the ratio of pAkt/GAPDH increased in the MCF-10CaCl1 cell line as compared to the MCF-10A **(Fig. 1A, B)**. When expressed by reference to total Akt, pAkt seemed to be specifically elevated in the malignant MCF-10CaCl1 cells **(Fig. 1C)** but the high standard deviation could not allow to conclude to a significant statistical difference. These experiments are currently being repeated to validate or not this observation.

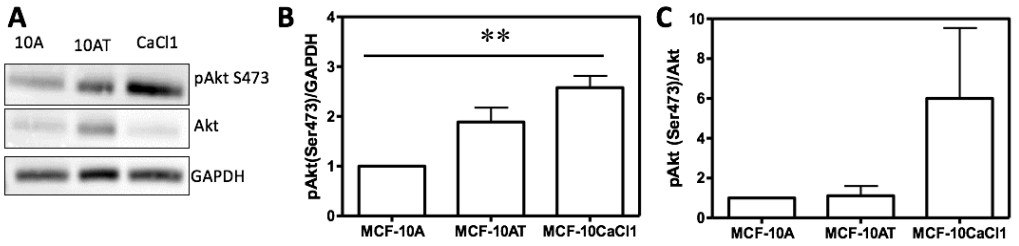

Fig 1. Increase of pAkt/GAPDH ratio in the MCF-10CaCl1 cell line as compared to the MCF-10A and -AT. A. Representative western blotting against phospho-Akt (Ser473), total Akt and GAPDH (control for protein loading). **B.** Quantification of pAkt/GAPDH. **C.** Quantification of pAkt/total Akt. One-way ANOVA with Bonferroni's multiple comparison post-test. Results are means of three independent experiments. **p< 0.01. Data from Mauriane Maja (Tyteca's group, DDUV Institute).

We then compared the spontaneous and oriented migration ability as well as the invasion potential of those three cell lines. As compared to the normal MCF-10A cells, the pre-malignant MCF-10AT cells exhibited a higher spontaneous migration in IBIDI chambers after 6 hours while malignant MCF10-CaCl1 migrated less. After 24 hours, both MCF-10A and MCF-10AT migrated more than the MCF-10CaCl1 cells **(Fig. 2A)**. Comparison of oriented migration in Transwell chambers suggested differences between MCF-10A and MCF-10AT after 6 hours, MCF-10AT cells exhibiting higher oriented motility than MCF-10A cells. Such differences were not seen after 24 hours **(Fig. 2B)**. Those data indicated that the malignant MCF-10CaCl1 cells were surprisingly the least able to migrate, both spontaneously and in an oriented manner. In contrast, upon invasion through a thin matrigel layer in Transwell chambers, they exhibited higher invasive potential than non-cancerous cells after both 6 and 24 hours **(Fig. 2C)**. Unfortunately, since these last results were from only one experiment in triplicates, further experiments are required to perform statistical analysis. Altogether those preliminary data suggested that the pre-malignant cells were the most apt to spontaneous and oriented migration and that malignant MCF-10CaCl1 cells were the most able to invasion through confined space.

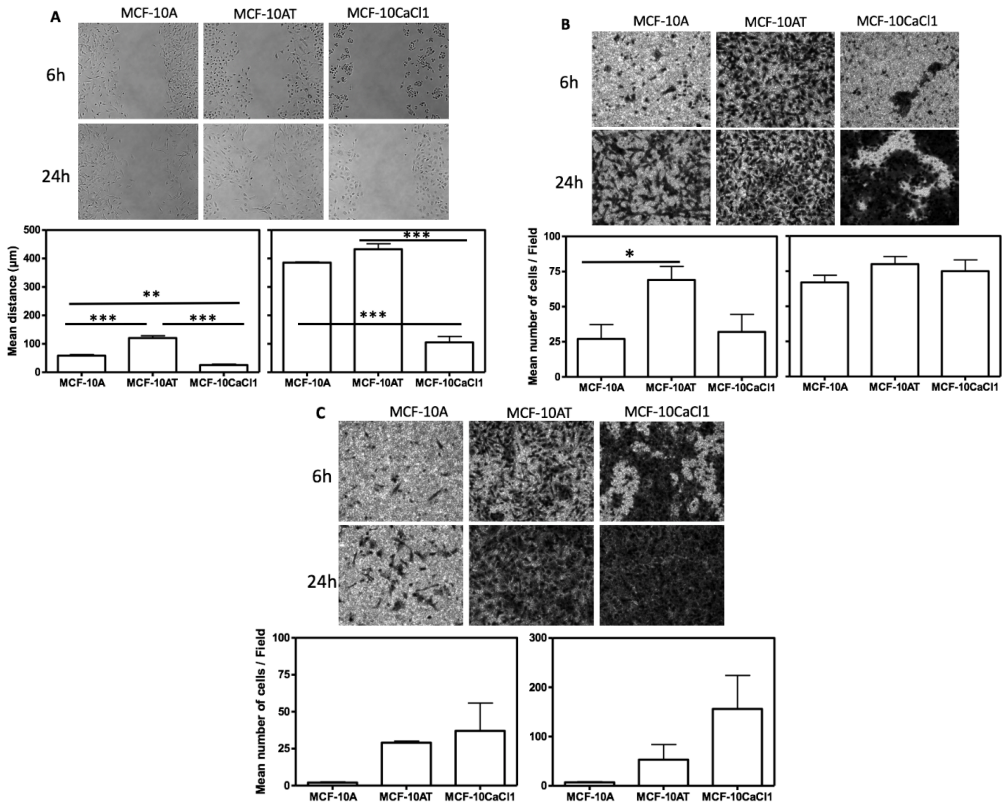

Fig 2. Differential spontaneous migration, oriented motility and invasion in the MCF-10A cell lines. **A.** Spontaneous migration in the cell-free area of IBIDI chambers for 6 and 24 hours. **B.** Oriented migration in Transwell assay toward 10% serum for 6 and 24 hours. **C.** Invasion in Transwell chambers with a matrigel layer (0.5mg/ml) toward 10% serum for 6 and 24 hours. Data from Mauriane Maja (Tyteca's group, DDUV). **A, B.** One-way ANOVA with Bonferroni's multiple comparison post-test. Results are means of three independent experiments in triplicates. *p<0.05; **p<0.01; ***p< 0.001. **C.** Results are means of one independent experiments in triplicates

To next evaluate whether the differential invasiveness of the three cells lines could correlate with a differential membrane stiffness, we used tapping-mode atomic force microscopy (AFM). This method measures the resistance of the cell to an externally induced deformation, by monitoring the interaction force of the tip of cantilever striking against the surface and detaching from the sample surface on each

oscillation cycle by using a large vibration amplitude. MCF-10AT and MCF-10CaCl1 cells were found to have an elasticity modulus significantly lower than the one of the benign MCF-10A **(Fig. 3)**. Thus, as expected from the literature[303, 304], (pre)malignant cells were softer than their counterparts, a property hypothesized to facilitate migration out of the primary tumor into circulation[305].

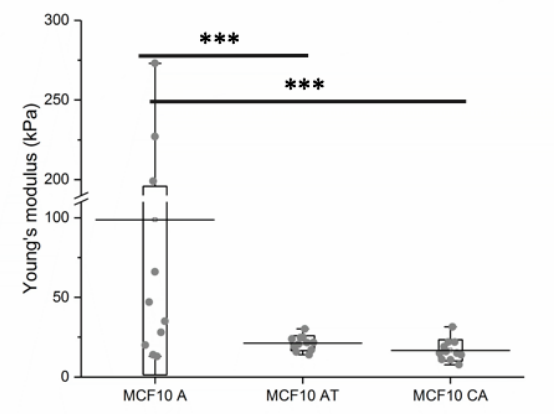

Fig 3. Lower stiffness of the MCF-10AT and MCF-10CaCl1 than MCF-10a cells. The stiffness of the cells is represented by its Young's modulus. Each point represents the averaged apparent Young's modulus of a single cell (11 cells/condition). One-way ANOVA with Bonferroni's multiple comparison post-test. ***p< 0.001. Data from Dr. Andra Dumitru (Alsteens's group, ISV, UClouvain-LLN).

As lower Chol levels in metastatic cells could correlate with a more deformable membrane and a higher ability to invade surrounding tissues[165, 173], we next determined if the change of membrane stiffness could be linked to a change of membrane lipid content. For this purpose, as a first step, we quantified global Chol, SM and total phospholipid contents. The three cell lines exhibited a similar Chol/phospholipid ratio **(Fig. 4, left)**. Concerning SM content, pre-malignant MCF-10AT cells showed an equivalent ratio of SM/phospholipid as compared to the MCF-10A, while malignant MCF-10CaCl1 cells exhibited a lower ratio **(Fig. 4, right)** which is in agreement with the literature[160]. To further test whether such modifications could be correlated with cell stiffness, it is required to analyze Chol and SM composition specifically in the PM upon isolation by cell fractionation. This analysis will be extended to PC as well as ganglioside species as they have been shown to cluster into lipid domains in RBCs. Hence, a particular attention will be given to lipid chain length and

unsaturation number (see section 2.2 as a state of the art).

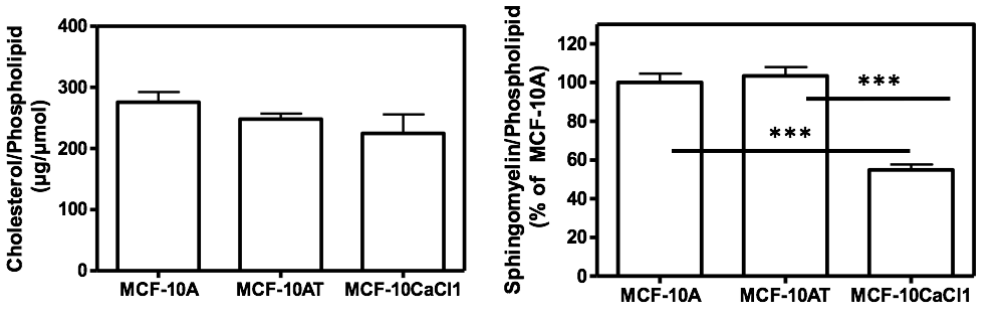

Fig 4. Similar Chol-to-phospholipid but lower SM-to-phospholipid ratio in MCF-10CaCl1 as compared to MCF-10A and MCF-10AT. Free Chol and SM levels were measured by Amplex red cholesterol assay and silica gel thin layer chromatography, respectively. Data were expressed to phospholipid content (phosphorus assay after lipid extraction). One-way ANOVA with Bonferroni's multiple comparison post-test. Results are means of three independent experiments in triplicates. ***p< 0.001.

Altogether those preliminary data seemed to indicate that malignant MCF-10CaCl1 cells differed from their counterpart by an increased invasion ability, a decreased SM content and a lower PM stiffness. We then explored if those changes could be accompanied by changes of lipid organization. We started by analyzing the PM distribution of GM1 and SM by labeling the three cell lines with two complementary unrelated probes: the fluorescent GM1 analog (BODIPY-GM1) on one hand and a toxin specific to endogenous SM (mCherry-lysenin; lysenin*) on the other hand[58]. Several fluorescent lipid analogs are available. Among those, we chose a fluorescent lipid in which the BODIPY fluorophore, which presents a good quantum yield and a higher photostability than other fluorophores (e.g. NBD), replaces a part of the lipid fatty acyl chain.. Although fluorescent lipid analogs are easy to use, they could present drawbacks due to insertion in the PM of exogenous lipids, even if they are used at trace level. Contrary to fluorescent lipid analogs, fluorescent toxin fragments, like lysenin*, allow direct labelling of endogenous lipids. Respective advantages and drawbacks of fluorescent lipid analogs and toxin fragments are described in [7]. Labelled cells were then analyzed by confocal vital imaging and colocalization between two probes was quantified using Zen software. As a first step, we evaluated the reliability of the method for colocalization analysis using images generated from cells labeled with two complementary probes for a same lipid, i.e. SM, by insertion of exogenous BODIPY-SM vs direct recognition using lysenin* **(Fig. 5**)

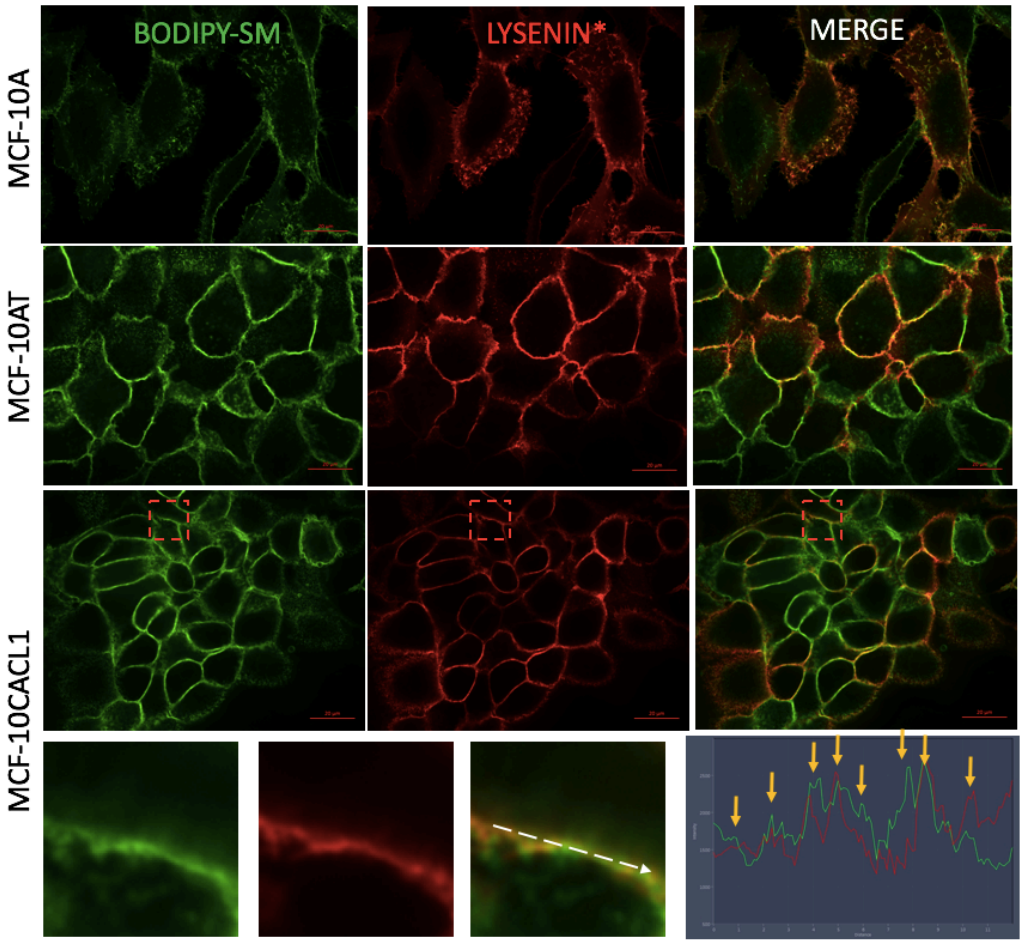

Fig 5. Large, but not perfect, overlap between two complementary SM probes (BODIPY-SM and lysenin*) in the three cell lines. MCF-10A (top), MCF-10AT (middle), MCF-10CaCl1 (below) cells were cultured on coverslips, labelled with BODIPY-SM (1 µM) for 15 min at 4°C and then with lysenin* (1,25 µM) also for 15 min at 4°C. All samples were then visualized by a spinning disk confocal microscope (COSD). Below, right: line intensity profile of BODIPY-SM (green) and lysenin* (red) signals measured along the white line on MCF-10CaCl1 cells. Yellow arrows indicate regions labeled by both BODIPY-SM and lysenin*. Representative images of 8-22 images. All scale bars, 20 µm.

For quantification, every pixel in the image is plotted in the scatter diagram based on its intensity level from each channel. Based on the scatter plot, the software automatically analyzes parameters, including:

- the Pearson's Correlation Coefficient (PCC), which reflects the correlation of the pixel intensities in the two channels. It measures the relationship between signals whether the signal value in one channel rises simultaneously with the other, or if one signal falls when the other rise. Values are between +1 and −1, where 1 reveals total positive linear correlation, 0 no linear correlation, and −1 total negative linear correlation. For pixel i in the images, R and G are intensities of the red and green channel respectively.

$$R_r = \frac{\sum (R_i - \bar{R}) \times (G_i - \bar{G})}{\sqrt{\sum (R_i - \bar{R})^2 \times \sum (G_i - \bar{G})^2}}$$

- Colocalization coefficient – M_{red} and M_{green}: M_{red} is the sum of the intensities of red pixels that have a green component divided by the total sum of red intensities. Ri, coloc= R_i if $G_i > 0$; Gi, coloc= G_i if $R_i > 0$.

$$M_{red} = \frac{\sum_i R_{i,coloc}}{\sum_i R_i} \qquad M_{green} = \frac{\sum_i G_{i,coloc}}{\sum_i G_i}$$

As shown in **Table 1**, BODIPY-SM and lysenin* showed a PCC of ~0.45, similar in the three cell lines. Same results were obtained once the labeling with the two probes was performed in the opposite order, i.e. lysenin* then BODIPY-SM (data not shown). Although those PCC values were closed to ~0.5, they are however lower than those obtained in experiments with RBCs showing an almost perfect colocalization between BODIPY-SM and lysenin* probes which reached PPC values of ~0.65[58]. Regarding the colocalization coefficient, more red pixels (lysenin*) overlapped with green pixels (BODIPY-SM) (Mred: ~0.77) than the opposite (Mgreen: ~0.52). Accordingly, Carquin et al. observed on RBCs that, at high lysenin* concentration (2.5 µM), lysenin*-labeled domains were equally labeled by BODIPY-SM whereas

accessibility of BODIPY-SM to lysenin*-saturated domains was strongly reduced[58]. It could therefore be useful to repeat the above experiments with a lower lysenin* concentration.

BODIPY-SM / lysenin*	PCC	Coloc. Coef - BODIPY-SM	Coloc. Coef – lysenin*
MCF-10A	0.469 ± 0.077	0.535 ± 0.148	0.769 ± 0.111
MCF-10AT	0.452 ± 0.073	0.502 ± 0.080	0.772 ± 0.119
MCF-10CaCl1	0.431 ± 0.065	0.518 ± 0.176	0.840 ± 0.09

Table 1. Similar Pearson's correlation coefficient (PCC) between BODIPY-SM and lysenin* in the three cell lines. SM was revealed by insertion in the PM of exogenous BODIPY-SM (1µM) and then by direct recognition upon labeling with lysenin* (1.25µM), both for 15 min at 4°C. Means and standard deviations of 8-22 images.

The distribution of SM in the PM was then compared to the one of GM1 upon labeling with lysenin* and BODIPY-GM1. In MCF-10A cells, BODIPY-GM1 and lysenin* signals largely overlapped (yellow arrows at **Fig. 6, top)** and the PCC between the two dyes was comparable to the one obtained between BODIPY-SM and lysenin*. In MCF-10AT cells, BODIPY-GM1 partially colocalized with lysenin* but additional spots were only labeled by BODIPY-GM1 (green arrows) or lysenin* (red arrows) **(Fig. 6, middle)**. This segregation between BODIPY-GM1 and lysenin* seemed to still increase in MCF-10CaCl1 cells **(Fig. 6, below)**, as revealed by the lowest PCC among the three cell lines **(Table 2)**. All those data suggested that cancer cells exhibited a higher segregation between SM and GM1 at the PM as compared to their counterpart. Regarding the colocalization coefficient, as previously observed with BODIPY-SM and lysenin*, more red pixels (lysenin*) overlapped with green pixels (BODIPY-GM1) than the opposite, with no differences between the three cell lines.

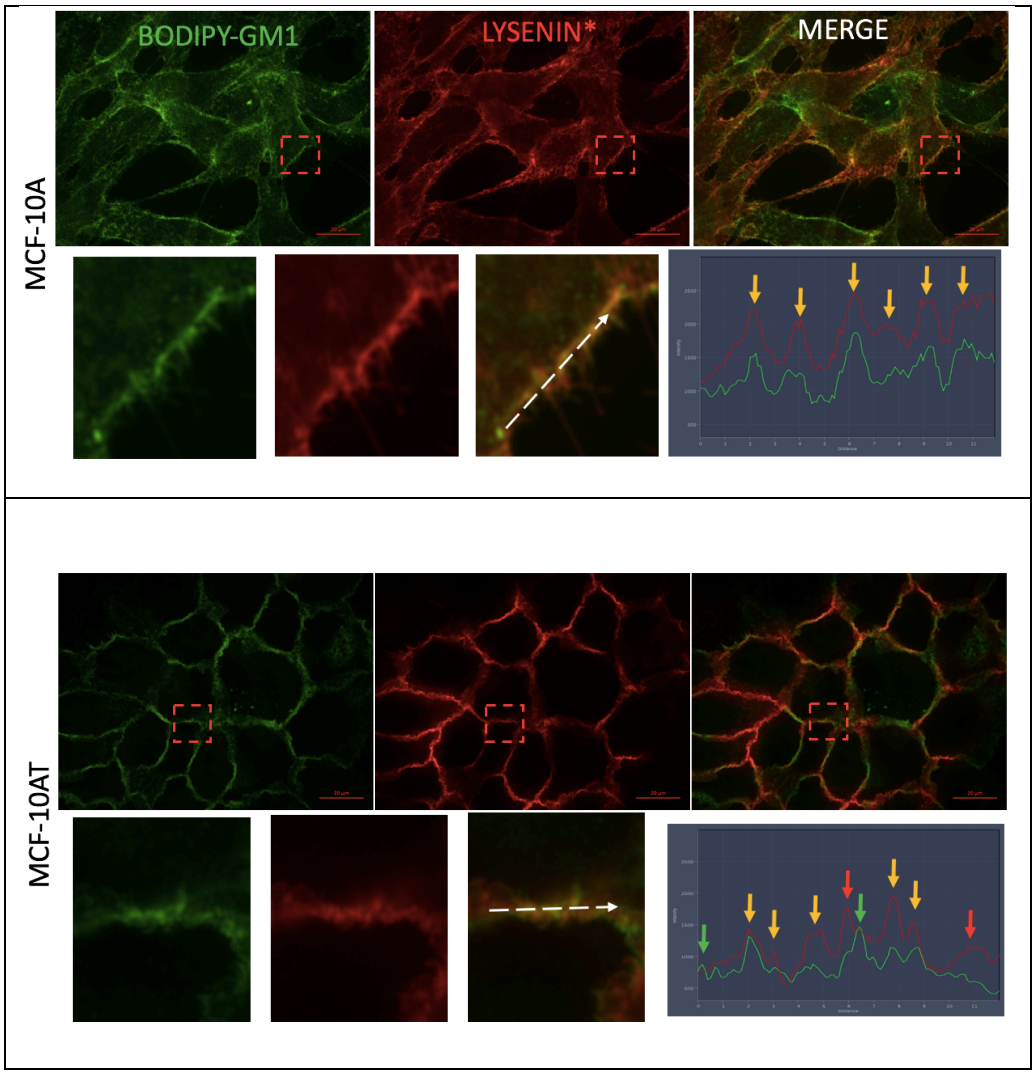
BODIPY-GM1
LYSENIN*
MERGE
MCF-10A
MCF-10AT

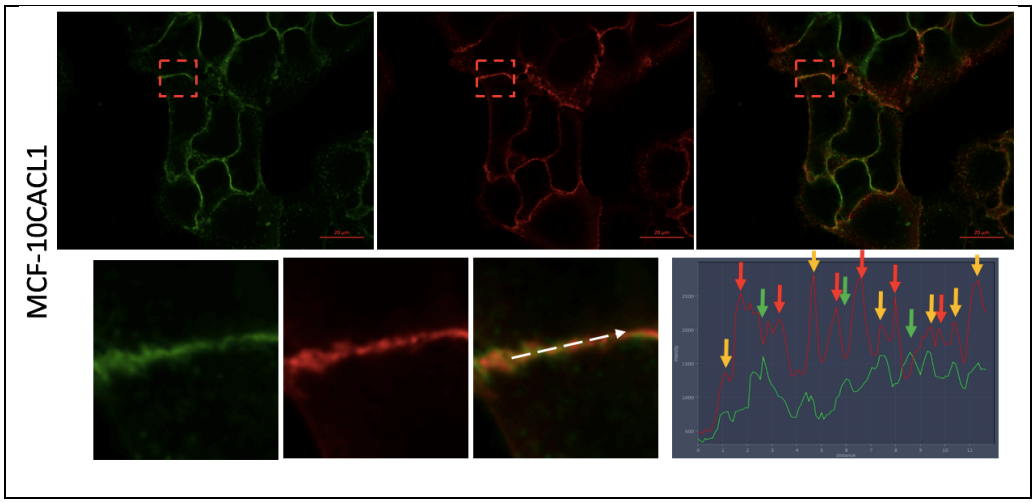

Fig 6. Decreased overlap between GM1 and SM signals in breast cancer cells as compared to non-cancer cells. MCF-10A (top), -AT (middle), -CaCl1 (below) cells were cultured on coverslips, labelled with BODIPY-GM1 (1 µM) for 15 min at 4°C and then with lysenin* (1,25 µM) for another 15 min at 4°C. All samples were then analyzed by confocal vital imaging using a spinning disk microscope. Line intensity profiles of BODIPY-GM1 (green) and lysenin* (red) signals were measured along the white lines. Yellow arrows indicate membrane areas labeled by both BODIPY-GM1 and lysenin* while green and red arrows indicate membrane regions labeled by BODIPY-GM1 or lysenin*, respectively. All scale bars, 20 µm. Representative of 12-15 images.

BODIPY-GM1/ lysenin	PCC	Coloc. Coef - Bodipy-GM1	Coloc. Coef-lysenin*
MCF-10A	0.465 ± 0.106	0.482 ± 0.138	0.663 ± 0.137
MCF-10AT	0.355 ± 0.068	0.538 ± 0.136	0.556 ± 0.149
MCF-10CaCl1	0.314 ± 0.087	0.453 ± 0.093	0.705 ± 0.055

Table 2. Lower Pearson's correlation coefficient between BODIPY-GM1 and lysenin* in breast cancer cells as compared to non-cancer cells. Cells were labelled by insertion of exogenous BODIPY-GM (1µM) for 15 min at 4°C and then by lysenin* (1.25µM) for another 15 min at 4°C. Mean and standard deviation of 12-15 images.

Since the increased Akt phosphorylation in cancer cells could potentially result from a decrease of phosphatidylinositol (4,5)-bisphosphate (PIP2) through PI3K activation, we also questioned PIP2 distribution at the inner PM leaflet thanks to the expression of the fluorescent protein marker PH-PLCδ1[63] while the lact-C2 marker was expressed to visualize the organization of PS[64]. Our preliminary data suggested that MCF-10AT showed a lower PCC between Lact-C2 and PH-PLCδ1 markers than MCF-10A and MCF-10CaCl1 cells. Additional experiments are necessary to confirm these preliminary data.

As mentioned in the introduction, our goal is to test whether ginsenoside Rh2 could affect tumor migration by targeting specific lipids or lipid regions at the PM. Before that, it was crucial to compare the different breast cancer cell lines for their migration/invasion potential but also for their membrane lipid composition, organization and biophysical properties. We started to determine non-cytotoxic doses of ginsenoside Rh2 to discriminate its apoptotic activity from its anti-metastatic potential (migration and invasion). For this purpose, the three cell lines were treated with increasing concentrations of Rh2 from 5 to 50 µM for 24 hours and tested for cell viability using 3-(4,5-dimethylthiazol-2-yl)-2,5-diphenyltetrazolium bromide (MTT) **(Fig. 7)**. Treatment with 20 and 50 µM Rh2 killed almost all the three cell lines. At a concentration of 10 µM, ginsenoside Rh2 decreased cell viability to a higher extent in MCF-10CaCl1 than MCF-10A. 5 µM of Rh2 showed no or very low toxicity and therefore will be used in the future to evaluate the effect of Rh2 on cell migration and invasion after 24 hours.

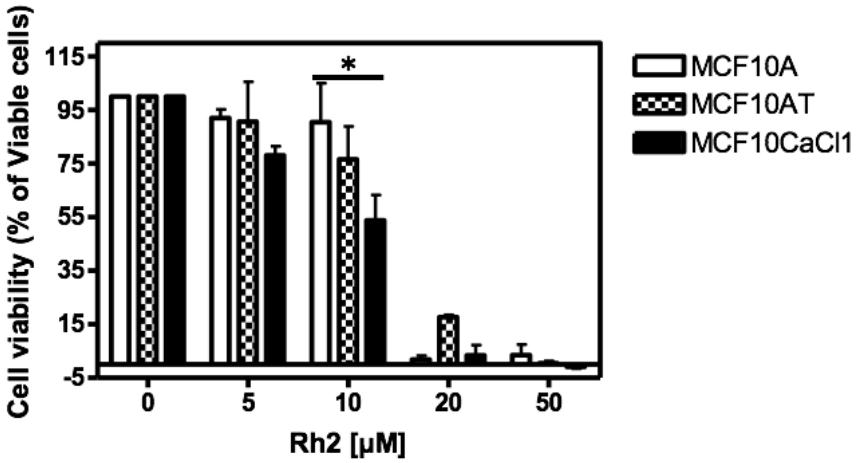

Fig 7. Higher decrease of cell viability in MCF-10CaCl1 than MCF-10A treated with 10 µM Rh2. Cell viability after treatment with increasing concentrations of Rh2 was determined by the colorimetric MTT assay. Viable cells contain NAD(P)H-dependent oxidoreductase enzymes which reduce the MTT reagent to formazan, an insoluble crystalline product with a deep purple color. Two-way ANOVA with Bonferroni's multiple comparison post-test. Results are means of three independent experiments in triplicates. *p< 0.05.

3.3 Summary

The above preliminary results indicated that MCF-10CaCl1 differed from their non-cancerous counterparts MCF-10A, exhibiting a lower SM content and a lower membrane stiffness. In addition, overlap between GM1 and SM in the outer PM leaflet decreased in premalignant MCF-10AT and malignant MCF-10CaCl1 as compared to non-cancer cells. Perspectives will be developed in the chapter IV.

CHAPTER IV: GENERAL DISCUSSION AND PERSPECTIVES

In this chapter, we first summarize the major published results obtained in this thesis (section 1) and highlight strengths and weaknesses of approaches used while proposing some alternatives (section 2). We then raise unsolved questions regarding the specific contribution of PM (section 3.1), lipids (section 3.2), lipid packing (section 3.3), lateral heterogeneity (section 3.4) and Akt protein (section 3.5) for the activity of Rh2. We then ask how the results obtained with Rh2 can be extended to other saponins (section 3.6). We finally dedicate a section to new chemotherapeutic agents interacting with membrane (section 3.7) and discuss the potential use of Rh2 as chemotherapeutic agent (sections 4,5, 6).

1. Summary of key findings regarding the Rh2 activity

The purpose of this research was to investigate the membrane-related effects and the apoptotic signaling pathway induced by ginsenoside Rh2 and to evaluate the respective importance of Chol and SM in these effects.

In the first part of this work, we used model systems including lipid monolayers and liposomes (LUVs and GUVs) while using biophysical techniques. It is important to stress that simplification of the lipid membrane composition is critical to understand the Rh2-membrane interaction and its lipid preferences at the molecular level. On lipid monolayers, we evidenced that Rh2 interacts more favorably with eSM and DOPC than with Chol and ePC. Using LUVs, we showed that Rh2 increases vesicle size, decreases membrane fluidity and induces membrane fusion and permeability. On GUVs, we evidenced that Rh2 generates positive curvatures in eSM-containing GUVs and small buds followed by intra-luminal vesicles in eSM-free GUVs. Our data indicate that eSM promotes and accelerates membrane-related effects induced by Rh2 whereas Chol slows down and depresses these effects.

In the second part, we turned to human cancer cell lines with differential Chol content (carcinomic human alveolar basal epithelial A549 cells, human monocytic leukemia THP-1 and U937 cells), allowing us to elucidate the role of this lipid in the Rh2-induced apoptosis. We observed higher cellular uptake of Rh2 upon Chol depletion explaining why apoptotic signaling pathway induced by Rh2 was observed earlier and to a higher extent in Chol-depleted cells as compared to non-depleted cells. Mechanisms involve the alteration of PM packing, the dephosphorylation of Akt and the activation of the intrinsic pathway of apoptosis (loss of mitochondrial membrane

potential, caspase-9 and -3 activation). All these features are induced faster in Chol-depleted cells. In contrast to Chol removal, SM depletion confers resistance towards Rh2-induced apoptosis.

In conclusion, our work challenges the usual view that most saponins mediate their membrane-related effects and cytotoxic activity through an interaction with Chol. Here the action of Rh2 is enhanced by the interaction with membrane SM but depressed by Chol.

2. Limitations of the work and alternatives

2.1 Model membranes

As biological membranes are very complex systems (section 1.3.6), this makes the importance of SM and Chol for Rh2-membrane interaction very difficult to investigate. For those reasons, we first started our experiments using artificial membrane models, as simplified systems in which physical and chemical parameters can be controlled. We used three different membrane models: lipid monolayers, LUVs and GUVs. Each model has its own advantages, already mentioned in section 1.3.6. However, it has to be kept in mind that these artificial model systems have some limitations as they do not capture the whole complexity of biological membrane. First, our experiments have been performed on symmetric LUVs and therefore do not take into account the asymmetry found in PMs. Second, our model membranes possess a limited lipid compositional complexity involving up three different lipid species, PC, SM and Chol considered as the three main lipids of the outer leaflet of eukaryotic cell PMs. We modified gradually the lipid composition from binary SM:PC (1:1) or PC:Chol (1:1) to ternary system SM:PC:Chol (1:1:1). The latter exhibits liquid disordered and liquid ordered phases. Although this system is commonly used in model raft studies (section 1.3.2.1), the lipid composition of PM between species and cell types within species can show a high degree of diversity (see Table 2). Thus, such a composition limited to three lipids contrasts with the heterogeneous nature of the biological membranes enclosing more than thousand different lipids[306]. Third, it is challenging to reconstitute membrane proteins in model membranes while these affect the membrane structure and contribute to membrane properties and functions. Fourth, model membranes do not possess cytoskeletal components which affect lipid and protein diffusion at the cell surface and consequently the phase behavior of cell membranes[27]. Altogether, while the simplification of the membrane system is essential for the study of specific molecular interactions at the membrane level, it can also be an obstacle to understand

some membrane functions.

The first three limitations mentioned above (membrane asymmetry and diversity of lipids and proteins) could be overcome by using (i) asymmetric vesicles and (ii) giant PM vesicles (GPMVs), respectively. For instance, multiple promising approaches have been developed to prepare **asymmetric LUVs**: enzymes that modify outer leaflet lipid headgroups[307], oil-in-water techniques[308, 309] or external addition of lipid carrier molecules like hydroxypropyl-α-cyclodextrin (HPαCD)-mediated lipid exchange[310]. We describe below the first approach as it was demonstrated to produce asymmetric LUVs closely resembling to mammalian PMs in terms of asymmetry with SM and PC outside while PE and PS inside, and in which Chol content can be readily varied between 0 and 50 mol%. This method consists of using a binary donor-acceptor system to engineer an asymmetric population, as depicted in **Fig. 1**[311]. The heavy-acceptor (LUVs) is composed of lipids destined to be on the inner leaflet, while the light-donor population (MLVs) provides the desired outer leaflet composition. The exchange begins with the incubation of the acceptors and donors alongside HPαCD which exchanges lipids. To separate LUVs from MLVs by ultracentrifugation, the heavy-acceptor LUVs contain a dense sucrose solution while the light-donor MLVs is hydrated in pure water or buffer. Sucrose inside LUVs could affect bilayer properties and even if these vesicles contain the most essential features of PM both in terms of lipid composition and asymmetry, this approach does not capture the whole complexity of the cells. However, asymmetric LUVs are closer to cell PM than symmetric LUVs used in this work.

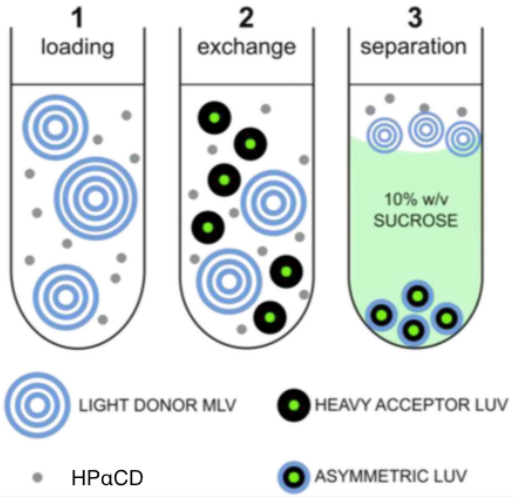

Fig 1. Schematic of asymmetric LUVs construction methods. (1) HPαCD is incubated with donor lipid MLVs suspended in a buffer and composed of the desired outer leaflet lipid; (2) HPαCD facilitates the exchange of the outer leaflet of the acceptor LUVs (entrapped with sucrose) with donor lipid; (3) the asymmetric LUVs are recovered after ultracentrifugation through sucrose cushion. Adapted from [311].

The overall lipid composition could be assessed by gas chromatography coupled to mass spectrometry (GC-MS) or ultra-high-performance liquid chromatography-MS (UHPLC-MS) which are sensitive to length and degree of unsaturation or lipids with same acyl chains but different headgroups, respectively. Besides approaches mentioned in section 1.3.3.3, the quantification of each leaflet's lipid composition could be determined by nuclear magnetic resonance (NMR) using the lanthanide shift reagent (e.g. Pr^{3+}) added externally and selectively interacting with the outer leaflet lipids.

➔ *It could be relevant to determine whether the transversal asymmetry affects Rh2 membrane activities (packing, fusion, permeability) and influence its interaction with membrane lipids, especially SM and Chol. As a first step, via isothermal titration calorimetry, we could incubate Rh2 with those asymmetric LUVs by varying SM and Chol levels and measure thermodynamic parameters such as the binding affinity (section 1.3.6).*

➔ *Based on our results, we hypothesize that Rh2 induces cell apoptosis through its interaction with the outer membrane leaflet mainly composed of SM, PC and Chol lipids leading to the alteration of biophysical membrane properties such as membrane packing. As proposed by the interleaflet lipid coupling mechanism (section 1.3.3.5), we suggest that the Rh2-induced alteration of the outer leaflet could affect the physical properties of the inner leaflet and prevent the binding of Akt or kinases such as PDK1 to the PM which conducts to prevent Akt phosphorylation and promote the mitochondrial apoptosis pathway. To test this hypothesis, we could begin to determine whether Rh2 could redistribute lipids from one leaflet to another in asymmetric LUVs resembling to mammalian PMs using NMR and reagents like 2,4,6-trinitrobenzen sulfonic acid (TNBS) (see section 1.3.3.3)[310].*

Besides asymmetric LUVs, **GPMVs** can be easily isolated by chemical vesiculants from almost any living cells and captures much of the compositional protein and lipid complexity of intact cell PM providing an alternative to vesicles constructed of synthetic or purified lipids[312]. Microscopically observed, GPMVs labeled with a fluorescent protein or lipid analog appear uniform on the micron-scale when imaged above the Tm, and separate into Lo and Ld phases (labelled with NBD-DPPE and rhodamine-DOPE, respectively) with differing membrane compositions and physical properties below this temperature[313]. The fluorescence spectroscopy of laurdan is often used to quantify the relative membrane order in GPMVs. One of the most notable uses of GPMVs is the assessing of lipid and protein partitioning between Lo and Ld phases through fluorescent labelling. However, it is important to keep in mind that several factors are still missing. The obvious notable limitations of GPMVs are the covalent modifications induced by chemical vesiculants. The more common preparation involves a combination of formaldehyde and dithiothreitol (DTT) which are nonspecific cross-linkers and reducers, respectively or *N*-ethyl maleimide which irreversibly reacts with terminal thiol (typically cysteine side chains)[314]. In addition, they are no longer coupled to cytoskeleton and have some signatures of loss of asymmetry[315]. Even with these important differences, GPMVs are membrane models that much more closely reproduce intact cell PM than do GUVs made of purified lipids.

➔ *As we evaluated by the GPex of laurdan that Rh2 increases eSM packing and Tm in LUVs, the use of GPMVs isolated from the three human breast cell lines with increasing malignant potential (MCF-10A, MCF-10AT, MCF-10CaCl1) will allow to evaluate whether Rh2 could change GPex and Tm and to what extent depending on the*

cell line. This technology will also provide a first indication regarding Lo and Ld in GPMVs and determine the potential effect of Rh2 on these vesicles. As one study showed the disorganization of lipid raft and inactivation of Akt by Rh2 in human epidermoid A431 carcinoma cell line[204], we could imagine to transfect the three breast cell lines with a plasmid expressing pEGFP-Akt (available in Addgene), prepare GPMvs from these cells and determine Akt localization in membrane phases and evaluate the impact of Rh2. To visualize these effects, we could use fluorescence imaging microscopy with ±250 nm resolution or stimulated emission depletion (STED) for a higher resolution (± 20-40nm)[316] (see section 1.3.2.1.1). GPMV formation anyway requires fixation step.

2.2 Tools for studying the role of lipids in the effects induced by Rh2

The concordance of results obtained through biophysical and cellular approaches dispel our concern regarding the use of SMase or MβCD to hydrolyze SM and generate Cer or remove Chol from the PM, respectively. Beside the pro-apoptotic activity of Cer (section 1.4.1.2) that we carefully evaluated and limited using a non-toxic concentration of SMase, Cer has been reported to promote transmembrane lipid motion, increase PM order and give rise to lateral phase separation[317]. Removal of Chol has been reported to decrease membrane packing of Ld phase[43, 318]. Since artificial membrane eSM:ePC LUVs are more sensitive to the Rh2 activity than ePC:Chol or eSM:ePC:Chol, we suggest that these potential biophysical properties changes have a minor impact regarding its preferential interaction for SM compared to Chol.

In addition, we confirmed that the faster and stronger effects induced by Rh2 in Chol-depleted cells compared to non-depleted cells are specific of the removal of Chol from PM by MβCD and does not result from an unspecific mechanism due to the pretreatment with MβCD. For instance, using the conventional anticancer drug etoposide, well-known to induce apoptosis in cancer cells[319], we did not observe significant difference between Chol-depleted and non-depleted cells (data not shown). In addition, depletion of Chol reduces the apoptosis induced by α-hederin, a saponin known to interact preferentially with Chol (section 3.2.1.6).

➔ *To confirm the importance of SM and Chol in the activity of Rh2, we could prevent SL and Chol synthesis using fumonisin B1 and statins, respectively. Fumonisin B1 inhibits sphingosine and Cer synthase while statins inhibit HMG-CoA reductase. However, as a consequence, there is an accumulation of intermediates of SL and Chol metabolism which could interfere with PM components and modify biophysical*

membrane properties[320]. This could potentially affect the activity of Rh2 and hinder its interaction with specific lipids such as SM and Chol.

3. Questions raised by this work

Since model membranes used in the first part of this thesis do not fully reflect the whole complexity of biological membranes, we also investigated the importance of Chol and SM in the cytotoxic activity of Rh2 in A549, THP-1 and U937 cells. Both biophysical and cellular approaches showed that the membrane-related effects and the cytotoxic activity of Rh2 are enhanced by SM but depressed by Chol. Therefore, even if artificial lipid bilayers are less complex than biological membranes, our data are consistent with those obtained in A549, THP-1 and U937 cells. The cytotoxic activity of Rh2 is inversely correlated with membrane Chol content in these cell lines differing by their membrane Chol level (carcinomic human alveolar basal epithelial A549 cells, human monocytic leukemia THP-1 and U937 cells; A549 > THP-1 > U937). However, this correlation is not observed in human breast epithelial MCF-10A cell line series with increasing malignancy potential. While malignant MCF-10CaCl1 cells has an equal Chol/phospholipid but a lower SM/phospholipid ratio compared to non-malignant MCF-10A cells, Rh2 seems to decrease the cell viability in higher extent in MCF-10CaCl1. Those results suggest that the membrane-related effects of Rh2 cannot be restricted to the global cell content in Chol and SM and several additional parameters should be considered, including (i) the surface *vs* intracellular accumulation of Rh2 (section 3.1); (ii) the intervention of other lipids than Chol and SM (section 3.2); (iii) the lipid packing (section 3.3); (iv) the heterogeneity of Chol and SM organization at the PM through lipid domains with differential lipid enrichment (section 3.4) and the role of Akt (section 3.5).

3.1 The main target for the action of Rh2?

The first hypothesis to explain the discrepancies between model membranes and A549, THP-1 and U937 cancer cells on one hand and the three breast cancer cell lines on the other hand is based on the possibility that the Rh2 main target is the PM and that Chol and SM contents at the cell surface could strongly vary from on cell type to another. For instance, while PM of myoblast contains 42mol% of Chol, PM of human macrophages exhibit only 8mol% compared to the total lipid fraction. Therefore, difference could be observed between the Chol abundance of PM and Chol content in the whole cells (the latter was measured in this thesis). In other words, while a

difference of 6-fold could be observed regarding Chol present in the PM of these cells, the Chol amount of the whole cells could attenuate or mask this difference.

➔ *To try to understand these discrepancies mentioned above, it will be essential to evaluate the ratio of SM/phospholipid in A549, THP-1 and U937 cells by thin layer chromatography and compare it to the ratio of the three breast cell lines. After that, it will be necessary to perform lipidomic analysis of PM of the three breast cell lines to evaluate a potential correlation between the levels of some lipids and the degree of malignant progression. After that, we could assess whether Rh2 could have a specific affinity for one of these lipids. In addition, the isolation of the PM from the whole cells will be also useful to determine the localization of Rh2 in the cells.*

Although a great variety of investigations on the biological activity of ginsenoside Rh2 is described through the modulation of many pathways, PM is poorly considered and little is known regarding the specific membrane lipid target of ginsenoside Rh2. For instance, *in silico* IMPALA methods used in this work indicated that Rh2 could not be able to cross the bilayer. In addition, the logP value (octanol-water partition coefficient) of Rh2 is 3.8. This value indicates that Rh2 is highly lipophilic which could suggest that Rh2 will be adsorbed or sequestered within the PM outer leaflet and will not flip-flop or diffuse into the cytosol. In addition, only 5 and 30 min were necessary to observe Rh2-induced membrane packing changes in cholesterol-depleted cells and non-depleted cells, respectively, whereas apoptosis markers induced by Rh2 (Akt inactivation, mitochondrial membrane depolarization and the activation of caspase-9 and -3) manifested later **(Fig. 2)**. These findings suggest that the primary action of Rh2 involved first changes of biophysical membrane properties leading then to dephosphorylation or cleavage of proteins. These effects take less time than slower events like gene modulation and protein expression proposed by some studies as the mechanism of action of Rh2[321, 322].

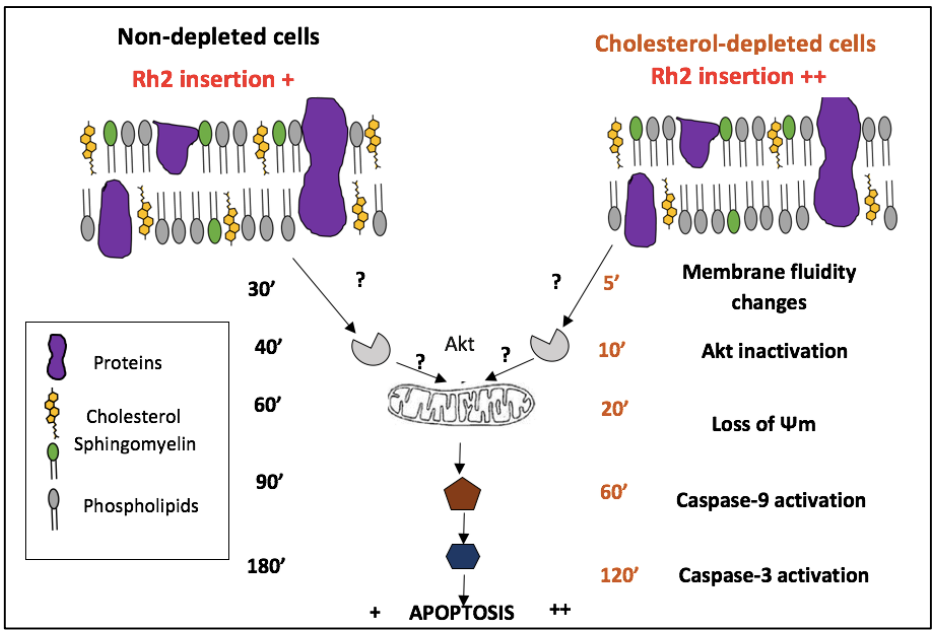

Fig 2. Schematic of Rh2-induced apoptosis in non-depleted and cholesterol-depleted cells. Rh2 decreases the phosphorylation of Akt and induces the activation of the intrinsic pathway of apoptosis through mitochondrial membrane depolarization and caspase-9 and -3 activations. All these features appear earlier in cholesterol-depleted cells as compared to non-depleted cells.

To reconcile these observations, we suggest that any change inflicted by Rh2 upon the biophysical membrane properties (membrane packing, fusion, permeability and budding) observed in model membrane could influence a range of membrane proteins (i.e Akt) involved in a huge number of cell signaling pathways which could, for example, modulate protein expression. In addition, as already mentioned, it is tempting to speculate that Rh2 could affect membrane organization in the outer leaflet which somehow influences the organization of the inner leaflet-associated proteins during signal transduction as proposed by the interleaflet coupling mechanism (section 1.3.3.5).

➔ *We could determine whether Rh2 is adsorbed or inserted within the PM from compression isotherm assay obtained by measuring the change of surface pressure (Π) that occurs when reducing the area occupied by one lipid or a binary or ternary lipid systems mixed with Rh2 (SM:PC vs PC:Chol vs SM:PC:Chol) spread at an air-buffer*

interface in a Langmuir trough. In addition, to evaluate the ability of Rh2 to penetrate into a lipid monolayer, we could determine an exclusion surface pressure by plotting the maximum surface pressure increase as a function of different initial surface pressures of lipid monolayers after the injection of Rh2 into the buffer subphase. This parameter corresponds to the initial surface pressure of the lipid monolayer above which no more Rh2 can penetrate the lipid film and increase the surface pressure. In other words, this parameter will give a hint regarding the membrane penetration power of the Rh2.

Even if these data seem to indicate that Rh2 is adsorbed or sequestered within the PM, we cannot exclude the possibility that the drug could enter the cytoplasm by facilitated diffusion via a transmembrane protein or by endocytosis and thereby affect organelles such as mitochondria and endoplasmic reticulum (ER). Unfortunately, in this thesis, quantification of Rh2 by HPLC MS/MS was realized in the whole cell without distinguishing the PM from the cytoplasm or intracellular organelles, hiding its exact cell localization.

Regarding the effects of Rh2 on mitochondria, we showed that Rh2 collapses mitochondrial membrane potential causing the activation of caspase-dependent apoptotic cell death. However, in this work, we do not know if Rh2 directly interacts with mitochondrial membrane or inactive Bcl-2 family proteins such Bcl-2 and Bcl-XL and promote the oligomerization of Bax and Bak required for mitochondrial permeabilization during apoptosis (section 1.4.1.1). Interestingly, it has been reported in human hepatoma SK-HEP-1 cells that Rh2 causes rapid and dramatic translocation of both Bak and Bax within mitochondrial membrane, which subsequently triggers mitochondrial cytochrome c release and consequent caspase activation[323]. These results suggest an indirect effect of Rh2 on mitochondrial membrane. Mobilization of ER calcium stores can initiate the activation of cytoplasmic death pathways through caspase-12 as well as sensitize mitochondria to direct pro-apoptotic stimuli[324]. Unlike other caspases, caspase-12 is remarkably specific to insults that elicit ER stress and is not proteolytically activated by other death stimuli.

➔ *To evaluate the impact of Rh2 on ER, we could assess the phosphorylation of the eukaryotic translation initiation factor 2 (eIF2) or the activation of the caspase-12. We could also envision to inhibit two well-characterized types of Ca^{2+}-channels in the ER, the inositol 1,4,5-triphosphate receptor (IP_3R) and the Ryanodine receptor (RyR) and evaluate the impact on the apoptosis after the treatment with Rh2.*

It is worth nothing that ER and mitochondria are mainly enriched in PC (40% - 50% of the total phospholipid) and exhibit only very low concentrations of Chol and SM in comparison with the PM [9]. If we confirm a direct effect of Rh2 with the membrane of these organelles, this could suggest that PC could also be involved in the activity of Rh2 as proposed in the next section.

3.2 Influence of specific membrane lipids for the activity of Rh2?

Even if we did not elucidate the location of Rh2 yet, it is tempting to speculate, based on similarity of Rh2 and Chol structures, that Rh2 could intercalate easier and faster into the membrane in Chol-depleted cells or in low amount or absence of Chol in artificial membranes by taking the place of Chol and/or interacting with SM. We suggest that the depressed effect of Chol could be explained through its favorable interaction with SM in lipid domains. Therefore, Chol could compete with Rh2, thereby depressing Rh2:SM interaction and related effects. However, even if the PM of RBCs contains a high level of Chol[15, 16], Rh2 is able to induce hemolysis[233], these results suggest that other lipids could be involved in the activity of Rh2. One study suggests that PC could be involved in the membrane activity of ginsenosides. For instance, the ginsenoside Rc showed stronger agglutinability with ePC than SM from bovine brain (major FA distribution: 18:0 (50%) and 24:1 (21%)). However, another ginsenoside Ro exhibited no lytic activity in ePC whatever the presence or absence of Chol (see section 3.2.2).

➔ *To evaluate the respective importance of specific lipids we could adopt a step-by-step approach, by modifying gradually the lipid ratio. For example, going from 1:1:1 to 1:1:3 SM:PC:Chol will be useful to confirm or not the protective role of Chol for the activity of Rh2.*

➔ *As we suggest that like Chol, Rh2 could interact more easily with SM than PC through the formation of a hydrogen bond between the OH group of Chol and the NH group of SM* ***(Fig. 2)****, we could compare the adsorption of Rh2 into pSM (N-palmitoyl-D-erythro-sphingosylphosphorylcholine) and POPC (1-palmitoyl-2-oleoyl-glycero-3-phosphocholine) monolayers using a Langmuir trough. The comparison of these lipids will give a hint regarding the importance of the amine group for the specificity of the membrane-Rh2 interaction. As lipid specificity is a key factor for the detailed understanding of the penetration and/or activity of lipid-interacting molecules, it is essential to extent our study to evaluate the potential role of other lipids in the activity of Rh2. In addition, we could also envision to perform small-angle X-ray scattering*

(SAXS) or attenuated total reflectance-infrared spectroscopy (ATR-FTIR) to provide relevant information at the molecular level regarding the interaction of Rh2 with specific lipid regions such as phospholipid phosphate groups or alkyl chains. Further investigation in that way should improve development of membrane-active molecules targeting specific lipid regions.

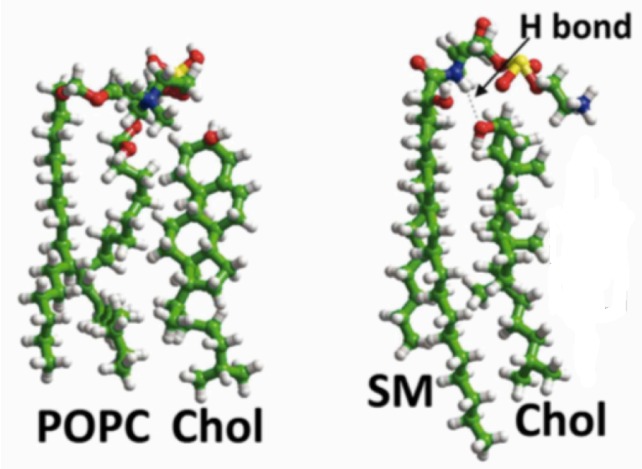

Fig 2. POPC or SM-Chol interactions. (Left) When Chol interacts with POPC, its OH group is not buried in the complex. **(Right)** However, when Chol interacts with SM, a hydrogen bond (H bond) is formed between the OH group of Chol and the NH group of the sphingolipid. This H bond orientates Chol with respect to SM. The OH group Chol is masked by the polar head of SM in a typical "umbrella" effect[325].

3.3 Influence of membrane packing for the activity of Rh2?

Besides the polar headgroup, the variations in the fatty acyl chain length and the degree of saturation could also influence the Rh2-membrane interaction. Regarding the interaction of Rh2 with ePC (major distribution: DOPC (18:1, 30%) and DPPC (16:0, 30%)), we showed that the binding affinity between Rh2 and ePC was lower than with DOPC vesicles. In addition, the ginsenoside Rc is more effective to induce liposomal agglutinability toward PCs with short and/or unsaturated fatty acyl chains[194]. As mentioned in section 1.3.1.2, these two parameters clearly influence the membrane packing. Regarding the role of this property in the Rh2 activity, we showed that eSM:ePC liposomes are more fluid than ePC:Chol and eSM:ePC:Chol liposomes and are also the most sensitive to Rh2. However, even if ePC:Chol and eSM:ePC:Chol liposomes are classified from the more fluid to the more rigid, ePC:Chol vesicles are less susceptible to the action of Rh2 as compared to eSM:ePC:Chol vesicles.

Altogether, we gave a hint regarding the key role of Chol and SM in the membrane activity of Rh2 but a series of experiments have to be done to fully decipher whether other parameters such as chain length or degree of saturation could influence the membrane activity of Rh2.

➔ *For this purpose, monolayers and LUVs composed of PC or SM with increasing acyl chain length or degree of unsaturation could be incubated with Rh2 to assess its adsorption and its binding affinity through Langmuir trough or ITC method, respectively.*

3.4 Role of membrane lateral heterogeneity for the activity of Rh2?

Two studies have reported the disorganization of lipid rafts by Rh2 leading to apoptosis, via either the FAS oligomerization in Hela cells[221] or inactivation of Akt in human epidermoid carcinoma A431 cells and in human breast cancer MBA-MB-231 cells[204]. In order to evaluate the influence of Rh2 on this Lo domain, we prepared GUVs composed of eSM:ePC:Chol (1:1:1) exhibiting a lipid phase coexistence (Lo an Ld labeling with NBD-DPPE and rhodamine-DOPE, respectively). Owing to its high molecular packing and enrichment of sterol and saturated lipids, the Lo phase is considered as the model for lipid rafts[40]. In this work, we showed that, over the course of Rh2 treatment, positive membrane curvature occurred and Ld phases tended to spontaneously reside in this curved region whereas Lo phases were preferentially localized in flat region. However, Rh2 does not seem to affect Lo domain. How can we explain this discrepancy between results obtained from artificial membranes and cell lines? It has to keep in mind that artificial models have number of caveats and limitations, which prevent direct translation of findings from model membranes to biological ones. Moreover, it is worth noting that experiments performed in these two studies such as detergent resistant membrane (DRM), MβCD treatment or staining GM1 by cholera enterotoxin subunit B precursor (CtxB) to evaluate the Rh2-induced disruption of lipid raft in cell lines are well-debated (section 1.3.2.1.1).

➔ *We could evaluate the effect of Rh2 on the coexistence of ordered and disordered domains in GMPVs (see above, section 2.1). In addition, it will be relevant to assess the impact of Rh2 on the membrane lateral heterogeneity on supported lipid bilayers composed of eSM:ePC:Chol (1:1:1) by using AFM, a powerful tool to observe phase-separated domains on the micro and nanoscales, and to monitor membrane remodeling and alteration upon interaction with molecules[16].*

The favorable interaction of Rh2 with eSM monolayer is reminiscent to the specific binding to membrane SM of pore-forming proteins actinoporins (*e.g.* lysenin from the earthworm *Eisenia foetida*) (section 1.3.5.2). Hence, binding of the toxins and their permeabilization ability only occur in model systems exhibiting phase coexistence (Lo and Ld)[326]. Regarding the Rh2 activity, we observed that whatever the presence and the type of GUV phase boundaries, Rh2 induced alterations of GUV morphology and membrane permeability. This could suggest that the lipid phase separation is not a major actor for the Rh2 action.

3.5 Role of Akt for the cytotoxic activity of Rh2?

In this study, we showed that Rh2 induces a decrease of Akt phosphorylation which could provoke the activation of caspase-9 and the intrinsic mitochondrial-involved apoptotic pathway (section 1.4.1.3). Unfortunately, we do not know whether Rh2 directly targets Akt or promotes its dephosphorylation through the activation of PTEN or prevents the kinase activity of proteins involved the PI3K/Akt pathway such as the receptor or PI3K located at the PM. As we suggest that the main target of Rh2 is the PM, it is tempting to speculate that Rh2 could prevent the tyrosine kinase activity of receptor or the insertion within the membrane of PI3K or Akt by changing the membrane fluidity[327].

➔ *To confirm the importance of Akt for the Rh2-induced apoptosis, it will be interesting to knock-down the Akt expression by transfecting Akt siRNA or using CRISPR/Cas9 technology in U937 cells (characterized by a constitutive phosphorylation of Akt[328]) and then evaluate the Rh2-induced apoptosis in these cells. In addition, to establish a direct correlation between the Akt dephosphorylation and the intrinsic apoptosis, it will be relevant to evaluate the phosphorylation state of Bad and caspase-9, two proteins phosphorylated by active Akt to prevent the apoptosis (see section 1.4.1.3).*

➔ *To study the role of PI3K in the Rh2-induced apoptosis, we could evaluate the ratio of PIP2/PIP3 after Rh2 treatment. In a more global approach, we could use phosphoproteomics to identify upstream targets of Rh2.*

In agreement with the literature [323, 329], we observed the activation of the caspase-8 using a colorimetric assay after the treatment with Rh2, which was confirmed by the attenuation of the apoptosis using a specific inhibitor of this caspase (Z-IETD-FMK, data not shown). These results clearly indicate that PI3K/Akt pathway is

not the only target leading to the cytotoxic activity of Rh2 and that the death receptor pathway is also involved (section 1.4.1.1), suggesting that Rh2 employs a multi pro-apoptotic pathway to execute cell death. This pathway could also be activated by the effects of Rh2 on the biophysical PM properties.

➔ *As a first step, we could use confocal microscopy and ZB4 anti-Fas antibody to analyze the effects of Rh2 on Fas receptor expression at the PM. Exposure of cells to recombinant sFas-L, which induces the clustering of Fas receptor at the membrane, will be used as a positive control. In addition, to test the possibility that Rh2 could also induce the recruitment of the adaptor protein FADD to Fas receptor, co-immunoprecipitation studies will be performed.*

3.6 How the results observed with Rh2 can be extended to other saponins? Focus on digitonin

Even if ginsenoside Rh2 is considered as a saponin like digitonin, it seems to interact differently with the lipid bilayer. In this section, we would like to highlight some similarities and differences regarding their effects and structures without pretending to provide a structure-activity relationship. Although both saponins increased vesicle size and induced membrane permeability, digitonin effects were only observed in the presence of Chol while this latter slowed down these effects of Rh2. In contrast to Rh2, digitonin decreased the membrane packing which could be explained by the removal of Chol from the membrane core through the formation of Chol−digitonin complexes on the membrane surface as proposed by Frenkel et al[188]. This study suggests that the sterical hindrance between saccharide residues in digitonin-sterol aglycone aggregates may induce changes in the curvature of the membrane composed of 1-stearoyl-2-oleoyl-sn-glycero-3-phosphocholine (SOPC)-Chol(4:1)[188]. We also observed that Rh2-membrane interaction lead to the formation of membrane curvature but we suspect that it is the consequence of the reduction of the line tension due to the increased membrane rigidity[330]. Structures of Rh2 and digitonin exhibit many difference such as the aglycon skeleton (dammarane *vs* spirostan) or the number and type of sugar groups in C-3 (1 sugar: glucose *vs* 5 sugars: 2 galactoses, 2 glucoses, xylose) **(Fig. 3)**. Lorent et al. has proposed that an increase in the sugar length of saponin could favor the interaction with Chol in membranes[185]. This might be due to an “umbrella” effect. The glycoside residues of saponin would shield the non-polar parts of Chol from water and thereby promote interaction between both molecules. In this line with this, successive removal of sugar residues from digitonin decreases the hemolytic activity[187]. Although it could be a criterion to discriminate Chol-dependent

and –independent saponin, clear evidences suggest other discriminating factors such as the importance of the aglycon skeleton. While chikusetsusaponin III has 3 sugars (xylose, 2 glucoses) attached in C-3 on its dammarane skeleton, its activity was somewhat higher for Chol-free liposomes. This work highlights the need to distinguish different activities of molecules classified as saponins.

➔ *Further investigations should be performed to discriminate Chol-dependent and –independent saponins. This will allow to establish a clear structure-relationship activity leading to the discovery or development of molecules which could interact only with Chol or SM.*

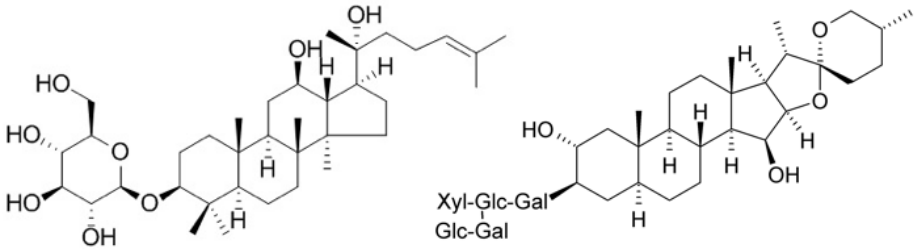

Ginsenoside Rh2 **Digitonin**

Fig 3. Structure of ginsenoside Rh2 and digitonin. Glc: glucose, gal: galactose, xyl: xylose.

3.7 Interaction of drugs with lipid membranes: new chemotherapeutic approach?

Evidences show that, during malignant transformation, cells suffer from alterations in their biophysical properties and membrane lipid profile. Accordingly, our preliminary data by AFM showed MCF-10AT and CaCl1 exhibit a softer membrane as compared to non-cancer cells. In addition, lower SM-to-PL ratio was measured in malignant MCF-10CaCl1 compared to "normal" MCF-10A and pre-malignant MCF-10AT cells. Although most cancer therapeutics are traditionally designed to interact with proteins and nucleic acids, membrane-lipid therapy has been proposed during the past few years and represents an important field of research to target alterations of biophysical membrane properties, lipid compositions and associated functionality in cancer cells[331, 332]. The effects of a large number of drugs on PM have been shown to affect PM characteristics with implication in their cytotoxic effects[294]. Escape of apoptotic signaling is a critical strategy commonly used for cancer tumorigenesis. Direct

activation of the cancer cell apoptotic machinery could thus constitute an appealing approach. The conventional drug cisplatin causes an increase in the Tm of model membranes composed of negatively charged PLs and, as a result, a decrease in membrane fluidity[333]. Alterations in membrane fluidity can profoundly alter functional properties of the cell and induce apoptotic pathways that can result in cell death[334]. In fact, studies using several cancer cell lines demonstrated that cisplatin triggers ligand-independent Fas apoptotic pathways in various cancer cells. Moreover, the membrane insertion of synthetic fatty acid 2-hydroxyoleic acid (2OHOA, Minerval) increased the packing of ordered domains and has proven to be efficacious against cancer without inducing the adverse side-effects. Studies revealed that 2OHOA can regulate SM synthase and recover the SM levels that are reported to be reduced in glioma cells. This molecule is currently being tested in clinical trials and it is expected to enter the market around 2020[159]. In this work, we reported that Rh2 increases the membrane packing before to induce apoptosis A549, THP-1 and U937 cancer cell lines. It is tempting to speculate that this effect could be useful to reduce cell migration and invasion by increasing the lower stiffness of the MCF-10AT and MCF-10CaCl1 than MCF-10A cells measured by AFM.

➔ *We are far from using this ginsenoside in membrane lipid therapy for the reasons explained in the next section. Before that, we should first continue to determine lipid organization at the outer PM leaflet using multiple probes for a same lipid (SM, PC, GM1, Chol). As we have set up the labelling of PIP2 and PS at the inner PM leaflet, we will also try to establish a potential relation between inner and outer leaflet lipids using labeling fluorescent toxins and fluorescent protein markers. In parallel, we will examine whether those lipids contribute to cell migration and invasion by testing if they could exhibit a gradient from the trailing to the leading edge upon migration by real time imaging. Then we will evaluate whether ginsenoside Rh2 could affect cell migration and invasion of the three breast cell lines using IBIDI and Transwell chambers and could target specific lipids or lipid regions.*

Owing to the progressive understanding of membrane lipid composition and membrane biophysical properties in healthy and cancer cells, the interplay between anticancer drugs and the cell membrane represents an important field of research and the development of new chemotherapeutic agents should take into account the role of the membrane in their activity.

4. Clinical studies and limitations of chemotherapeutic use of Rh2

Panax ginseng is an herbal medicine used for a long time worldwide for a wide range of indications. Ginsenosides are the major active ingredients and seem to be the responsible for the anticancer activities. Studies have reported that Rh2 administered at a dose 120 mg/kg exhibit a peak plasma concentration of 19 µg/ml in mice bearing tumors established following subcutaneous injection of PC-3 human prostate cancer cells. This dose induces a significant delay in PC-3 tumor growth, an increase in apoptotic index, and a decrease in tumor cell proliferation without measurable toxicity. Regarding the biodistribution, Rh2 levels appear to be highest in the small intestines and in the liver of mice. This was also observed in rats[335]. Interestingly, 0,08% and 0,3% of the administered dose were found in the prostate and in the PC-3 tumor tissue respectively, suggesting a certain tumor selectivity[336]. In addition, Nakata et al. demonstrated that a daily oral administration of Rh2 (1.6 mg/kg, every day for 90 days from the day of tumor inoculation) in nude mice bearing HRA human ovarian cancer xenograft has a dose-dependent inhibitory effect on the tumor growth resulting in a significant increase of the survival[289]. Though ginsenoside Rh2 shows a clear anticancer activity in xenograft tumor models, it is imperative to observe their effects in human subjects. Many clinical studies have revealed beneficial effects of ginseng in patients with different types and stages of cancers. For more detail regarding these studies please refer to [281, 337]. However, it is difficult to actually attribute the anticancer properties of ginseng specifically to ginsenosides as ginseng possesses other constituents such as polysaccharides and phenolic compounds[338].

➔ *Active studies demonstrating the therapeutic effects of single ginsenoside Rh2 are in high demand to provide a rationale for the development of Rh2 as a novel chemotherapy. Further evaluations will also be needed to determine why ginsenosides have selective toxicity towards tumor cells and how this selectivity is achieved[337].*

The absence of clinical trial regarding the anticancer activity of ginsenoside Rh2 could be explained by four caveats: (i) hemolysis, (ii) poor absorption and potential degradation, (iii) undesirable interactions, and (iv) limited quantity.

(i) Treatment with Rh2 has been shown to swell and rupture erythrocytes causing a release of hemoglobin. Rh2 can only be used pharmacologically if they don't induce important hemolysis or if they do not pass into the

blood stream[233].

(ii) Rh2 has low oral bioavailability and shows difficult absorption due to three impact factors: (1) low solubility; (2) low membrane permeability; (3) pre-systemic elimination. For example, the bioavailability of Rh2 is about 5% in rats and 16% in dogs[335].

➔ *Using drug delivery systems such as liposomes to integrate Rh2 could provide a tool to increase the therapeutic index of the molecules by reducing hemolysis and potential degradation and increasing absorption therefore improving its anti-cancer activities (see section 6).*

(iii) The cytotoxic effect of Rh2 is reduced in presence of serum components. Ginsenoside Rh2 induces faster apoptosis on cells incubated in medium with delipidated foetal calf serum (FCS) *vs* those incubated in FCS. This effect is amplified in serum-free medium (data not shown). Moreover, it has been reported that serum impairs the activity of Rh2 due to its interaction with human or bovine serum albumin, main proteins of blood produced in the liver[339]. In addition, it has been reported that after oral dosing in rats, the circulating fraction of Rh2 bound to plasma proteins is around 70%[335].

(iv) While the ginseng root contains only 2-3% ginsenosides, ginsenoside Rh2 accounts for less than 0.01% of dried *Panax ginseng* roots which cannot satisfy the scientific researches and the clinical requirements. Therefore, synthetic biology strategy to artificially produce ginsenoside Rh2 is expected. To overcome this limitation, a researcher group recently built an high efficient ginsenoside Rh2 biosynthetic in *Saccharomyces cerevisiae* cell factory[340].

Ginsenosides Rh2 integrated in drug delivery systems could be a promising candidate for cancer treatments, particularly if it can be more bioavailable, efficacious, safe, and affordable. Combination therapy of Rh2 with conventional chemotherapeutic drugs has been proposed to be more effective (section 3.4.5.1.4). However, these therapies warrant further investigation using additional animal studies and large cohort clinical trials.

5. How Rh2 by interacting with membrane could act as a potential anti-cancer drug?

Beside membrane-related anticancer effects of ginsenosides already mentioned in section 3.4.5, we would like to propose the alternative hypothesis that Rh2 could preferentially alter SM-enriched domains and thereby cancer cell proliferation and squeezing. This hypothesis is based on the following literature data regarding the importance of SM-enriched domains in cell division and squeezing. Firstly, SM-enriched domains in the outer leaflet are required for the localization of PIP2 to the cleavage furrow, which is a prerequisite for the proper translocation of small GTPase Rho and the progression of cytokinesis, the final stage of cell division[341]. Interestingly, the depletion of SM from the PM inhibits the completion of cytokinesis. Secondly, an increase of SM-enriched domain abundance occurs during the Ca^{2+} efflux upon red blood cell shape restoration after stretching[67, 68]. As highly deformable metastatic cells need to restore their shape after squeezing through tight space, it is tempting to speculate that Rh2, through its interaction with SM, could prevent this shape restoration thereby precluding new cell deformations.

➔ *To confirm or reject these hypothetic mechanisms, it is first essential to continue to characterize membrane lipid composition and organization in breast cancer cell lines with increasing malignancy potential (see results, part 3). Then, it would be appealing to investigate whether and how lipid domains could also be involved in the (re)shaping processes of these cells. Interestingly, our preliminary data showed a higher segregation between SM and GM1 at the PM of cancer cells as compared to their counterpart. After the PM characterization, next step will be to evaluate the effects of Rh2 on these lipid-enriched regions and its impact on tumor proliferation and migration.*

As we showed that Rh2 interacts more favorably with SM in comparison with Chol, this suggests that PM of cells enriched with SM but not in Chol could be the first target for the induction of apoptosis by Rh2. Certain healthy tissues such as brain, peripheral nervous tissue and ocular lenses having a higher SM contents could therefore also be affected by Rh2 treatment limiting its therapeutic use[342]. However, the biodistribution of Rh2 following oral administration to nude mice (120 mg/kg) in PC-3 human xenograft model indicates that Rh2 is not quantifiable in the brain. This was also confirmed in rats[335].

Beside its potential influence on SM-enriched domains, Rh2 could reduce

cancer cell migration and invasion by increasing the membrane packing. Indeed, AFM data clearly showed that pre-metastatic and metastatic breast cancer cell lines (MCF-10AT and MCF-10CaCl1) exhibit a softer membrane as compared to non-cancer cells. This intrinsic membrane property seems to facilitate migration out of the primary tumor into circulation[305].

6. Specific membrane lipid interaction of Rh2 as a magic bullet?

Although conventional chemotherapeutic drugs provide benefits up to certain extent for treatment and management of cancers, most of them have poor pharmacokinetics profiles and are distributed non-specifically in the body leading to systemic toxicity associated with serious side effects. In this context, the tumor targeting of liposomal formulation-based therapeutics has emerged as one approach to protect drug from environmental factors, provide effective drug delivery and overcome the lack of specificity of conventional chemotherapeutic agents[343]. This concept was inspired by Paul Ehrlich which coined the term “magic bullet” to describe a highly selective substance to precisely target other toxic substances or organisms that caused disease and to neutralize their effects[344]. Liposome technologies offer unique characteristics in an attempt to optimize specific drug delivery to tumor cells[345]. Liposomes can be covered with polymers such as polyethylene glycol to exhibit prolonged half-life in blood circulation. To enhance target specificity, the surface of liposomes can be conjugated to ligands such as antibody which bind to appropriate receptors overexpressed by tumor cells and not expressed by normal cells. Recently, temperature-sensitive liposomes have been investigated to enhance the release of the loaded drug at Tm (between 40-45°C)[346]. Lipid components mainly DPPC and myristoylstearoyl PC present in the liposome undergo a gel to liquid transition above the Tm, making it more permeable, and thus releasing the drug. Local tissue temperature is generally elevated by radiofrequency ablation or microwave hyperthermia or high-intensity focused ultrasound. For instance, ThermoDox® is being tested in phase III clinical trial and uses temperature-triggered liposomal technology to encapsulate doxorubicin for the treatment of various solid tumors[347]. Recently, it has been observed that the lipid membrane composition of liposomes could itself influence the specific delivery of drugs to cancer cells. For instance, the high dependency of cancer cells on saturated FA can be exploited to increase tumor-drug delivery, as loading drugs in liposomes enriched in saturated PC has been shown to reduce the metastatic spread of pancreatic cancer in vivo[348]. Development of multifunctional liposomes should be pursued to combine different technologies

(polyethylene glycol, temperature-responsive, ligand, lipids, Rh2?) to enhance the delivery of chemotherapeutic drugs to the tumor sites.

➔ *Whether we clearly identify one specific lipid or lipid region contributing to the preferential interaction of Rh2 with cancer cells compared to their counterpart, we could envision to design anticancer drug loaded-liposomes combining the above technologies with Rh2 in their membrane. Besides enhancing the specific targeting, Rh2 could serve as fusogenic and permeabilizing molecule to promote the release of the loaded drug. First, we have to evaluate in vitro the anticancer activity of Rh2 alone or incorporated in these liposomal membranes loaded or not with anticancer drugs in MCF-10AT and MCF-10CaCl1 as compared to MCF-10A. For that purpose, we could assess its effects on cell proliferation (using bromo-deoxyuridine (BrdU)), apoptosis (using DAPI staining), P-gp efflux pump (using rhodamine 123 efflux assay), lipid organization (lipid labelling, see above), cell migration (using Ibidi chamber) and invasion (using Transwell chamber). If results are promising, we could envision to investigate its activity on tumor xenograft bearing mice. For that purpose, each cell line will be injected subcutaneously in immunodeficient mice and we could evaluate tumor growth, ex vivo apoptosis (using caspase-3 staining), proliferation (using Ki67 staining (ex vivo) and 18F-FLT positron emission tomography (in vivo))[349, 350].*

7. Conclusion

Our work evidenced the importance of membrane lipid nature for molecule activity. For instance, SM promotes and accelerates the activity of the steroid saponin ginsenoside Rh2 whereas Chol slows down and depresses it. From a more global point-of-view, the favorable interaction of a molecule with a membrane lipid could provide a powerful tool to (i) evidence this lipid or (ii) target the latter in a pathophysiological context such as tumor growth and metastasis. First, as extensively studied, pore-forming toxins represent a unique class of highly specific lipid-binding proteins. Non-toxic (NT) pore-forming toxin derivatives are commonly used to visualize lipids in live cells and reveal the presence of specific lipid domains in the cell membrane. Since these probes have a larger size than the targeted lipid (15-fold larger surface projection than endogenous lipids) predicting steric hindrance[58, 59], the use of smaller molecules to visualize membrane lipid represents an undeniable advantage. Second, specific lipid-binding molecules could be a bullet fired to target membrane lipid alteration in cancer cells as revealed by lipidomic analysis in comparison to their counterpart. These changes modify the biophysical membrane properties of tumors such as membrane

lateral organization or fluidity potentially facilitating their invasion into neighboring tissues. At the end of this work, one question remains: could ginsenoside Rh2 be used a bullet to tackle this disease?

CHAPTER V: BIBLIOGRAPHY

1. Gorter E, Grendel F: **On Bimolecular Layers of Lipoids on the Chromocytes of the Blood**. *J Exp Med* 1925, **41**(4):439-443.
2. Danielli JFD, H. : **A contribution to the theory of permeability of thin films**. *J Cell Physiol* 1935, **5**(4):495-508.
3. Singer SJ, Nicolson GL: **The fluid mosaic model of the structure of cell membranes**. *Science* 1972, **175**(4023):720-731.
4. Lombard J: **Once upon a time the cell membranes: 175 years of cell boundary research**. *Biol Direct* 2014, **9**:32.
5. Simons K, Ikonen E: **Functional rafts in cell membranes**. *Nature* 1997, **387**(6633):569-572.
6. Kusumi A, Fujiwara TK, Chadda R, Xie M, Tsunoyama TA, Kalay Z, Kasai RS, Suzuki KG: **Dynamic organizing principles of the plasma membrane that regulate signal transduction: commemorating the fortieth anniversary of Singer and Nicolson's fluid-mosaic model**. *Annu Rev Cell Dev Biol* 2012, **28**:215-250.
7. Carquin M, D'Auria L, Pollet H, Bongarzone ER, Tyteca D: **Recent progress on lipid lateral heterogeneity in plasma membranes: From rafts to submicrometric domains**. *Prog Lipid Res* 2016, **62**:1-24.
8. Escriba PV: **Membrane-lipid therapy: A historical perspective of membrane-targeted therapies - From lipid bilayer structure to the pathophysiological regulation of cells**. *Biochim Biophys Acta* 2017, **1859**(9 Pt B):1493-1506.
9. van Meer G, Voelker DR, Feigenson GW: **Membrane lipids: where they are and how they behave**. *Nat Rev Mol Cell Biol* 2008, **9**(2):112-124.
10. Pollard T EW, Lippincott-Schwartz J, Johnson G: **Membrane structure and dynamics**. In: *Cell biology.* Edited by Elsevier; 2017.
11. Hofmann K, Dixit VM: **Ceramide in apoptosis--does it really matter?** *Trends Biochem Sci* 1998, **23**(10):374-377.
12. Salmaso S, Caliceti P: **Stealth properties to improve therapeutic efficacy of drug nanocarriers**. *J Drug Deliv* 2013, **2013**:374252.

13. Desmond E, Gribaldo S: **Phylogenomics of sterol synthesis: insights into the origin, evolution, and diversity of a key eukaryotic feature**. *Genome Biol Evol* 2009, **1**:364-381.
14. Lange Y, Swaisgood MH, Ramos BV, Steck TL: **Plasma membranes contain half the phospholipid and 90% of the cholesterol and sphingomyelin in cultured human fibroblasts**. *J Biol Chem* 1989, **264**(7):3786-3793.
15. Wolkers WF, Crowe LM, Tsvetkova NM, Tablin F, Crowe JH: **In situ assessment of erythrocyte membrane properties during cold storage**. *Mol Membr Biol* 2002, **19**(1):59-65.
16. Deleu M, Crowet JM, Nasir MN, Lins L: **Complementary biophysical tools to investigate lipid specificity in the interaction between bioactive molecules and the plasma membrane: A review**. *Biochim Biophys Acta* 2014, **1838**(12):3171-3190.
17. Biro E, Akkerman JW, Hoek FJ, Gorter G, Pronk LM, Sturk A, Nieuwland R: **The phospholipid composition and cholesterol content of platelet-derived microparticles: a comparison with platelet membrane fractions**. *J Thromb Haemost* 2005, **3**(12):2754-2763.
18. Fauvel J, Chap H, Roques V, Levy-Toledano S, Douste-Blazy L: **Biochemical characterization of plasma membranes and intracellular membranes isolated from human platelets using Percoll gradients**. *Biochimica et biophysica acta* 1986, **856**(1):155-164.
19. Pankov R, Markovska T, Antonov P, Ivanova L, Momchilova A: **The plasma membrane lipid composition affects fusion between cells and model membranes**. *Chemico-biological interactions* 2006, **164**(3):167-173.
20. Cezanne L, Navarro L, Tocanne JF: **Isolation of the plasma membrane and organelles from Chinese hamster ovary cells**. *Biochim Biophys Acta* 1992, **1112**(2):205-214.
21. Calderon RO, DeVries GH: **Lipid composition and phospholipid asymmetry of membranes from a Schwann cell line**. *Journal of neuroscience research* 1997, **49**(3):372-380.

22. Perkins RG, Scott RE: **Plasma membrane phospholipid, cholesterol and fatty acyl composition of differentiated and undifferentiated L6 myoblasts**. *Lipids* 1978, **13**(5):334-337.
23. Sahu S, Lynn WS: **Lipid composition of human alveolar macrophages**. *Inflammation* 1977, **2**(2):83-91.
24. Garrett RH, and Charles M. Grisham. 2010. Biochemistry. Belmont, CA: Brooks/Cole, Cengage Learning. In.
25. Recktenwald DJ, McConnell HM: **Phase equilibria in binary mixtures of phosphatidylcholine and cholesterol**. *Biochemistry* 1981, **20**(15):4505-4510.
26. Ladbrooke BD, Williams RM, Chapman D: **Studies on lecithin-cholesterol-water interactions by differential scanning calorimetry and X-ray diffraction**. *Biochim Biophys Acta* 1968, **150**(3):333-340.
27. Eeman M, Deleu, M: **From biological membranes to biomimetic model membranes**. *Biotechnol Agron Soc Environ* 2010, **14**(4):719-736.
28. Goni FM, Alonso A, Bagatolli LA, Brown RE, Marsh D, Prieto M, Thewalt JL: **Phase diagrams of lipid mixtures relevant to the study of membrane rafts**. *Biochim Biophys Acta* 2008, **1781**(11-12):665-684.
29. de Almeida RF, Fedorov A, Prieto M: **Sphingomyelin/phosphatidylcholine/cholesterol phase diagram: boundaries and composition of lipid rafts**. *Biophys J* 2003, **85**(4):2406-2416.
30. Bagatolli LA, Ipsen JH, Simonsen AC, Mouritsen OG: **An outlook on organization of lipids in membranes: searching for a realistic connection with the organization of biological membranes**. *Prog Lipid Res* 2010, **49**(4):378-389.
31. Elson EL, Fried E, Dolbow JE, Genin GM: **Phase separation in biological membranes: integration of theory and experiment**. *Annu Rev Biophys* 2010, **39**:207-226.
32. Harris FM, Best KB, Bell JD: **Use of laurdan fluorescence intensity and polarization to distinguish between changes in membrane fluidity and phospholipid order**. *Biochim Biophys Acta* 2002, **1565**(1):123-128.

33. Parasassi T, De Stasio G, Ravagnan G, Rusch RM, Gratton E: **Quantitation of lipid phases in phospholipid vesicles by the generalized polarization of Laurdan fluorescence**. *Biophys J* 1991, **60**(1):179-189.
34. do Canto A, Robalo JR, Santos PD, Carvalho AJP, Ramalho JPP, Loura LMS: **Diphenylhexatriene membrane probes DPH and TMA-DPH: A comparative molecular dynamics simulation study**. *Biochim Biophys Acta* 2016, **1858**(11):2647-2661.
35. Lentz BR: **Membrane "fluidity" as detected by diphenylhexatriene probes**. *Chem Phys Lipids* 1989, **50**(3-4):171-190.
36. Zhao H, Lappalainen P: **A simple guide to biochemical approaches for analyzing protein-lipid interactions**. *Mol Biol Cell* 2012, **23**(15):2823-2830.
37. Starling AP, East JM, Lee AG: **Effects of gel phase phospholipid on the Ca(2+)-ATPase**. *Biochemistry* 1995, **34**(9):3084-3091.
38. Sharom FJ: **Complex Interplay between the P-Glycoprotein Multidrug Efflux Pump and the Membrane: Its Role in Modulating Protein Function**. *Front Oncol* 2014, **4**:41.
39. Ernst R, Ejsing CS, Antonny B: **Homeoviscous Adaptation and the Regulation of Membrane Lipids**. *J Mol Biol* 2016, **428**(24 Pt A):4776-4791.
40. Sezgin E, Levental I, Mayor S, Eggeling C: **The mystery of membrane organization: composition, regulation and roles of lipid rafts**. *Nat Rev Mol Cell Biol* 2017, **18**(6):361-374.
41. Simons K, Toomre D: **Lipid rafts and signal transduction**. *Nat Rev Mol Cell Biol* 2000, **1**(1):31-39.
42. Heerklotz H: **Triton promotes domain formation in lipid raft mixtures**. *Biophys J* 2002, **83**(5):2693-2701.
43. Sanchez SA, Gunther G, Tricerri MA, Gratton E: **Methyl-beta-cyclodextrins preferentially remove cholesterol from the liquid disordered phase in giant unilamellar vesicles**. *J Membr Biol* 2011, **241**(1):1-10.
44. Goni FM, Sot J, Alonso A: **Biophysical properties of sphingosine, ceramides and other simple sphingolipids**. *Biochem Soc Trans* 2014, **42**(5):1401-1408.

45. Munro S: **Lipid rafts: elusive or illusive?** *Cell* 2003, **115**(4):377-388.
46. Cheng X, Smith JC: **Biological Membrane Organization and Cellular Signaling**. *Chem Rev* 2019, **119**(9):5849-5880.
47. Sydor AM, Czymmek KJ, Puchner EM, Mennella V: **Super-Resolution Microscopy: From Single Molecules to Supramolecular Assemblies**. *Trends Cell Biol* 2015, **25**(12):730-748.
48. Sezgin E, Levental I, Grzybek M, Schwarzmann G, Mueller V, Honigmann A, Belov VN, Eggeling C, Coskun U, Simons K *et al*: **Partitioning, diffusion, and ligand binding of raft lipid analogs in model and cellular plasma membranes**. *Biochim Biophys Acta* 2012, **1818**(7):1777-1784.
49. Levental I, Veatch S: **The Continuing Mystery of Lipid Rafts**. *J Mol Biol* 2016, **428**(24 Pt A):4749-4764.
50. Parton RG, del Pozo MA: **Caveolae as plasma membrane sensors, protectors and organizers**. *Nat Rev Mol Cell Biol* 2013, **14**(2):98-112.
51. Patel HH, Insel PA: **Lipid rafts and caveolae and their role in compartmentation of redox signaling**. *Antioxid Redox Signal* 2009, **11**(6):1357-1372.
52. Cheng JPX, Nichols BJ: **Caveolae: One Function or Many?** *Trends Cell Biol* 2016, **26**(3):177-189.
53. Simons K, Vaz WL: **Model systems, lipid rafts, and cell membranes**. *Annu Rev Biophys Biomol Struct* 2004, **33**:269-295.
54. Kabeche R, Madrid M, Cansado J, Moseley JB: **Eisosomes Regulate Phosphatidylinositol 4,5-Bisphosphate (PI(4,5)P2) Cortical Clusters and Mitogen-activated Protein (MAP) Kinase Signaling upon Osmotic Stress**. *J Biol Chem* 2015, **290**(43):25960-25973.
55. Guiney EL, Goldman AR, Elias JE, Cyert MS: **Calcineurin regulates the yeast synaptojanin Inp53/Sjl3 during membrane stress**. *Mol Biol Cell* 2015, **26**(4):769-785.
56. Kiyokawa E, Baba T, Otsuka N, Makino A, Ohno S, Kobayashi T: **Spatial and functional heterogeneity of sphingolipid-rich membrane domains**. *J Biol Chem* 2005, **280**(25):24072-24084.
57. Mound A, Lozanova V, Warnon C, Hermant M, Robic J, Guere C, Vie K, Lambert de Rouvroit C, Tyteca D, Debacq-Chainiaux F *et al*: **Non-senescent keratinocytes organize in plasma membrane**

submicrometric lipid domains enriched in sphingomyelin and involved in re-epithelialization. *Biochim Biophys Acta Mol Cell Biol Lipids* 2017, **1862**(9):958-971.

58. Carquin M, Pollet H, Veiga-da-Cunha M, Cominelli A, Van Der Smissen P, N'Kuli F, Emonard H, Henriet P, Mizuno H, Courtoy PJ *et al*: **Endogenous sphingomyelin segregates into submicrometric domains in the living erythrocyte membrane**. *J Lipid Res* 2014, **55**(7):1331-1342.
59. Carquin M, Conrard L, Pollet H, Van Der Smissen P, Cominelli A, Veiga-da-Cunha M, Courtoy PJ, Tyteca D: **Cholesterol segregates into submicrometric domains at the living erythrocyte membrane: evidence and regulation**. *Cell Mol Life Sci* 2015, **72**(23):4633-4651.
60. Tyteca D, D'Auria L, Der Smissen PV, Medts T, Carpentier S, Monbaliu JC, de Diesbach P, Courtoy PJ: **Three unrelated sphingomyelin analogs spontaneously cluster into plasma membrane micrometric domains**. *Biochim Biophys Acta* 2010, **1798**(5):909-927.
61. D'Auria L, Van der Smissen P, Bruyneel F, Courtoy PJ, Tyteca D: **Segregation of fluorescent membrane lipids into distinct micrometric domains: evidence for phase compartmentation of natural lipids?** *PLoS One* 2011, **6**(2):e17021.
62. D'Auria L, Fenaux M, Aleksandrowicz P, Van Der Smissen P, Chantrain C, Vermylen C, Vikkula M, Courtoy PJ, Tyteca D: **Micrometric segregation of fluorescent membrane lipids: relevance for endogenous lipids and biogenesis in erythrocytes**. *J Lipid Res* 2013, **54**(4):1066-1076.
63. Stauffer TP, Ahn S, Meyer T: **Receptor-induced transient reduction in plasma membrane PtdIns(4,5)P2 concentration monitored in living cells**. *Curr Biol* 1998, **8**(6):343-346.
64. Yeung T, Gilbert GE, Shi J, Silvius J, Kapus A, Grinstein S: **Membrane phosphatidylserine regulates surface charge and protein localization**. *Science* 2008, **319**(5860):210-213.
65. Dumitru AC, Conrard L, Lo Giudice C, Henriet P, Veiga-da-Cunha M, Derclaye S, Tyteca D, Alsteens D: **High-resolution mapping and recognition of lipid domains using AFM with toxin-derivatized probes**. *Chem Commun (Camb)* 2018, **54**(50):6903-6906.

66. Orsini F, Cremona A, Arosio P, Corsetto PA, Montorfano G, Lascialfari A, Rizzo AM: **Atomic force microscopy imaging of lipid rafts of human breast cancer cells**. *Biochim Biophys Acta* 2012, **1818**(12):2943-2949.
67. Leonard C, Conrard L, Guthmann M, Pollet H, Carquin M, Vermylen C, Gailly P, Van Der Smissen P, Mingeot-Leclercq MP, Tyteca D: **Contribution of plasma membrane lipid domains to red blood cell (re)shaping**. *Sci Rep* 2017, **7**(1):4264.
68. Conrard L, Stommen A, Cloos AS, Steinkuhler J, Dimova R, Pollet H, Tyteca D: **Spatial Relationship and Functional Relevance of Three Lipid Domain Populations at the Erythrocyte Surface**. *Cell Physiol Biochem* 2018, **51**(4):1544-1565.
69. Bretscher MS: **Asymmetrical lipid bilayer structure for biological membranes**. *Nat New Biol* 1972, **236**(61):11-12.
70. Gordesky SE, Marinetti GV, Segel GB: **Differences in the reactivity of phospholipids with FDNB in normal RBC, sickle cells and RBC ghosts**. *Biochem Biophys Res Commun* 1972, **47**(5):1004-1009.
71. Muller P, Herrmann A: **Rapid transbilayer movement of spin-labeled steroids in human erythrocytes and in liposomes**. *Biophys J* 2002, **82**(3):1418-1428.
72. Ramstedt B, Slotte JP: **Membrane properties of sphingomyelins**. *FEBS Lett* 2002, **531**(1):33-37.
73. Kobayashi T, Menon AK: **Transbilayer lipid asymmetry**. *Curr Biol* 2018, **28**(8):R386-R391.
74. Pomorski T, Menon AK: **Lipid flippases and their biological functions**. *Cell Mol Life Sci* 2006, **63**(24):2908-2921.
75. Elvas F, Stroobants S, Wyffels L: **Phosphatidylethanolamine targeting for cell death imaging in early treatment response evaluation and disease diagnosis**. *Apoptosis* 2017, **22**(8):971-987.
76. Bretscher MS: **Phosphatidyl-ethanolamine: differential labelling in intact cells and cell ghosts of human erythrocytes by a membrane-impermeable reagent**. *J Mol Biol* 1972, **71**(3):523-528.
77. Verkleij AJ, Zwaal RF, Roelofsen B, Comfurius P, Kastelijn D, van Deenen LL: **The asymmetric distribution of phospholipids in the human red cell**

membrane. A combined study using phospholipases and freeze-etch electron microscopy. *Biochim Biophys Acta* 1973, **323**(2):178-193.

78. Murate M, Kobayashi T: **Revisiting transbilayer distribution of lipids in the plasma membrane**. *Chem Phys Lipids* 2016, **194**:58-71.
79. Katz DH, Chiorazzi N, McDonald J, Katz LR: **Cell interactions between histoincompatible T an B lymphocytes. IX. The failure of histoincompatible cells is not due to suppression and cannot be circumvented by carrier-priming T cells with allogeneic macrophages**. *J Immunol* 1976, **117**(5 Pt.2):1853-1859.
80. Lentz BR: **Exposure of platelet membrane phosphatidylserine regulates blood coagulation**. *Prog Lipid Res* 2003, **42**(5):423-438.
81. Li MO, Sarkisian MR, Mehal WZ, Rakic P, Flavell RA: **Phosphatidylserine receptor is required for clearance of apoptotic cells**. *Science* 2003, **302**(5650):1560-1563.
82. Lin Q, London E: **The influence of natural lipid asymmetry upon the conformation of a membrane-inserted protein (perfringolysin O)**. *J Biol Chem* 2014, **289**(9):5467-5478.
83. Shahidullah K, Krishnakumar SS, London E: **The effect of hydrophilic substitutions and anionic lipids upon the transverse positioning of the transmembrane helix of the ErbB2 (neu) protein incorporated into model membrane vesicles**. *J Mol Biol* 2010, **396**(1):209-220.
84. Putzel GG, Uline MJ, Szleifer I, Schick M: **Interleaflet coupling and domain registry in phase-separated lipid bilayers**. *Biophys J* 2011, **100**(4):996-1004.
85. Kiessling V, Wan C, Tamm LK: **Domain coupling in asymmetric lipid bilayers**. *Biochim Biophys Acta* 2009, **1788**(1):64-71.
86. Nickels JD, Smith JC, Cheng X: **Lateral organization, bilayer asymmetry, and inter-leaflet coupling of biological membranes**. *Chem Phys Lipids* 2015, **192**:87-99.
87. May S: **Trans-monolayer coupling of fluid domains in lipid bilayers** *Soft Matter* 2009, **5**(17):3148-3156.
88. Dinic J, Ashrafzadeh P, Parmryd I: **Actin filaments attachment at the plasma membrane in live cells cause the formation of ordered lipid domains**. *Biochim Biophys Acta* 2013, **1828**(3):1102-1111.

89. Raghupathy R, Anilkumar AA, Polley A, Singh PP, Yadav M, Johnson C, Suryawanshi S, Saikam V, Sawant SD, Panda A *et al*: **Transbilayer lipid interactions mediate nanoclustering of lipid-anchored proteins**. *Cell* 2015, **161**(3):581-594.
90. Johnna R. St. Clair QW, Guangtao Li, and Erwin London: **Preparation and Physical Properties of Asymmetric Model Membrane Vesicles**. In: *The Biophysics of Cell Membranes.* Edited by Martinac B, vol. 19; 2017.
91. Janmey PA, Kinnunen PK: **Biophysical properties of lipids and dynamic membranes**. *Trends Cell Biol* 2006, **16**(10):538-546.
92. Seddon JM: **Structure of the inverted hexagonal (HII) phase, and non-lamellar phase transitions of lipids**. *Biochim Biophys Acta* 1990, **1031**(1):1-69.
93. Leonard C, D. Alsteens, A. Dumitru, M. Mingeot-Leclercq, and D. Tyteca. 2017a. Lipid domains and membrane (re)shaping : from biophysics to biology. In the role of the physical properties of membranes in influencing biological phenomena. J. Ruysschaert and R. Epand, editors. Springer series in biophysics. Vol. 19 pp 121-175
94. Siegel DP: **Energetics of intermediates in membrane fusion: comparison of stalk and inverted micellar intermediate mechanisms**. *Biophys J* 1993, **65**(5):2124-2140.
95. Cullis PRHMJ: **Physical properties and functional roles of lipids in membranes**. In: *New Comprehensive Biochemistry.* Edited by JE VDV, vol. 20; 1991.
96. Kawamoto S, Klein ML, Shinoda W: **Coarse-grained molecular dynamics study of membrane fusion: Curvature effects on free energy barriers along the stalk mechanism**. *J Chem Phys* 2015, **143**(24):243112.
97. Lorin AF, C; Thomas, A; Brasseur, R: **Les liposomes : description, fabrication et applications**. *Biotechnol Agron Soc Environ* 2004, **8**(3):163-176.
98. Duzgunes N: **Fluorescence assays for liposome fusion**. *Methods Enzymol* 2003, **372**:260-274.
99. Loura LM, Prieto M: **FRET in Membrane Biophysics: An Overview**. *Front Physiol* 2011, **2**:82.

100. Hoekstra D, de Boer T, Klappe K, Wilschut J: **Fluorescence method for measuring the kinetics of fusion between biological membranes**. *Biochemistry* 1984, **23**(24):5675-5681.
101. Jahn R, Lang T, Sudhof TC: **Membrane fusion**. *Cell* 2003, **112**(4):519-533.
102. Jahn R, Scheller RH: **SNAREs--engines for membrane fusion**. *Nat Rev Mol Cell Biol* 2006, **7**(9):631-643.
103. Yang NJ, Hinner MJ: **Getting across the cell membrane: an overview for small molecules, peptides, and proteins**. *Methods Mol Biol* 2015, **1266**:29-53.
104. Le CF, Fang CM, Sekaran SD: **Intracellular Targeting Mechanisms by Antimicrobial Peptides**. *Antimicrob Agents Chemother* 2017, **61**(4).
105. Fuertes G, Gimenez D, Esteban-Martin S, Garcia-Saez A, Sanchez O, Salgado J: **Role of membrane lipids for the activity of pore forming peptides and proteins**. *Adv Exp Med Biol* 2010, **677**:31-55.
106. Sukumwang N, Umezawa K: **Earthworm-derived pore-forming toxin lysenin and screening of its inhibitors**. *Toxins (Basel)* 2013, **5**(8):1392-1401.
107. Colombini M: **Ceramide channels and mitochondrial outer membrane permeability**. *J Bioenerg Biomembr* 2017, **49**(1):57-64.
108. Anishkin A, Sukharev S, Colombini M: **Searching for the molecular arrangement of transmembrane ceramide channels**. *Biophys J* 2006, **90**(7):2414-2426.
109. Checkervarty A, Werner M, Sommer JU: **Formation and stabilization of pores in bilayer membranes by peptide-like amphiphilic polymers**. *Soft Matter* 2018, **14**(13):2526-2534.
110. Unsay JD, Garcia-Saez AJ: **AFM to Study Pore-Forming Proteins**. *Methods Mol Biol* 2019, **1886**:191-202.
111. Hallett FR, Marsh J, Nickel BG, Wood JM: **Mechanical properties of vesicles. II. A model for osmotic swelling and lysis**. *Biophys J* 1993, **64**(2):435-442.
112. Dalla Serra M, Menestrina G: **Liposomes in the study of pore-forming toxins**. *Methods Enzymol* 2003, **372**:99-124.

113. Weinstein JN, Yoshikami S, Henkart P, Blumenthal R, Hagins WA: **Liposome-cell interaction: transfer and intracellular release of a trapped fluorescent marker**. *Science* 1977, **195**(4277):489-492.
114. Pomorski TG, Nylander T, Cardenas M: **Model cell membranes: discerning lipid and protein contributions in shaping the cell**. *Adv Colloid Interface Sci* 2014, **205**:207-220.
115. Ichim G, Tait SW: **A fate worse than death: apoptosis as an oncogenic process**. *Nat Rev Cancer* 2016, **16**(8):539-548.
116. Tait SW, Green DR: **Mitochondria and cell death: outer membrane permeabilization and beyond**. *Nat Rev Mol Cell Biol* 2010, **11**(9):621-632.
117. Obeid LM, Linardic CM, Karolak LA, Hannun YA: **Programmed cell death induced by ceramide**. *Science* 1993, **259**(5102):1769-1771.
118. Stancevic B, Kolesnick R: **Ceramide-rich platforms in transmembrane signaling**. *FEBS Lett* 2010, **584**(9):1728-1740.
119. Corre I, Guillonneau M, Paris F: **Membrane signaling induced by high doses of ionizing radiation in the endothelial compartment. Relevance in radiation toxicity**. *Int J Mol Sci* 2013, **14**(11):22678-22696.
120. Wymann MP, Schneiter R: **Lipid signalling in disease**. *Nat Rev Mol Cell Biol* 2008, **9**(2):162-176.
121. Bollinger CR, Teichgraber V, Gulbins E: **Ceramide-enriched membrane domains**. *Biochim Biophys Acta* 2005, **1746**(3):284-294.
122. Bourbon NA, Sandirasegarane L, Kester M: **Ceramide-induced inhibition of Akt is mediated through protein kinase Czeta: implications for growth arrest**. *J Biol Chem* 2002, **277**(5):3286-3292.
123. Huang WC, Chen CL, Lin YS, Lin CF: **Apoptotic sphingolipid ceramide in cancer therapy**. *J Lipids* 2011, **2011**:565316.
124. Vivanco I, Sawyers CL: **The phosphatidylinositol 3-Kinase AKT pathway in human cancer**. *Nat Rev Cancer* 2002, **2**(7):489-501.
125. Franke TF, Hornik CP, Segev L, Shostak GA, Sugimoto C: **PI3K/Akt and apoptosis: size matters**. *Oncogene* 2003, **22**(56):8983-8998.
126. Igney FH, Krammer PH: **Death and anti-death: tumour resistance to apoptosis**. *Nat Rev Cancer* 2002, **2**(4):277-288.

127. Lasserre R, Guo XJ, Conchonaud F, Hamon Y, Hawchar O, Bernard AM, Soudja SM, Lenne PF, Rigneault H, Olive D *et al*: **Raft nanodomains contribute to Akt/PKB plasma membrane recruitment and activation**. *Nat Chem Biol* 2008, **4**(9):538-547.
128. Reis-Sobreiro M, Roue G, Moros A, Gajate C, de la Iglesia-Vicente J, Colomer D, Mollinedo F: **Lipid raft-mediated Akt signaling as a therapeutic target in mantle cell lymphoma**. *Blood Cancer J* 2013, **3**:e118.
129. Gao X, Lowry PR, Zhou X, Depry C, Wei Z, Wong GW, Zhang J: **PI3K/Akt signaling requires spatial compartmentalization in plasma membrane microdomains**. *Proc Natl Acad Sci U S A* 2011, **108**(35):14509-14514.
130. Calay D, Vind-Kezunovic D, Frankart A, Lambert S, Poumay Y, Gniadecki R: **Inhibition of Akt signaling by exclusion from lipid rafts in normal and transformed epidermal keratinocytes**. *J Invest Dermatol* 2010, **130**(4):1136-1145.
131. Mollinedo F, Gajate C: **Lipid rafts and clusters of apoptotic signaling molecule-enriched rafts in cancer therapy**. *Future Oncol* 2010, **6**(5):811-821.
132. Beloribi-Djefaflia S, Vasseur S, Guillaumond F: **Lipid metabolic reprogramming in cancer cells**. *Oncogenesis* 2016, **5**:e189.
133. Mayor R, Etienne-Manneville S: **The front and rear of collective cell migration**. *Nat Rev Mol Cell Biol* 2016, **17**(2):97-109.
134. Lee K, Gallop JL, Rambani K, Kirschner MW: **Self-assembly of filopodia-like structures on supported lipid bilayers**. *Science* 2010, **329**(5997):1341-1345.
135. Saarikangas J, Zhao H, Lappalainen P: **Regulation of the actin cytoskeleton-plasma membrane interplay by phosphoinositides**. *Physiol Rev* 2010, **90**(1):259-289.
136. van Rheenen J, Song X, van Roosmalen W, Cammer M, Chen X, Desmarais V, Yip SC, Backer JM, Eddy RJ, Condeelis JS: **EGF-induced PIP2 hydrolysis releases and activates cofilin locally in carcinoma cells**. *J Cell Biol* 2007, **179**(6):1247-1259.
137. Wang W, Eddy R, Condeelis J: **The cofilin pathway in breast cancer invasion and metastasis**. *Nat Rev Cancer* 2007, **7**(6):429-440.

138. Bourne HR: **Rac and cell migration: CDM proteins integrate signals**. *Nat Cell Biol* 2005, **7**(8):777-778.
139. Keren K: **Cell motility: the integrating role of the plasma membrane**. *Eur Biophys J* 2011, **40**(9):1013-1027.
140. Kundu M, Mahata B, Banerjee A, Chakraborty S, Debnath S, Ray SS, Ghosh Z, Biswas K: **Ganglioside GM2 mediates migration of tumor cells by interacting with integrin and modulating the downstream signaling pathway**. *Biochim Biophys Acta* 2016, **1863**(7 Pt A):1472-1489.
141. Huang X, Li Y, Zhang J, Xu Y, Tian Y, Ma K: **Ganglioside GM3 inhibits hepatoma cell motility via down-regulating activity of EGFR and PI3K/AKT signaling pathway**. *J Cell Biochem* 2013, **114**(7):1616-1624.
142. Gomez-Mouton C, Abad JL, Mira E, Lacalle RA, Gallardo E, Jimenez-Baranda S, Illa I, Bernad A, Manes S, Martinez AC: **Segregation of leading-edge and uropod components into specific lipid rafts during T cell polarization**. *Proc Natl Acad Sci U S A* 2001, **98**(17):9642-9647.
143. Bi J, Wang R, Zeng X: **Lipid rafts regulate the lamellipodia formation of melanoma A375 cells via actin cytoskeleton-mediated recruitment of beta1 and beta3 integrin**. *Oncol Lett* 2018, **16**(5):6540-6546.
144. del Pozo MA, Alderson NB, Kiosses WB, Chiang HH, Anderson RG, Schwartz MA: **Integrins regulate Rac targeting by internalization of membrane domains**. *Science* 2004, **303**(5659):839-842.
145. Pierini LM, Eddy RJ, Fuortes M, Seveau S, Casulo C, Maxfield FR: **Membrane lipid organization is critical for human neutrophil polarization**. *J Biol Chem* 2003, **278**(12):10831-10841.
146. Long J, Zhang CJ, Zhu N, Du K, Yin YF, Tan X, Liao DF, Qin L: **Lipid metabolism and carcinogenesis, cancer development**. *Am J Cancer Res* 2018, **8**(5):778-791.
147. Baenke F, Peck B, Miess H, Schulze A: **Hooked on fat: the role of lipid synthesis in cancer metabolism and tumour development**. *Dis Model Mech* 2013, **6**(6):1353-1363.
148. Blom T, Somerharju P, Ikonen E: **Synthesis and biosynthetic trafficking of membrane lipids**. *Cold Spring Harb Perspect Biol* 2011, **3**(8):a004713.

149. Mullen PJ, Yu R, Longo J, Archer MC, Penn LZ: **The interplay between cell signalling and the mevalonate pathway in cancer**. *Nat Rev Cancer* 2016, **16**(11):718-731.
150. de Gonzalo-Calvo D, Lopez-Vilaro L, Nasarre L, Perez-Olabarria M, Vazquez T, Escuin D, Badimon L, Barnadas A, Lerma E, Llorente-Cortes V: **Intratumor cholesteryl ester accumulation is associated with human breast cancer proliferation and aggressive potential: a molecular and clinicopathological study**. *BMC Cancer* 2015, **15**:460.
151. Flavin R, Peluso S, Nguyen PL, Loda M: **Fatty acid synthase as a potential therapeutic target in cancer**. *Future Oncol* 2010, **6**(4):551-562.
152. Kuhajda FP: **Fatty acid synthase and cancer: new application of an old pathway**. *Cancer Res* 2006, **66**(12):5977-5980.
153. Perrotti F, Rosa C, Cicalini I, Sacchetta P, Del Boccio P, Genovesi D, Pieragostino D: **Advances in Lipidomics for Cancer Biomarkers Discovery**. *Int J Mol Sci* 2016, **17**(12).
154. Ogretmen B, Hannun YA: **Biologically active sphingolipids in cancer pathogenesis and treatment**. *Nat Rev Cancer* 2004, **4**(8):604-616.
155. Riboni L, Campanella R, Bassi R, Villani R, Gaini SM, Martinelli-Boneschi F, Viani P, Tettamanti G: **Ceramide levels are inversely associated with malignant progression of human glial tumors**. *Glia* 2002, **39**(2):105-113.
156. Knapp P, Bodnar L, Blachnio-Zabielska A, Swiderska M, Chabowski A: **Plasma and ovarian tissue sphingolipids profiling in patients with advanced ovarian cancer**. *Gynecol Oncol* 2017, **147**(1):139-144.
157. Leong WI, Saba JD: **S1P metabolism in cancer and other pathological conditions**. *Biochimie* 2010, **92**(6):716-723.
158. Bonnaud S, Niaudet C, Pottier G, Gaugler MH, Millour J, Barbet J, Sabatier L, Paris F: **Sphingosine-1-phosphate protects proliferating endothelial cells from ceramide-induced apoptosis but not from DNA damage-induced mitotic death**. *Cancer Res* 2007, **67**(4):1803-1811.
159. Barcelo-Coblijn G, Martin ML, de Almeida RF, Noguera-Salva MA, Marcilla-Etxenike A, Guardiola-Serrano F, Luth A, Kleuser B, Halver JE, Escriba PV: **Sphingomyelin and sphingomyelin synthase (SMS) in the malignant transformation of glioma cells and in 2-hydroxyoleic acid therapy**. *Proc Natl Acad Sci U S A* 2011, **108**(49):19569-19574.

160. Wang S, Chen X, Luan H, Gao D, Lin S, Cai Z, Liu J, Liu H, Jiang Y: **Matrix-assisted laser desorption/ionization mass spectrometry imaging of cell cultures for the lipidomic analysis of potential lipid markers in human breast cancer invasion**. *Rapid Commun Mass Spectrom* 2016, **30**(4):533-542.
161. Saha S, Mohanty KC: **Correlation of gangliosides GM2 and GM3 with metastatic potential to lungs of mouse B16 melanoma**. *J Exp Clin Cancer Res* 2003, **22**(1):125-134.
162. Rysman E, Brusselmans K, Scheys K, Timmermans L, Derua R, Munck S, Van Veldhoven PP, Waltregny D, Daniels VW, Machiels J *et al*: **De novo lipogenesis protects cancer cells from free radicals and chemotherapeutics by promoting membrane lipid saturation**. *Cancer Res* 2010, **70**(20):8117-8126.
163. Hilvo M, Denkert C, Lehtinen L, Muller B, Brockmoller S, Seppanen-Laakso T, Budczies J, Bucher E, Yetukuri L, Castillo S *et al*: **Novel theranostic opportunities offered by characterization of altered membrane lipid metabolism in breast cancer progression**. *Cancer Res* 2011, **71**(9):3236-3245.
164. MacLennan M, Ma DW: **Role of dietary fatty acids in mammary gland development and breast cancer**. *Breast Cancer Res* 2010, **12**(5):211.
165. Zeisig R, Koklic T, Wiesner B, Fichtner I, Sentjurc M: **Increase in fluidity in the membrane of MT3 breast cancer cells correlates with enhanced cell adhesion in vitro and increased lung metastasis in NOD/SCID mice**. *Arch Biochem Biophys* 2007, **459**(1):98-106.
166. Connor J, Bucana C, Fidler IJ, Schroit AJ: **Differentiation-dependent expression of phosphatidylserine in mammalian plasma membranes: quantitative assessment of outer-leaflet lipid by prothrombinase complex formation**. *Proc Natl Acad Sci U S A* 1989, **86**(9):3184-3188.
167. Utsugi T, Schroit AJ, Connor J, Bucana CD, Fidler IJ: **Elevated expression of phosphatidylserine in the outer membrane leaflet of human tumor cells and recognition by activated human blood monocytes**. *Cancer Res* 1991, **51**(11):3062-3066.

168. Stafford JH, Thorpe PE: **Increased exposure of phosphatidylethanolamine on the surface of tumor vascular endothelium**. *Neoplasia* 2011, **13**(4):299-308.
169. Van Blitterswijk WJ, De Veer G, Krol JH, Emmelot P: **Comparative lipid analysis of purified plasma membranes and shed extracellular membrane vesicles from normal murine thymocytes and leukemic GRSL cells**. *Biochim Biophys Acta* 1982, **688**(2):495-504.
170. Dessi S, Batetta B, Pulisci D, Spano O, Cherchi R, Lanfranco G, Tessitore L, Costelli P, Baccino FM, Anchisi C *et al*: **Altered pattern of lipid metabolism in patients with lung cancer**. *Oncology* 1992, **49**(6):436-441.
171. Kolanjiappan K, Ramachandran CR, Manoharan S: **Biochemical changes in tumor tissues of oral cancer patients**. *Clin Biochem* 2003, **36**(1):61-65.
172. Bernardes N, Fialho AM: **Perturbing the Dynamics and Organization of Cell Membrane Components: A New Paradigm for Cancer-Targeted Therapies**. *Int J Mol Sci* 2018, **19**(12).
173. Sok M, Sentjurc M, Schara M, Stare J, Rott T: **Cell membrane fluidity and prognosis of lung cancer**. *Ann Thorac Surg* 2002, **73**(5):1567-1571.
174. Peetla C, Vijayaraghavalu S, Labhasetwar V: **Biophysics of cell membrane lipids in cancer drug resistance: Implications for drug transport and drug delivery with nanoparticles**. *Adv Drug Deliv Rev* 2013, **65**(13-14):1686-1698.
175. Sakai K, Okuyama H, Yura J, Takeyama H, Shinagawa N, Tsuruga N, Kato K, Miura K, Kawase K, Tsujimura T *et al*: **Composition and turnover of phospholipids and neutral lipids in human breast cancer and reference tissues**. *Carcinogenesis* 1992, **13**(4):579-584.
176. Doria ML, Cotrim CZ, Simoes C, Macedo B, Domingues P, Domingues MR, Helguero LA: **Lipidomic analysis of phospholipids from human mammary epithelial and breast cancer cell lines**. *J Cell Physiol* 2013, **228**(2):457-468.
177. Kim HY, Lee KM, Kim SH, Kwon YJ, Chun YJ, Choi HK: **Comparative metabolic and lipidomic profiling of human breast cancer cells with different metastatic potentials**. *Oncotarget* 2016, **7**(41):67111-67128.

178. He M, Guo S, Li Z: **In situ characterizing membrane lipid phenotype of breast cancer cells using mass spectrometry profiling**. *Sci Rep* 2015, **5**:11298.
179. Kang HS, Lee SC, Park YS, Jeon YE, Lee JH, Jung SY, Park IH, Jang SH, Park HM, Yoo CW *et al*: **Protein and lipid MALDI profiles classify breast cancers according to the intrinsic subtype**. *BMC Cancer* 2011, **11**:465.
180. Kawashima M, Iwamoto N, Kawaguchi-Sakita N, Sugimoto M, Ueno T, Mikami Y, Terasawa K, Sato TA, Tanaka K, Shimizu K *et al*: **High-resolution imaging mass spectrometry reveals detailed spatial distribution of phosphatidylinositols in human breast cancer**. *Cancer Sci* 2013, **104**(10):1372-1379.
181. Cifkova E, Holcapek M, Lisa M, Vrana D, Gatek J, Melichar B: **Determination of lipidomic differences between human breast cancer and surrounding normal tissues using HILIC-HPLC/ESI-MS and multivariate data analysis**. *Anal Bioanal Chem* 2015, **407**(3):991-1002.
182. Merchant TE, Meneses P, Gierke LW, Den Otter W, Glonek T: **31P magnetic resonance phospholipid profiles of neoplastic human breast tissues**. *Br J Cancer* 1991, **63**(5):693-698.
183. Lorent JH, Quetin-Leclercq J, Mingeot-Leclercq MP: **The amphiphilic nature of saponins and their effects on artificial and biological membranes and potential consequences for red blood and cancer cells**. *Org Biomol Chem* 2014, **12**(44):8803-8822.
184. Vincken JP, Heng L, de Groot A, Gruppen H: **Saponins, classification and occurrence in the plant kingdom**. *Phytochemistry* 2007, **68**(3):275-297.
185. Lorent J, Le Duff CS, Quetin-Leclercq J, Mingeot-Leclercq MP: **Induction of highly curved structures in relation to membrane permeabilization and budding by the triterpenoid saponins, alpha- and delta-Hederin**. *J Biol Chem* 2013, **288**(20):14000-14017.
186. Bangham AD, Horne RW, Glauert AM, Dingle JT, Lucy JA: **Action of saponin on biological cell membranes**. *Nature* 1962, **196**:952-955.
187. Nishikawa M, Nojima S, Akiyama T, Sankawa U, Inoue K: **Interaction of digitonin and its analogs with membrane cholesterol**. *J Biochem* 1984, **96**(4):1231-1239.

188. Frenkel N, Makky A, Sudji IR, Wink M, Tanaka M: **Mechanistic investigation of interactions between steroidal saponin digitonin and cell membrane models**. *J Phys Chem B* 2014, **118**(50):14632-14639.
189. Keukens EA, de Vrije T, van den Boom C, de Waard P, Plasman HH, Thiel F, Chupin V, Jongen WM, de Kruijff B: **Molecular basis of glycoalkaloid induced membrane disruption**. *Biochim Biophys Acta* 1995, **1240**(2):216-228.
190. Armah CN, Mackie AR, Roy C, Price K, Osbourn AE, Bowyer P, Ladha S: **The membrane-permeabilizing effect of avenacin A-1 involves the reorganization of bilayer cholesterol**. *Biophys J* 1999, **76**(1 Pt 1):281-290.
191. Lin F, Wang R: **Hemolytic mechanism of dioscin proposed by molecular dynamics simulations**. *J Mol Model* 2010, **16**(1):107-118.
192. Hu M, Konoki K, Tachibana K: **Cholesterol-independent membrane disruption caused by triterpenoid saponins**. *Biochim Biophys Acta* 1996, **1299**(2):252-258.
193. Nakamura TI, K; Nojima. S; Sankawa. U; Shoji. J; Kawasaki. T; Shibata. S: **Interaction of saponins with red blood cells as well as with th phosphatidylcholine liposomal membranes**. *JPharm Dyn* 1979, **2**(6):375-382.
194. Fukuda K, Utsumi H, Shoji J, Hamada A: **Saponins can cause the agglutination of phospholipid vesicles**. *Biochim Biophys Acta* 1985, **820**(2):199-206.
195. Liu CX, Xiao PG: **Recent advances on ginseng research in China**. *J Ethnopharmacol* 1992, **36**(1):27-38.
196. Nag SA, Qin JJ, Wang W, Wang MH, Wang H, Zhang R: **Ginsenosides as Anticancer Agents: In vitro and in vivo Activities, Structure-Activity Relationships, and Molecular Mechanisms of Action**. *Front Pharmacol* 2012, **3**:25.
197. Li W, Liu Y, Zhang JW, Ai CZ, Xiang N, Liu HX, Yang L: **Anti-androgen-independent prostate cancer effects of ginsenoside metabolites in vitro: mechanism and possible structure-activity relationship investigation**. *Arch Pharm Res* 2009, **32**(1):49-57.

198. Wang W, Zhao Y, Rayburn ER, Hill DL, Wang H, Zhang R: **In vitro anti-cancer activity and structure-activity relationships of natural products isolated from fruits of Panax ginseng**. *Cancer Chemother Pharmacol* 2007, **59**(5):589-601.
199. Chen RJ, Chung TY, Li FY, Lin NH, Tzen JT: **Effect of sugar positions in ginsenosides and their inhibitory potency on Na+/K+-ATPase activity**. *Acta Pharmacol Sin* 2009, **30**(1):61-69.
200. Attele AS, Wu JA, Yuan CS: **Ginseng pharmacology: multiple constituents and multiple actions**. *Biochem Pharmacol* 1999, **58**(11):1685-1693.
201. Lorent JH, Diaz-Rohrer B, Lin X, Spring K, Gorfe AA, Levental KR, Levental I: **Structural determinants and functional consequences of protein affinity for membrane rafts**. *Nat Commun* 2017, **8**(1):1219.
202. van Meer G: **Cellular lipidomics**. *EMBO J* 2005, **24**(18):3159-3165.
203. Lorent J, Lins L, Domenech O, Quetin-Leclercq J, Brasseur R, Mingeot-Leclercq MP: **Domain formation and permeabilization induced by the saponin alpha-hederin and its aglycone hederagenin in a cholesterol-containing bilayer**. *Langmuir* 2014, **30**(16):4556-4569.
204. Park EK, Lee EJ, Lee SH, Koo KH, Sung JY, Hwang EH, Park JH, Kim CW, Jeong KC, Park BK *et al*: **Induction of apoptosis by the ginsenoside Rh2 by internalization of lipid rafts and caveolae and inactivation of Akt**. *Br J Pharmacol* 2010, **160**(5):1212-1223.
205. Kwon HY, Kim EH, Kim SW, Kim SN, Park JD, Rhee DK: **Selective toxicity of ginsenoside Rg3 on multidrug resistant cells by membrane fluidity modulation**. *Arch Pharm Res* 2008, **31**(2):171-177.
206. Yang WZ, Hu Y, Wu WY, Ye M, Guo DA: **Saponins in the genus Panax L. (Araliaceae): a systematic review of their chemical diversity**. *Phytochemistry* 2014, **106**:7-24.
207. Qi LW, Wang CZ, Yuan CS: **Ginsenosides from American ginseng: chemical and pharmacological diversity**. *Phytochemistry* 2011, **72**(8):689-699.
208. Israelachvili JN, Mitchell DJ, Ninham BW: **Theory of self-assembly of lipid bilayers and vesicles**. *Biochimica et biophysica acta* 1977, **470**(2):185-201.

209. Morein B, Lovgren K, Hoglund S, Sundquist B: **The ISCOM: an immunostimulating complex**. *Immunology today* 1987, **8**(11):333-338.
210. Xiong J, Guo J, Huang L, Meng B, Ping Q: **Self-micelle formation and the incorporation of lipid in the formulation affect the intestinal absorption of Panax notoginseng**. *International journal of pharmaceutics* 2008, **360**(1-2):191-196.
211. Dai X, Shi X, Wang Y, Qiao Y: **Solubilization of saikosaponin a by ginsenoside Ro biosurfactant in aqueous solution: mesoscopic simulation**. *J Colloid Interface Sci* 2012, **384**(1):73-80.
212. Dai X, Shi X, Yin Q, Ding H, Qiao Y: **Multiscale study on the interaction mechanism between ginsenoside biosurfactant and saikosaponin a**. *J Colloid Interface Sci* 2013, **396**:165-172.
213. Song X, Zang L, Hu S: **Amplified immune response by ginsenoside-based nanoparticles (ginsomes)**. *Vaccine* 2009, **27**(17):2306-2311.
214. Hou G, Niu J, Song F, Liu Z, Liu S: **Studies on the interactions between ginsenosides and liposome by equilibrium dialysis combined with ultrahigh performance liquid chromatography-tandem mass spectrometry**. *J Chromatogr B Analyt Technol Biomed Life Sci* 2013, **923-924**:1-7.
215. Ota T, Fujikawa-yamamoto K, Zong ZP, Yamazaki M, Odashima S, Kitagawa I, Abe H, Arichi S: **Plant-glycoside modulation of cell surface related to control of differentiation in cultured B16 melanoma cells**. *Cancer Res* 1987, **47**(14):3863-3867.
216. Korchowiec B, Gorczyca M, Wojszko K, Janikowska M, Henry M, Rogalska E: **Impact of two different saponins on the organization of model lipid membranes**. *Biochim Biophys Acta* 2015, **1848**(10 Pt A):1963-1973.
217. Sudji IR, Subburaj Y, Frenkel N, Garcia-Saez AJ, Wink M: **Membrane Disintegration Caused by the Steroid Saponin Digitonin Is Related to the Presence of Cholesterol**. *Molecules* 2015, **20**(11):20146-20160.
218. Yu BS, Kim A, Chung HH, Yoshikawa W, Akutsu H, Kyogoku Y: **Effects of purified ginseng saponins on multilamellar liposomes**. *Chem Biol Interact* 1985, **56**(2-3):303-319.
219. Verstraeten SL, Albert M, Paquot A, Muccioli GG, Tyteca D, Mingeot-Leclercq MP: **Membrane cholesterol delays cellular apoptosis induced**

by ginsenoside Rh2, a steroid saponin. *Toxicol Appl Pharmacol* 2018, **352**:59-67.

220. Verstraeten SL, Deleu M, Janikowska-Sagan M, Claereboudt EJS, Lins L, Tyteca D, Mingeot-Leclercq MP: **The activity of the saponin ginsenoside Rh2 is enhanced by the interaction with membrane sphingomyelin but depressed by cholesterol**. *Sci Rep* 2019, **9**(1):7285.
221. Yi JS, Choo HJ, Cho BR, Kim HM, Kim YN, Ham YM, Ko YG: **Ginsenoside Rh2 induces ligand-independent Fas activation via lipid raft disruption**. *Biochem Biophys Res Commun* 2009, **385**(2):154-159.
222. Jiang YS, Jin ZX, Umehara H, Ota T: **Cholesterol-dependent induction of dendrite formation by ginsenoside Rh2 in cultured melanoma cells**. *Int J Mol Med* 2010, **26**(6):787-793.
223. Tachikawa E, Kudo K, Nunokawa M, Kashimoto T, Takahashi E, Kitagawa S: **Characterization of ginseng saponin ginsenoside-Rg(3) inhibition of catecholamine secretion in bovine adrenal chromaffin cells**. *Biochem Pharmacol* 2001, **62**(7):943-951.
224. Zhou XM, Cao YL, Dou DQ: **Protective effect of ginsenoside-Re against cerebral ischemia/reperfusion damage in rats**. *Biol Pharm Bull* 2006, **29**(12):2502-2505.
225. Sung WS, Lee DG: **The combination effect of Korean red ginseng saponins with kanamycin and cefotaxime against methicillin-resistant Staphylococcus aureus**. *Biol Pharm Bull* 2008, **31**(8):1614-1617.
226. Sung WS, Lee DG: **In vitro candidacidal action of Korean red ginseng saponins against Candida albicans**. *Biol Pharm Bull* 2008, **31**(1):139-142.
227. Diaz-Rohrer BB, Levental KR, Simons K, Levental I: **Membrane raft association is a determinant of plasma membrane localization**. *Proceedings of the National Academy of Sciences of the United States of America* 2014, **111**(23):8500-8505.
228. Yun UJ, Lee JH, Koo KH, Ye SK, Kim SY, Lee CH, Kim YN: **Lipid raft modulation by Rp1 reverses multidrug resistance via inactivating MDR-1 and Src inhibition**. *Biochem Pharmacol* 2013, **85**(10):1441-1453.
229. Kang MS, Baek SH, Chun YS, Moore AZ, Landman N, Berman D, Yang HO, Morishima-Kawashima M, Osawa S, Funamoto S *et al*: **Modulation of lipid kinase PI4KIIalpha activity and lipid raft association of presenilin**

1 underlies gamma-secretase inhibition by ginsenoside (20S)-Rg3. *J Biol Chem* 2013, **288**(29):20868-20882.

230. Qiu J, Li W, Feng SH, Wang M, He ZY: **Ginsenoside Rh2 promotes nonamyloidgenic cleavage of amyloid precursor protein via a cholesterol-dependent pathway**. *Genet Mol Res* 2014, **13**(2):3586-3598.
231. Liu Y, Yang G, Bu X, Liu G, Ding J, Li P, Jia W: **Cell-type-specific regulation of raft-associated Akt signaling**. *Cell Death Dis* 2011, **2**:e145.
232. Park B, Lee YM, Kim JS, Her Y, Kang JH, Oh SH, Kim HM: **Neutral sphingomyelinase 2 modulates cytotoxic effects of protopanaxadiol on different human cancer cells**. *BMC Complement Altern Med* 2013, **13**:194.
233. Li GX, Liu ZQ: **The protective effects of ginsenosides on human erythrocytes against hemin-induced hemolysis**. *Food Chem Toxicol* 2008, **46**(3):886-892.
234. Nah SY: **Ginseng ginsenoside pharmacology in the nervous system: involvement in the regulation of ion channels and receptors**. *Front Physiol* 2014, **5**:98.
235. Lee BH, Jeong SM, Ha TS, Park CS, Lee JH, Kim JH, Kim DH, Han JS, Kim HC, Ko SR *et al*: **Ginsenosides regulate ligand-gated ion channels from the outside**. *Mol Cells* 2004, **18**(1):115-121.
236. Lee BH, Lee JH, Lee SM, Jeong SM, Yoon IS, Lee JH, Choi SH, Pyo MK, Rhim H, Kim HC *et al*: **Identification of ginsenoside interaction sites in 5-HT3A receptors**. *Neuropharmacology* 2007, **52**(4):1139-1150.
237. Lee JH, Choi SH, Lee BH, Shin TJ, Pyo MK, Hwang SH, Kim BR, Lee SM, Bae DH, Rhim H *et al*: **The effects of ginsenoside Rg(3) on human Kv1.4 channel currents without the N-terminal rapid inactivation domain**. *Biol Pharm Bull* 2009, **32**(4):614-618.
238. Kim S, Kim T, Ahn K, Park WK, Nah SY, Rhim H: **Ginsenoside Rg3 antagonizes NMDA receptors through a glycine modulatory site in rat cultured hippocampal neurons**. *Biochem Biophys Res Commun* 2004, **323**(2):416-424.
239. Lee E, Kim S, Chung KC, Choo MK, Kim DH, Nam G, Rhim H: **20(S)-ginsenoside Rh2, a newly identified active ingredient of ginseng,**

inhibits NMDA receptors in cultured rat hippocampal neurons. *Eur J Pharmacol* 2006, **536**(1-2):69-77.

240. Gao S, Kushida H, Makino T: **Ginsenosides, ingredients of the root of Panax ginseng, are not substrates but inhibitors of sodium-glucose transporter 1**. *J Nat Med* 2017, **71**(1):131-138.
241. Li G, Kim J, Huang Z, St Clair JR, Brown DA, London E: **Efficient replacement of plasma membrane outer leaflet phospholipids and sphingolipids in cells with exogenous lipids**. *Proceedings of the National Academy of Sciences of the United States of America* 2016, **113**(49):14025-14030.
242. Tanaka A, Yamamoto A, Murota K, Tsujiuchi T, Iwamori M, Fukushima N: **Polyunsaturated fatty acids induce ovarian cancer cell death through ROS-dependent MAP kinase activation**. *Biochemical and biophysical research communications* 2017, **493**(1):468-473.
243. Sultana R, Perluigi M, Allan Butterfield D: **Lipid peroxidation triggers neurodegeneration: a redox proteomics view into the Alzheimer disease brain**. *Free radical biology & medicine* 2013, **62**:157-169.
244. Ye R, Yang Q, Kong X, Han J, Zhang X, Zhang Y, Li P, Liu J, Shi M, Xiong L *et al*: **Ginsenoside Rd attenuates early oxidative damage and sequential inflammatory response after transient focal ischemia in rats**. *Neurochem Int* 2011, **58**(3):391-398.
245. Deng HL, Zhang JT: **Anti-lipid peroxilative effect of ginsenoside Rb1 and Rg1**. *Chin Med J (Engl)* 1991, **104**(5):395-398.
246. Liu ZQ, Luo XY, Liu GZ, Chen YP, Wang ZC, Sun YX: **In vitro study of the relationship between the structure of ginsenoside and its antioxidative or prooxidative activity in free radical induced hemolysis of human erythrocytes**. *J Agric Food Chem* 2003, **51**(9):2555-2558.
247. Wu Q, Deng J, Fan D, Duan Z, Zhu C, Fu R, Wang S: **Ginsenoside Rh4 induces apoptosis and autophagic cell death through activation of the ROS/JNK/p53 pathway in colorectal cancer cells**. *Biochem Pharmacol* 2017, **148**:64-74.
248. Xia T, Wang YN, Zhou CX, Wu LM, Liu Y, Zeng QH, Zhang XL, Yao JH, Wang M, Fang JP: **Ginsenoside Rh2 and Rg3 inhibit cell proliferation and**

induce apoptosis by increasing mitochondrial reactive oxygen species in human leukemia Jurkat cells. *Mol Med Rep* 2017, **15**(6):3591-3598.
249. Mollinedo F, Gajate C: **Lipid rafts as major platforms for signaling regulation in cancer**. *Adv Biol Regul* 2015, **57**:130-146.
250. Huang J, Peng K, Wang L, Wen B, Zhou L, Luo T, Su M, Li J, Luo Z: **Ginsenoside Rh2 inhibits proliferation and induces apoptosis in human leukemia cells via TNF-alpha signaling pathway**. *Acta Biochim Biophys Sin (Shanghai)* 2016, **48**(8):750-755.
251. Kim HS, Lee EH, Ko SR, Choi KJ, Park JH, Im DS: **Effects of ginsenosides Rg3 and Rh2 on the proliferation of prostate cancer cells**. *Arch Pharm Res* 2004, **27**(4):429-435.
252. Zhang YL, Zhang R, Xu HL, Yu XF, Qu SC, Sui DY: **20(S)-protopanaxadiol triggers mitochondrial-mediated apoptosis in human lung adenocarcinoma A549 cells via inhibiting the PI3K/Akt signaling pathway**. *Am J Chin Med* 2013, **41**(5):1137-1152.
253. Li S, Gao Y, Ma W, Guo W, Zhou G, Cheng T, Liu Y: **EGFR signaling-dependent inhibition of glioblastoma growth by ginsenoside Rh2**. *Tumour Biol* 2014, **35**(6):5593-5598.
254. Li S, Guo W, Gao Y, Liu Y: **Ginsenoside Rh2 inhibits growth of glioblastoma multiforme through mTor**. *Tumour Biol* 2015, **36**(4):2607-2612.
255. Gorrini C, Harris IS, Mak TW: **Modulation of oxidative stress as an anticancer strategy**. *Nat Rev Drug Discov* 2013, **12**(12):931-947.
256. Sodrul IMD, Wang C, Chen X, Du J, Sun H: **Role of ginsenosides in reactive oxygen species-mediated anticancer therapy**. *Oncotarget* 2018, **9**(2):2931-2950.
257. Kim SS, Seong S, Kim SY: **Synergistic effect of ginsenoside Rg3 with verapamil on the modulation of multidrug resistance in human acute myeloid leukemia cells**. *Oncol Lett* 2014, **7**(4):1265-1269.
258. Kim SW, Kwon HY, Chi DW, Shim JH, Park JD, Lee YH, Pyo S, Rhee DK: **Reversal of P-glycoprotein-mediated multidrug resistance by ginsenoside Rg(3)**. *Biochem Pharmacol* 2003, **65**(1):75-82.
259. Feng. SL, Lua. HB, Zhan. J, B W, Chen. YJ, Zhan HX, Jiang ZH, Y. X: **Ginsenoside Rg5 overcomes chemotherapeutic multidrug resistance**

mediated by ABCB1 transporter: in vitro and in vivo study. *Journal of ginseng research* 2018.

260. Kikuchi Y, Sasa H, Kita T, Hirata J, Tode T, Nagata I: **Inhibition of human ovarian cancer cell proliferation in vitro by ginsenoside Rh2 and adjuvant effects to cisplatin in vivo**. *Anticancer Drugs* 1991, **2**(1):63-67.
261. Nakhjavani M, Hardingham JE, Palethorpe HM, Tomita Y, Smith E, Price TJ, Townsend AR: **Ginsenoside Rg3: Potential Molecular Targets and Therapeutic Indication in Metastatic Breast Cancer**. *Medicines (Basel)* 2019, **6**(1).
262. Namba T, Yoshizaki M, Tominori T, Kobashi K, Mitsui K: **Hemolytic and its protective activity of ginseng saponins**. *Chem Pharm Bull (Tokyo)* 1973, **21**(2):459-461.
263. Sun HX, Chen Y, Ye Y: **Ginsenoside Re and notoginsenoside R1: Immunologic adjuvants with low haemolytic effect**. *Chem Biodivers* 2006, **3**(7):718-726.
264. Sun HX, Qin F, Ye YP: **Relationship between haemolytic and adjuvant activity and structure of protopanaxadiol-type saponins from the roots of Panax notoginseng**. *Vaccine* 2005, **23**(48-49):5533-5542.
265. Yang ZG, Ye YP, Sun HX: **Immunological adjuvant effect of ginsenoside Rh4 from the roots of Panax notoginseng on specific antibody and cellular response to ovalbumin in mice**. *Chem Biodivers* 2007, **4**(2):232-240.
266. Kim H, Lee JH, Kim JE, Kim YS, Ryu CH, Lee HJ, Kim HM, Jeon H, Won HJ, Lee JY *et al*: **Micro-/nano-sized delivery systems of ginsenosides for improved systemic bioavailability**. *J Ginseng Res* 2018, **42**(3):361-369.
267. Xu. L; Yu. H; Yin. S ZRZYLJ: **Liposome-based delivery systems for ginsenoside Rh2: in vitro and in vivo comparisons**. *J Nanopart Res* 2015, **17**:415.
268. Jin X, Yang Q, Cai N: **Preparation of ginsenoside compound-K mixed micelles with improved retention and antitumor efficacy**. *Int J Nanomedicine* 2018, **13**:3827-3838.
269. Yu X, Xu H, Hu M, Luan X, Wang K, Fu Y, Zhang D, Li J: **Ginsenoside Rg3 bile salt-phosphatidylcholine-based mixed micelles: design,**

characterization, and evaluation. *Chem Pharm Bull (Tokyo)* 2015, **63**(5):361-368.

270. Zare-Zardini H, Taheri-Kafrani A, Amiri A, Bordbar AK: **New generation of drug delivery systems based on ginsenoside Rh2-, Lysine- and Arginine-treated highly porous graphene for improving anticancer activity**. *Sci Rep* 2018, **8**(1):586.
271. Morrissey JP, Osbourn AE: **Fungal resistance to plant antibiotics as a mechanism of pathogenesis**. *Microbiol Mol Biol Rev* 1999, **63**(3):708-724.
272. Défago. G, Kern. H: **Induction of Fusarium solani mutants insensitive to tomatine, their pathogenicity and aggressiveness to tomato fruits and pea plants**. *Physiological Plant Pathology* 1983, **22**(1):29-37.
273. Zhao X, Gao J, Song C, Fang Q, Wang N, Zhao T, Liu D, Zhou Y: **Fungal sensitivity to and enzymatic deglycosylation of ginsenosides**. *Phytochemistry* 2012, **78**:65-71.
274. Yousef LF, Bernards MA: **In vitro metabolism of ginsenosides by the ginseng root pathogen Pythium irregulare**. *Phytochemistry* 2006, **67**(16):1740-1749.
275. Kazan K, Gardiner DM: **Targeting pathogen sterols: Defence and counterdefence?** *PLoS Pathog* 2017, **13**(5):e1006297.
276. Kachur K, Suntres ZE: **The antimicrobial properties of ginseng and ginseng extracts**. *Expert Rev Anti Infect Ther* 2016, **14**(1):81-94.
277. Xue P, Yao Y, Yang XS, Feng J, Ren GX: **Improved antimicrobial effect of ginseng extract by heat transformation**. *J Ginseng Res* 2017, **41**(2):180-187.
278. Kim SH, Ha US, Sohn DW, Lee SJ, Kim HW, Han CH, Cho YH: **Preventive effect of ginsenoid on chronic bacterial prostatitis**. *J Infect Chemother* 2012, **18**(5):709-714.
279. Zhang J, Sun Y, Wang Y, Lu M, He J, Liu J, Chen Q, Zhang X, Zhou F, Wang G *et al*: **Non-antibiotic agent ginsenoside 20(S)-Rh2 enhanced the antibacterial effects of ciprofloxacin in vitro and in vivo as a potential NorA inhibitor**. *Eur J Pharmacol* 2014, **740**:277-284.
280. Sharif Makhmal Zadeh B, Esfahani G, Salimi A: **Permeability of Ciprofloxacin-Loaded Polymeric Micelles Including Ginsenoside as P-**

glycoprotein Inhibitor through a Caco-2 Cells Monolayer as an Intestinal Absorption Model. *Molecules* 2018, **23**(8).

281. Yu SE, Mwesige B, Yi YS, Yoo BC: **Ginsenosides: the need to move forward from bench to clinical trials**. *J Ginseng Res* 2019, **43**(3):361-367.
282. Li JQ, Zhang JT: **[Effects of age and ginsenoside RG1 on membrane fluidity of cortical cells in rats]**. *Yao Xue Xue Bao* 1997, **32**(1):23-27.
283. Fukuda K, Utsumi H, Soda S, Shoji J, Hamada A: **Specific interaction of arabinose residue in ginsenoside with egg phosphatidylcholine vesicles**. *Biochim Biophys Acta* 1987, **900**(2):267-274.
284. Chen F, Zhang B, Sun Y, Xiong ZX, Peng H, Deng ZY, Hu JN: **The Octyl Ester of Ginsenoside Rh2 Induces Lysosomal Membrane Permeabilization via Bax Translocation**. *Nutrients* 2016, **8**(5).
285. Lee JH, Lee BH, Choi SH, Yoon IS, Pyo MK, Shin TJ, Choi WS, Lim Y, Rhim H, Won KH *et al*: **Ginsenoside Rg3 inhibits human Kv1.4 channel currents by interacting with the Lys531 residue**. *Mol Pharmacol* 2008, **73**(3):619-626.
286. Tian J, Zhang S, Li G, Liu Z, Xu B: **20(S)-ginsenoside Rg3, a neuroprotective agent, inhibits mitochondrial permeability transition pores in rat brain**. *Phytother Res* 2009, **23**(4):486-491.
287. Ye R, Kong X, Yang Q, Zhang Y, Han J, Zhao G: **Ginsenoside Rd attenuates redox imbalance and improves stroke outcome after focal cerebral ischemia in aged mice**. *Neuropharmacology* 2011, **61**(4):815-824.
288. Wu Q, Deng J, Fan D, Duan Z, Zhu C, Fu R, Wang S: **Ginsenoside Rh4 induces apoptosis and autophagic cell death through activation of the ROS/JNK/p53 pathway in colorectal cancer cells**. *Biochem Pharmacol* 2018, **148**:64-74.
289. Nakata H, Kikuchi Y, Tode T, Hirata J, Kita T, Ishii K, Kudoh K, Nagata I, Shinomiya N: **Inhibitory effects of ginsenoside Rh2 on tumor growth in nude mice bearing human ovarian cancer cells**. *Jpn J Cancer Res* 1998, **89**(7):733-740.
290. Santner SJ, Dawson PJ, Tait L, Soule HD, Eliason J, Mohamed AN, Wolman SR, Heppner GH, Miller FR: **Malignant MCF10CA1 cell lines derived from premalignant human breast epithelial MCF10AT cells**. *Breast Cancer Res Treat* 2001, **65**(2):101-110.

291. Bravo-Cordero JJ, Hodgson L, Condeelis J: **Directed cell invasion and migration during metastasis**. *Curr Opin Cell Biol* 2012, **24**(2):277-283.
292. Lambert AW, Pattabiraman DR, Weinberg RA: **Emerging Biological Principles of Metastasis**. *Cell* 2017, **168**(4):670-691.
293. Leonard C, D. Alsteens, A. Dumitru, M. Mingeot-Leclercq, and D. Tyteca: **Lipid domains and membrane (re)shaping : from biophysics to biology**, vol. 19; 2017.
294. Alves AC, Ribeiro D, Nunes C, Reis S: **Biophysics in cancer: The relevance of drug-membrane interaction studies**. *Biochim Biophys Acta* 2016, **1858**(9):2231-2244.
295. Ran S, Downes A, Thorpe PE: **Increased exposure of anionic phospholipids on the surface of tumor blood vessels**. *Cancer Res* 2002, **62**(21):6132-6140.
296. Riedl S, Rinner B, Asslaber M, Schaider H, Walzer S, Novak A, Lohner K, Zweytick D: **In search of a novel target - phosphatidylserine exposed by non-apoptotic tumor cells and metastases of malignancies with poor treatment efficacy**. *Biochim Biophys Acta* 2011, **1808**(11):2638-2645.
297. Sherbet GV: **Membrane fluidity and cancer metastasis**. *Exp Cell Biol* 1989, **57**(4):198-205.
298. Galeotti T, Borrello S, Minotti G, Masotti L: **Membrane alterations in cancer cells: the role of oxy radicals**. *Ann N Y Acad Sci* 1986, **488**:468-480.
299. Luo J, Manning BD, Cantley LC: **Targeting the PI3K-Akt pathway in human cancer: rationale and promise**. *Cancer Cell* 2003, **4**(4):257-262.
300. Ren G, Shi Z, Teng C, Yao Y: **Antiproliferative Activity of Combined Biochanin A and Ginsenoside Rh(2) on MDA-MB-231 and MCF-7 Human Breast Cancer Cells**. *Molecules* 2018, **23**(11).
301. Kadota M, Sato M, Duncan B, Ooshima A, Yang HH, Diaz-Meyer N, Gere S, Kageyama S, Fukuoka J, Nagata T *et al*: **Identification of novel gene amplifications in breast cancer and coexistence of gene amplification with an activating mutation of PIK3CA**. *Cancer Res* 2009, **69**(18):7357-7365.

302. Lim SJ, Choi HG, Jeon CK, Kim SH: **Increased chemoresistance to paclitaxel in the MCF10AT series of human breast epithelial cancer cells**. *Oncol Rep* 2015, **33**(4):2023-2030.
303. Li QS, Lee GY, Ong CN, Lim CT: **AFM indentation study of breast cancer cells**. *Biochem Biophys Res Commun* 2008, **374**(4):609-613.
304. Wang B, Guo P, Auguste DT: **Mapping the CXCR4 receptor on breast cancer cells**. *Biomaterials* 2015, **57**:161-168.
305. Suresh S: **Biomechanics and biophysics of cancer cells**. *Acta Biomater* 2007, **3**(4):413-438.
306. Vestergaard M, Hamada T, Takagi M: **Using model membranes for the study of amyloid beta:lipid interactions and neurotoxicity**. *Biotechnol Bioeng* 2008, **99**(4):753-763.
307. Holopainen JM, Angelova MI, Kinnunen PK: **Vectorial budding of vesicles by asymmetrical enzymatic formation of ceramide in giant liposomes**. *Biophys J* 2000, **78**(2):830-838.
308. Pautot S, Frisken BJ, Weitz DA: **Engineering asymmetric vesicles**. *Proc Natl Acad Sci U S A* 2003, **100**(19):10718-10721.
309. de Matos MBC, Miranda BS, Rizky Nuari Y, Storm G, Leneweit G, Schiffelers RM, Kok RJ: **Liposomes with asymmetric bilayers produced from inverse emulsions for nucleic acid delivery**. *J Drug Target* 2019, **27**(5-6):681-689.
310. Lin Q, London E: **Preparation of artificial plasma membrane mimicking vesicles with lipid asymmetry**. *PLoS One* 2014, **9**(1):e87903.
311. Doktorova M, Heberle FA, Eicher B, Standaert RF, Katsaras J, London E, Pabst G, Marquardt D: **Preparation of asymmetric phospholipid vesicles for use as cell membrane models**. *Nat Protoc* 2018, **13**(9):2086-2101.
312. Baumgart T, Hammond AT, Sengupta P, Hess ST, Holowka DA, Baird BA, Webb WW: **Large-scale fluid/fluid phase separation of proteins and lipids in giant plasma membrane vesicles**. *Proc Natl Acad Sci U S A* 2007, **104**(9):3165-3170.
313. Gerstle Z, Desai R, Veatch SL: **Giant Plasma Membrane Vesicles: An Experimental Tool for Probing the Effects of Drugs and Other Conditions on Membrane Domain Stability**. *Methods Enzymol* 2018, **603**:129-150.

314. Sezgin E, Kaiser HJ, Baumgart T, Schwille P, Simons K, Levental I: **Elucidating membrane structure and protein behavior using giant plasma membrane vesicles**. *Nat Protoc* 2012, **7**(6):1042-1051.
315. Levental KR, Levental I: **Giant plasma membrane vesicles: models for understanding membrane organization**. *Curr Top Membr* 2015, **75**:25-57.
316. Sezgin E, Schneider F, Zilles V, Urbancic I, Garcia E, Waithe D, Klymchenko AS, Eggeling C: **Polarity-Sensitive Probes for Superresolution Stimulated Emission Depletion Microscopy**. *Biophys J* 2017, **113**(6):1321-1330.
317. Alonso A, Goni FM: **The Physical Properties of Ceramides in Membranes**. *Annu Rev Biophys* 2018, **47**:633-654.
318. Lopez CA, de Vries AH, Marrink SJ: **Computational microscopy of cyclodextrin mediated cholesterol extraction from lipid model membranes**. *Sci Rep* 2013, **3**:2071.
319. Wang C, Zhang F, Cao Y, Zhang M, Wang A, Xu M, Su M, Zhang M, Zhuge Y: **Etoposide Induces Apoptosis in Activated Human Hepatic Stellate Cells via ER Stress**. *Sci Rep* 2016, **6**:34330.
320. Riley RT, Merrill AH, Jr.: **Ceramide synthase inhibition by fumonisins: a perfect storm of perturbed sphingolipid metabolism, signaling, and disease**. *J Lipid Res* 2019, **60**(7):1183-1189.
321. Lee H, Lee S, Jeong D, Kim SJ: **Ginsenoside Rh2 epigenetically regulates cell-mediated immune pathway to inhibit proliferation of MCF-7 breast cancer cells**. *J Ginseng Res* 2018, **42**(4):455-462.
322. An IS, An S, Kwon KJ, Kim YJ, Bae S: **Ginsenoside Rh2 mediates changes in the microRNA expression profile of human non-small cell lung cancer A549 cells**. *Oncol Rep* 2013, **29**(2):523-528.
323. Guo XX, Guo Q, Li Y, Lee SK, Wei XN, Jin YH: **Ginsenoside Rh2 induces human hepatoma cell apoptosisvia bax/bak triggered cytochrome C release and caspase-9/caspase-8 activation**. *Int J Mol Sci* 2012, **13**(12):15523-15535.
324. Breckenridge DG, Germain M, Mathai JP, Nguyen M, Shore GC: **Regulation of apoptosis by endoplasmic reticulum pathways**. *Oncogene* 2003, **22**(53):8608-8618.

325. Fantini J, Barrantes FJ: **How cholesterol interacts with membrane proteins: an exploration of cholesterol-binding sites including CRAC, CARC, and tilted domains**. *Front Physiol* 2013, **4**:31.
326. Schon P, Garcia-Saez AJ, Malovrh P, Bacia K, Anderluh G, Schwille P: **Equinatoxin II permeabilizing activity depends on the presence of sphingomyelin and lipid phase coexistence**. *Biophys J* 2008, **95**(2):691-698.
327. Ge G, Wu J, Lin Q: **Effect of membrane fluidity on tyrosine kinase activity of reconstituted epidermal growth factor receptor**. *Biochem Biophys Res Commun* 2001, **282**(2):511-514.
328. Chen CC, Wu ML, Ho CT, Huang TC: **Blockade of the Ras/Raf/ERK and Ras/PI3K/Akt Pathways by Monacolin K Reduces the Expression of GLO1 and Induces Apoptosis in U937 Cells**. *J Agric Food Chem* 2015, **63**(4):1186-1195.
329. Guo XX, Li Y, Sun C, Jiang D, Lin YJ, Jin FX, Lee SK, Jin YH: **p53-dependent Fas expression is critical for Ginsenoside Rh2 triggered caspase-8 activation in HeLa cells**. *Protein Cell* 2014, **5**(3):224-234.
330. Garcia-Saez AJ, Chiantia S, Schwille P: **Effect of line tension on the lateral organization of lipid membranes**. *J Biol Chem* 2007, **282**(46):33537-33544.
331. Escriba PV: **Membrane-lipid therapy: a new approach in molecular medicine**. *Trends Mol Med* 2006, **12**(1):34-43.
332. Escriba PV: **Membrane-lipid therapy: A historical perspective of membrane-targeted therapies - From lipid bilayer structure to the pathophysiological regulation of cells**. *Biochim Biophys Acta Biomembr* 2017, **1859**(9 Pt B):1493-1506.
333. Speelmans G, Sips WH, Grisel RJ, Staffhorst RW, Fichtinger-Schepman AM, Reedijk J, de Kruijff B: **The interaction of the anti-cancer drug cisplatin with phospholipids is specific for negatively charged phospholipids and takes place at low chloride ion concentration**. *Biochim Biophys Acta* 1996, **1283**(1):60-66.
334. Baritaki S, Apostolakis S, Kanellou P, Dimanche-Boitrel MT, Spandidos DA, Bonavida B: **Reversal of tumor resistance to apoptotic stimuli by**

alteration of membrane fluidity: therapeutic implications. *Adv Cancer Res* 2007, **98**:149-190.

335. Gu Y, Wang GJ, Sun JG, Jia YW, Wang W, Xu MJ, Lv T, Zheng YT, Sai Y: **Pharmacokinetic characterization of ginsenoside Rh2, an anticancer nutrient from ginseng, in rats and dogs**. *Food Chem Toxicol* 2009, **47**(9):2257-2268.
336. Musende AG, Eberding A, Wood C, Adomat H, Fazli L, Hurtado-Coll A, Jia W, Bally MB, Guns ET: **Pre-clinical evaluation of Rh2 in PC-3 human xenograft model for prostate cancer in vivo: formulation, pharmacokinetics, biodistribution and efficacy**. *Cancer Chemother Pharmacol* 2009, **64**(6):1085-1095.
337. Wong AS, Che CM, Leung KW: **Recent advances in ginseng as cancer therapeutics: a functional and mechanistic overview**. *Nat Prod Rep* 2015, **32**(2):256-272.
338. Hou JP: **The chemical constituents of ginseng plants**. *Comp Med East West* 1977, **5**(2):123-145.
339. Lin Y, Li Y, Song ZG, Zhu H, Jin YH: **The interaction of serum albumin with ginsenoside Rh2 resulted in the downregulation of ginsenoside Rh2 cytotoxicity**. *J Ginseng Res* 2017, **41**(3):330-338.
340. Wang P, Wei W, Ye W, Li X, Zhao W, Yang C, Li C, Yan X, Zhou Z: **Synthesizing ginsenoside Rh2 in Saccharomyces cerevisiae cell factory at high-efficiency**. *Cell Discov* 2019, **5**:5.
341. Abe M, Makino A, Hullin-Matsuda F, Kamijo K, Ohno-Iwashita Y, Hanada K, Mizuno H, Miyawaki A, Kobayashi T: **A role for sphingomyelin-rich lipid domains in the accumulation of phosphatidylinositol-4,5-bisphosphate to the cleavage furrow during cytokinesis**. *Mol Cell Biol* 2012, **32**(8):1396-1407.
342. Slotte JP: **Biological functions of sphingomyelins**. *Prog Lipid Res* 2013, **52**(4):424-437.
343. Danhier F, Feron O, Preat V: **To exploit the tumor microenvironment: Passive and active tumor targeting of nanocarriers for anti-cancer drug delivery**. *J Control Release* 2010, **148**(2):135-146.
344. Strebhardt K, Ullrich A: **Paul Ehrlich's magic bullet concept: 100 years of progress**. *Nat Rev Cancer* 2008, **8**(6):473-480.

345. Nisini R, Poerio N, Mariotti S, De Santis F, Fraziano M: **The Multirole of Liposomes in Therapy and Prevention of Infectious Diseases**. *Front Immunol* 2018, **9**:155.
346. Kneidl B, Peller M, Winter G, Lindner LH, Hossann M: **Thermosensitive liposomal drug delivery systems: state of the art review**. *Int J Nanomedicine* 2014, **9**:4387-4398.
347. Bulbake U, Doppalapudi S, Kommineni N, Khan W: **Liposomal Formulations in Clinical Use: An Updated Review**. *Pharmaceutics* 2017, **9**(2).
348. Graeser R, Bornmann C, Esser N, Ziroli V, Jantscheff P, Unger C, Hopt UT, Schaechtele C, von Dobschuetz E, Massing U: **Antimetastatic effects of liposomal gemcitabine and empty liposomes in an orthotopic mouse model of pancreatic cancer**. *Pancreas* 2009, **38**(3):330-337.
349. Karroum O, Mignion L, Kengen J, Karmani L, Leveque P, Danhier P, Magat J, Bol A, Labar D, Gregoire V *et al*: **Multimodal imaging of tumor response to sorafenib combined with radiation therapy: comparison between diffusion-weighted MRI, choline spectroscopy and 18F-FLT PET imaging**. *Contrast Media Mol Imaging* 2013, **8**(3):274-280.
350. Mignion L, Dutta P, Martinez GV, Foroutan P, Gillies RJ, Jordan BF: **Monitoring chemotherapeutic response by hyperpolarized 13C-fumarate MRS and diffusion MRI**. *Cancer Res* 2014, **74**(3):686-694.

CHAPTER VI: APPENDIX

Contents lists available at ScienceDirect

Toxicology and Applied Pharmacology

journal homepage: www.elsevier.com/locate/ytaap

Subcellular mechanisms involved in apoptosis induced by aminoglycoside antibiotics: Insights on p53, proteasome and endoplasmic reticulum

Sophie Denamur [a], Lidvine Boland [a], Maxime Beyaert [b], Sandrine L. Verstraeten [a], Marianne Fillet [c], Paul M. Tulkens [a], Françoise Bontemps [b], Marie-Paule Mingeot-Leclercq [a]

[a] Université catholique de Louvain, Louvain Drug Research Institute, Cellular and Molecular Pharmacology, UCL B1.73.05, avenue E. Mounier, 73 – B1200 Brussels, Belgium
[b] Université catholique de Louvain, de Duve Institute, Laboratory of Physiological Chemistry, UCL B1.75.08, avenue Hippocrate, 75 B -1200 Brussels, Belgium
[c] University of Liege, CIRM, Department of Pharmacy, Laboratory for the Analysis of Medicines, Quartier Hopital, Avenue Hippocrate, 15, B36, Tower 4, 4000 Liège 1, Belgium

ARTICLE INFO

Article history:
Received 19 April 2016
Revised 20 August 2016
Accepted 22 August 2016
Available online 26 August 2016

Keywords:
Aminoglycosides
Gentamicin
Apoptosis
p53
Proteasome
Endoplasmic reticulum

ABSTRACT

Gentamicin, an aminoglycoside used to treat severe bacterial infections, may cause acute renal failure. In the renal cell line LLC-PK1, gentamicin accumulates in lysosomes, induces alterations of their permeability, and triggers the mitochondrial pathway of apoptosis via activation of caspase-9 and -3 and changes in Bcl-2 family proteins. Early ROS production in lysosomes has been associated with gentamicin induced lysosomal membrane permeabilization. In order to better understand the multiple interconnected pathways of gentamicin-induced apoptosis and ensuing renal cell toxicity, we investigated the effect of gentamicin on p53 and p21 levels. We also studied the potential effect of gentamicin on proteasome by measuring the chymotrypsin-, trypsin- and caspase-like activities, and on endoplasmic reticulum by determining phopho-eIF2α, caspase-12 activation and GRP78 and 94. We observed an increase in p53 levels, which was dependent on ROS production. Accumulation of p53 resulted in accumulation of p21 and of phospho-eIF2α. These effects could be related to an impairment of proteasome as we demonstrated an inhibition of trypsin-and caspase-like activities. Moderate endoplasmic reticulum stress could also participate to cellular toxicity induced by gentamicin, with activation of caspase-12 without change in GRP74 and GRP98. All together, these data provide new mechanistic insights into the apoptosis induced by aminoglycoside antibiotics on renal cell lines.

1. Introduction

Gentamicin is a commonly used aminoglycoside antibiotic for the treatment of serious and life-threatening infections caused by Gram-negative aerobes. Although displaying desirable properties such as rapid and high bactericidal activity, low cost and controlled levels of resistance, nephrotoxicity induced by aminoglycosides remain a serious limiting factor in their daily use. The mechanisms of aminoglycoside-induced nephrotoxicity have been extensively studied for many years (Mingeot-Leclercq and Tulkens, 1999; Quiros et al., 2011; Lopez-Novoa et al., 2011), but remain incompletely deciphered. Unraveling these mechanisms at the cellular level might open new avenues for decreasing their toxicity.

The observation that aminoglycosides induce apoptosis in vivo at therapeutically-relevant doses (El Mouedden et al., 2000a) was an important step in our appreciation of the importance of the early stages in cell dysfunction leading to nephrotoxicity. Apoptosis, detected in proximal tubules of rats treated with low therapeutic doses of gentamicin, can be reproduced in the porcine proximal tubular cell line LLC-PK1 (El Mouedden et al., 2000b), where gentamicin accumulates in lysosomes following adsorptive and/or receptor-mediated endocytosis (Sastrasinh et al., 1982; Moestrup et al., 1995). Within these subcellular organites, vital confocal imaging revealed that gentamicin induces ROS production (Denamur et al., 2011). ROS production appears prior to, and at lower drug concentrations than what is required for lysosomal permeabilization, which is observed only 6 h after incubation of cells with gentamicin (Servais et al., 2006; Servais et al., 2005). ROS antioxidants or scavengers, such as catalase or *N*-acetylcysteine, largely prevent these events (Denamur et al., 2011). Deferoxamine, an iron chelator, which is endocytosed and accumulates in lysosomes, also largely reduces gentamicin-induced ROS production as well as apoptosis (Denamur et al., 2011). After lysosomal membrane permeabilisation, the intrinsic pathway of apoptosis is then activated with disruption of mitochondrial membrane potential, release of cytochrome *c* and activation of caspase-3 (Servais et al., 2005). Bcl-2 and Bax are involved in this process since Bcl-2 overexpression (through transfection) prevents apoptosis-induced by gentamicin (El Mouedden et al., 2000b) and significant increases of the cellular levels of Bax and ubiquinitated Bax (without changes in Bax mRNA) (Servais et al., 2005; Servais et al., 2006) were observed.

http://dx.doi.org/10.1016/j.taap.2016.08.020
0041-008X/

The link between lysosomal membrane permeabilization and activation of the mitochondrial intrinsic apoptotic pathway has been the object of much attention. In the past few years, lysosomes have been identified as important actors of cell death induction (see (Kirkegaard and Jaattela, 2009; Villamil Giraldo et al., 2014) for review), mainly via the release of lysosomal proteases such as cathepsins. Beside a potential role of the release of proteases, gentamicin-induced apoptosis probably involves other ways of interaction between lysosomes and mitochondria. Indeed, electroporation of cells in the presence of very low concentrations of gentamicin (allowing the drug to directly reach the cytoplasm and avoiding the need of lysosomal membrane permeabilization) induces a marked increase of Bax and ubiquinitated Bax as well as apoptosis (Servais et al., 2006). This suggests that gentamicin, released from lysosomes to cytosol after lysosomal membrane permeabilization or moving by retrograde trafficking through the Golgi apparatus and the endoplasmic reticulum (Sandoval and Molitoris, 2004), could play an important role in the apoptotic process. Direct interactions of gentamicin with mitochondria has been hypothesized (Mather and Rottenberg, 2001), but other organelles as proteasome or endoplasmic reticulum could also play a critical role, as suggested in a variety of models ranging from in vitro to in vivo experiments (Servais et al., 2006; Peyrou and Cribb, 2007; Peyrou et al., 2007; Horibe et al., 2004).

A possible inhibition of the ubiquitin-proteasome pathway by gentamicin has been suggested based on our previous results. We indeed observed an increase of the cytosolic protein Bax together with its ubiquitinated form, upon incubation of cells with gentamicin while competitive RT-PCR failed to reveal significant changes in the cell content of Bax mRNA (Servais et al., 2006). Moreover, since H_2O_2 has been linked to 26S proteasome disassembly (Wang et al., 2010), gentamicin-induced ROS production (Denamur et al., 2011) could modulate proteasome activities. Such effect could trigger alterations of endoplasmic reticulum since proteasome is involved in part of the endoplasmic reticulum-associated machinery for protein degradation that removes unfolded and misfolded proteins from endoplasmic reticulum (Oyadomari et al., 2006). In turn, this could induce eIF2α phosphorylation as a cellular stress response against proteasome inhibition (Jiang and Wek, 2005; Baird and Wek, 2012) and accumulation of p53, a transcription factor often involved in apoptosis induced by nephrotoxicants (Molitoris et al., 2009) and normally kept at low concentration by the proteasome (Zhang et al., 2011; Pant and Lozano, 2014). An increase of p53 levels induces expression of its downstream genes involved in diverse cellular stress responses including cell cycle arrest via the cell cycle inhibitor p21 (An et al., 2000), DNA damage response (Meek, 2015) or apoptosis (Dashzeveg and Yoshida, 2015; Meek, 2015). Another critical actor for cell cycle arrest, and apoptosis are the ceramides which may interplay (Sawada et al., 2001; Kim et al., 2002; El Assaad et al., 2003) or not (Yang and Duerksen-Hughes, 2001; Kim et al., 2000) with p53.

Our study was designed to further decipher the cellular and molecular mechanisms involved in gentamicin-induced apoptosis. We first considered a possible role of p53 as well as sphingomyelinase pathway in apoptosis induced by gentamicin. The importance of ROS for changes in p53 was investigated. Second, we studied the inhibition of proteasome activity induced by gentamicin by following the chymotrypsin-, trypsin- and caspase-like activities of proteasome. Then, we investigated the potential effect of gentamicin on endoplasmic reticulum by looking for phosphorylation of eIF2α, caspase-12 activation and up-regulation of the chaperones GRP78 and GRP94. Collectively, all these results have been integrated for giving new insights about the molecular and cellular mechanisms involved in aminoglycoside antibiotics induced apoptosis.

2. Material and methods

2.1. Materials

Dulbecco's Modified Eagle's Medium (DMEM) and trypsin-EDTA were purchased from Life Technologies, Paisley, UK. Gentamicin sulfate (Gentalline®) was from Schering-Plough (Merck, Whitehouse Station, NJ, USA). Proteasome substrates Suc-LLVY-amc, Ac-RLR-amc and Ac-nLPnLD-amc were purchased from Bachem (Bachem AG, Bubendorf, Switzerland). Tunicamycin, cisplatin, epoxomicin, nocodazole, ribonuclease A, propidium iodide, *N*-acetylcystein and glucosamine hydrochloride were from Sigma Aldrich (St-Louis, MO, USA). 4′, 6′-diamidine-2′-phenylindole (DAPI) was from Roche (Basel, Switzerland).

2.2. Cells and treatments

All experiments were performed with LLC-PK1 (Lilly Laboratories Culture-Pig Kidney Type 1) cells obtained from American Tissue Culture Collection (LGC Promochem, Teddington, UK) as ATCC CL-101. Cultures were grown in Dubelcco's Modified Eagle's medium (DMEM) supplemented with 10% fetal calf serum in an atmosphere of 95% air - 5% CO_2. Cells were subcultured twice a week and used when reaching approximately 80% of confluence. All solutions for incubation were adjusted to pH 7.4 prior being added to the culture medium or to lysis buffers.

2.3. Short interference RNA and transfection

p53 protein expression was knocked down using p53 siRNA (Santa Cruz Biotechnology, Inc., Santa Cruz, CA). Transient transfections were performed when the cells had reached 60% confluence in a 6 well-plate using Lipofectamine® RNAiMAX Reagent (Invitrogen; Carlsbad, CA, USA) in accordance with the manufacturer's protocol. Briefly, cells were first washed with phosphate-buffered saline (PBS) and cultured with fresh Opti-MEM Medium (Invitrogen, Carlsbad, CA, USA). A mix of transfection reagent and 60 pmol of p53 siRNA was then added to the wells. Mock groups were treated with the transfection reagent only. Twenty four hours after transfection, cells were treated, or not, with gentamicin 3 mM for 24 h. To assess gene silencing, p53 protein levels were evaluated by Western Blot and cell apoptosis was assessed by DAPI labeling.

2.4. Western blot analysis

p21 and p27, phosphorylated eIF2α, ER chaperones GRP78 and 94, and caspase-12 were analyzed by western blot analysis. After incubation for 24 h with gentamicin, tunicamycin (as positive control of eIF2α phosphorylation and ER stress (Peyrou and Cribb, 2007)), cisplatin (as positive control of caspase 12 activation and p21 overexpression (Liu and Baliga, 2005)) or epoxomicin (as positive control of inhibition of chymotrypsin- and caspase-like activities of proteasome (Giguere and Schnellmann, 2008), supernatant was kept. Cells were washed with PBS and therafter detached by trypsinization, pelleted by centrifugation at 290g for 7 min and washed two times with gentle resuspension and repelleting in ice-cold PBS. Cells were then resuspended in RIPA buffer (Tris-HCl 25 mM, pH 7.6; NaCl 150 mM, NP-40 1%; SDS 0.1%; sodium deoxycholate 1%) supplemented with protease and phosphatase inhibitor cocktail, lysed by sonication, and centrifuged for 15 min at 14,000 g and 4 °C. The protein content of cellular lysates was assessed using the bicinchoninic acid (BCA) method (Pierce, Rockford, IL). Western blots were performed using the NuPAGE electrophoresis system (Invitrogen, Paisley, UK). Appropriate quantities of proteins were mixed to 4× NuPAGE LDS sample buffer and 10× NuPAGE reducing agent, then heated at 70 °C for 10 min. Samples were loaded on acrylamide gels (NuPAGE 1% Bis-Tris Gel, Invitrogen). After migration, proteins were electro-transferred on a PVDF membrane (0.45 μM, Pierce), which was blocked by a 1 h incubation with bovine serum albumin (BSA) 5% in Tris-buffered saline (TBS; 20 mM Tris-HCl, 500 mM NaCl pH 7.5). Membranes were then incubated for 2 h at room temperature with the primary antibodies anti-ubiquitin (sc-47,721, Santa Cruz Biotechnologies, Santa Cruz), anti-p21 (sc-397, Santa Cruz Biotechnologies), anti-GRP78 (76-E6) (sc-13,539, Santa Cruz Biotechnologies),

anti-GRP94 (SPA-850F, Stressgen, Enzo Life Sciences, Farmingdale, NY, USA) and anti-caspase-12 (2202, Cell Signaling Technology) or overnight at 4 °C with anti-eIF2α (2103, Cell Signaling Technology) or anti-phosphorylated eIF2α antibodies (3597, Cell Signaling Technology, Danvers, MA, USA), to detect ubiquitin, p21, GRP78, GRP94, caspase-12, and eiF2α and its phosphorylated form, respectively. Then, membranes were exposed to appropriate horseradish peroxidase-coupled secondary antibodies for 1 h. Blots were revealed by chemiluminescence (SuperSignal West Pico, Pierce). Membranes were then washed with Restore Western Blot Stripping Buffer (Pierce) for 30 min, and anti-actin polyclonal antibodies (sc-1616, Santa Cruz Biotechnologies) were used as loading control.

Given the failure to detect p53 protein by this procedure, the protocol was adapted for p53 western blot as followed. Cells were resuspended in a lysis buffer (Tris-HCl 50 mM, pH 7.6; DTT 2 mM; EDTA 1 mM; EGTA 1 mM; β-glycerophosphate 1 mM; NaF 10 mM; NP-40 0.5%, glycerol 20%; p-toluenesulfonyl fluoride 1 mM; benzamidin 5 mM; sodium orthovanadate 1 mM, leupeptin 5 μg/ml; antipain 5 μg/ml), kept for 20 min on ice and centrifuged for 10 min at 18,000 g and 4 °C. The protein content of cellular lysates was assessed using the Bradford method (Pierce, Rockford, IL). Before migration, samples were boiled (100 °C) for 5 min in Laemmli buffer containing SDS 8%, Tris 125 mM (pH 6.8), sucrose 40% (w/v), bromophenol blue 0.03% (w/v) and DTT 40 mM. Migration of proteins (50 μg) was made on 12% acrylamide gels at 200 V for 1 h. Semi-dry transfer on PVDF membrane (1 h 15 min, 100 mA/gel) was followed by blocking and marking steps as described above. Anti-p53 (DO-1) antibody (sc-126, Santa Cruz Biotechnologies) was used to detect p53. For investigating the potential role of ROS in p53 expression, cells were preincubated for 3 h with medium containing *N*-acetylcysteine (1 mM) which is kept during incubation with gentamicin.

2.5. Proteasome activity assay

Chymotrypsin-, trypsin-, and caspase-like activities of proteasome were evaluated by generation of the fluorescent species amino-methyl-coumarin (amc) from peptides substrates of each proteasome hydrolytic activity (Kisselev and Goldberg, 2005). Chymotrypsin-like activity was assessed with Suc-LLVY-amc, trypsin-like activity with Ac-RLR-AMC and caspase-like activity with Ac-nLPnLD-amc.

Cells were scrapped in extraction buffer containing Tris-HCl 10 mM pH 7.5, 1 mM EDTA, 2 mM ATP, 5 mM DTT, 20% (V/V) glycerol. Samples were sonicated for 10 s and centrifuged for 15 min at 15,000 g and 4 °C. Supernatants were collected and protein contents measured using the Bradford's method. Assays were performed in polypropylene black 96-well plates, to avoid proteasome adsorption. Adequate quantity of proteins (25 μg for chymotrypsin-like, 10 μg for trypsin-like, and 100 μg for caspase-like activity assay) were incubated for 1 h at 37 °C in extraction buffer containing the indicated concentrations of gentamicin or epoxomicin (a proteasome inhibitor used as positive control (Giguere and Schnellmann, 2008)). Fifty microliter of reaction buffer (Tris-HCl 50 mM pH 7.4, EDTA 0.5 mM) containing suitable substrate concentrations (100 μM for Suc-LLVY-amc, 200 μM for Ac-RLR-amc and 100 μM for Ac-nLPnLD-amc) were then added in the wells, and the fluorescence was read immediately and after 4 h incubation at 37 °C with a FluoroCount Microplate Fluorometer (Packard Instruments Company, Downers Grove, IL, USA) with excitation wavelength set at 380 nm and readings made at 460 nm. We checked that neither gentamicin nor epoxomicin interfered with AMC fluorescence.

2.6. Counting of apoptotic cells

Apoptotic nuclear fragmentation, revealed by DNA staining with 4′,6′-diamidine-2′-phenylindole (DAPI) (Servais et al., 2006), was identified by random counting of 500 cells per condition. Clusters of apoptotic bodies were given a single count. Data were expressed as the percentage of apoptotic nuclei relative to total number of nuclei counted.

2.7. Measurement of intracellular ceramide levels

The intracellular levels of ceramides after incubation of LLC-PK1 with gentamicin (1 and 2 mM) for 15 min up to 24 h were measured as described previously (Fillet et al., 2003) using liquid chromatography-electrospray ionization tandem-mass spectrometry (LC-ESI-MS/MS). Ceramides were separated by liquid chromatography on a C18 column and eluted using a solvent gradient made of a mixture of water, acetonitrile and 2-propanol. MS detection was carried out using a Ultima triple quadrupole instrument (Waters, Manchester, UK) configured with a electrospray ionization source used in positive ion mode. Collision-induced fragmentations conducted on ceramides produced a well characteristic product ion at *m/z* 264, making multiple reactions monitoring (MRM) well suited for various ceramides quantitative measurements (Fillet et al., 2002).

For LC-ESI-MS/MS quantitative purpose, standard solutions were prepared by dissolving ceramides (Acros Organics, Gell, Belgium) in a 99.8/0.2 (v/v) mixture of ethanol/formic acid to reach a concentration of 1 μg/ml. For extraction of cellular lipids, cells were rinsed twice with ice-cold PBS, then scraped in PBS and centrifuged at 800*g*. The resulting pellet was homogenized in distilled water by sonication. An aliquot of the cell homogenate was reserved for determination of protein levels. Ten nanogram of C12-ceramide (as an internal standard) was added to samples of cell lysates containing 300 μg of protein. Lipids were extracted using Folch's partition with a mixture of chloroform and methanol (2/1, v/v). Samples were then centrifuged at 1500*g* and washed with chloroform, methanol and water (5/48/47, v/v/v). The organic phase was evaporated to near dryness under a gentle stream of dry nitrogen. The samples were reconstituted by vortexing with 100 μl of a mixture of ethanol/formic acid (99.8/0.2) until they were completely dissolved. To avoid any loss of lipids, the entire procedure was performed in siliconized glassware.

The analysis showed that C16-, C18-, C20-, C22- and C24-ceramides were present in our cell model. The levels of each ceramide species were expressed as their relative abundance compared with ceramide level in untreated cells. All determinations have been done on cells incubated with gentamicin in conditions where apoptosis was described.

2.8. Acidic and neutral sphingomyelinase assays

Apart the production of ceramide by de novo synthesis through the sequential activation of serine-palmitoyl transferase, ceramide synthetase, and dehydro-ceramide desaturase (Hannun and Luberto, 2000; Zeidan and Hannun, 2010), ceramides can also arise from the hydrolysis of sphingomyelin by the activation of the two major known types of sphingomyelinases, the acidic sphingmomyelinase with an optimum pH close to 4.8 (Goni and Alonso, 2002) and the neutral sphingomyelinase which exhibits a pH optimum around 7.5 and is a membrane-bound and Mg^{2+}-dependent (Kitatani et al., 2008) enzyme. Briefly, the activities of neutral- and acidic sphingomyelinases were determined as follows. After culture, cell pellets were suspended in distilled water and sonicated (3 × 15 s). Cell lysates were incubated at 37 °C for the indicated periods with sphingomyelin and [*N*-methyl^{14}C]-sphingomyelin. For the determination of the activity of acidic sphingomyelinase (EC 3.1.4.12), the reaction was performed in acetate buffer 200 mM, pH 5.5 in presence of EDTA (4 mM), taurocholate de sodium (1%), and Triton X-100 (1%). For the measure of the activity of neutral sphingomyelinase, Tris buffer 100 mM, pH 7.5 containing dithiothreitol (10 mM), Triton X-100 (1%), and $MgCl_2$ (10 mM) was used. After incubation, serum bovine albumin and TCA were added. The mixture was placed at 0 °C for 30 min before centrifugation. The radioactivity associated to the supernatant was counted.

2.9. Gentamicin dosage

Gentamicin concentrations were measured by microbiological assay. *Bacillus subtilis* ATCC 6633 was used as the test organism (lowest limit of detection, 1 μg/ml; linearity [$R^2 = 0.934$], concentrations up to 256 μg/ml) and antibiotic medium #11 was adjusted at pH 8 (Carryn et al., 2002).

2.10. Statistical analysis

All statistical analyses were performed with the GraphPad Prism 6.0 software and GraphPad InStat 3.06 (GraphPad software, San Diego, CA, USA). The comparison of 3 or more groups of data was performed using the one- or two-way ANOVA followed by the Tukey's post hoc test to compare values to control, and with Sidak's post hoc test to compare all values.

3. Results

3.1. p53 pathway is involved in gentamicin-induced apoptosis

3.1.1. Gentamicin increased p53 levels. p53 is known to play a critical role in renal cell apoptosis (Jiang et al., 2004) including when induced by known nephrotoxicants such as cisplatin (Sanchez-Perez et al., 2010). To determine if gentamicin-induced apoptosis was also dependent on p53, we first measured the effect of gentamicin on p53 levels (Fig. 1).

After incubation for 8 h and 24 h with 2 and 3 mM of gentamicin, an increase of p53 was observed reaching around 1.7 and 3.7 fold increase respectively, as compared to controls. The increase was similar after 8 and 24 h of incubation. No statistically significant increase was observed when cells were incubated with gentamicin 1 mM. For investigating the potential downstream effect of DNA damage, we also measured the cellular levels of phosphoSer15-p53. No statistically-significant change was observed whatever the concentration of gentamicin and the time of incubation used (data not shown).

3.1.2. Role of p53 in apoptosis induced by gentamicin: effect of p53 inhibitor and of p53 siRNA. To confirm the role of p53 in apoptosis induced by gentamicin, cells were incubated with pifithrin- α, an inhibitor of the transcriptional pathway of p53 (Yano et al., 2007; Zeng et al., 2016) described for protecting against genotoxic agents, including cisplatin (Jiang et al., 2004) or UV-induced damages (Komarov et al., 1999). The percentage of apoptotic cells after incubation with 1–3 mM gentamicin for 24 h was determined by DAPI staining (Fig. 2).

We observed a decrease of apoptosis induced by gentamicin by >50% after 24 h incubation. For longer time of incubation (48 h), the same observation was done with again a partial protective effect afforded by pifithrin-α. After incubation with 3 mM gentamicin for 48 h, gentamicin induced 17.15% apoptosis in absence of pifithrin-α and 9.6% apoptosis in presence of this inhibitor of transcriptional pathway of p53. The cellular gentamicin content after incubation with pifithrin-α was assessed by a disc-plate microbiological technique using *Bacillus subtilis* (ATCC 6633) as previously described (Tulkens and Trouet, 1978), and no statistically significant change in gentamicin accumulation was observed (data not shown).

To confirm the involvement of p53 protein in gentamicin-induced apoptosis, we also performed p53 siRNA-mediated gene silencing experiments. First, we evaluated the effects of the p53-targeting siRNA on the expression of endogenous p53 protein in LLC-PK1 cells. We assessed the expression of p53 by western blotting. p53 siRNA induced a reduction in the expression of endogenous p53 in comparison with the mock (Fig. 3, Top). We then investigated whether p53 protein knockdown decreased the gentamicin-induced apoptosis using DAPI labeling (Fig. 3, Below). p53 siRNA transfection reduced gentamicin-induced nuclear fragmentation, both after 24 and 48 h of incubation. This result is in accordance with those of the experiments using the p53 inhibitor pifithrin-α.

Thus, in this first set of experiments, we demonstrated an increase of p53 levels induced by gentamicin and partial protection against apoptosis induced by gentamicin afforded by the p53 inhibitor, pifithrin-α, and by p53 siRNA suggesting implication of both p53 transcriptional-dependent and -independent pathways in apoptosis-induced by gentamicin.

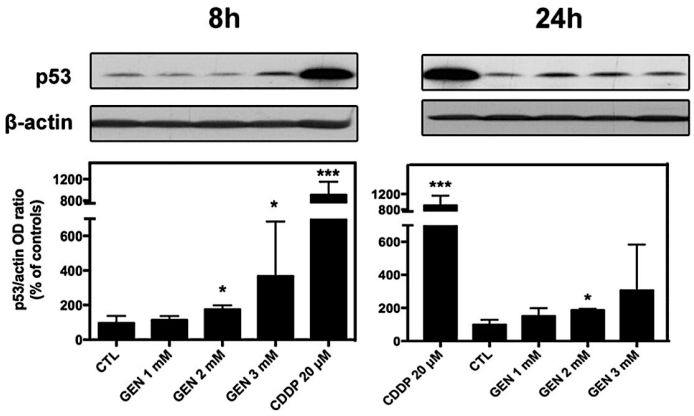

Fig. 1. Effect of gentamicin on p53 protein levels. Cells were incubated for 8 h (left) or 24 h (right) without (controls, CTL) or with gentamicin (GEN 1–3 mM). Densitometric values of p53 protein are normalized to β-actin. The blot presented is representative from 3 independent experiments. Data are given as means ± SD (*$p < 0.05$; ***$p < 0.001$). Cisplatin (CDDP), known to induce apoptosis in LLC-PK1 cells via p53 (Sanchez-Perez et al., 2010), was used as positive control.

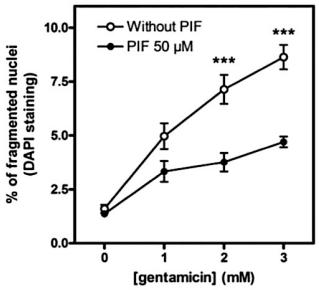

Fig. 2. Prevention by the p53 inhibitor pifithrin-α of gentamicin-induced apoptosis. Cells were pre-incubated or not for 1 h with 50 µM pifithrin-α and then incubated with gentamicin (1–3 mM) for 24 h, in continued presence of pifithrin-α. Data are given as means ± SD ($n = 6$ from 2 separate experiments). Statistical analysis: Two-way analysis of variances, with Bonferroni post-tests to compare points treated with the same concentration of gentamicin together (***$p < 0.001$).

3.1.3. ROS is involved in p53 increase induced by gentamicin. Because we had demonstrated an increase of reactive oxygen species (ROS) after incubation of LLC-PK1 with gentamicin (Denamur et al., 2011) and since ROS production is involved in p53 activation in renal cells (Jiang et al., 2007; Ju et al., 2014), we next investigated the potential role of ROS in the increase of p53 level induced by gentamicin (Fig. 4).

Cells were pre-incubated with *N*-acetylcysteine, an antioxidant known to inhibit ROS-dependent apoptosis (Curtin et al., 2002) including apoptosis induced by gentamicin (Denamur et al., 2011). Pre-incubation of cells with *N*–acetylcysteine induced a marked decrease of the p53 accumulation observed after incubation for 24 h with 2 or 3 mM of gentamicin. *N*-acetylcysteine also decreased p53 levels in control cells or in cells incubated with 1 mM gentamicin but the effect was not statistically significant.

These data suggest that ROS exert an important role in the increase of p53 levels induced by gentamicin.

3.1.4. Increase of p53 induced by gentamicin leads to p21 increase. We examined whether overexpression of p53 induced by gentamicin could allow it to accumulate in the nucleus and to transcriptionally regulate genes to control the cell's fate. For instance, p53 can lead to an increase of cellular levels of cyclin-dependant kinases inhibitors like p21 (Lu and Hunter, 2010), which are substrate for proteasomal degradation. We therefore monitored the potential effect of gentamicin on p21 protein levels (Fig. 5).

We showed a marked and statistically significant increase (up to 180%) in p21 protein levels after treatment with 2 and 3 mM gentamicin (Fig. 5).

To determine the implication of p53 activation in the increase in p21 levels, we measured the p21 cellular levels in cells exposed to gentamicin in the presence of the p53 transcription inhibitor pifithrin-α. Fig. 6 shows that the increase in cellular levels of p21 induced by gentamicin was considerably reduced when pifithrin-α was present, suggesting that p21 accumulation is related to gentamicin-induced p53 activation.

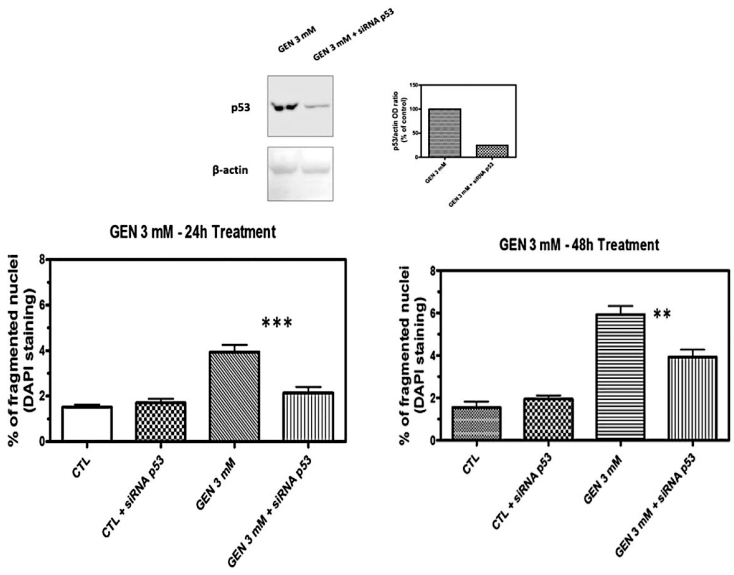

Fig. 3. (Top) Reduction of p53 expression by p53-targeting small interfering (si)RNA (p53 siRNA) in LLC-PK1 incubated with gentamicin 3 mM for 24 h. The p53 protein levels were assessed by western blotting analysis. β-actin levels were also assessed and served as a loading control. A representative blot is shown from three independent experiments with identical results. (Below) Prevention by the p53 siRNA of gentamicin-induced apoptosis. Transfected cells were incubated with gentamicin (3 mM) for 24 h or 48 h. Data are given as means ± SD (n = 6 from 2 separate experiments). Statistical analysis: Two-way analysis of variances, with Bonferroni post-tests to compare points treated with the same concentration of gentamicin together (**$p < 0.01$; ***$p < 0.001$).

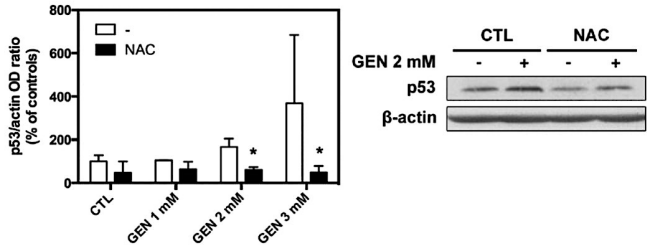

Fig. 4. Effect of N-acetylcysteine on gentamicin induced increase of p53 protein levels. Cells were incubated for 24 h without (controls, CTL) or with gentamicin (GEN 1–3 mM) after preincubation or not with *N*-acetylcysteine (1 mM). Densitometric values are normalized to β-actin (* $p < 0.05$). The blot presented is representative from 3 independent experiments performed after incubation with gentamicin 2 mM.

3.2. Sphingomyelinase pathway is not involved in gentamicin-induced apoptosis

3.2.1. Gentamicin decreased ceramides levels by inhibiting the activity of acidic sphingomyelinase. The partial protection afforded by the p53 inhibitor, pifithrin-α (Fig. 2), as well as by p53 siRNA (Fig. 3) against apoptosis induced by gentamicin suggests that other signaling pathways are probably involved. Ceramide accumulation has been observed in response to various extracellular stimuli including p53 upregulation (Heffernan-Stroud and Obeid, 2011; Kim et al., 2002; El Assaad et al., 2003), and cause apoptosis and/or cell cycle arrest (Dbaibo et al., 1998; Fillet et al., 2002; Fillet et al., 2003). To investigate the potential role of ceramides in apoptosis induced by gentamicin, we determined the effect of gentamicin on the amounts of endogenous ceramides in LLC-PK1. We incubated LLC-PK1 cells with gentamicin at extracellular concentrations of 1 or 2 mM and for periods of time ranging from 15 min to 24 h before measurement of C-14 to C-24 ceramides contents by LC-ESI-MS/MS. No major change was observed when cells were incubated with gentamicin 2 mM for 5 min up to 3 h (Fig. 7). Thereafter, we observed a marked decrease of ceramide levels in cells incubated with gentamicin as compared to control cells (Fig. 7). Similar results were found after incubation with 1 mM of gentamicin (data not shown).

To decipher the mechanism involved in the decrease of ceramide levels in cells incubated with gentamicin, and since previous studies have shown a decrease of lysosomal sphingomyelinase in presence of gentamicin (Laurent et al., 1982), we measured the activities of neutral and acidic sphingomylinases in LLC-PK1 cells incubated with gentamicin. Results of a typical experiment in which LLC-PK1 were cultivated over a period of 24 h in a control medium or in presence of gentamicin 2 mM are shown in Fig. 8.

The activity of acidic sphingomyelinase in gentamicin treated cells dropped to significantly lower values as compared to controls, for pH lower than 6.5. Similar results were obtained with gentamicin 1 mM (data not shown). The measurement of neutral sphingomyelinase showed no detectable changes (data not shown).

Decrease of ceramides contents resulting from inhibition of acidic sphingomyelinase suggests that sphingomyelinase pathway is not involved in apoptosis induced by gentamicin.

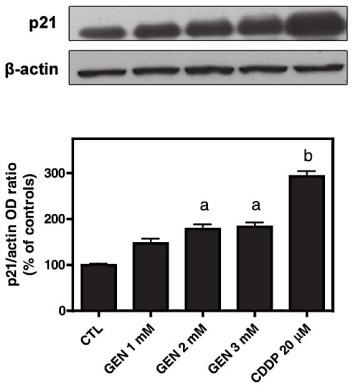

Fig. 5. Effect of gentamicin on p21 protein levels. Cells were incubated for 24 h without (controls, CTL) or with gentamicin (GEN 1–3 mM) or cisplatin (CDDP 20 μM). Densitometric values are normalized to β-actin. The blot presented is representative from 3 independent experiments, data are means ± SD ($n = 3$) (bars with different letters are significantly different from each other; $^*p < 0.05$).

3.3. Involvement of proteasome and endoplasmic reticulum in apoptosis induced by gentamicin

3.3.1. Gentamicin increased the ubiquitin conjugates.. Increase of p53 and p21 levels after gentamicin incubation, two proteins normally kept at low cellular concentration by a rapid degradation by the proteasome and involved in cell apoptosis as well as accumulation of ubiquitinated protein Bax (Servais et al., 2006) pushed us to investigate the global impact of gentamicin on cellular accumulation of ubiquitinated proteins.

We used ubiquitin immunoblotting to assess the effects of gentamicin on accumulation of ubiquitin-conjugates (Fig. 9). LLC-PK1 cells were incubated for 24 h with the antibiotic or with epoxomicin, a highly selective and potent inhibitor of the proteasome (Giguere and Schnellmann, 2008) used as positive control (EPX, 20 μM). A concentration-dependant increase of ubiquitinated proteins in the cells incubated with gentamicin that was statistically significant for an extracellular concentration of 3 mM.

3.3.2. Gentamicin inhibited the trypsine-like activity of proteasome. To further assess the potential effects of gentamicin on proteasome, we assayed the activities of the three types of active sites of proteasome (chymotrypsin-like, trypsin-like and caspase-like) using lysates of LLC-PK1 cells incubated with gentamicin (Fig. 10). These lysates were collected and crude extracts incubated for 1 h at 37 °C with increasing concentrations of gentamicin (0 up to 30 mM) before adding specific

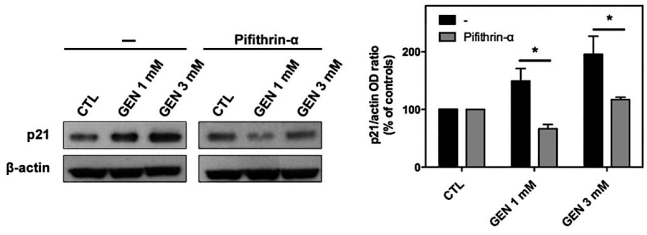

Fig. 6. Effect of pifithrin-α on gentamicin-induced accumulation of cellular p21 proteins. Cells were pre-incubated or not for 1 h with 50 μM pifithrin-α and then incubated with gentamicin (1 and 3 mM) for 24 h, in continued presence of pifithrin-α. Data are given as means ± SD ($n = 3$; $^*p < 0.05$).

fluorogenic substrates of each catalytic activity. The proteasome inhibitor epoxomicin was used as positive control.

While chymotrypsin-like activity was completely inhibited by epoxomicin since the fluorescence level detected with this inhibitor is quite the same as the fluorescence emitted by the substrate alone (SA, Fig. 10a), incubation with gentamicin induced an increase of chymotrypsin-like activity at 5 mM, followed by a slight decrease of activity up to 30 mM.

In contrast, gentamicin induced an important decrease in trypsin-like activity, from the first concentration tested (5 mM) and which becomes complete (same fluorescence level as the substrate alone) from 15 mM. Note that trypsin-like activity was not inhibited by epoxomicin (Fig. 10b), as described previously (Naujokat et al., 2007).

Caspase-like activity, after undergoing an increase of activity at 5 and 10 mM, was inhibited by gentamicin at higher concentrations (Fig. 10c). As for chymotrypsin-like activity, epoxomicin induced an important inhibition of this proteasomal activity.

3.3.3. Gentamicin increased the phospho-eIF2α protein levels. A well-known consequence of proteasome inhibition is the activation of GCN2 kinase and the resulting phosphorylation of the translation initiation factor eIF2α, which leads to apoptosis (Jiang and Wek, 2005). We measured the cellular levels of eIF2α and of its phosphorylated form

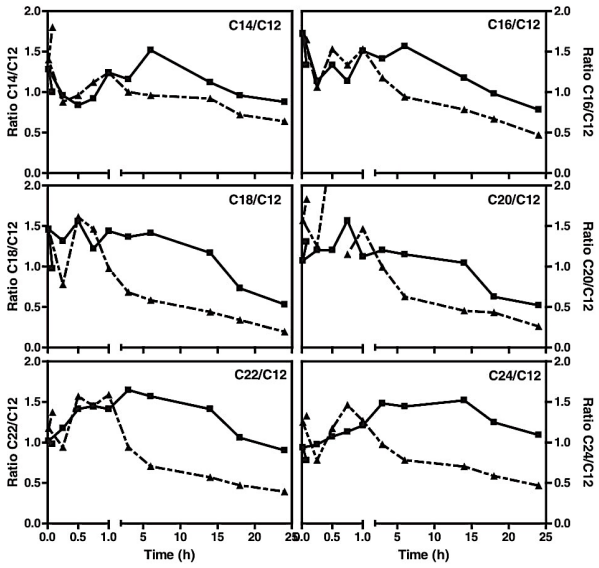

Fig. 7. Ceramide levels in LLC-PK1 incubated with gentamicin. Cells were treated with 2 mM gentamicin for various periods of time from 15 min to 24 h before assessment of C14–24-ceramide levels by LC-ESI-MS/MS. The results are expressed in function of an internal standard (C-12 ceramide). Results obtained for controls and cells incubated with 2 mM of gentamicin are represented as continuous (squares) and dotted lines (triangles), respectively. $n = 3$; 2 independent experiments.

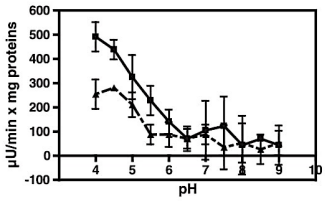

Fig. 8. Effect of gentamicin on the activity of acidic sphingomyelinase at pH ranging from 4 to 9. The cells were incubated for 24 h in absence (full lines; squares) and presence of 2 mM gentamicin (dotted lines; triangles) $n = 3$.

to test for this hypothesis in our model and the results are illustrated in Fig. 11.

Despite the absence of statistical significance, these experiments showed an increase in the cellular levels of eIF2α to up to 200% after incubation with gentamicin 3 mM (Fig. 11a). Regarding the cellular levels of phosphorylated eIF2α, these increased in a dose-dependent fashion with gentamicin reaching 315% for cells incubated with 3 mM of gentamicin and all differences vs control were statistically significant (Fig. 11b).

3.3.4. Gentamicin induced activation of caspase-12 without change in ER chaperones GRP78 and GRP94. In addition to the link between inhibition of the proteasome and phosphorylation of eIF2, the latter is also connected to ER stress. The hypothesis of an ER implication in gentamicin-induced apoptosis would be consistent with the binding of ER chaperones proteins by gentamicin (Horibe et al., 2004) and the observation of markers of ER stress in rats treated for 7 days with 100 mg gentamicin (Peyrou et al., 2007). To investigate this hypothesis, we evaluated caspase-12 activation by immunoblotting (Fig. 12).

As shown in Fig. 12, treatment of cells with gentamicin induced an activation of caspase-12 by cleavage of the pro-form (detected at 55 kDa) into cleaved active caspase-12 (42 kDa), the cellular levels of which increased after gentamicin treatment. The small subunit is detected at 20 kDa. Bands detected at 85 and 110 kDa could correspond to dimers of (pro) caspase-12, which also correspond to activation of caspase-12 (Yoneda et al., 2001). Gentamicin induced a significant increase of caspase-12 (42 kDa) fragment. There was no statistically significant difference in the effect induced by 1 mM of gentamicin as compared to that observed for cells incubated with 3 mM of gentamicin. An increase caspase-12 (20 kDa) was also observed.

As cleavage of caspases is a common indicator of their activation, and since caspase-12 can be specifically activated by apoptotic signals with an ER stress component (Nakagawa et al., 2000), we wanted to investigate if gentamicin could induce ER stress in LLC-PK1 cells. Specifically, we determined the potential role of ER chaperones by incubating cells with or without gentamicin (1–3 mM) for 24 h and measuring the expression levels of two ER chaperones, GRP78 and GRP94 (Fig. 13, a–b). Tunicamycin (5 μl/ml), a specific inhibitor of *N*-linked glycosylation which prevents post-translational maturation of proteins and is known as ER stress inducer in LLC-PK1 cells (Peyrou and Cribb, 2007) was used as positive control for ER stress markers induction.

While tunicamycin induced a marked increase in GRP94 and GRP78 cellular levels, treatment with gentamicin did not induce any change in the expression of these chaperones in our conditions.

4. Discussion

After endocytosis by proximal tubular cells, gentamicin mainly accumulates in lysosomes inducing lysosomal membrane permeabilisation (Denamur et al., 2011). At therapeutically-relevant doses, gentamicin induces mitochondrial pathway of apoptosis (Servais et al., 2006; Servais et al., 2005). The present work moves us one step ahead in the understanding of the cellular mechanisms underlying the apoptosis induced in cells by gentamicin by focusing on p53 and sphingomyelinase pathways as well as on the effect of gentamicin on proteasome and endoplasmic reticulum.

On LLC-PK1 proximal tubular cells, we demonstrate that p53 is a key cornerstone in apoptosis induced by gentamicin as suggested by the increase of its level upon gentamicin treatment and by the partial protective effect afforded by pifithrin-α or by transfection with p53 siRNA. Upon stress signals, p53 undergoes a series of post translational modifications as phosphorylation at Ser15. Even any effect was observed towards this specific phosphorylation, other post translational modifications could be involved in p53 activation induced by gentamicin. First, Ser-46 phosphorylation is required for p53-dependent transcriptional activation of the apoptotic gene p53AIP1. Second, in addition to phosphorylation, mediating p53 stabilization, the acetylation of p53 has also been shown to be a key signal, promoting its activation upon DNA damage (Kruse and Gu, 2009; Tang et al., 2008).

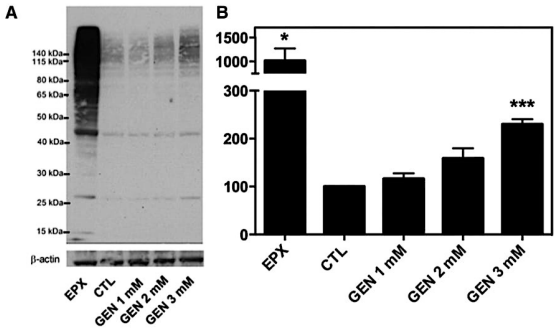

Fig. 9. Effect of gentamicin on ubiquitin conjugates. Ubiquitin immunoblot of lysates of LLC-PK1 cells incubated for 24 h with or without (control, CTL) gentamicin (GEN 1–3 mM) or epoxomicin (EPX, 20 μM). Densitometric values detected for ubiquitin was normalized to β-actin and results are expressed in % of ratio obtained for control cells. Data are means ± SD ($n = 3$; $^{*}p < 0.05$, $^{***}p < 0.001$).

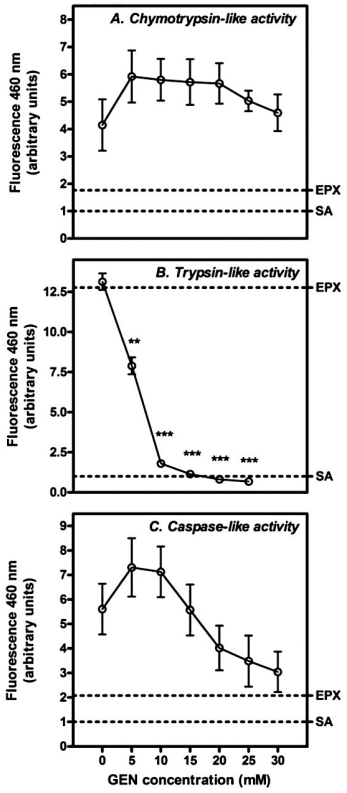

Fig. 10. Effect of gentamicin on proteasome catalytic activities, determined by measuring fluorescence produced by fluorogenic specific substrates of the three proteasomal activities. Results are expressed in arbitrary units, fluorescence of the substrate alone being considered as having a value of 1. Cellular lysates were incubated at 37 °C for 1 h with (or without) gentamicin (GEN) at indicated concentrations. Epoxomicin (EPX) 20 μM was used as positive control. Chymotrypsin-like activity (A), trypsin-like activity (B) and peptidyl-glutamyl peptide hydrolyzing or caspase-like activity (C) were determined with Suc-LLVY-amc, Ac-RLR-amc and Ac-nLPnLD-amc respectively. Fluorescence was read at the end of 4 h incubation at 37 °C after addition of the substrate. On each graph, fluorescence level of the substrate alone (SA, substrate not incubated with cell lysates) and of lysates incubated with epoxomicin (EPX) are represented by a dotted-line. Data are means ± SD ($n = 6$ from 3 separate experiments; where not visible, error bars are included in the symbol). Statistical analysis was performed using one-way ANOVA with Dunnett's multiple comparison post-test to compare each point to control value (without gentamicin) (**$p < 0.01$, ***$p < 0.001$, where not indicated, differences are not significant).

Especially, acetylation at lysine 164 could play a critical role for blocking repression of p53, mediated by Mdm2- and Mdmx, by preventing their recruitment to target promoters (Kruse and Gu, 2009; Tang et al., 2008).

The partial protective effect afforded by pifithrin-α and by siRNA p53 suggest a potential activation of both p53 transcriptional-dependent- and independent pathways, as also demonstrated for toxicities induced by cisplatin (Rebillard et al., 2008) or manganese (Wan et al., 2014) or in radio-resistant head and neck squamous carcinoma cells (Bionda et al., 2007). The potential role of p53 transcriptional pathway in gentamicin-induced apoptosis is in agreement with what was observed by microarray experiments on rats treated with gentamicin (Ozaki et al., 2010). Activation of the transcription factor NFκB, for which p65 subunit could activate the p53 promoter (Wu and Lozano, 1994), is consistent with the increase of NFκB activation demonstrated after incubation of renal tubular cells with gentamicin (Chen et al., 2011; Juan et al., 2007). JNK pathway activation (Yang et al., 2004) could be also involved even though this pathway is dependent upon the cell strains. Indeed, no modification of JNK or pJNK expression levels was observed in proximal tubular cells after 24 h of incubation with gentamicin 3 mM despite an increase of p53 expression (Chen et al., 2011), although JNK implication has been demonstrated after gentamicin treatment of mesangial cells (Martinez-Salgado et al., 2005) and increase of Jun. transcription was evidenced by microarray studies (Ozaki et al., 2010). Even most p53 functions are mediated by transcriptional activation of its target genes in response to various stress signals, cytoplasmic p53 was also shown to directly bind to proteins like Bax to trigger mitochondrial outer membrane permeabilization (MOMP) and apoptosis (Green and Kroemer, 2009; Nikoletopoulou et al., 2013). This could be critical for apoptosis induced by gentamicin since Bcl-2 and Bax are involved in this process. Indeed, Bcl-2 overexpression (through transfection) prevents apoptosis-induced by gentamicin (El Mouedden et al., 2000b) and significant increases of the cellular levels of Bax and ubiquinitated Bax (without changes in Bax mRNA) (Servais et al., 2005; Servais et al., 2006) were observed. In addition, sphingomyelinase pathway could also be important. Sphingomyelinases are responsible for the conversion of sphingomyelin to ceramides which have been proposed to play a key role in apoptosis and in cellular responses to stresses (Mullen and Obeid, 2012) including activation of proapoptotic receptors (CD95/Fas and TNFR). However, we observed a marked decrease of ceramides which we related to the inhibition of acidic sphingomyelinase activity, in agreement with previous studies (Laurent et al., 1982). Sphingomyelinase pathway would be therefore not be involved in apoptosis induced by gentamicin and could even afford partial protection against gentamicin-induced apoptosis.

One potential mechanism explaining the increase of p53 levels induced by gentamicin is ROS production. By measuring fluorescence of 2′,7′-dichlorofluoresceine production (DCF) resulting from H_2DCF conversion and by vital confocal imaging, we showed that gentamicin-induced ROS production occurs in lysosomes. Moreover, gentamicin-induced ROS production as well as apoptosis was largely prevented by deferoxamine, an iron chelator, which is endocytosed and accumulates in lysosomes. We also reported that gentamicin induced ROS production prior to, and at lower drug concentrations than required for apoptosis (Denamur et al., 2011). The effect afforded by *N*-acetylcysteine on p53 levels is consistent with this hypothesis. The role of lysosome for ROS production is is in accordance with numerous publications revealing that autophagosomes and/or lysosomes are the major sites for basal ROS generation in addition to mitochondria (Kubota et al., 2010; Hu et al., 2016; Walker and Shah, 1987). Moreover, an interconnected pathway could be involved since the release of mitochondrial ROS leads to subsequent lysosomal membrane permeabilization.

This role of ROS could be critical since, as suggested in literature, ROS could also interact with the functions of the proteasome by inhibiting its ability to breakdown proteins (Meek, 2015). This could explain (i) the increased cell content in ubiquitinated Bax in cells exposed to gentamicin (Servais et al., 2006; Servais et al., 2005), (ii) the increase in total ubiquitinated proteins shown here after cell incubation with gentamicin and (iii) the inhibition of trypsin- and caspase-like activities by gentamicin in cellular lysates (this study). While the role of these two activities is limited in yeast protein, where chymotrypsin-like is considered as rate-limiting in protein breakdown (Heinemeyer et al., 1997), all three types of active sites contribute to protein breakdown in

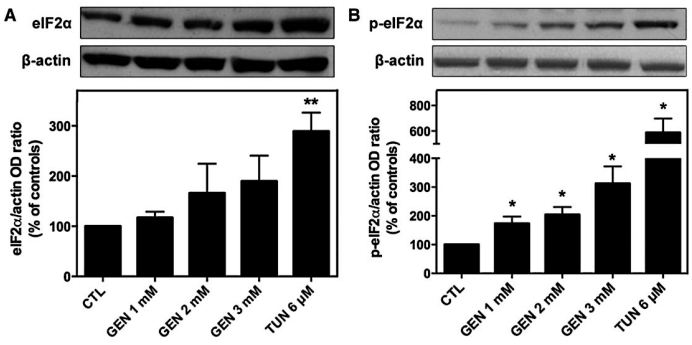

Fig. 11. Effect of gentamicin on eIF2α and p-eIF2α protein levels. Cells were incubated for 24 h without (controls, CTL) or with gentamicin (GEN 1–3 mM) or tunicamycin (TUN 6 µM). eIF2α (panel A) and its phosphorylated form (panel B) bands were detected at 38 kDa; densitometric values are normalized to β-actin. The blot presented is representative from 3 independent experiments, data are means ± SD ($n = 3$; $^{*}p < 0.05$, $^{**}p < 0.01$).

mammalian cells, even though the respective importance of each catalytic site varies widely with the substrate. So, simultaneous inhibition of trypsin- and caspase-like activities reduces the degradation of model proteins by pure 26S proteasome between 30 and 56% depending on the substrate used (Kisselev et al., 2006). Although the effect of gentamicin on proteasome could result from direct interaction of the antibiotic with the proteasome, such as observed in vitro (Horibe et al., 2004), it is likely that ROS production induced by gentamicin accumulated in lysosomes could also alter the proteasomal activity since ROS are able to disassembly 26S proteasome (Wang et al., 2010). ROS production in itself and the redox oxidized proteins signaling pathways could activate kinase cascades and gene transcription aimed at rescuing oxidized proteins, which might disrupt important cellular processes including proteasome-mediated protein degradation (Demasi et al., 2015; Hohn et al., 2014; Lee et al., 2001). Induction of ROS by gentamicin could therefore be responsible for further lysosomal membrane permeabilization, and decreased catalytic activity of the proteasome. The question of the dose of gentamicin needed for inhibiting proteasome activities has also to be questioned but gentamicin could bind to intracellular sites (membranes or even proteins, making interpretations of the concentrations data quite difficult to analyze.

The increase in p53 cellular levels we observed can fully explain the increase of p21, another target of degradation by the proteasome. p21 is known for its role in cell cycle inhibition and apoptosis modulation. We showed here an increased expression of p21 protein levels that most probably results from p53 transcription factor activation since it is completely inhibited by co-treatment with pifithrin-α. The role of p21 in apoptosis is dependent upon its localization and p21 is supposed to be protective since bortezomib-induced apoptosis is markedly enhanced in the p21 knock-out cells (Yu et al., 2003). Besides on their effect in apoptosis, the expression levels of the p21 family CDK inhibitors play an important role in the regulation of cyclin-dependant kinases activity, which are responsible for cell cycle progression. However, since human adult renal proximal tubular cells present a low rate of proliferation (Nadasdy et al., 1994), the roles of p21 as cyclin-dependent

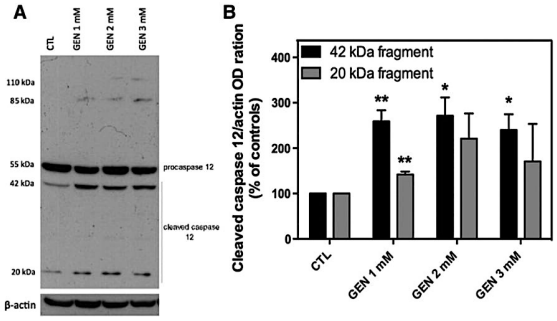

Fig. 12. Effect of gentamicin on caspase 12 activation. Cells were incubated for 24 h without (controls, CTL) or with gentamicin (GEN 1–3 mM). Pro-caspase12 band is detected at 55 kDa, and cleaved caspase-12 at 42 kDa (large subunit) and 20 kDa (small subunit). Bands appearing at 110 and 85 kDa could correspond to dimers of (pro) caspase-12. Densitometric values are normalized to β-actin. The blot presented is representative from 3 independent experiments, data are means ± SD ($n = 3$), statistical analysis compares values to correspondent controls ($^{*}p < 0.05$, $^{**}p < 0.01$).

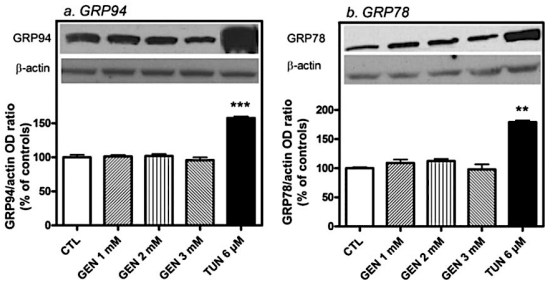

Fig. 13. Effect of gentamicin on cellular levels of GRP94 (a), GRP78 (b). Cells were incubated for 24 h with or without (control, CTL) gentamicin (GEN) or tunicamycin (TUN) at indicated concentrations. Densitometric values are normalized with β-actin, results are presented as percentage of OD ratio obtained for control cells. Values are means ± SD ($n = 3$, from 3 separate experiments; $^{**}p < 0.01$, $^{***}p < 0.01$). GRP94 and GRP78 were detected at 94 and 78 kDa respectively.

kinases inhibitor is probably not crucial in the process of toxicity induced by gentamicin in patients.

In addition to increase in p53 cellular levels induced by gentamicin, we also evidence here an increase in eIF2α phosphorylation. This could indirectly result from proteasome inhibition through phosphorylation by eIF2α kinases such as GCN2 (Jiang and Wek, 2005; Yu et al., 2003; Zhang et al., 2011) or following endoplasmic reticulum stress induction (Teske et al., 2011; Chauhan et al., 2008). Such signs of endoplasmic reticulum stress induction after treatment of rats with gentamicin have been previously described (Peyrou et al., 2007). In the present work, however, we show that activation of caspase-12 occurs independently of chaperones upregulation as already been described for cisplatin, without real explanation of this phenomenon (Peyrou and Cribb, 2007). Studies showing chaperones induction and caspase-12 activation upon gentamicin treatment of animals have been conducted with very high doses of the drug (160 mg/kg), while apoptosis is observed in vivo at much lower and more therapeutically significant dosages (typically 10 mg/kg; (Mingeot-Leclercq and Tulkens, 1999; El Mouedden et al., 2000a).

A summary of the most likely current view of cellular mechanisms involved in gentamicin toxicity, as derived from the results of this study and our previous observations is illustrated in Fig. 14. The new data are that p53 is a key element in the signaling pathway leading to apoptosis following its increased expression mediated by ROS. Since

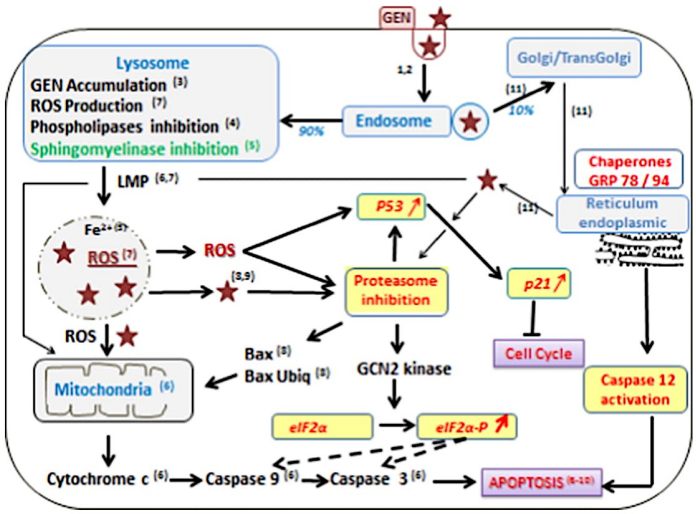

Fig. 14. Proposed signaling pathway triggered by gentamicin. Observations from current study which result to- or protect against- apoptosis (in red and green, respectively). The upper number referred to results from previous studies from our group: [1]Sastrasinh et al. (1982), [2]Moestrup et al. (1995), [3]Tulkens and Trouet (1978), [4]Mingeot-Leclercq et al. (1988), [5]Laurent et al. (1982), [6]Servais et al. (2005), [7]Denamur et al. (2011), [8]Servais et al. (2006), [9]Denamur et al. (2008), [10]El Mouedden et al. (2000a; 2000b), [11]Sandoval and Molitoris (2004). (For interpretation of the references to color in this figure legend, the reader is referred to the web version of this article.)

the protective effect against apoptosis exerted by the p53 transcription inhibitor pifithrin-α and by p53 siRNA is only partial, the process could implicate p53 transcription-dependent and –independent pathways. We also demonstrated an increase in p21 protein levels directly related with p53 increase. A complex interplay between subcellular organites is probably involved since we showed an inhibition of trypsin- and caspase-like activities of proteasome in addition with an effect of gentamicin on reticulum endoplasmic stress as demonstrated by the increase of phosphorylation of eIF2α, and caspase 12-cleavage without chaperones accumulation. The role played by p53 and endoplasmic reticulum in pathways leading to apoptosis induced gentamicin might be extended to other nephrotoxicants such as cisplatin (dos Santos et al., 2012) and cyclosporine A (Xiao et al., 2013).

In a nutshell, incubation of renal cells with gentamicin induced (i) activation of p53 pathway (as demonstrated by measuring the expression of p53 and the effect induced by an inhibitor of transcriptional effect of p53 [pifithrin-α] or p53 siRNA approach), (ii) inhibition of proteasomal activity and (iii) response of endoplasmic reticulum, which in turn resulted in apoptosis. How these pathways are interconnected is not entirely solved yet but autophagy could be a key process. Indeed, data from literature suggested that (i) perturbation of either endoplasmic reticulum homeostasis or endoplasmic reticulum functions increases autophagy and apoptotic cell death (Nikoletopoulou et al., 2013), (ii) endoplasmic reticulum-induced autophagy has an important role in disposing of unwanted polyubiquinitated protein aggregates, thus protecting against cell death and (iii) there is a link between p53 and autophagy, by inhibition of mTor via activation of AMP kinase (Feng et al., 2005).

This work could help in deciphering the cellular and molecular mechanisms involved in aminoglycoside-induced nephrotoxicity and designing new approaches to improve the treatment of critically-ill patients. The results could also help in deciphering the most interesting options to consider in the research of sensitive and reliable biomarkers to detect early toxicity induced by toxicants such as aminoglycosides.

Transparency document

The Transparency document associated to this article can be found, in the online version.

Acknowledgements

We thank M. C. Cambier for cell culture expertise. SD was recipient of a *bourse de doctorat* of the *Université catholique de Louvain*. This work was supported by the Belgian *Fonds de la Recherche Scientifique Médicale* (FRSM 3.4.588.10F) and the *Université catholique de Louvain*.

References

An, W.G., Hwang, S.G., Trepel, J.B., Blagosklonny, M.V., 2000. Protease inhibitor-induced apoptosis: accumulation of wt p53, p21WAF1/CIP1, and induction of apoptosis are independent markers of proteasome inhibition. Leukemia 14, 1276–1283.

Baird, T.D., Wek, R.C., 2012. Eukaryotic initiation factor 2 phosphorylation and translational control in metabolism. Adv. Nutr. 3, 307–321.

Bionda, C., Hadchity, E., Alphonse, G., Chapet, O., Rousson, R., Rodriguez-Lafrasse, C., Ardail, D., 2007. Radioresistance of human carcinoma cells is correlated to a defect in raft membrane clustering. Free Radic. Biol. Med. 43, 681–694.

Carryn, S., Van Bambeke, F., Mingeot-Leclercq, M.P., Tulkens, P.M., 2002. Comparative intracellular (THP-1 macrophage) and extracellular activities of beta-lactams, azithromycin, gentamicin, and fluoroquinolones against *Listeria monocytogenes* at clinically relevant concentrations. Antimicrob. Agents Chemother. 46, 2095–2103.

Chauhan, D., Singh, A., Brahmandam, M., Podar, K., Hideshima, T., Richardson, P., Munshi, N., Palladino, M.A., Anderson, K.C., 2008. Combination of proteasome inhibitors bortezomib and NPI-0052 trigger in vivo synergistic cytotoxicity in multiple myeloma. Blood 111, 1654–1664.

Chen, Y.C., Chen, C.H., Hsu, Y.H., Chen, T.H., Sue, Y.M., Cheng, C.Y., Chen, T.W., 2011. Leptin reduces gentamicin-induced apoptosis in rat renal tubular cells via the PI3K-Akt signaling pathway. Eur. J. Pharmacol. 658, 213–218.

Curtin, J.F., Donovan, M., Cotter, T.G., 2002. Regulation and measurement of oxidative stress in apoptosis. J. Immunol. Methods 265, 49–72.

Dashzeveg, N., Yoshida, K., 2015. Cell death decision by p53 via control of the mitochondrial membrane. Cancer Lett. 367, 108–112.

Dbaibo, G.S., Pushkareva, M.Y., Rachid, R.A., Alter, N., Smyth, M.J., Obeid, L.M., Hannun, Y.A., 1998. p53-dependent ceramide response to genotoxic stress. J. Clin. Invest. 102, 329–339.

Demasi, M., Simoes, V., Bonatto, D., 2015. Cross-talk between redox regulation and the ubiquitin-proteasome system in mammalian cell differentiation. Biochim. Biophys. Acta 1850, 1594–1606.

Denamur, S., Tyteca, D., Marchand-Brynaert, J., Van Bambeke, F., Tulkens, P.M., Courtoy, P.J., Mingeot-Leclercq, M.P., 2011. Role of oxidative stress in lysosomal membrane permeabilization and apoptosis induced by gentamicin, an aminoglycoside antibiotic. Free Radic. Biol. Med. 51, 1656–1665.

Denamur, S., Van Bambeke, F., Mingeot-Leclercq, M.P., Tulkens, P.M., 2008. Apoptosis induced by aminoglycosides in LLC-PK1 cells: comparative study of neomycin, gentamicin, amikacin, and isepamicin using electroporation. Antimicrob. Agents Chemother. 52, 2236–2238.

dos Santos, N.A., Carvalho Rodrigues, M.A., Martins, N.M., dos Santos, A.C., 2012. Cisplatin-induced nephrotoxicity and targets of nephroprotection: an update. Arch. Toxicol. 86, 1233–1250.

El Assaad, W., Kozhaya, L., Araysi, S., Panjarian, S., Bitar, F.F., Baz, E., El Sabban, M.E., Dbaibo, G.S., 2003. Ceramide and glutathione define two independently regulated pathways of cell death initiated by p53 in Molt-4 leukaemia cells. Biochem. J. 376, 725–732.

El Mouedden, M., Laurent, G., Mingeot-Leclercq, M.P., Tulkens, P.M., 2000b. Gentamicin-induced apoptosis in renal cell lines and embryonic rat fibroblasts. Toxicol. Sci. 56, 229–239.

El Mouedden, M., Laurent, G., Mingeot-Leclercq, M.P., Taper, H.S., Cumps, J., Tulkens, P.M., 2000a. Apoptosis in renal proximal tubules of rats treated with low doses of aminoglycosides. Antimicrob. Agents Chemother. 44, 665–675.

Feng, Z., Zhang, H., Levine, A.J., Jin, S., 2005. The coordinate regulation of the p53 and mTOR pathways in cells. Proc. Natl. Acad. Sci. U. S. A. 102, 8204–8209.

Fillet, M., Bentires-Alj, M., Deregowski, V., Greimers, R., Gielen, J., Piette, J., Bours, V., Merville, M.P., 2003. Mechanisms involved in exogenous C2- and C6-ceramide-induced cancer cell toxicity. Biochem. Pharmacol. 65, 1633–1642.

Fillet, M., Van Heugen, J.C., Servais, A.C., De Graeve, J., Crommen, J., 2002. Separation, identification and quantitation of ceramides in human cancer cells by liquid chromatography-electrospray ionization tandem mass spectrometry. J. Chromatogr. A 949, 225–233.

Giguere, C.J., Schnellmann, R.G., 2008. Limitations of SLLVY-AMC in calpain and proteasome measurements. Biochem. Biophys. Res. Commun. 371, 578–581.

Goni, F.M., Alonso, A., 2002. Sphingomyelinases: enzymology and membrane activity. FEBS Lett. 531, 38–46.

Green, D.R., Kroemer, G., 2009. Cytoplasmic functions of the tumour suppressor p53. Nature 458, 1127–1130.

Hannun, Y.A., Luberto, C., 2000. Ceramide in the eukaryotic stress response. Trends Cell Biol. 10, 73–80.

Heffernan-Stroud, L.A., Obeid, L.M., 2011. p53 and regulation of bioactive sphingolipids. Adv. Enzym. Regul. 51, 219–228.

Heinemeyer, W., Fischer, M., Krimmer, T., Stachon, U., Wolf, D.H., 1997. The active sites of the eukaryotic 20 S proteasome and their involvement in subunit precursor processing. J. Biol. Chem. 272, 25200–25209.

Hohn, A., Jung, T., Grune, T., 2014. Pathophysiological importance of aggregated damaged proteins. Free Radic. Biol. Med. 71, 70–89.

Horibe, T., Matsui, H., Tanaka, M., Nagai, H., Yamaguchi, Y., Kato, K., Kikuchi, M., 2004. Gentamicin binds to the lectin site of calreticulin and inhibits its chaperone activity. Biochem. Biophys. Res. Commun. 323, 281–287.

Hu, J., Kholmukhamedov, A., Lindsey, C.C., Beeson, C.C., Jaeschke, H., Lemasters, J.J., 2016. Translocation of iron from lysosomes to mitochondria during acetaminophen-induced hepatocellular injury: Protection by starch-desferal and minocycline. Free Radic. Biol. Med. 97, 418–426 http://dx.10.1016/j.freeradbiomed.2016.06.024. Epub 2016 Jun 23.

Jiang, H.Y., Wek, R.C., 2005. Phosphorylation of the alpha-subunit of the eukaryotic initiation factor-2 (eIF2alpha) reduces protein synthesis and enhances apoptosis in response to proteasome inhibition. J. Biol. Chem. 280, 14189–14202.

Jiang, M., Wei, Q., Pabla, N., Dong, G., Wang, C.Y., Yang, T., Smith, S.B., Dong, Z., 2007. Effects of hydroxyl radical scavenging on cisplatin-induced p53 activation, tubular cell apoptosis and nephrotoxicity. Biochem. Pharmacol. 73, 1499–1510.

Jiang, M., Yi, X., Hsu, S., Wang, C.Y., Dong, Z., 2004. Role of p53 in cisplatin-induced tubular cell apoptosis: dependence on p53 transcriptional activity. Am. J. Physiol. Ren. Physiol. 287, F1140–F1147.

Ju, S.M., Pae, H.O., Kim, W.S., Kang, D.G., Lee, H.S., Jeon, B.H., 2014. Role of reactive oxygen species in p53 activation during cisplatin-induced apoptosis of rat mesangial cells. Eur. Rev. Med. Pharmacol. Sci. 18, 1135–1141.

Juan, S.H., Chen, C.H., Hsu, Y.H., Hou, C.C., Chen, T.H., Lin, H., Chu, Y.L., Sue, Y.M., 2007. Tetramethylpyrazine protects rat renal tubular cell apoptosis induced by gentamicin. Nephrol. Dial. Transplant. 22, 732–739.

Kim, S.S., Chae, H.S., Bach, J.H., Lee, M.W., Kim, K.Y., Lee, W.B., Jung, Y.M., Bonventre, J.V., Suh, Y.H., 2002. P53 mediates ceramide-induced apoptosis in SKN-SH cells. Oncogene 21, 2020–2028.

Kim, W.H., Kang, K.H., Kim, M.Y., Choi, K.H., 2000. Induction of p53-independent p21 during ceramide-induced G1 arrest in human hepatocarcinoma cells. Biochem. Cell Biol. 78, 127–135.

Kirkegaard, T., Jaattela, M., 2009. Lysosomal involvement in cell death and cancer. Biochim. Biophys. Acta 1793, 746–754.

Kisselev, A.F., Goldberg, A.L., 2005. Monitoring activity and inhibition of 26S proteasomes with fluorogenic peptide substrates. Methods Enzymol. 398, 364–378.

Kisselev, A.F., Callard, A., Goldberg, A.L., 2006. Importance of the different proteolytic sites of the proteasome and the efficacy of inhibitors varies with the protein substrate. J. Biol. Chem. 281, 8582–8590.

Kitatani, K., Idkowiak-Baldys, J., Hannun, Y.A., 2008. The sphingolipid salvage pathway in ceramide metabolism and signaling. Cell. Signal. 20, 1010–1018.
Komarov, P.G., Komarova, E.A., Kondratov, R.V., Christov-Tselkov, K., Coon, J.S., Chernov, M.V., Gudkov, A.V., 1999. A chemical inhibitor of p53 that protects mice from the side effects of cancer therapy. Science 285, 1733–1737.
Kruse, J.P., Gu, W., 2009. Modes of p53 regulation. Cell 137, 609–622.
Kubota, C., Torii, S., Hou, N., Saito, N., Yoshimoto, Y., Imai, H., Takeuchi, T., 2010. Constitutive reactive oxygen species generation from autophagosome/lysosome in neuronal oxidative toxicity. J. Biol. Chem. 285 (1), 667–674 http://dx.10.1074/jbc.M109.053058, Epub 2009 Oct 22, PMID: 19850931.
Laurent, G., Carlier, M.B., Rollman, B., Van Hoof, F., Tulkens, P., 1982. Mechanism of aminoglycoside-induced lysosomal phospholipidosis: in vitro and in vivo studies with gentamicin and amikacin. Biochem. Pharmacol. 31, 3861–3870.
Lee, M.H., Hyun, D.H., Jenner, P., Halliwell, B., 2001. Effect of proteasome inhibition on cellular oxidative damage, antioxidant defences and nitric oxide production. J. Neurochem. 78, 32–41.
Liu, H., Baliga, R., 2005. Endoplasmic reticulum stress-associated caspase 12 mediates cisplatin-induced LLC-PK1 cell apoptosis. J. Am. Soc. Nephrol. 16, 1985–1992.
Lopez-Novoa, J.M., Quiros, Y., Vicente, L., Morales, A.I., Lopez-Hernandez, F.J., 2011. New insights into the mechanism of aminoglycoside nephrotoxicity: an integrative point of view. Kidney Int. 79, 33–45.
Lu, Z., Hunter, T., 2010. Ubiquitylation and proteasomal degradation of the p21(Cip1), p27(Kip1) and p57(Kip2) CDK inhibitors. Cell Cycle 9, 2342–2352.
Martinez-Salgado, C., Rodriguez-Barbero, A., Eleno, N., Lopez-Novoa, J.M., 2005. Gentamicin induces Jun-AP1 expression and JNK activation in renal glomeruli and cultured mesangial cells. Life Sci. 77, 2285–2298.
Mather, M., Rottenberg, H., 2001. Polycations induce the release of soluble intermembrane mitochondrial proteins. Biochim. Biophys. Acta 1503, 357–368.
Meek, D.W., 2015. Regulation of the p53 response and its relationship to cancer. Biochem. J. 469, 325–346.
Mingeot-Leclercq, M.P., Tulkens, P.M., 1999. Aminoglycosides: nephrotoxicity. Antimicrob. Agents Chemother. 43, 1003–1012.
Mingeot-Leclercq, M.P., Laurent, G., Tulkens, P.M., 1988. Biochemical mechanism of aminoglycoside-induced inhibition of phosphatidylcholine hydrolysis by lysosomal phospholipases. Biochem. Pharmacol. 37, 591–599.
Moestrup, S.K., Cui, S., Vorum, H., Bregengard, C., Bjorn, S.E., Norris, K., Gliemann, J., Christensen, E.I., 1995. Evidence that epithelial glycoprotein 330/megalin mediates uptake of polybasic drugs. J. Clin. Invest. 96, 1404–1413.
Molitoris, B.A., Dagher, P.C., Sandoval, R.M., Campos, S.B., Ashush, H., Fridman, E., Brafman, A., Faerman, A., Atkinson, S.J., Thompson, J.D., Kalinski, H., Skaliter, R., Erlich, S., Feinstein, E., 2009. siRNA targeted to p53 attenuates ischemic and cisplatin-induced acute kidney injury. J. Am. Soc. Nephrol. 20, 1754–1764.
Mullen, T.D., Obeid, L.M., 2012. Ceramide and apoptosis: exploring the enigmatic connections between sphingolipid metabolism and programmed cell death. Anti Cancer Agents Med. Chem. 12, 340–363.
Nadasdy, T., Laszik, Z., Blick, K.E., Johnson, L.D., Silva, F.G., 1994. Proliferative activity of intrinsic cell populations in the normal human kidney. J. Am. Soc. Nephrol. 4, 2032–2039.
Nakagawa, T., Zhu, H., Morishima, N., Li, E., Xu, J., Yankner, B.A., Yuan, J., 2000. Caspase-12 mediates endoplasmic-reticulum-specific apoptosis and cytotoxicity by amyloid-beta. Nature 403, 98–103.
Naujokat, C., Berges, C., Hoh, A., Wieczorek, H., Fuchs, D., Ovens, J., Miltz, M., Sadeghi, M., Opelz, G., Daniel, V., 2007. Proteasomal chymotrypsin-like peptidase activity is required for essential functions of human monocyte-derived dendritic cells. Immunology 120, 120–132.
Nikoletopoulou, V., Markaki, M., Palikaras, K., Tavernarakis, N., 2013. Crosstalk between apoptosis, necrosis and autophagy. Biochim. Biophys. Acta 1833, 3448–3459.
Oyadomari, S., Yun, C., Fisher, E.A., Kreglinger, N., Kreibich, G., Oyadomari, M., Harding, H.P., Goodman, A.G., Harant, H., Garrison, J.L., Taunton, J., Katze, M.G., Ron, D., 2006. Cotranslocational degradation protects the stressed endoplasmic reticulum from protein overload. Cell 126, 727–739.
Ozaki, N., Matheis, K.A., Gamber, M., Feidl, T., Nolte, T., Kalkuhl, A., Deschl, U., 2010. Identification of genes involved in gentamicin-induced nephrotoxicity in rats–a toxicogenomic investigation. Exp. Toxicol. Pathol. 62, 555–566.
Pant, V., Lozano, G., 2014. Limiting the power of p53 through the ubiquitin proteasome pathway. Genes Dev. 28, 1739–1751.
Peyrou, M., Cribb, A.E., 2007. Effect of endoplasmic reticulum stress preconditioning on cytotoxicity of clinically relevant nephrotoxins in renal cell lines. Toxicol. In Vitro 21, 878–886.
Peyrou, M., Hanna, P.E., Cribb, A.E., 2007. Cisplatin, gentamicin, and p-aminophenol induce markers of endoplasmic reticulum stress in the rat kidneys. Toxicol. Sci. 99, 346–353.
Quiros, Y., Vicente-Vicente, L., Morales, A.I., Lopez-Novoa, J.M., Lopez-Hernandez, F.J., 2011. An integrative overview on the mechanisms underlying the renal tubular cytotoxicity of gentamicin. Toxicol. Sci. 119, 245–256.
Rebillard, A., Rioux-Leclercq, N., Muller, C., Bellaud, P., Jouan, F., Meurette, O., Jouan, E., Vernhet, L., Le Quement, C., Carpinteiro, A., Schenck, M., Lagadic-Gossmann, D., Gulbins, E., Dimanche-Boitrel, M.T., 2008. Acid sphingomyelinase deficiency protects from cisplatin-induced gastrointestinal damage. Oncogene 27, 6590–6595.
Sanchez-Perez, Y., Morales-Barcenas, R., Garcia-Cuellar, C.M., Lopez-Marure, R., Calderon-Oliver, M., Pedraza-Chaverri, J., Chirino, Y.I., 2010. The alpha-mangostin prevention on cisplatin-induced apoptotic death in LLC-PK1 cells is associated to an inhibition of ROS production and p53 induction. Chem. Biol. Interact. 188, 144–150.
Sandoval, R.M., Molitoris, B.A., 2004. Gentamicin traffics retrograde through the secretory pathway and is released in the cytosol via the endoplasmic reticulum. Am. J. Physiol. Ren. Physiol. 286, F617–F624.
Sastrasinh, M., Knauss, T.C., Weinberg, J.M., Humes, H.D., 1982. Identification of the aminoglycoside binding site in rat renal brush border membranes. J. Pharmacol. Exp. Ther. 222, 350–358.
Sawada, M., Nakashima, S., Kiyono, T., Nakagawa, M., Yamada, J., Yamakawa, H., Banno, Y., Shinoda, J., Nishimura, Y., Nozawa, Y., Sakai, N., 2001. p53 regulates ceramide formation by neutral sphingomyelinase through reactive oxygen species in human glioma cells. Oncogene 20, 1368–1378.
Servais, H., Jossin, Y., Van Bambeke, F., Tulkens, P.M., Mingeot-Leclercq, M.P., 2006. Gentamicin causes apoptosis at low concentrations in renal LLC-PK1 cells subjected to electroporation. Antimicrob. Agents Chemother. 50, 1213–1221.
Servais, H., Van Der, S.P., Thirion, G., Van der, E.G., Van Bambeke, F., Tulkens, P.M., Mingeot-Leclercq, M.P., 2005. Gentamicin-induced apoptosis in LLC-PK1 cells: involvement of lysosomes and mitochondria. Toxicol. Appl. Pharmacol. 206, 321–333.
Tang, Y., Zhao, W., Chen, Y., Zhao, Y., Gu, W., 2008. Acetylation is indispensable for p53 activation. Cell 133, 612–626.
Teske, B.F., Wek, S.A., Bunpo, P., Cundiff, J.K., McClintick, J.N., Anthony, T.G., Wek, R.C., 2011. The eIF2 kinase PERK and the integrated stress response facilitate activation of ATF6 during endoplasmic reticulum stress. Mol. Biol. Cell 22, 4390–4405.
Tulkens, P., Trouet, A., 1978. The uptake and intracellular accumulation of aminoglycoside antibiotics in lysosomes of cultured rat fibroblasts. Biochem. Pharmacol. 27, 415–424.
Villamil Giraldo, A.M., Appelqvist, H., Ederth, T., Ollinger, K., 2014. Lysosomotropic agents: impact on lysosomal membrane permeabilization and cell death. Biochem. Soc. Trans. 42, 1460–1464.
Walker, P.D., Shah, S.V., 1987. Gentamicin enhanced production of hydrogen peroxide by renal cortical mitochondria. Am. J. Phys. 253, C495–C499.
Wan, C., Ma, X., Shi, S., Zhao, J., Nie, X., Han, J., Xiao, J., Wang, X., Jiang, S., Jiang, J., 2014. Pivotal roles of p53 transcription-dependent and -independent pathways in manganese-induced mitochondrial dysfunction and neuronal apoptosis. Toxicol. Appl. Pharmacol. 281, 294–302.
Wang, X., Yen, J., Kaiser, P., Huang, L., 2010. Regulation of the 26S proteasome complex during oxidative stress. Sci. Signal. 3, ra88.
Wu, H., Lozano, G., 1994. NF-kappa B activation of p53. A potential mechanism for suppressing cell growth in response to stress. J. Biol. Chem. 269, 20067–20074.
Xiao, Z., Shan, J., Li, C., Luo, L., Lu, J., Li, S., Long, D., Li, Y., 2013. Mechanisms of cyclosporine-induced renal cell apoptosis: a systematic review. Am. J. Nephrol. 37, 30–40.
Yang, J., Duerksen-Hughes, P.J., 2001. Activation of a p53-independent, sphingolipid-mediated cytolytic pathway in p53-negative mouse fibroblast cells treated with N-methyl-N-nitro-N-nitrosoguanidine. J. Biol. Chem. 276, 27129–27135.
Yang, Y., Ikezoe, T., Saito, T., Kobayashi, M., Koeffler, H.P., Taguchi, H., 2004. Proteasome inhibitor PS-341 induces growth arrest and apoptosis of non-small cell lung cancer cells via the JNK/c-Jun/AP-1 signaling. Cancer Sci. 95, 176–180.
Yano, T., Itoh, Y., Matsuo, M., Kawashiri, T., Egashira, N., Oishi, R., 2007. Involvement of both tumor necrosis factor-alpha-induced necrosis and p53-mediated caspase-dependent apoptosis in nephrotoxicity of cisplatin. Apoptosis 12, 1901–1909.
Yoneda, T., Imaizumi, K., Oono, K., Yui, D., Gomi, F., Katayama, T., Tohyama, M., 2001. Activation of caspase-12, an endoplastic reticulum (ER) resident caspase, through tumor necrosis factor receptor-associated factor 2-dependent mechanism in response to the ER stress. J. Biol. Chem. 276, 13935–13940.
Yu, J., Tiwari, S., Steiner, P., Zhang, L., 2003. Differential apoptotic response to the proteasome inhibitor Bortezomib [VELCADE, PS-341] in Bax-deficient and p21-deficient colon cancer cells. Cancer Biol. Ther. 2, 694–699.
Zeidan, Y.H., Hannun, Y.A., 2010. The acid sphingomyelinase/ceramide pathway: biomedical significance and mechanisms of regulation. Curr. Mol. Med. 10, 454–466.
Zeng, F., Yu, X., Sherry, J.P., Dixon, B., Duncker, B.P., Bols, N.C., 2016. The p53 inhibitor, pifithrin-alpha, disrupts microtubule organization, arrests growth, and induces polyploidy in the rainbow trout gill cell line, RTgill-W1. Comp Biochem. Physiol C. Toxicol. Pharmacol. 179, 1–10.
Zhang, L., Hu, J.J., Gong, F., 2011. MG132 inhibition of proteasome blocks apoptosis induced by severe DNA damage. Cell Cycle 10, 3515–3518.